Geology and Genesis of the Prince Darwin Prospect, Western Tasmania

Xin Ni Seow

BSc. (Honours)

Submitted in fulfillment of the requirements for the degree of Bachelor of Science with Honours

Oct, 2018

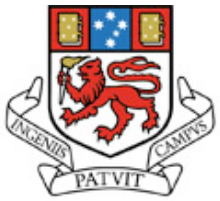

UNIVERSITY OF TASMANIA

CODES ARC CENTRE OF EXCELLENCE IN ORE DEPOSITS

TMVC TRANSFORMING THE MINING VALUE CHAIN

Corona Resources

Mineral Resources Tasmania mrt

Declaration of Originality

This thesis contains no materials which has been accepted for a degree or diploma by the University or and other institution, except by way of background information and duly acknowledged in the thesis, and to the best of my knowledge and belief, contains no material previously published or written by another person except where due acknowledgment is made in the text of the thesis.

Date:

Signature:

Authority of Access

Copying and communication of any part of this thesis is prohibited until May 2020 (1.5 years after acceptance); following that time, limited copying and communication is permitted in accordance with the *Copyright Act 1968*.

Abstract

Prince Darwin is an-intrusion-related prospect containing copper, gold, iron and rare earth element (REE) mineralisation. It is hosted within the Central Volcanic Complex (CVC) in the south of the Mount Read Volcanics (MRV), western Tasmania. Host rocks include submarine rhyolite and dacite that were deposited during the middle Cambrian. These volcanic rocks were intruded by the Darwin granite and a quartz porphyry in the middle to late Cambrian. The Darwin granite comprises two intrusive phases: Pink granite (syeno-granite) and White granite (granodiorite). The intrusive and volcanic rocks form part of suite I of the MRV, which are the least REE-enriched rocks of the sequence. Whole-rock geochemical data suggests that the volcanic rocks and quartz porphyry were co-genetic. However, the volcanic rocks and quartz porphyry are not co-magmatic with the Darwin granite.

Copper, gold, iron and REE mineralisation at Prince Darwin occurs in magmatic-hydrothermal breccias that are associated with the Darwin granite. The surrounding intrusive and volcanic rocks have been intensely altered, obscuring most primary features. Hydrothermal alteration at Prince Darwin consists of K-feldspar – magnetite – tourmaline – hematite, magnetite – apatite, chlorite, phengite, allanite – biotite and carbonate assemblages. The prevalent magnetite alteration within the granite is consistent with an I-type granite series association. Copper and gold mineralisation at Prince Darwin is characterised by sulfide mineral assemblages occurring with two different alteration stages: chalcopyrite hosted within early K-feldspar – magnetite-rich alteration, and bornite – chalcopyrite associated later-stage quartz – chlorite – phengite veins.

The chemistry of key alteration minerals (e.g., chlorite, epidote, allanite and tourmaline) is consistent with multiple episodes of hydrothermal fluid flow associated with the multi-stage emplacement of the Darwin granite and quartz porphyry. Heavy sulfur isotopic values (+8.6–15.8‰) at Prince Darwin are consistent with significant involvement of Cambrian seawater. Variability in the sulfur isotopic compositions of different alteration stages can be explained by relative differences in redox conditions.

Prince Darwin shows similarities with porphyry Cu, skarn, and IOCG deposits. However, no single model can explain the heavy sulfur isotopic compositions, REE-rich mineralisation, REE-depleted volcanic and intrusive rock compositions, mineralisation styles and presence of F- and P-rich fluids. Consequently, Prince Darwin potentially represents a hybrid ore deposit type that differs from other MRV-hosted base metal prospects.

Acknowledgements

I've received a lot of help and supports throughout my Honours year. It has been a pleasure to collaborate with people from different scientific aspects and backgrounds. I would like to acknowledge my gratitude to my supervisors, Mike and Evan who have given me a lot of guidance, advice and encouragements. Thank you for organising always having so much patience with me in the compilation of this project.

Thanks to Corona Minerals Ltd., Mineral Resources Tasmania (MRT) and CODES for the financial and logistical support for this project. Big thanks go to Charles Hughes from the Corona Minerals for providing guidance, unpublished reports, geological maps of the study area and geochemical data. Thank you to Ralph Botrill from MRT for sharing ideas, providing guidance and lending me thin sections. Dave Green is also thanked for processing the spectral data for the drill holes and helping me with the data interpretation.

I would like to thank staffs from CODES and the Earth Sciences department at the University Tasmania, in particular: Jay Thompson, Paul Olin, Sebastian Meffre, Sasha Stepanov, Alexander Cuison. I would also like to thank Angela Escolme for providing insights into the mineral system of my study area. Thanks to a variety of staffs from University of Tasmania, in particular to Martin Jutzeler, Jane Higgins, Deborah Macklin, Helen Scott Sandrin Feig, Karsten Goemann, Christin Cooke and Christine Dietz for technical and administrative support throughout the year.

I would like to thank my family back in Malaysia who have always supported me and had my back. Big thanks to my friends and Honours fellows that I met during my time at university: Fatin, Briedie, Josh, Ben, Tom, Emmet, Riquan, Lexi, Jaynnie, Jinning, Joyce, Wesley, Calvin, Lijia, Jiahui and many more. Thanks for the comfort, joy and laughter. You all made my stressed Honours year bearable.

Table of Contents

Digital Appendices

List of Figures

Chapter 1

Chapter 2

Chapter 3

Chapter 4

Chapter 5

Chapter 6

Chapter 7

List of Tables

Chapter 3

Chapter 4

Chapter 5

Chapter 6

Chapter 7

Chapter 8

Chapter 1

Introduction

1.1 Introduction

The Prince Darwin prospect is an intrusion-related Cu-Au-Fe-REE prospect discovered in 2011-2012 by Corona Minerals Ltd. It forms part of the South Darwin prospect tenement owned by Corona Minerals Ltd. Mineralization is associated with the Darwin granite which intruded the Central Volcanic Complex (CVC) in the south portion of the Mount Read Volcanic (MRV) belt in western Tasmania (Fig. 1.1). Previous studies have demonstrated a spatial and genetic association between the Darwin granite and several minor Cu-Au prospects nearby that collectively form a regionally significant belt of hydrothermal alteration and mineralization known as the Jukes-Darwin mineral field (White, 1975; Jones, 1993; Wyman, 2001); however, the genesis and mineralization style of the Prince Darwin prospect is still poorly understood.

1.2 Aims

This project aims to study the geology and alteration mineral chemistry of the Prince Darwin prospect, in order to define the paragenesis of mineralization and its relationship to the wider Cambrian metallogenic belt of western Tasmania. This has included: (1) identification and description of the key rock types through the combination of field mapping and sampling, drill core logging and sampling, and interpretation of spectral data, (2) documentation the styles of hydrothermal alteration across the Prince Darwin prospect in order to constrain the paragenetic relationship between the various rock types, mineralization and alteration assemblages, (3) mineral chemistry analysis of key alteration minerals to define their most likely origin and assess the trace element and REE deportment and anomalism, and (4) construct a genetic model of the mineralization at the Prince Darwin prospect and evaluate its relationship to other Cu-Au prospects along the same metallogenic belt.

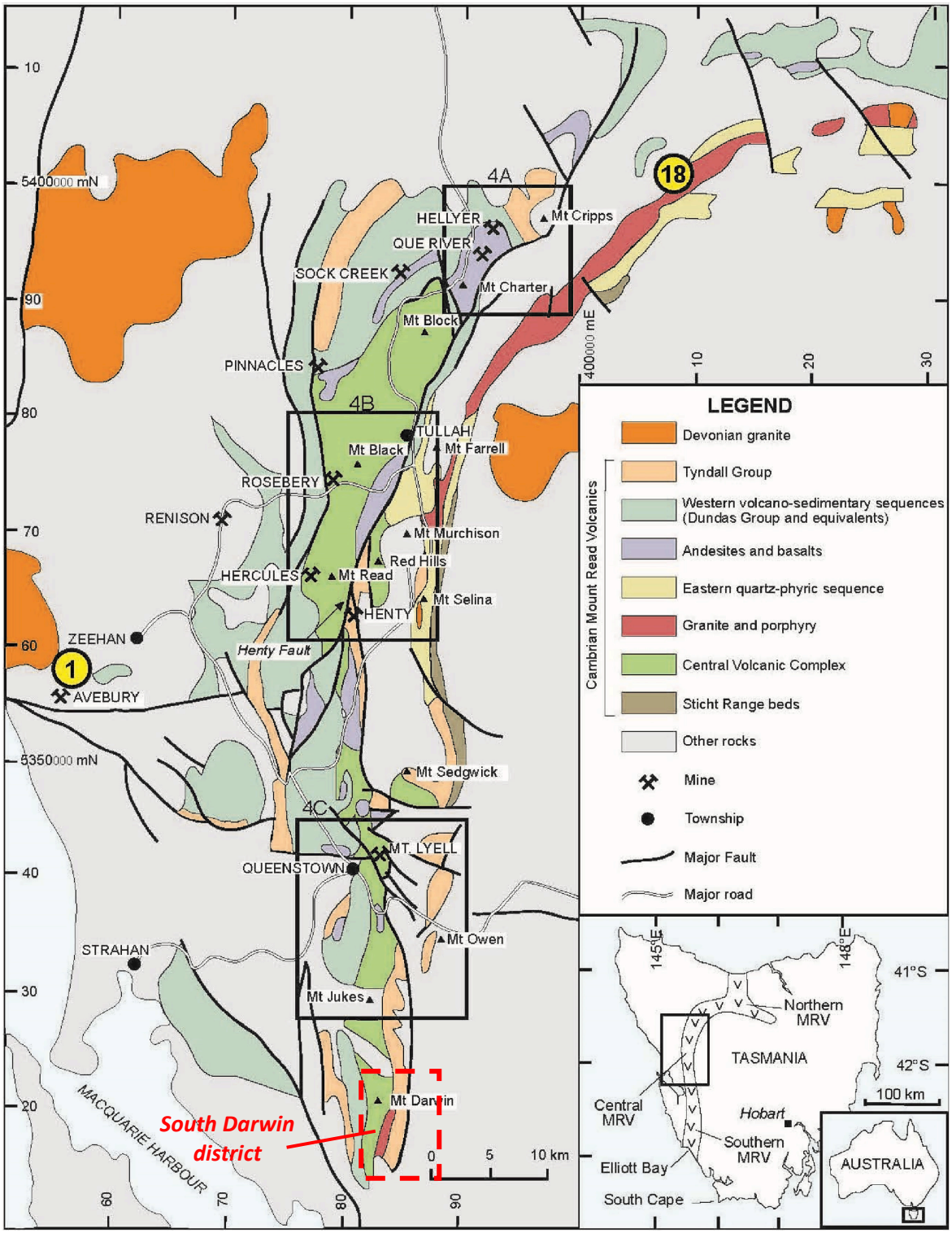

Figure 1.1: Simplified geological map of the central Mount Read Volcanic (MRV) in western Tasmania. Distribution of major lithologic units in the Mount Read Volcanics belt associated Cambrian – Protorozoic sequences, and the locations of the South Darwin district and major base metal propsecrs are indicated (after Mortensen et al., 2015).

1.3 Location and access

The Prince Darwin prospect is located in proximity to the Darwin granite at the southern end of the Cambrian Mount Read Volcanic (MRV) belt within the South Darwin

prospect area (Fig. 1.2). The study area, incorporating the South Darwin prospect, is located at Mount Darwin, approximately 20 km south of the Queenstown, western Tasmania. Access to the area is gained via the Jukes Road south from Queenstown and several four-wheel drive tracks. Access to the Darwin Plateau is via 4WD tracks.

1.4 Exploration and mining history

Documentation of old mining activities within the Mt. Darwin – South Darwin Peak region Studies by Hills (1914), Corbett and Cuffley (1970), Reid (1977), Corona Minerals (2011) have documented old mining activities in the Jukes-Darwin area. A number of minor Cu-Au prospects at several localities have been discovered since the 19th century, following the discovery of Cu-Au prospects at Mt. Lyell in 1880's (Hills, 1914). The major discoveries of Cu-Au mineralisation in the Jukes-Darwin region include Lake Jukes, Prince Darwin, East Darwin and Jukes Proprietary Prospect (Fig. 1.2; Hills, 1914; Reid, 1977; Green et al., 1988). Principal Cu ore minerals of these prospects are chalcopyrite, with minor Au, Ag and Pb (Hills, 1914).

South Darwin prospect has been continuously explored since 1900's. Mining activities in the district have however been limited due to poor infrastructure, rugged terrain and remote conditions which hamper the establishment of profitable mining operations (Corona Minerals, 2011). The South Darwin prospect was initially being prospected for copper-bearing magnetite-rich orebodies at Prince Darwin adits in 1900's but no production has been documented (Corona Minerals, 2011). Hills (1914) reported that the grab samples from the Prince Darwin adit yielded geochemical assay data up to 7 % Cu and 60 g/t Ag. No data on average grades have however been reported.

At present day, there is only very little modern exploration being conducted in the South Darwin prospect. Limited airborne magnetics and ground self-potential surveys were undertaken across the region (Large et al., 1996). High tenor magnetic anomalies greater than 5 km modelled over the outcrop area of the Darwin granites were interpreted to relate to magnetite veining and alteration, as well as possible skarn deposits, within and around the granite and the surrounding volcanic rock packages (Large et al., 1996). Followed-up drilling by Corona Minerals Ltd. in 2011/2012 in the study area later confirmed mineralisation at depth, with the best assay results to 2.7 Cu %, 0.74 Au g/t, 9.6 g/t Ag, 29.9 % Fe and 2 % TREO (Total Rare Earth Oxide). The ore grades gradually improve downhole (Corona Minerals, 2011).

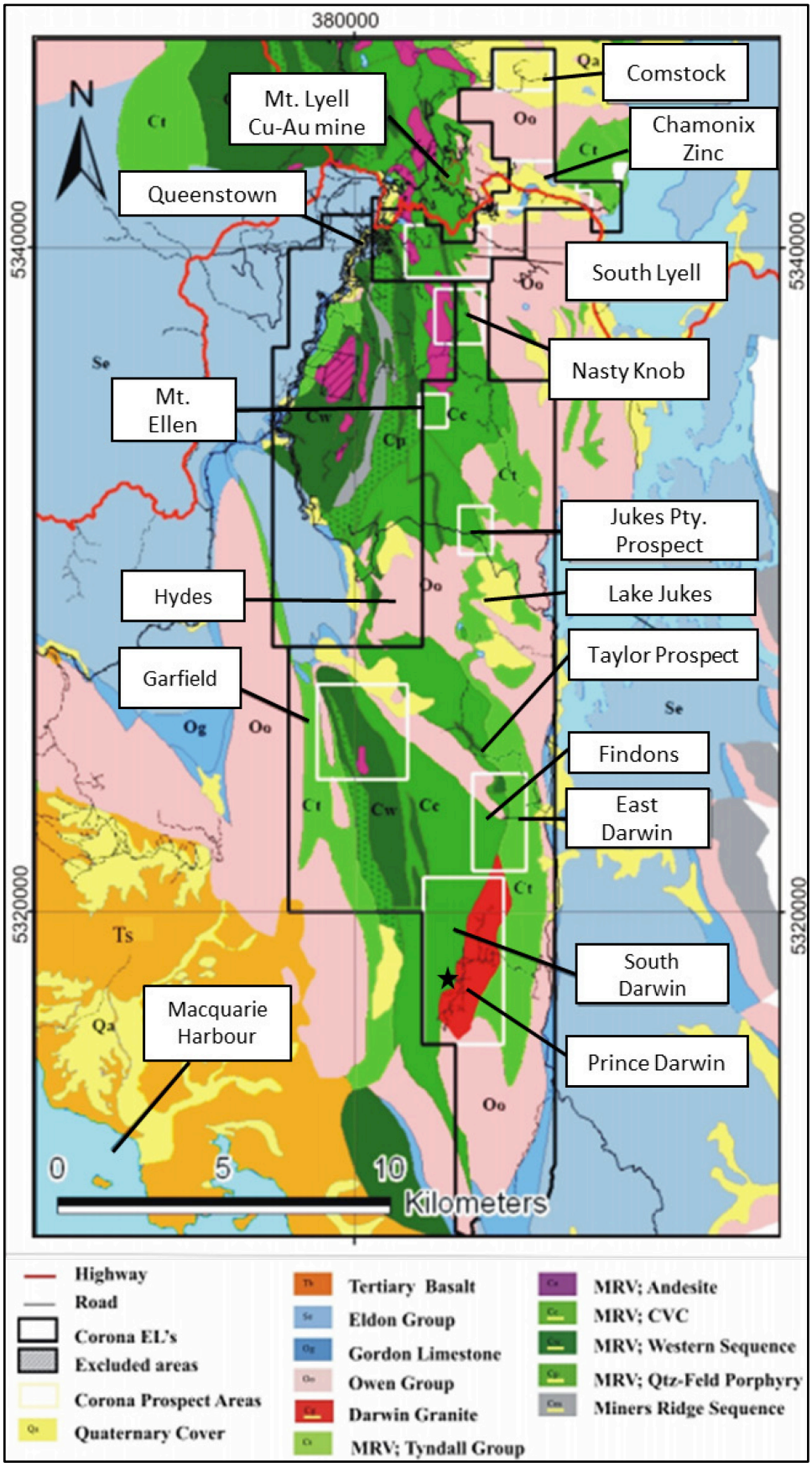

Figure 1.2: Regional map showing the locations of study area (Prince Darwin prospect), pre-existing old mines and known prospects associated Darwin granite along the MRV belt in western Tasmania (after Hills, 1914; Green, 1988; Wyman, 2001; Corona Minerals, 2011). Copper and gold are the main exploration targets in the southern MRV (e.g. Jukes Proprietary prospect, Doyle, 1990; East Darwin prospect, Gadaloff, 1996; Garfield prospect, Halley et al., 1996; Duncan, 1997; Jukes-Darwin prospect, Wyman, 2001).

1.5 Previous studies

Previous studies by Hills (1914), Corbett and Cuffley (1970), White (1975), Corbett (1993) and Large et al. (1996) have documented the structural, lithologic and stratigraphic relationships between the volcanic units in the Mount Read Volcanics (e.g., Tyndall Group and Central Volcanic Complex) and the Cambrian granites that intrude them (e.g., Murchison and Darwin granites), but their implications with regards to hydrothermal alteration and mineralization associated with the granitic intrusions were not covered. Hydrothermal alteration associated with the Cambrian granites were mapped and documented by Eastoe et al. (1987), Jones (1993) and Wyman (2001). Several minor prospects along the same metallogenic belt associated with the Darwin granites were also evaluated by numerous studies (Fig. 1.2). The Jukes-Darwin area was included in a regional sulphur isotope study of the entire MRV by Solomon et al. (1988). Solomon (1960), Leanman and Richardson (1989), and Large et al. (1996) carried out regional geophysical studies of gravity and magnetic data to delineate and interpret the morphology of the Cambrian granites. Large et al. (1996) also provided a review on the hydrothermal alteration and mineralization styles in the Jukes-Darwin area and the Mt. Lyell district, and proposed a genetic model linking two prospects.

1.6 Thesis organisation

This thesis comprises seven chapters and is structured follows:

Chapter 2 (Regional Geology) provides an introduction to the regional geology and tectonic setting of the MRV belt in the western Tasmania.

Chapter 3 (Local Geology) documents the detailed descriptions of the key rock types at the Prince Darwin prospect based on fieldwork, petrographic studies, graphic core logging completed by author. This is followed by geochronological constraints on the absolute timing of intrusive emplacement associated with the Prince Darwin prospect. Evidence of deformation recorded by local structures are also briefly discussed.

Chapter 4 (Hydrothermal Alteration and Mineralisation) documents paragenetic relationship of hydrothermal alteration, mineralisation and host rocks at the Prince Darwin prospect. In total, ten hydrothermal alteration and twelve vein types were recognised. Detailed descriptions were given to each alteration and vein stage, based on the observations on surface samples, drill holes and thin sections. These alteration and vein stages are

summarised in a table. A cross section was also reconstructed to show the distribution of the key hydrothermal alteration and mineralisation, with the aid of graphic core logging and drill hole assay data from Corona Minerals.

Chapter 5 (Igneous Geochemistry) documents of the whole-rock geochemistry of the volcanic and igneous rocks in the Prince Darwin prospect. Data from previous studies across the South Darwin prospect, least altered CVC rocks, and Murchison granite were included for comparative purposes and interpretation on their genetic relationship.

Chapter 6 (Hydrothermal Mineral Chemistry) documents and discusses the chemistry of the key hydrothermal minerals, including chlorite, epidote, allanite and tourmaline from Prince Darwin. Within each mineral group, samples were grouped to different sub-types based on their modes of occurrence. Trace element chemistry of each sub-type within each mineral group was compared to gain insights into the chemistry of the hydrothermal fluids.

Chapter 7 (Sulfur Isotopes) presents the sufur isotopic compositions of pyrites (n = 12) from the Prince Darwin prospect. A table, summarising the data compiled from previous studies on other MRV-hosted prospects, is presented and used to compare with results of this study. The data were used to infer the likely source of the hydrothermal fluid.

Chapter 8 (Genetic Model and Conclusion) provides a discussion on the genetic model of the Prince Darwin prospect by comparing the geological and geochemical results presented in previous chapters with some relevant porphyry-related ore deposit models. This is followed by the implications of this study for future exploration activities and recommendation for future studies.

Chapter 2

Regional Geology

2.1 Introduction

The Cambrian Mt. Read Volcanic Belt (MRV) is the main mineralized belt that hosts world-class base metal deposits in western Tasmania (Fig. 1.1 and 2.1). The MRV is a post-collisional volcanic belt composed of a diverse sequence of submarine felsic to intermediate volcanic rocks (Corbett, 1992). It occurs as a continuous linear belt that infills the eastern margin of mid-Cambrian extensional basin known as the Dundas trough (Crawford et al., 1992). The volcanic sequences of the MRV overlie the Precambrian Tyennan region to the east and are intercalated with Cambrian sedimentary sequences of the Dundas Group to the west (Corbett, 1992). The MRV was unconformably overlain by the late Cambrian to early Ordovician Owen Conglomerate (Corbett and Solomon, 1989) and was intruded by Cambrian and Devonian granites at different localities. These granitic intrusions are typically small and pipe-like or sheet-like in dimension. Solomon (1981) interpreted the Cambrian granites as subvolcanic intrusions genetically related to the emplacement of the surrounding volcanic piles in a volcanic arc that was accreted onto continental crust, whereas Crawford and Berry (1992) argued that the granites are post-collisional intrusions that were emplaced after arc-continent collision. The Cambrian granites are spatially related to the volcanic-hosted Cu-Au-Fe-Pb-Zn deposits of the MRV whereas Devonian granites are related to Sn mineralization elsewhere in the Dundas Trough (Large et al., 1996). Summaries of the key lithostratigraphic units that comprise the MRV are documented by Berry (1994), Corbett (1990, 1992, 2002), Crawford et al. (1992), McPhie and Allen (1992), Pemberton and Corbett (1992), Seymour and Calver (1995, 1998), White and McPhie (1996), Selley (1997), Seymour et al. (2006, 2007) and Corbett et al. (2014).

2.2 Regional geology

The MRV consists of calc-alkaline felsic to intermediate volcanic rocks, dominated by rhyolites and dacites, with minor andesites and rare basalts (Corbett and Solomon, 1989). Crawford (1992) summarised that the MRV is representative of short-lived post-collisional

volcanism in Cambrian. He further concluded that the MRV is a package of intensely altered, metamorphosed and deformed submarine volcanics that host a variety of world-class economic massive sulfide deposits. The MRV has been subdivided into several stratigraphic units, including the Sticht Range Beds, Western Volcano-Sedimentary Sequence (WVS), Central Volcanic Complex (CVC), Eastern Quartz-Phyric Sequence (EQPS) and the Tyndall Group, andesitic to basaltic volcanics, and tholeiitic mafic rocks (Fig. 2.1; Corbett, 2002; Mortensen et al., 2015).

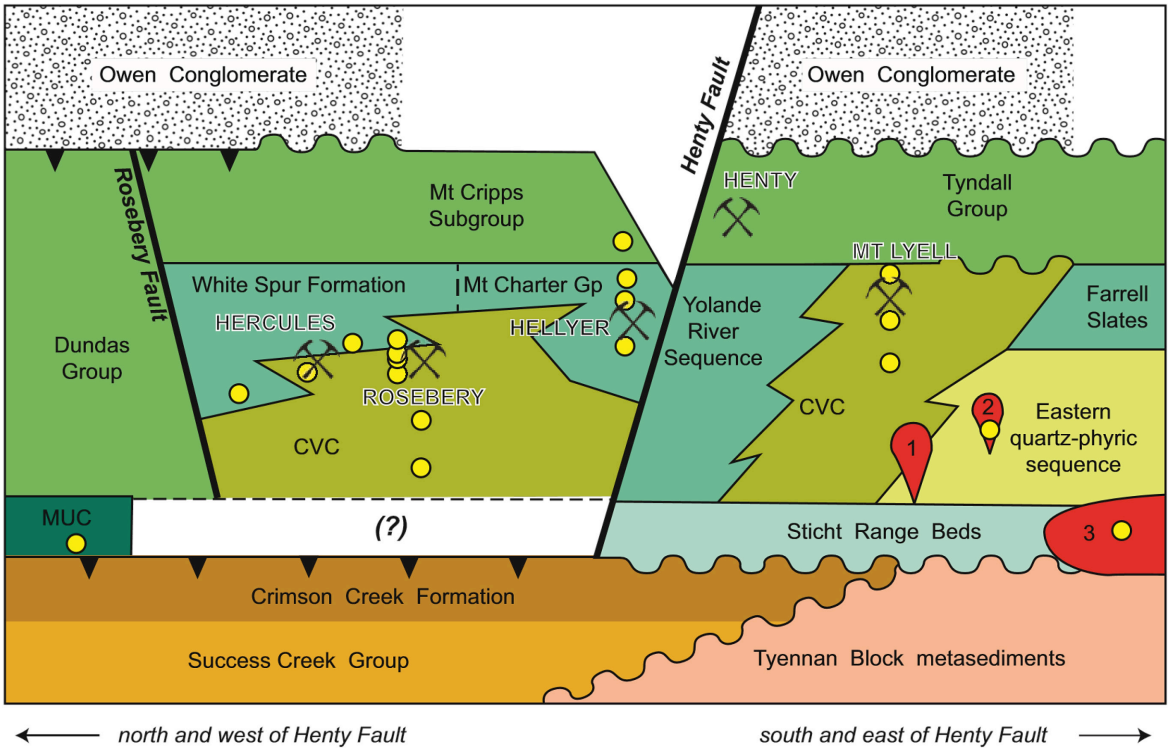

Figure 2.1: Simplified cross section illustrating the stratigraphic relationships within the Mount Read Volcanic (MRV) belt. The stratigraphic positions of the main VHMS deposits in the belt are also indicated (from Mortensen 2015). Darwin granite (1), Murchison granite (2) and the Bonds Range Porphyry (3) are labelled in numbers.

2.2.1 The Sticht Range beds

These consist of several hundred metres of west-dipping, thinly bedded Precambrian siliceous pebbles, conglomerate, boulders, and minor micaceous siltstone that directly overlies the Tyennan basement to the east of the Dundas Trough (Carey and Banks, 1954; Corbett, 1992). Various proportion of Interbedded volcanic detritus (Baillie, 1989) and volcaniclastic units (McNeil and Corbett, 1992) have been reported. A tribolite of a probable age of middle Cambrian was recovered the the Sticht Range beds (Bailie, 1989). Bailie (1989) consider that this unit reflects a progression from fluvial to shallow- to deep-marine

environment. The sedimentology, structure and formation of the Sticht Range Beds have been discussed in detail by Baillie (1989).

2.2.2 Western Volcano-Sedimentary Sequences (WVS)

The WVS is the oldest volcanic sequence in the MRV. This sequence typically comprises fossiliferous mid to late Cambrian sedimentary successions, micaceous siltstone, tuffaceous mudstone, black shale, interbedded volcaniclastic turbidites, quartz-phyric lavas and porphyritic intrusions, and with localized minor andesitic and basaltic lavas (Corbett and Solomon, 1989; Corbett, 1992). The Henty Fault has divided WVS into the Dundas Group (north of the Henty Fault), Yolande River Sequence (south of the Henty Fault) and Mt. Charter Group (Hellyer area; Corbett, 1992). The Yolande River Sequence, exposed to the west of Mt. Darwin and the south Darwin Plateau, is a mixed sequence of quartz-phyric lavas and volcaniclastics intercalated with sandstone, mudstone and black shale (Wyman, 2001).

2.2.3 Central Volcanic Complex (CVC)

The CVC is the main rock package within the central portion of the MRV and is dominated by feldspar-porphyritic lavas and associated volcaniclastics with minor sedimentary layers (Corbett, 1989; 1992; 2002; Corbett et al., 1993; Gifkins and Kimber, 2003). It is typically characterized by the abundance of pink hematite-dusted feldspar phenocrysts and lack of quartz phenocrysts in the felsic groundmass. Flow banding and autobreccia are common in the CVC. Current interpretation of the setting in which most of the CVC formed is of a submarine environment of variable depth, despite the presence of a thick pumaceous mass flow unit (Corbett, 1992; Crawford et al., 1992; McPhie and Allen, 1992; 2003). This unit is intruded by the Darwin and Elliott Bay granites in the south of the MRV (White, 1975). The interfingering relationship between the WVS and CVC to the west, in addition to fault disruption and lateral variations, has made differentiation between two stratigraphic sequences difficult (e.g., Wyman, 2001). A more detailed description of the CVC units within the area of this study will be presented in Chapter 3.

2.2.4 Eastern Quartz-Phyric Sequence (EQPS)

The EQPS is a succession comprising quartz-feldspar porphyritic lavas, volcaniclastic rocks and abundant quartz-feldspar (± biotite) phyric porphyry intrusions, with subordinate mudstones and siltstones (Corbett, 1992; Corbett et al., 1993; Wyman, 2001). The occurrence of large (2-3 mm) quartz phenocrysts throughout the volcanic facies is characteristic of this unit. The EQPS lies adjacent to and to the east of the CVC, and may

be intercalated with the CVC. This has made the strict stratigraphic definition between them challenging (e.g., Halley and Roberts, 1997). Some authors envisage that the EQPS is a time equivalent of the CVC (e.g., Corbett, 2002) or part of Tyndall Group (Murphy et al., 2004).

2.2.5 Tyndall Group

The Tyndall Group consists primarily of crystal-rich tuffaceous mass flow breccias, sandstones and volcanolithic conglomerates (Corbett et al., 1993). The Tyndall Group crops out to the east of the Darwin granite, approximately 5 km to the north of the South Darwin prospect. It is overlain by the siliciclastic Owen Conglomerate (Corbett, 1992). Where the Tyndall Group is in contact with the Darwin granite, it contains rounded clasts of sericite-altered coarse-grained pink Darwin granite and CVC volcanic clasts (Jones, 1993). An U-Pb age of 5494.4 ± 3.8 Ma was yielded from a volcaniclastic units in the Tyndall Group (Seymour et al., 1995). Detailed lithostratigraphic descriptions of the Tyndall Group and its correlates have been discussed by numerous authors (Corbett, 1992; Corbett et al., 1993; Jones, 1993; White and McPhie, 1996; Wyman, 2001).

2.2.6 Andesitic-basaltic and tholeiitic mafic rocks

Andesitic and basaltic volcanic rocks occur as lenses within the WVS and throughout the upper part of the CVC. Their associated geochemistry and petrogenesis in the MRV were described by Crawford et al. (1992). Tholeiitic mafic rocks, with substantial ultramafic layers, lies to the west of the MRV. Corbett (1992) and Crawford et al. (1992) noted that these rocks are geochemically distinct from the typical calc-alkaline MRV.

2.2.7 Darwin granite

The MRV was intruded by Cambrian granites at several localities, shortly after or coeval with the formation of the MRV (White, 1975). Five Cambrian granites have been mapped and studied in western Tasmania: the Murchison, Darwin, Elliott Bay, Timbertop and Dove granites (White, 1975; Leanman and Richardson, 1989; Jones, 1993).

In the study area, the CVC is intruded by the Darwin granite in the south of the MRV (Fig. 2.1). Two distinct phases of the Darwin granite have been recognized by White (1975): the ‘Pink’ and ‘White’ granite, based on their mineralogy. Jones (1993) described the Darwin Pink and White granite as ‘equigranular granite’ and ‘granodiorite’ respectively based on modal classification. Abbott (1992) described the Darwin granite as a high-K, magnetite series granite following the classification of Ishihara (1981). Two other minor phases, a

microgranite and quartz-feldspar porphyry were mapped by Wyman (2001). Detailed investigation on the geochemistry of each phase was inducted by Jones (1993) and Wyman (2001).

The Pink granite is the most common phase of the Darwin granite, followed by the white granite. The contact with the CVC is sharp and well-defined in the west, whereas the contact with the Tyndall Group to the east is an erosional unconformity (Wyman, 2001). The erosional contact suggests that the emplacement of the Darwin granite occurred after the deposition, cooling, uplift and erosion of the CVC volcanics, and prior to the deposition of the Tyndall Group rocks (Jones, 1993). Several theories have been put forward as to the genesis of the Darwin granite (e.g., Solomon, 1960; Crawford, 1987; Corbett and Solomon, 1989; Jones, 1993; Wyman, 2001). Jones (1993) suggested that the Darwin granite is a mid to lower epizonal intrusion, given by the fact that there is a lack of porphyritic texture (rapid cooling). Jones (1993) also suggested that the Darwin granite is thought to have already been highly crystallized upon its emplacement and was not a hot intrusion due to the lack of high grade contact metamorphism in the surrounding volcanic rocks. A more detailed description of the Darwin granite within the area of this study will be presented in Chapter 3.

2.3 Regional structures

Western Tasmania has been subjected to several major orogenic events since the Cambrian. Local unconformities, disconformities, multiphase folding and faulting, reactivation of early fold and fault structures, and contradictory structural relationships are therefore common in the Cambro-Ordovician sequences as the consequence of the complex deformation and metamorphism (Berry, 1994). The Cambro-Ordovician regional deformation (e,g, Tyennan-Delamarian and Tabberabberan Orogeny) was also accompanied with greenschist facies metamorphism (Stacey and Berry, 2004; Chmielowski, 2009). This was followed by widespread post-tectonic granitoid intrusions in the Late Devonian and Early Carboniferous. The main deformational events that have affected western Tasmania have been discussed in many previous studies (e.g., Berry and Keele, 1993a; 1993b; 1997; Crawford and Berry, 1992; Jones, 1993; Berry, 1994; Cayley et al., 2002; Stacey and Berry, 2004; Seymour et al., 2007; Chmielowski, 2009; Corbett et al., 2014). Cambro-Devonian orogenesis is the main tectonic event recorded in the MRV in western Tasmania. Stacey and Berry (2004) considered that most of the fold trends in western Tasmania are a result of

tightening of the Cambrian structures during the Devonian. Major tectonic events that have affected the MRV are listed below:

1. Formation of passive margin (late Neoproterozoic to early Cambrian): deposition of an early shallow water sequence (including cross-bedded quartz sandstone, laminated siltstone, pyritic shale and dolomite) of Rocky Cape Group, which has been widely considered as a block of the authochthonous basement of Paleozoic Tasmania, followed by tholeiitic volcanism (Berry, 1994).

2. Oceanic arc-continental collision and obduction (c. 525 – 510 Ma): corresponds to the earliest phase of the Tyennan Orogeny (Stacey and Berry, 2004). The east of the proto-Australian passive margin collided with an oceanic arc, with major slices of mafic-ultramafic complexes being thrust over Tasmania (Crawford and Berry, 1992). This led to high-pressure metamorphism in the underlying rocks (Stacey and Berry, 2004).

3. Tyennan (-Delamarian Orogeny) (c. 515 - 510 Ma): involved multiphase deformation. The mid-Cambrian post-collisional phase was characterized by rapid subsidence, complex extensional fault geometry (graben formation), active syn-orogenic deposition, major post-collisional felsic to intermediate volcanism (MRV) and VHMS mineralisation (Berry, 1993b; Stacey and Berry, 2004; Seymour et al., 2007). The tectonism during MRV formation was E-W extensional, as shown by the orientation of the hydrothermal veins at the Heyller deposit (Gemmell and Large, 1992), a basaltic dyke in the Henty Fault zone and growth faults underlying the Roseberry deposit (Gifkins and Kimber, 2003). During the mid to late Cambrian, N-S compression was followed by extension and granitoid intrusions (e.g., the Darwin, Elliott Bay and Murchison granites) and deposition of Tyndall Group (Stacey and Berry, 2004). The late Cambrian was characterized by E-W compression and basin inversion, with extensive reactivation of the early-formed extensional faults as reverse faults (e.g., Henty Fault) and development of upright N-trending open folds (Berry et al., 2007). Low to high grade metamorphic assemblages in Tyennan region is attributed to Tyennan Orogeny (Berry, 1994; Meffre et al., 2000; Holm and Berry, 2002; Corbett et al., 2014). The Tyennan block was later uplifted and unconformably overlain by the Owen Conglomerate (Seymour et al., 2007).

4. Ordovician to Early Devonian: cyclic shallow water deposition (renewal of shelf sedimentation; Seymour et al., 2007).

5. *Middle Devonian Tabberabberan Orogeny (c. 430 – 380 Ma):* the main deformational event to have affected the MRV, characterized complexity in fold orientations as a result of

reactivation of Cambrian folds (Turner et al., 1998; Stacey and Berry, 2004; Seymour et al., 2007; Chmielowski and Berry, 2012). This orogenic event superimposed pre-existing structures formed during the Cambrian Tyennan Orogeny. The fold trends developed in Tabberabberan Orogeny were strongly controlled by the geometry of the Cambrian folds, resulting in transection of Devonian cleavage orientations and axial plane of associated folds in places. It has been difficult to separate Cambrian and Devonian structures. Seymour (1980) separated Tabberabbera-related deformation events into four phases: E-W (D_1), NE-SW (D_2), N-S (D_3) and NW-SE trending folds at a regional scale. Williams et al. (1989) suggested that the initial phase of NE-SW compression developed NW-SW to WNW-ESE trending asymmetrical to symmetrical folds, faults and axial cleavage, followed by a later stage of E-W shortening. Consequently, NW-SE trending folds and N-S to NW-SE dominated faults, with minor brittle wrench faulting, developed across the region (e.g., Henty Fault, Rosebery Fault, Great Lyell Fault; Berry and Keele, 1992; Berry, 1993a, 1993b, 1994; Stacey and Berry, 2004; Corbett et al., 2014), disrupting the lithostratigraphy of the MR (Crawford and Berry, 1992). Prehnite-pumpellyite to lower greenschist facies regional metamorphism in Mount Read Volcanics was involved in the Tabberabberan Orogeny, accompanied with local hydrothermal alteration and associated contact metamorphism during post-tectonic granitoid emplacements (Walshe and Solomon, 1981; Williams et al., 1989; Corbett, 1992; Crawford et al., 1992; Jones, 1999; Corbett et al., 2014).

Chapter 3

Local Geology

3.1 Introduction

The Prince Darwin prospect is located on the Darwin Plateau towards the southern end of the MRV. Out of the major geological formations in the MRV, the CVC is the only unit exposed in the Prince Darwin area. The CVC has been intruded by the Darwin granite to the east. This chapter documents the petrology and geochronology of the major geological units encountered in this study.

3.2 Methods

Field mapping was conducted using a geological map, previously produced by Corona Minerals, as base map (Fig. 3.1). The CVC and Darwin granite are well-exposed in the field area; however, strongly weathered rocks and accessibility issues in the western part of the study area have resulted in some sampling limitations. The primary textures of the surface volcanic samples have been partly to completely destroyed. With the aid of drill core from near the Prince Darwin adit in the west of the prospect, relatively fresh volcanic samples were examined. An undefined quartz porphyry, which does not crop out in the field area, was logged in drill core (Appendix D). Petrographic analysis of 20 polished thin sections from surface and drill core samples, supplemented by 18 thin sections provided by MRT, have been carried out to observe primary and secondary minerals and textures, and to evaluate the mineral modal abundances of each geological unit. The following descriptions are based on the least-altered samples from each geological unit observed in this study.

3.3 Darwin granite

The Darwin granite is approximately 5 km long and 1 km wide, extending in a N-S direction across the Darwin Plateau (Fig. 3.1). Two dominant phases have been mapped in

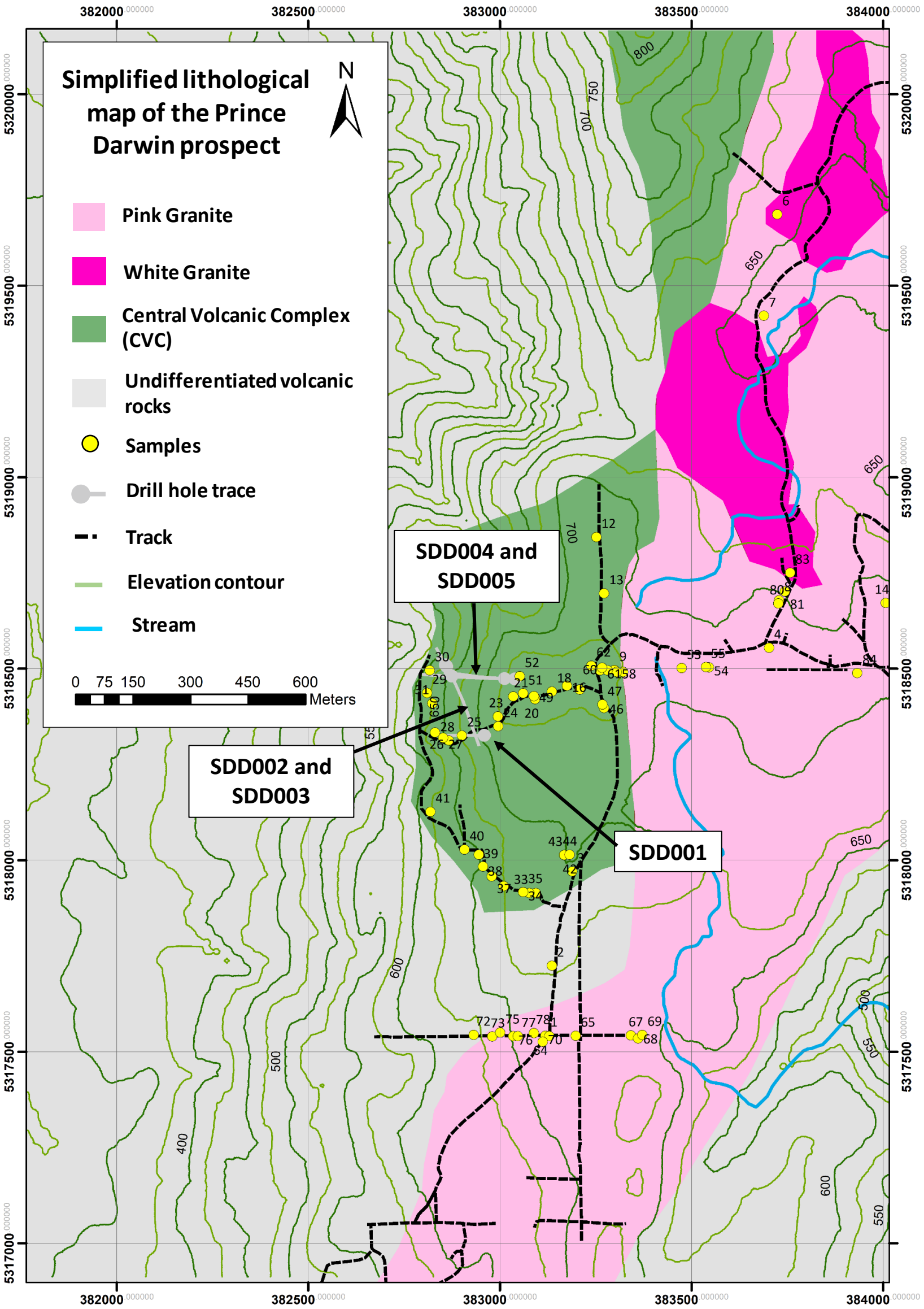

Figure 3.1: Simplified surface geology map of the Prince Darwin prospect (after Corona Minerals, 2011). The eastern margin of the Central Volcanic Complex at Prince Darwin was intruded by the Pink Granite, followed by the White granite. The west of the volcanic rocks was later intruded by another intrusion, namely quartz porphyry that does not outcrop in the field area (see Appendix D). Distribution of collected field samples and locations of drill holes are labelled (see Appendix B).

the field area: the Pink granite and White granite. Minor phases of microgranite dykes, described by Jones (1993), and quartz-feldspar porphyry, described by Wyman (2001), were not encountered in the field.

3.3.1 Pink granite

The Pink granite is the dominant phase of the Darwin granite. It is generally well-exposed in the field area but has been strongly oxidised and weathered (Fig. 3.2A). The Pink granite is characterised by equigranular and phaneritic texture. The presence of pink to red K-feldspar and intense chlorite – phengite alteration of plagioclase crystals, imparts the distinctive pink-green colouration that is characteristic of this intrusive phase (Fig 3.2A). The hematite dusting of K-feldspar gives the rocks a mottled texture (Fig. 3.2A). Locally, primary biotite has been intensely alterered to chlorite and (Fig 3.2B). Estimated modal abundance of minerals for the Pink granite are: 40–50% K-feldspar, 20–25% quartz, 20–25% plagioclase, minor biotite and white micas, and accessory zircon, monazite, hornblende, rutile, magnetite, titanite and apatite. Quartz crystals are typically anhedral with straight or sutured grain boundaries in places where quartz has recrystallised. Plagioclase crystals are euhedral to subhedral and have been altered to phengite (Fig.3.2C). K-feldspar occurs as subhedral to anhedral crystals with cleavages delineated by selective replacement of phengite. Microperthitic and granophyric textures are locally present.

3.3.2 White granite

The White granite is the other major phase of the Darwin granite, and it has intruded the Pink granite. It is volumetrically less abundant than the Pink granite and primarily crops out in the north part of the Darwin plateau (Fig. 3.1). The contact between the White granite and the Pink granite is sharp; however, no chilled margin has been clearly mapped in the field. The White granite has a diagnostic creamy white to pale yellow colour, imparted by abundant plagioclase and moderate to intense phengite alteration after plagioclase (Fig. 3.2D). The intensity of the phengite alteration in this unit increases towards the contact with the Pink granite. The White granite is compositionally and texturally distinct compared with the Pink granite. The White granite contains significantly more plagioclase and less K-feldspar. The estimated modal composition is 45–50% plagioclase, 20–25% K-feldspar and 20–25% quartz, with accessory white mica, biotite, magnetite and titanite.

White granite generally has phanerocrystalline and equigranular texture, although variation in grain size (coarse- to fine-grained) was observed (Fig. 3.2E and 3.2F). There are porphyritic and equigranular domains in the White granite. Texturally, the White granite is

more diverse than the Pink granite. Quartz crystals are typically euhedral in the porphyritic domains and subhedral to anhedral in the equigranular domains. Quartz recrystallisation has been observed in both cases where development of sutured grain boundaries. Plagioclase have been intensely altered to phengite, albite twinning is still intact in some crystals. K-feldspar, conversely, occurs as subhedral to anhedral crystals and has been weakly phengite-altered (Fig. 3.2 F). Rare biotites are observed and they have been partly altered to phengite and chlorite.

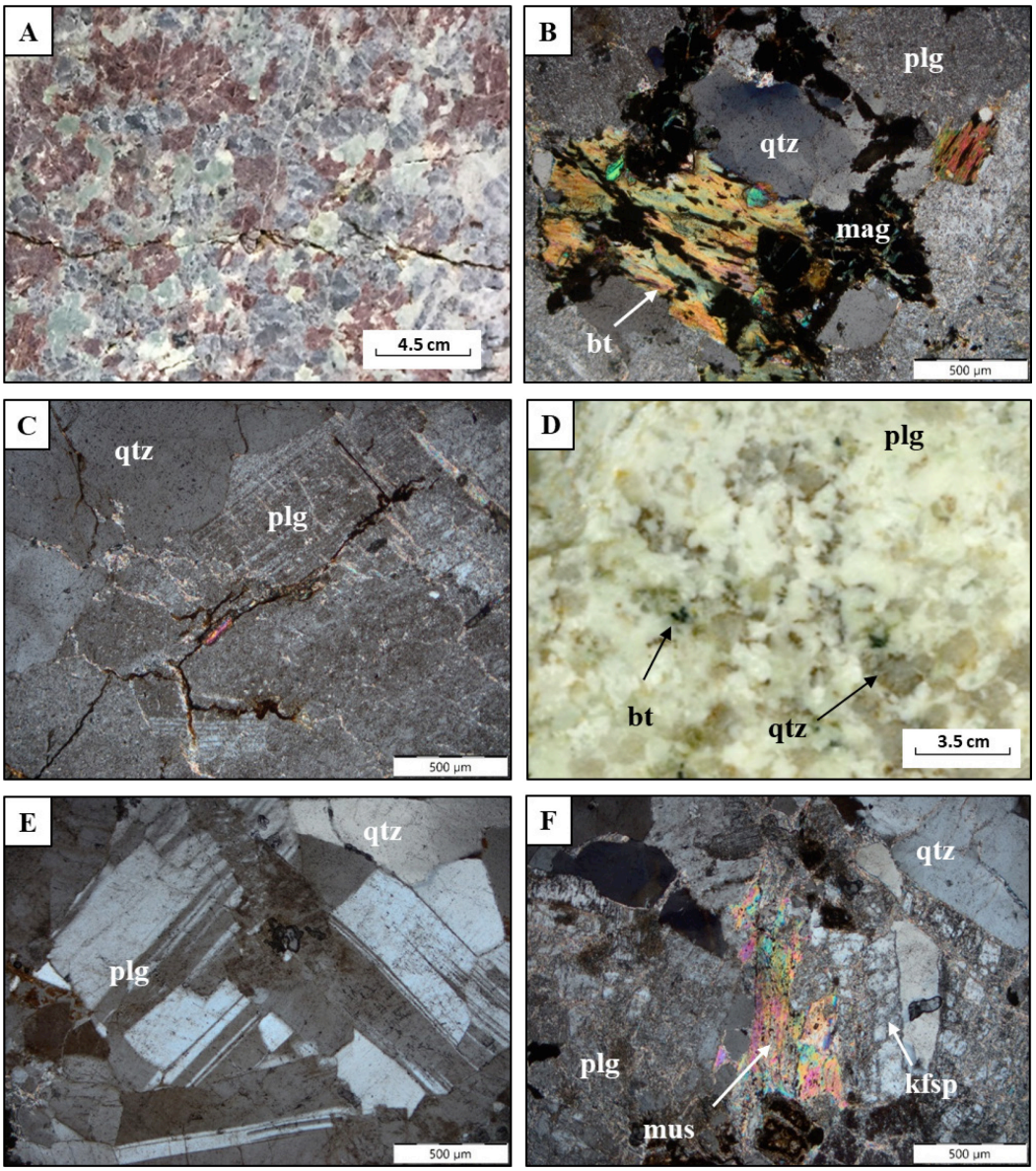

Figure 3.2: Photographs of the Darwin granite from the Prince Darwin prospect. **(A):** Hand specimen photograph of the Pink granite characterised by mottled texture as the consequence of intense K-feldspar and chlorite – phengite alteration. **(B):** Cross-polarised photomicrograph of partially chlorite – magnetite-altered biotite grains in the Pink granite. **(C):** Cross-polarised photomicrograph of phengite-altered Pink granite. Phengite selectively replaced plagioclase along the cleavages. **(D):** Hand specimen photograph of the White granite. Intense phengite alteration imparts creamy yellow appearance in the White granite. **(E):** Cross-polarised photomicrograph of unaltered White granite. Plagioclase is more abundant relative to K-feldspar within White granite. **(F):** Cross-polarised photomicrograph of phengite-altered White granite. K-feldspar is relatively less phengite-altered compared to plagioclase. Primary muscovite has also been partially replaced by phengite. Abbreviations: bt = biotite, kfsp = K-feldspar, mus = muscovite, plg = plagioclase, qtz = quartz.

3.4 Central Volcanic Complex (CVC)

The CVC forms an exposed ridge along the western edge of the Darwin Plateau (Fig. 3.1). It has not been possible to accurately distinguish the host rocks and map the geological contact between rhyolite and dacite in the field as the units are fine-grained and massive and have been intensely altered due to metamorphism and hydrothermal alteration.

The volcanic units in the study area are predominantly coherent, with minor volcaniclastic sandstone. The CVC rocks are typically brecciated and magnetite – tourmaline-cemented. Rare peperite was observed from the drill core and it has been strongly deformed. The volcanic rocks in the field area are characterised by distinctive pink to orange colour due to intense feldspar alteration (Fig. 3.3A). The CVC rocks near to the contact with the granites are intensely silicified due to contact metamorphism. Primary rock textures have been mostly destroyed due to metamorphism and hydrothermal alteration, which makes petrographic classification difficult (Fig. 3.3A).

The CVC rocks in the study area have been subdivided into two facies: dacite and rhyolite. This classification is based on the whole-rock geochemistry, phases of phenocrysts present, and the relative proportion of quartz, K-feldspar and plagioclase phenocrysts. The contact between the dacite and rhyolite has been interpreted as a fault contact (Hughes, 2015).

3.4.1 Dacite

Feldspar-phyric dacite is the dominant volcanic phase within the CVC across the Darwin Plateau. In most cases, only fine-grained feldspar phenocrysts, with sparse fine-grained quartz crystals, can be recognised within an aphanitic groundmass characterised by pink-orange colour due to regional scale K-feldspar alteration (Fig. 3.2A). In general, the phenocrysts make up 15–20% of the rocks, with variable proportion of quartz phenocrysts (generally <5% of the total rock). At some localities, this unit can be aphanitic. Feldspar phenocrysts are commonly replaced by phengite, chlorite and carbonate (Fig. 3.3B). Phengite and chlorite alteration give cloudy textures to the feldspars and destroy the twinning features, making the determination of the relative proportion between K-feldspar and plagioclase difficult (Fig. 3.3C). In some cases, the crystal outlines of feldspars are still recognisable. Feldspar crystals are commonly subhedral to euhedral ranging from <0.5 to 1.5 mm in size. Quartz crystals have variable crystal shapes and they typically display undulose extinction in thin sections. Quartz recrystallisation is recognisable in some places. The groundmass is composed of fine-grained quartz and sericite – chlorite-altered feldspar.

Schistosity, defined by the alignment of chlorite and sericite, has been observed in the dacitic unit. Acicular chlorite is locally common in some samples. Biotite are invariably chloritised. This unit has been intruded by the quartz porphyry. Flow banded textures develop near to the contact with quartz porphyry (Fig. 3.3D).

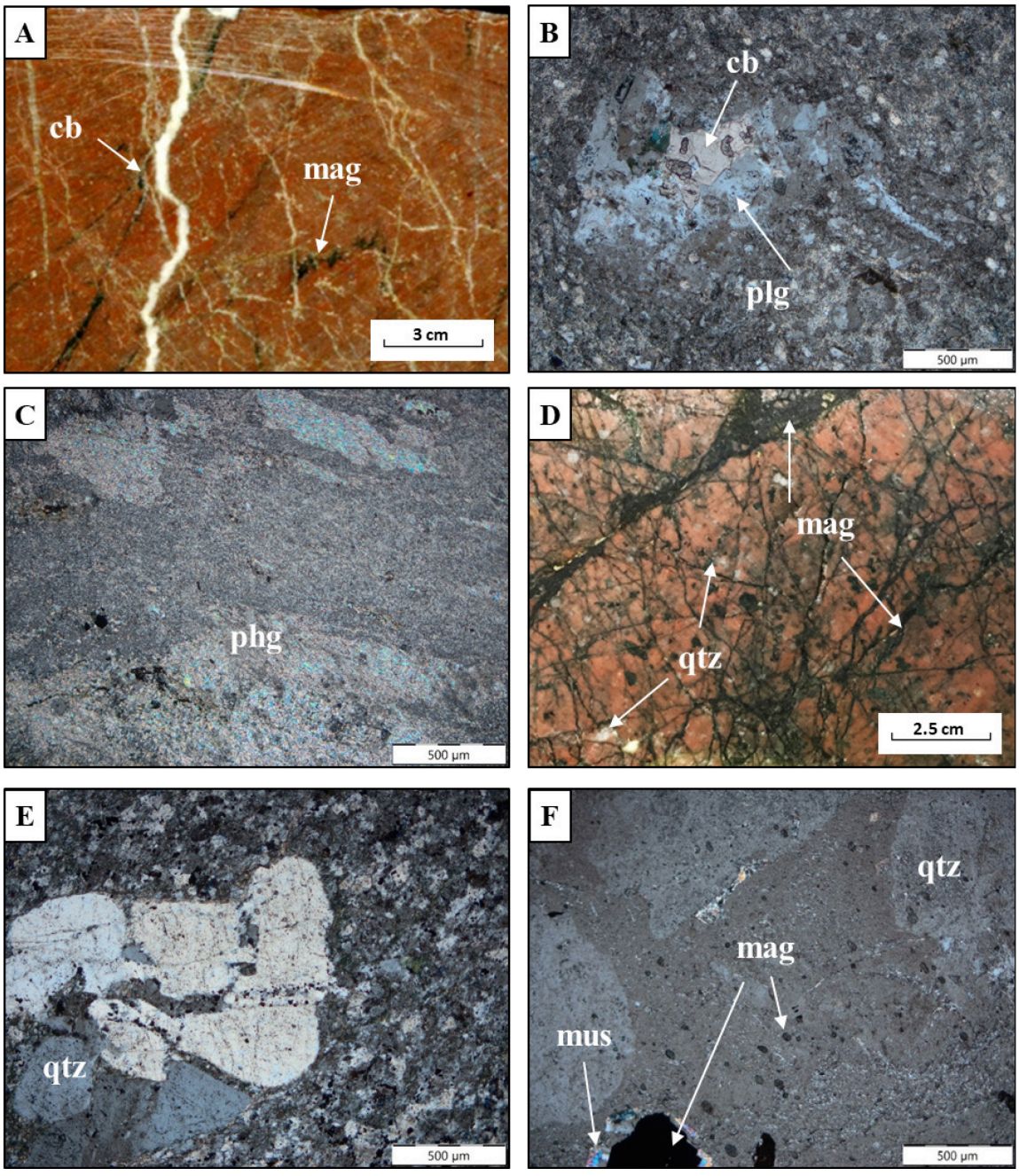

Figure 3.3. Representative photographs of dacite and rhyolite of the Central Volcanic Complex (CVC). **(A):** Hand specimen photograph of intensely K-feldspar altered CVC rocks. The primary texture has been completely destroyed due to intense K-feldspar alteration. **(B):** Cross-polarised photomicrograph of carbonate ± chlorite ± phengite-altered plagioclase phenocrysts in the dacite. Groundmass has also been invariably altered to phengite. **(C):** Cross-polarised of photomicrograph of intensely phengite-altered feldspar-phyric dacite, with no twining preserved. **(D):** Interval of K-feldspar – magnetite-altered quartz-phyric rhyolite. **(E):** Cross-polarised photomicrograph of quartz-phyric rhyolite with microcrystalline groundmass. Groundmass has been variably altered to chlorite. **(F):** Cross-polarised photomicrograph of quartz-phyric rhyolite with aphanitic groundmass. Magnetite grains are scattered throughout the groundmass. Abbreviations: cb = carbonate, mag = magnetite, mus = muscovite, phg = phengite, plg = plagioclase, qtz = quartz.

3.4.2 Rhyolite

Feldspar – quartz-phyric rhyolite crops out towards the west of the study area, representing another dominant volcanic host within the Prince Darwin prospect (Fig. 3.1). The quartz and feldspar phenocrysts and minor biotite, are set within a fine-grained K-feldspar-altered groundmass (Fig. 3.3D). The quartz and feldspar phenocrysts commonly make up to 15–20% of the rock. They can, however, comprise as little as 5% of the rock in some localities. Quartz is the dominant phenocryst with varying grain sizes (0.3 mm to 3 mm). Feldspar phenocrysts in places may be coarser than quartz phenocrysts but generally lower in abundance relative to quartz. In places, the feldspars are completely repalced by sericite; whereas, carlsbad twinning is preserved in some phenocrysts. The groundmass is typically quartz-rich with minor fine-grained chlorite – phengite – altered feldspar crystals, and has a microcrystalline to aphanitic texture (Fig. 3.3E to 3.3F). In some cases, quartz recrystallisation occurs within the groundmass. Foliation defined by alignment of sericite and chlorite ± biotite is common in deformed regions. Finely disseminated magnetite crystals are locally abundant (Fig. 3.3F). Chlorite and magnetite veins, locally stockwork, are common. Hydrothermal alteration in the rhyolite is not as intense as in the dacitic unit.

3.5 Quartz porphyry

Quartz porphyry does not outcrop in the field area, it is only present at the end of drill hole SDD005 in the west of the study area (Fig. 3.1). It has intruded the feldspar-phyric dacite with which it formed a sharp contact. It is characterised by quartz and chlorite-altered feldspar phenocrysts within fine-grained groundmass (Fig. 3.4A and 3.4B).

The groundmass is composed of fine-grained quartz and feldspar, with minor biotite and finely-disseminated magnetite, particularly near to the contact with the dacite. Flow banded textures are recognised near the intrusive contact. In thin section, the groundmass varies from unfoliated to moderately foliated, with increasing degree of foliation towards the intrusive margin. There is variation in size and proportion of quartz and feldspar phenocrysts from the interior of the porphyry towards the intrusive margin, likely due to different cooling rates. In the interior part of the porphyry, the quartz and feldspar phenocrysts make up to 45 to 50% of the total rock. The proportion between quartz and feldspar varies throughout the rock. Quartz is more abundant than feldspar in the interior of the porphyry (Fig. 3.4A); whereas, there are more feldspar towards the lower intrusive margin (Fig. 3.4B).

Compositionally, the quartz porphyry is composed of 40–50% quartz, 25–35% feldspar, and 5–10% chlorite and minor magnetite.

Quartz phenocrysts have euhedral to subrounded shapes (Fig. 3.4C). Quartz phenocrysts comprise up to 20% of the rock with variable sizes ranging from 0.25 mm to 7 mm. Different from the volcanic rocks and the Darwin granites, quartz crystals in the porphyry are characterised by the lack of undulose extinction in thin section, implying the lack of dynamic strain upon and after their emplacement (Fig. 3.4C). Feldspar have been intensely altered by different alteration assemblages at different depths (see Chapter 4). At the deepest part, feldspar phenocryst have been completely altered to carbonate – chlorite ± phengite assemblages (Fig. 3.4D). Weak to moderate carbonate replacement is locally abundant. The intense alteration makes the estimation of the proportion between plagioclase and K-feldspar difficult due to twinning destruction.

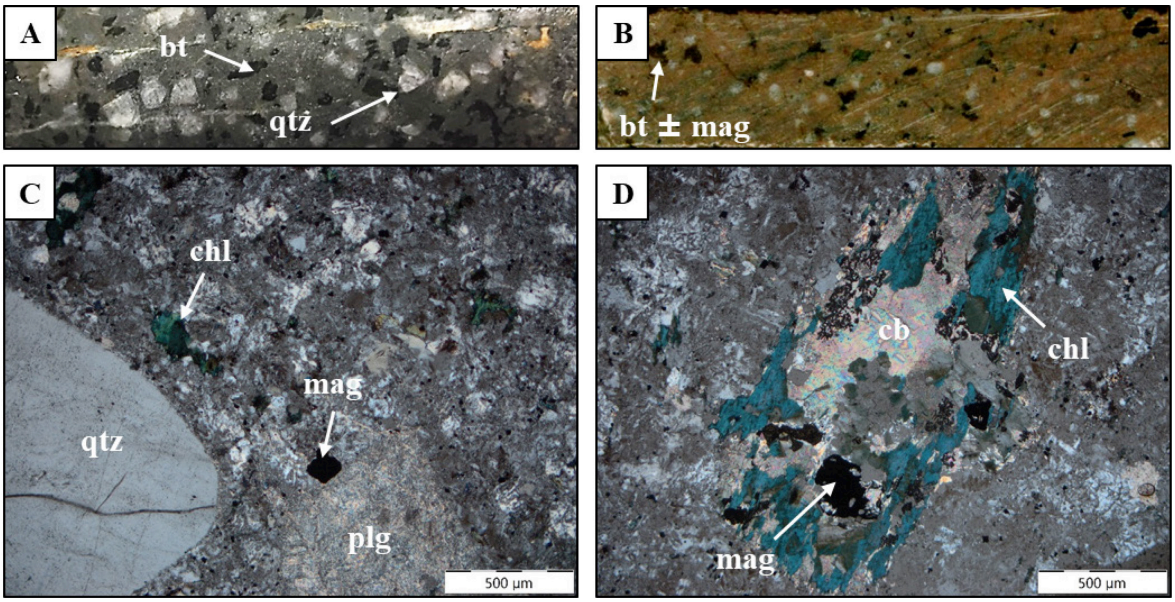

Figure 3.4: Representative photographs of quartz porphyry. **(A)** Hand specimen photography of the quartz porphyry from the interior part of the intrusion. Selective chlorite alteration of feldspar phenocrysts results in dark green speckles in the rock. (B): Core interval of K-feldspar ± magnetite-altered quartz porphyry. The finer grain size of the phenocrysts reflects faster cooling rate, relative to Fig. 3.4A. **(C):** Cross-polarised photo of quartz porphyry. Quartz remains unaltered, whereas plagioclase phenocryst and groundmass have been altered to secondary phengite and chlorite. **(D):** Cross-polarised phot of carbonate – chlorite ± magnetite-altered feldspar phenocryst in quartz porphyry. Abbreviations: bt = biotite, cb = carbonate, chl = chlorite, mag = magnetite, plg = plagioclase, qtz = quartz.

3.6 Local structures

The CVC outcrops provide some evidence of deformation in the area. Parasitic folds and crenulation (S-C fabric) have been observed in silicified CVC, implying there was likely

to have been more than one deformation event that affected the rocks (Fig. 3.5A). Chlorite alignment also occurs in the CVC. An NS-trending dextral strike-slip fault of unknown displacement has also been recognised, given by the development of extensional veins and deflected veins in outcrops of the CVC (Fig. 3.5B). Stepped and shear magnetite veins also provide evidence of multi-stage deformation (Fig. 3.5C and 3.5D).

Different vein types recognised in the field include magnetite – apatite, quartz, chlorite, tourmaline and specular hematite veins. Detailed descriptions of each vein type will be presented in Chapter 4. Table 3.1 summarises the orientations of these veins measured in the field. Biotite – allanite and carbonate veins have only been observed in drill core. No structural measurements have been taken in the drill core. Two dominant vein trends, NW-SE and NE-SW, have been widely recognised across the study area. Magnetite and boudin-neck fibre quartz veins are most common. Magnetite – apatite veins within the Darwin granite and CVC have similar orientations. The orientation of quartz veins is more varied than others. Chlorite veins are rare in the CVC in the field area and there is thus a lack of corresponding structural data.

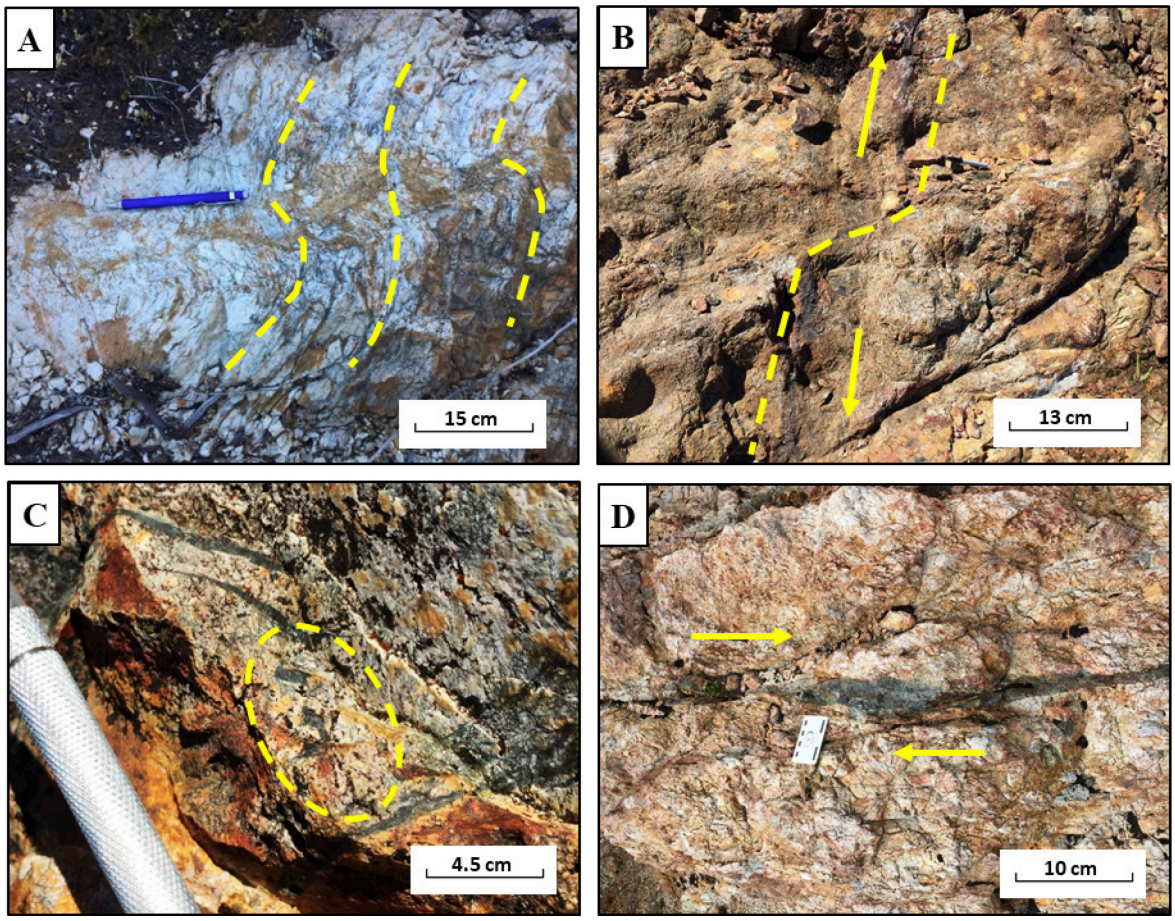

Figure 3.5: Field photographs of local structures at Prince Darwin. **(A):** Photographs of parasitic fold in silicified CVC. **(B):** Foliated magnetite vein in the CVC. **(C):** Stepped magnetite vein in the CVC. **(D):** N-S trending dextral strike-slip fault located in the CVC near to the intrusive contact with the Darwin granite.

Table 3.1: The general trends of each vein type recognised in the study area. Abbreviations: PG = Pink granite, WG = White granite; CVC = Cambrian Volcanic Complex, QP = quartz porphyry.

Veining	Occurrence	Darwin granite	CVC
Magnetite-apatite	PG, WG, CVC	NW, NE	NW, NE
Quartz	All	NW, NNE to E	NW, E
Tourmaline	PC, WG, CVC	NW	NW and NE
Chlorite	PG, CVC, QP	NW	?
Specular hematite	CVC	-	NW

3.7 Geochronology

Due to the interfingering relationship and overlapping nature of the volcanic rocks within the CVC, it has been a challenging to produce a detailed volcanic stratigraphy. However, there is good biostratigraphic constrains on the age of the Mt. Read Volcanic belt (mid to late Cambrian). Recent research by Mortensen et al. (2015) conducted more precise chronostratigraphic studies on the MRV and provide more comprehensive insights into the stratigraphic relationships between the volcanic sequences, intrusive rocks and base metal mineralisation in the MRV. The Darwin granite and quartz porphyry have been dated in this study (Table 3.2). The U–Pb zircon age dating results yielded ages of 497.3 ± 8.2 Ma for the Pink granite, 501.0 ± 4.8 Ma for the White granite and 492.4 ± 3.1 Ma for the quartz porphyry. The ages of the Pink granite and White granite overlap with uncertainty. The U–Pb age dating work in this study provides a better constraint on the age of Pink granite compared to the previously reported age of 510 Ma (+64, -21 Ma) by Adams et al. (1985). The considerable range of uncertainty in the age of Pink granite is mostly due to the complications of Pb loss and inheritance in the zircons. The quartz porphyry is the youngest intrusion at the Prince Darwin prospect.

3.8 Discussion

The Darwin granite compositions are interpreted using the QAP modal classification system of plutonic rocks developed by Streckeisen (1974; Figure 3.6). Results show that the Pink granite data plots within the syenogranite field; whereas, the White granite data plots within the granodiorite field. This interpretation is congruent with the previous interpretations from the studies by Jones (1993) and Wyman (2001). Quartz porphyry is classified as quartz-rich granitoids.

Table 3.2: Geochronology of the Darwin granite, quartz porphyry and CVC located towards the southern end of the MRV (Adams et al., 1985; Perkins and Walshe, 1993; Black et al., 1997; Turner et al., 1998; Mortensen et al., 2015).

Lithology	Dating Method	Material	Age (Ma)	Reference
Southern Central Volcanic Complex				
Concordant Age	U–Pb	Igneous zircons	502.6 ± 3.5	Perkins and Walshe (1993)
Mount Black Dacite	U–Pb	Igneous zircons	494.9 ± 4.3	Perkins and Walshe (1993)
Noddy Ck Volcanics	U-Pb	Igneous zircons	502.8 ± 8.8	Perkins and Walshe (1993)
Jukes Lava	U–Pb	Igneous zircons	503.6 ± 6.9	Black et al. (1997)
Jukes Road Lava	U–Pb	Igneous zircons	499.7 ± 4.4	Turner et al. (1998)
Mt. Jukes rhyodacite	U–Pb	Igneous zircons	503.3 ± 13.8	Mortensen et al. (2015)
Darwin granites				
Pink granite	U–Pb	Igneous zircons	510, +64, -21	Adams et al. (1985)
Pink granite	U–Pb	Igneous zircons	497.3 ± 8.2	This study
White granite	U–Pb	Igneous zircons	501.0 ± 4.8	This study
Quartz porphyry	U–Pb	Igneous zircons	492.4 ± 3.1	This study

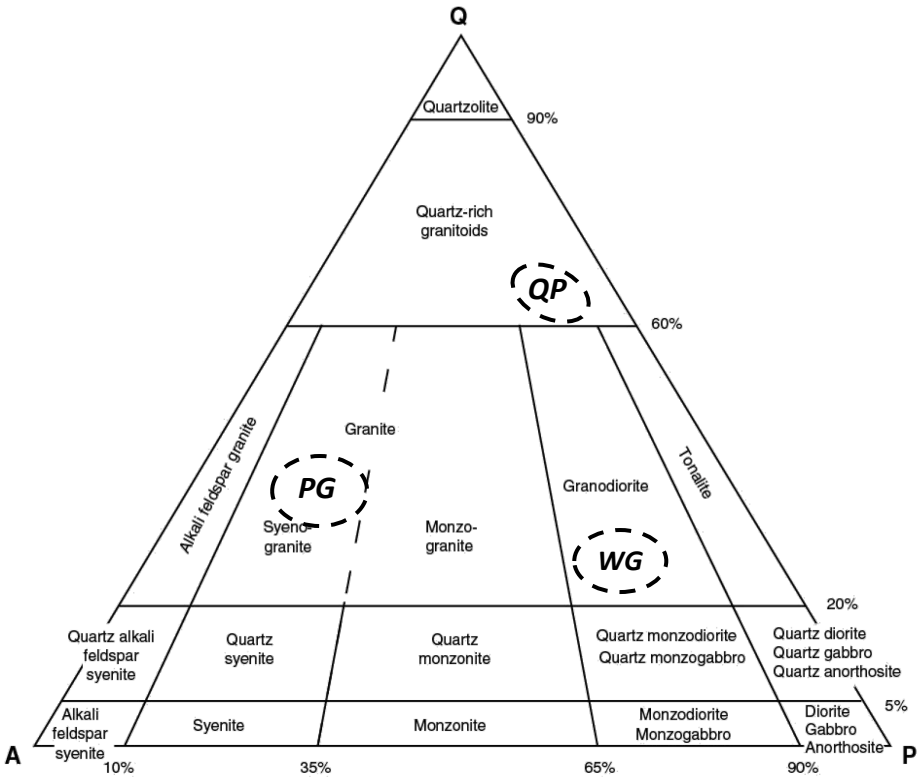

Figure 3.6: Lithotype interpretation of the Darwin granite and quartz porphyry using the QAP modal classification scheme of plutonic rocks (Streckeisen, 1974). Pink granite, White granite and quartz porphyry are classified as syno-granite, granodiorite and quartz-rich granitoid respectively. Abbreviations: PG = Pink granite, WG =White granite. QP = quartz porphyry.

Early geological mapping completed by Corona Minerals has reported that mineralisation at the Prince Darwin prospect is controlled by major NNE-striking regional faults, namely the Darwin Fault and other minor ENE-trending faults (Hughes, 2015). Jones (1993) have interpreted that the quartz veins in the South Darwin district are Devonian-aged. The trends of the veins observed in the field area are largely consistent with the previous interpretation made by Jones (1993), Wyman (2001) and Corona Minerals (2012). The orientations as recorded by the veins and fault trends in the Prince Darwin prospect are largely comparable to the Devonian Tabberabberan Orogeny (Stacey and Berry, 2004).

3.9 Summary

The Prince Darwin prospect is hosted within Cambrian-aged volcanics and intrusives, with the earliest deposition being volcanic rocks of the CVC, followed by the intrusion of the Darwin granites and quartz porphyry in the mid- to late-Cambrian. The Darwin granite is composed of two compositionally distinct phases: Pink granite (syeno-granite) and White granite (granodiorite). Field relationships provide strong evidence that the Pink granite was intruded by the White granite, although their U–Pb zircon ages are indistinguishable within uncertainty. Quartz porphyry is petrographically classified as quartz-rich granitoid and it is the youngest intrusive rock at Prince Darwin. The development of local structures in the Darwin prospect is related to the Tabberaberan Orogeny as recorded by the veins and fault trends observed in the field area.

Chapter 4

Hydrothermal Alteration and Mineralisation

4.1 Introduction

This chapter provides descriptions for the various hydrothermal alteration assemblages, veins, and copper-gold-iron-REE mineralisation events from the Prince Darwin prospect. A relative paragenesis of host rocks, alteration and mineralisation is included, as well as cross-sections illustrating the spatial distribution of select hydrothermal alteration domains in relation to the occurrence of mineralisation and geological structures.

4.2 Methods

Intense surface weathering has obscured the alteration patterns in the field area. Most of the alteration descriptions are based on observations made from drill core logging and thin section analysis, with the aid of Terraspec and HyLogger in identifying sericite and carbonate composition. Additional drill core assay data was provided by Corona Minerals. Cross sections were produced to illustrate the spatial distribution of different alteration stages. A table of relative paragenetic relationships has been constructed based on overprinting and crosscutting relationships observed during core logging and petrographic studies (Table 4.1).

4.3 Previous studies

There are several studies on alteration and mineralisation features from the South Darwin region (e.g., Jones, 1993; Wyman, 2001; Hughes, 2015). Jones (1993) reported the presence of several veins, including quartz, tourmaline and barite veins, in the Darwin granite and CVC, and interpreted their relative time of formation based on their stratigraphic relationships with the Tyndall Group and Owen Conglomerate, which overly the Darwin granite and CVC. Wyman (2001) provided more detailed descriptions of the hydrothermal alteration and mineralisation found in the South Darwin-Mt Darwin region. He documented

an inner zone of intense K-feldspar alteration associated with copper mineralisation that zones outwards to a chlorite – sericite domain. Wyman (2001) reported that mineralisation style changes with distance from the Darwin granite, from an inner zone of iron-oxide veins and stockworks that contain pyrite and chalcopyrite ± specular-hematite ± tourmaline, through to quartz – pyrite – chalcopyrite veins and pyrite – chalcopyrite ± covellite disseminations, to quartz ± bornite ± neodigenite ± chalcopyrite ± hematite veins. Wyman (2001) further postulated that the Jukes prospect and Mt. Darwin region represent different parts of the same hydrothermal system. A recent study by Hughes (2015) provides more comprehensive descriptions on paragenetic relationships at the Prince Darwin prospect.

4.4 Alteration and mineralisation

Albite ± chlorite alteration (Stage PD-M1)

Stage PD-M1 is potentially related to diagenesis of the MRV during Cambrian-Devonian deformation as described by Gifkins et al. (2005). This stage has only been observed within the volcanic rocks in drill core, giving the rocks a distinctive white to grey appearance (Fig. 4.1). This alteration is typically overprinted by all other alteration and vein phases, suggesting that Stage PD-M1 is the earliest formed alteration stage at Price Darwin.

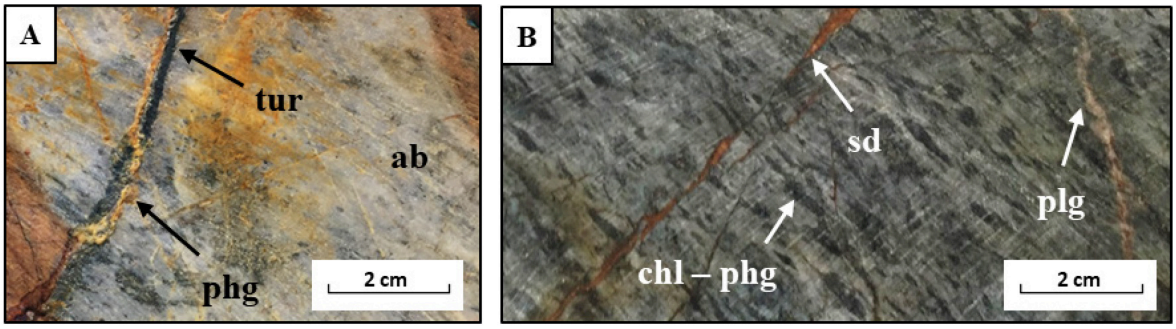

Figure 4.1: Examples of albite ± chlorite alteration (Stage PD-M1). **(A):** Photo of albite-altered volcanic rocks crosscut by early-stage tourmaline veins (Stage PD-2A) and phengite veins (Stage PD-5). **(B):** Hand specimen photograph of intensely albite-altered dacite that has been crosscut by a pink plagioclase vein (PD-9) and siderite vein (PD-11B). Abbreviations: ab = albite, chl = chlorite, phg = phengite, plg = plagioclase, sd = siderite, tur = tourmaline.

Phengite ± phengitic illite ± chlorite alteration (Stage PD-M2)

Stage PD-M2 is characterised by pervasive, moderate to intense phengite alteration, which results in prominent pale green domains within the Pink granite. This alteration was only recognised towards the south of Prince Darwin. Where present, chlorite occurs as fine disseminations. Fine- to medium-grained quartz crystals are apparent and randomly

distributed within this alteration domain. Where crosscutting relationships are observed, this alteration has been crosscut by quartz veins (Stage PD-7B; Fig. 4.2A) and tourmaline veins (Stage PD-2A; Fig. 4.2B). This crosscutting relationship suggests that Stage PD-M2 predates the hydrothermal alteration associated with the Darwin granite.

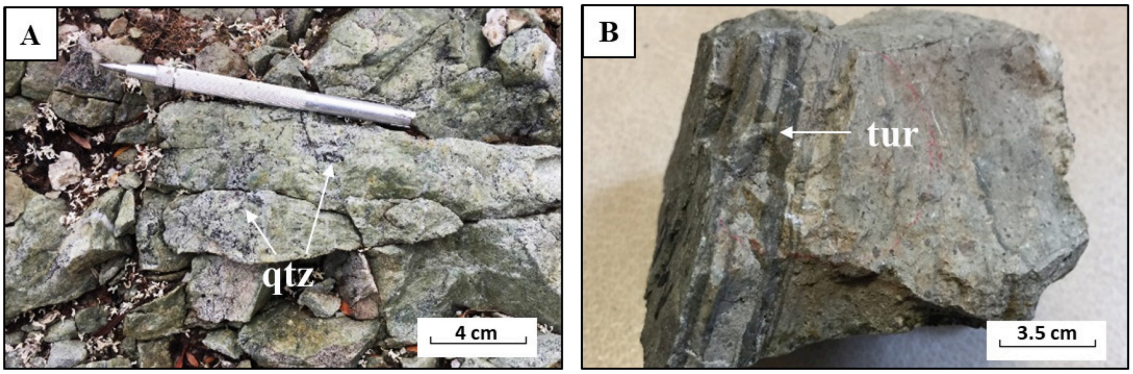

Figure 4.2: Examples of phengite ± phengitic illite ± chlorite alteration (Stage PD-M2). **(A):** Pale green phengite – chlorite-altered surface outcrop crosscut by quartz veins (Stage PD-7B). **(B):** Rock chip sample of intensely phengite – chlorite-altered Pink granite that has been crosscut by tourmaline veins (Stage PD-2A). Abbreviations: qtz = quartz, tur = tourmaline.

K-feldspar – magnetite – tourmaline ± hematite alteration (Stage PD-1)

Stage PD-1 occurs as breccia cement, domainal replacements and as disseminations. This stage is the most widespread alteration style at Prince Darwin and occurs within all geological units. Pervasive and intense alteration imparts a distinctive pink colouration and mottled texture to the Pink granite (Fig. 4.3A). In the volcanic rocks and quartz porphyry, the groundmass has been altered to K-feldspar and are typically hematite-stained. This results in a diagnostic red colouration (Fig. 4). Magnetite and tourmaline typically occur as cement in the volcanic breccias (Fig. 4.3C) and as disseminations within intrusions.

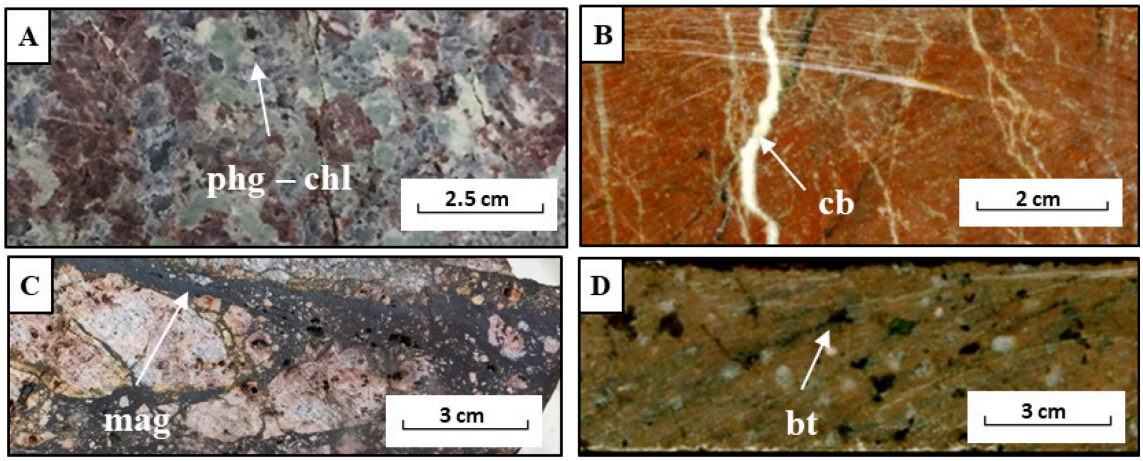

Figure 4.3: Examples of K-feldspar – magnetite – tourmaline alteration (Stage PD-1). **(A):** K-feldspar – phengite – chlorite-altered Pink granite with mottled texture. **(B):** Interval of intensely K-feldspar-altered dacite crosscut by late-stage carbonate vein (Stage PD-12B). **(C)**: Hand specimen photograph of magnetite-cemented K-feldspar-altered volcanic breccia. **(D):** Hand specimen photograph of quartz porphyry with intensely K-feldspar-altered groundmass. Abbreviations: bt = biotite, cb = carbonate, chl = chlorite, mag = magnetite, phg = phengite.

Magnetite – quartz ± tourmaline ± K-feldspar ± chlorite ± hematite veins (Stage PD-1A)

Magnetite veins and stockworks are abundant within the Pink granite and CVC but are typically absent in the White granite and quartz porphyry (Fig. 4.4). Absence of magnetite veins in the Tyndall Group and the Owen Conglomerate has been reported by Jones (1993), suggesting that the deposition of these two units occurred after the magnetite alteration. In the Pink granite, magnetite veins are commonly discontinuous (Fig. 5.4A). Magnetite veins in the CVC are typically wider and longer than in the Pink granite. (Fig. 4.4B and 4.4C) The veins can be up to 0.5 m wide and over 5 m long. Some PD-1A veins in dacite are enveloped by pinkish to reddish feldspar halos with a thickness ranging from 7 to 15 mm (Fig. 4.4C and D). In some places, magnetite veins have been partly replaced by hematite due to oxidation. Crenulated, sheeted and stepped magnetite veins are common and are suggestive of deformation after vein formation (Fig. 4.4E; Chapter 3).

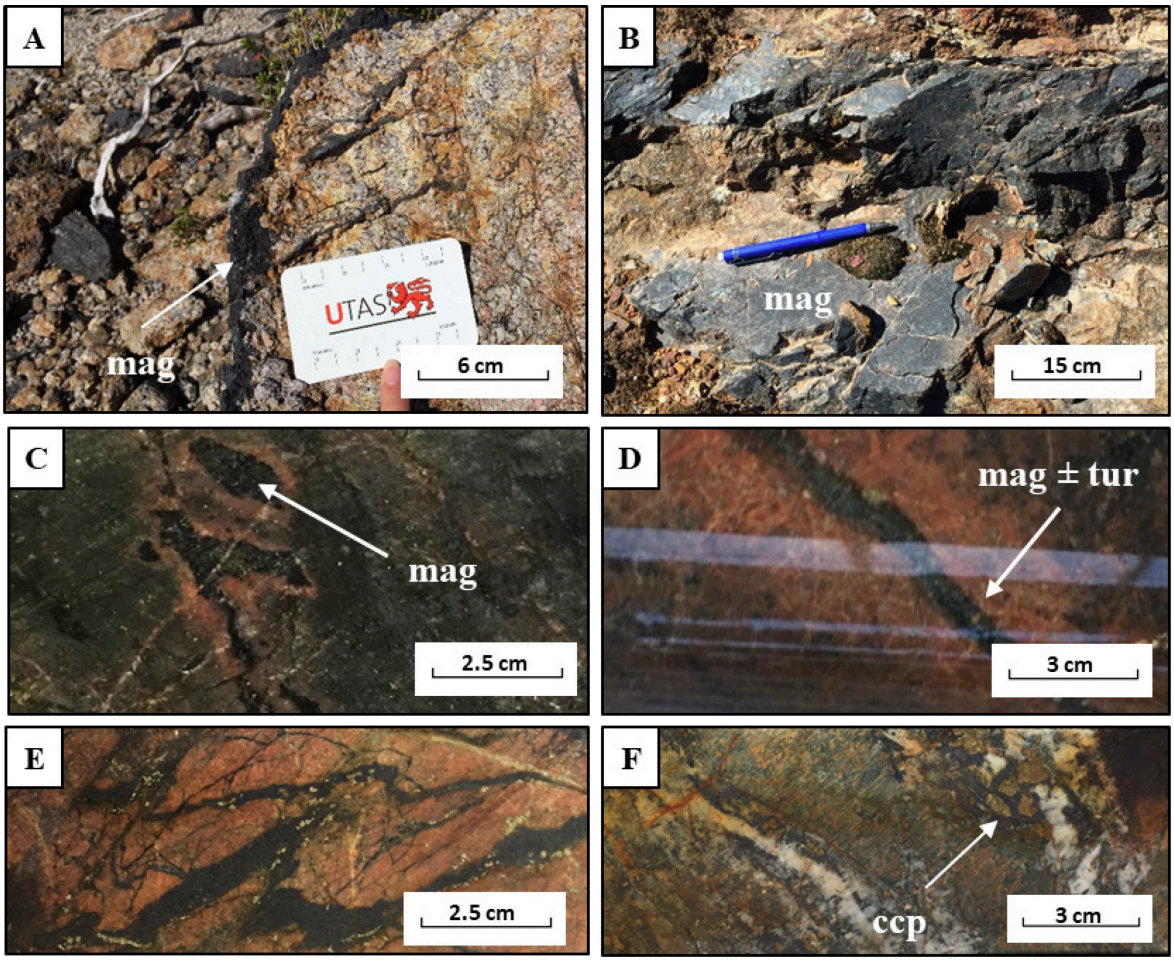

Figure 4.4: Examples of magnetite – quartz ± tourmaline ± K-feldspar ± chlorite ± hematite veins (Stage PD-1A). **(A):** Magnetite stockwork observed within the Pink granite. **(B):** Field photograph of a thick magnetite vein in volcanic rock. **(C):** Thin feldspar halo enveloping around magnetite in the dacite. **(D):** Magnetite ± tourmaline vein with pinkish feldspar selvage in dacite. **(E):** Wispy magnetite vein with pyrite ± chalcopyrite dissemination in intensely K-feldspar – magnetite-altered dacite (Stage PD-1). **(F):** Core interval of pyritic magnetite – quartz vein in albite-altered dacite. Abbreviations: ccp = chalcopyrite, mag = magnetite, tur = tourmaline.

PD-1A veins are associated with Cu-Au mineralisation in the volcanic rocks but not in any of the documented intrusions at Prince Darwin. Ore minerals (chalcopyrite ± bornite) occur as disseminations or clots within the magnetite veins (Fig. 4.4E and 4.4F).

Specularite ± quartz ± magnetite veins (Stage PD-1B)

PD-1B veins are exclusive to the intensely silicified and K-feldspar-altered CVC rocks near the intrusive contact with the Pink granite (Fig. 4.5A). Specularite veins trend in a NW-direction and typically dip at a low angle. These veins are commonly thin (mostly <3 cm-wide) and discontinuous. Quartz and magnetite may occur as minor phases (Fig. 4.5B). Specularite and quartz within the veins display bladed or comb texture (Fig. 4.5A). Due to its sparse occurrence at Prince Darwin, no crosscutting relationships with other stages have been observed. Stage PD-1B is classified as an early-stage vein because of the magnetite association.

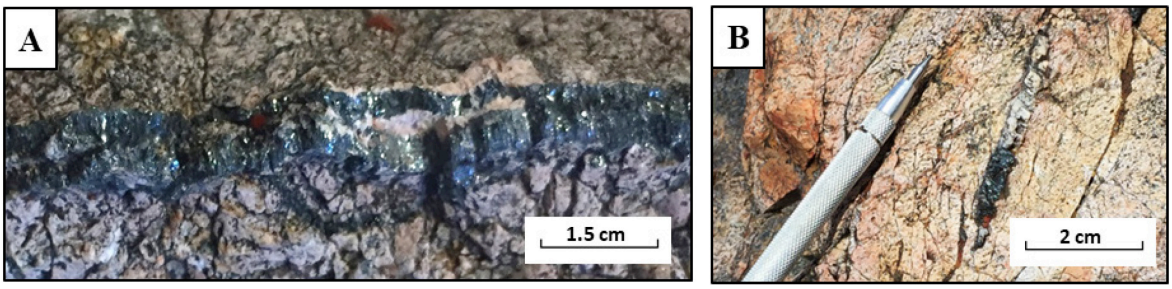

Figure 4.5: Examples of specularite ± quartz ± magnetite ± pyrite ± chalcopyrite veins (Stage PD-1B)**. (A)** Hand specimen photograph of a specular hematite vein within intensely silicified and K-feldspar-altered volcanic rock. **(B)** Field photograph of the discontinuous hematite – quartz ± magnetite vein in the K-feldspar-altered volcanic rock.

Tourmaline ± magnetite ± chlorite ± pyrite veins (Stage PD-2A)

Tourmaline veins occur in volcanic rocks and Darwin granite at Prince Darwin. Stage PD-2A is more common in the volcanic rocks and the Pink granite relative to the White granite. Tourmaline veins in the Darwin granites are generally discontinuous and thinner, varying from 0.5 cm to 1.5 cm wide (Fig. 4.6A). Tourmaline veins in the CVC are generally 0.5 cm to 10 cm wide and can be followed along strike up to 4 m (Fig. 4.6B). In the CVC, tourmaline veins and magnetite veins crosscut each other, implying that they have a close timing relationship. Tourmaline veins have also been crosscut by chlorite veins (Stage PD-9).

Tourmaline-cemented breccia (Stage PD-2B)

Tourmaline breccias are confined within the CVC, with the largest breccia crosscutting the strongly silicified volcanic rocks within 150 m from the contact with the Pink granite (Fig. 4.6C). Tourmaline breccias in the CVC typically contain a crackle to mosaic organisation of fragments derived from the host rocks. The clast size varies from 0.3 cm to 2.5 cm in diameter. The tabular and angular character of the breccias implies that they are related to hydrothermal brecciation (Fig. 4.6C; Rio Blanco, Chile: Frikken, 2003; Copper Creek, U.S.: Eichenlaub, 2007). No preferential orientations have been observed in the breccias and tourmaline cement, suggesting that they have a hydrothermal origin rather than tectonic, which would otherwise preserve some evidence of deformation such as clast alignment within the cement. No tourmaline veins have been recognised in the Tyndall Group and Owen Conglomerate (Jones, 1993). This stratigraphic relationship may provide evidence that tourmaline veins formed during or right after the emplacement of the Darwin granite and before the deposition of Tyndall Group and Owen Conglomerate.

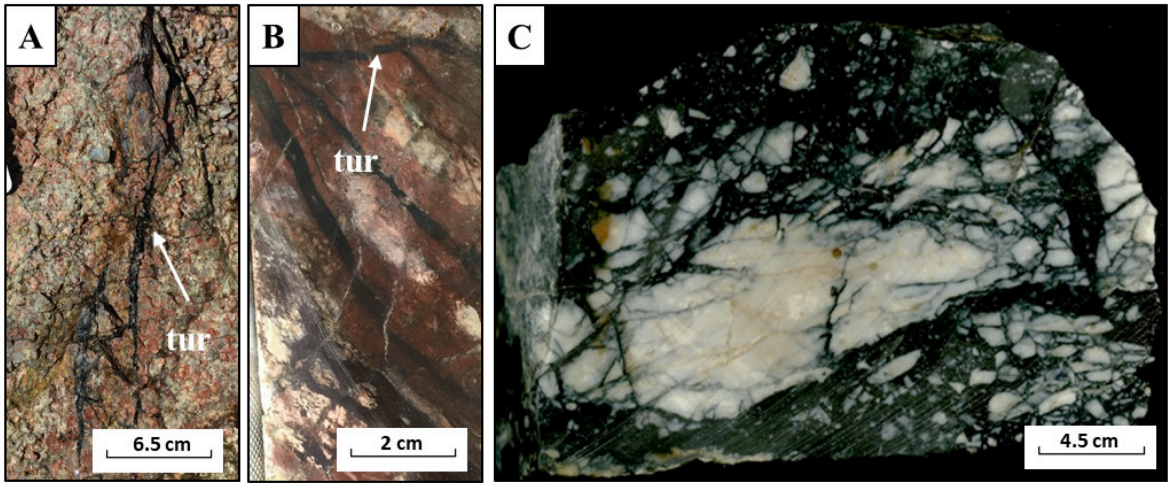

Figure 4.6: Examples of tourmaline ± magnetite ± chlorite ± pyrite veins (Stage PD-2A) and tourmaline-cemented breccias (Stage PD-2B). **(A):** Field photograph of tourmaline veins in the Pink granite. **(B):** Drill core interval of intensely K-feldspar-altered (Stage PD-1) dacite that has been crosscut by tourmaline veins. **(C):** Hand specimen photo of tourmaline-cemented, tabular to angular silicified breccia (Stage PD-2B). Abbreviations: tur = tourmaline.

Magnetite – apatite ± chlorite ± pyrite ± chalcopyrite ± bornite replacement (Stage PD-3)

Intense to moderate massive magnetite replacement occurs at the contact between the rhyolite and dacite units, which may be skarn (A. Crawford, pers. comm., 2018). Apatite is locally abundant and occurs as white amorphous crystals, which make it distinguishable from quartz (Fig. 4.7A). Pyrite and chalcopyrite are typically associated with this assemblage (Fig. 4.7B).

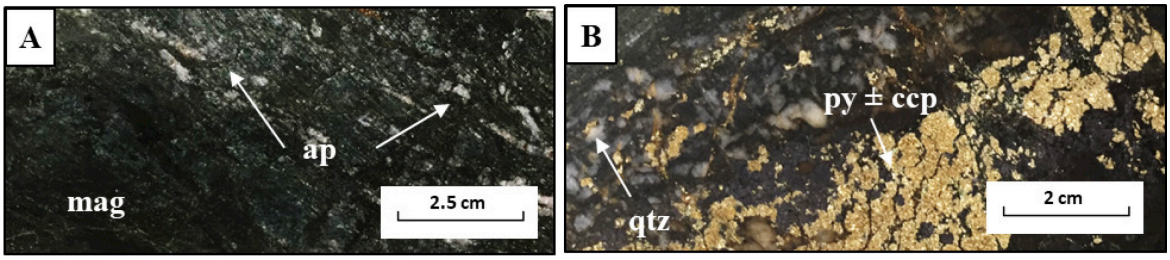

Figure 4.7: Examples of magnetite – apatite ± chlorite ± pyrite ± chalcopyrite ± bornite replacement (Stage PD-3). **(A):** Representative hand specimen photograph of magnetite – apatite-altered volcanic rocks. The white amorphous crystals are apatite. **(B):** Interval of magnetite – apatite-altered volcanic rocks with a pyrite ± chalcopyrite clot. Quartz fragments, probably from the precursor lithotype, may be locally abundant. Abbreviations: ap = apatite, ccp = chalcopyrite, mag = magnetite, py = pyrite, qtz = quartz.

Allanite – biotite ± fluorapatite ± monazite ± carbonate ± chlorite alteration (Stage PD-4)

Stage PD-4 is the main host of REEs at Prince Darwin. Occurrence of stage PD-4 is typically restricted to CVC dacite. Allanite has a characteristic dark brown to black colour (Fig. 4.8A). Biotite with disseminated apatite, fluorapatite and carbonate are commonly associated with the occurrence of allanite (Fig. 4.8B and 4.8C). Allanite crystals typically have subrounded to blocky crystal shapes. Biotite has been incipiently chloritised or are unaltered, which contrasts with the complete chloritisation of most biotite grains present in the CVC host rocks and the Pink granite.

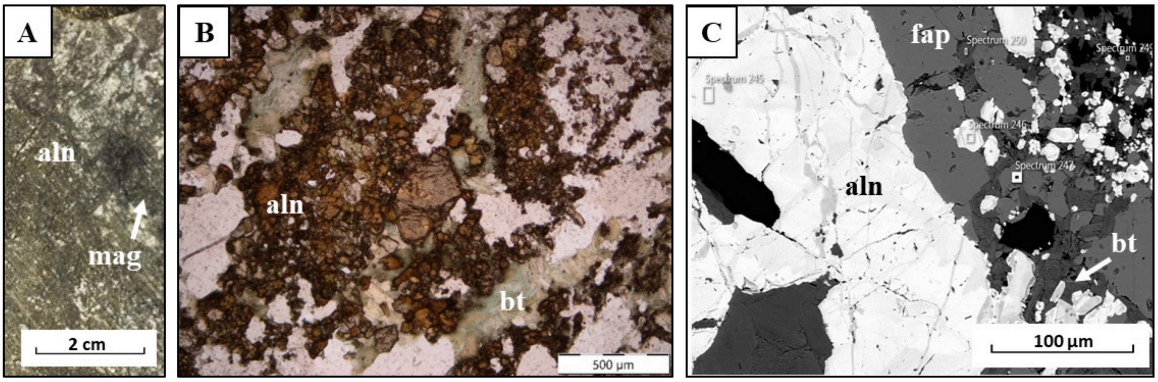

Figure 4.8: Examples of allanite – biotite ± fluorapatite ± monazite ± carbonate ± chlorite alteration (Stage PD-4). **(A):** Hand specimen photograph of allanite-bearing dacite. **(B):** Plane-polarised photomicrograph of allanite – biotite assemblages in dacite. **(C):** SEM image illustrating common association of allanite with biotite and fluorapatite. Abbreviations: aln = allanite, bt = biotite, fap = fluorapatite, mag = magnetite.

Phengite ± illite ± muscovite ± chlorite alteration (Stage PD-5)

There is multi-stage sericite alteration at Prince Darwin. Stage PD-5 has been repeatedly re-introduced with each successive intrusive phase. It may be weak to strong in intensity, selective to pervasive, diffusive to disseminated in style. Spectral data shows that the secondary sericites are predominantly phengitic in composition. Phengite ± chlorite has

selectively feldspar phenocryst in each rock type. This alteration is most intense within the CVC rocks, where most of the feldspar phenocrysts have been completely replaced by fine-grained phengite aggregates with complete textural destruction (Fig. 4.9A). Secondary muscovite and illite are present but rare. Feldspar phenocrysts in the Darwin granite are relatively less phengite-altered compared to those in the volcanic rocks (Fig. 4.9C). Primary muscovite in the Darwin granite, if present, have been partly altered to phengite (Fig. 4.9D). Intense and pervasive phengite alteration in the Pink granite and White granite results in pale green and creamy white appearance respectively.

Phengite ± illite veins (Stage PD-5A)

Stage PD-5A is characterised by straight-walled, continuous to discontinuous, phengite ± illite veins (Fig. 4.9E). Phengite ± illite veins typically have a reddish-purplish and flaky appearance. The distinct colour may be due to weathering. PD-5A veins are not common but can be locally abundant. The occurrence of these veins has only been recognised within the CVC dacite. Magnetite – pyrite veins (stage PD-1A) are crosscut by PD-5A veins (Fig. 4.9E).

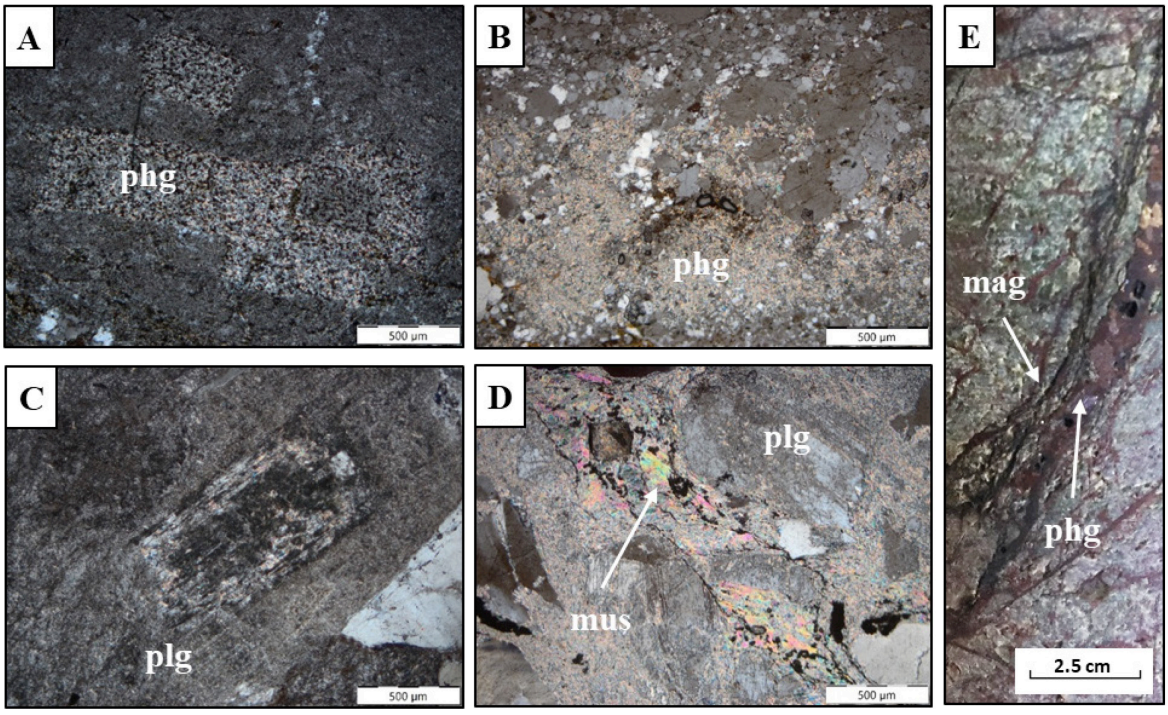

Figure 4.9: Examples of multi-stage phengite ± illite ± muscovite ± chlorite alteration (Stage PD-5) and phengite ± illite veins (Stage PD-5A). **(A):** Cross-polarised photomicrograph of complete replacement of feldspar phenocryst by phengite in the dacite. **(B):** Cross-polarised photomicrograph showing the phengite-altered groundmass in the rhyolite. **(C):** Cross-polarised photomicrograph of partially phengite-altered plagioclase phenocrysts in the Pink granite. Relict multiple twinning is still discerned in the plagioclase phenocryst. Groundmass has also invariably been phengite-altered. **(D):** Cross-polarised photomicrograph of phengite alteration after primary muscovite and feldspar in the Pink granite. **(E):** Hand specimen photograph of phengite – illite vein (Stage PD-5A) that crosscuts the early magnetite vein (Stage PD-1A). Abbreviations: chl = chlorite, mag = magnetite, mus = muscovite, phg = phengite; plg = plagioclase.

Epidote ± quartz ± biotite ± chlorite ± plagioclase ± allanite veins (Stage PD-6)

Epidote veins have only been recognised in the Pink granite, with only two occurrences observed in the central area of the Darwin Plateau. Epidote veins have a characteristic pistachio green appearance (Fig. 4.10A). In thin section, epidotes are lath-shaped and are aligned. Subordinate fine-grained quartz and feldspar crystals are present in the epidote vein (Fig. 4.10B).

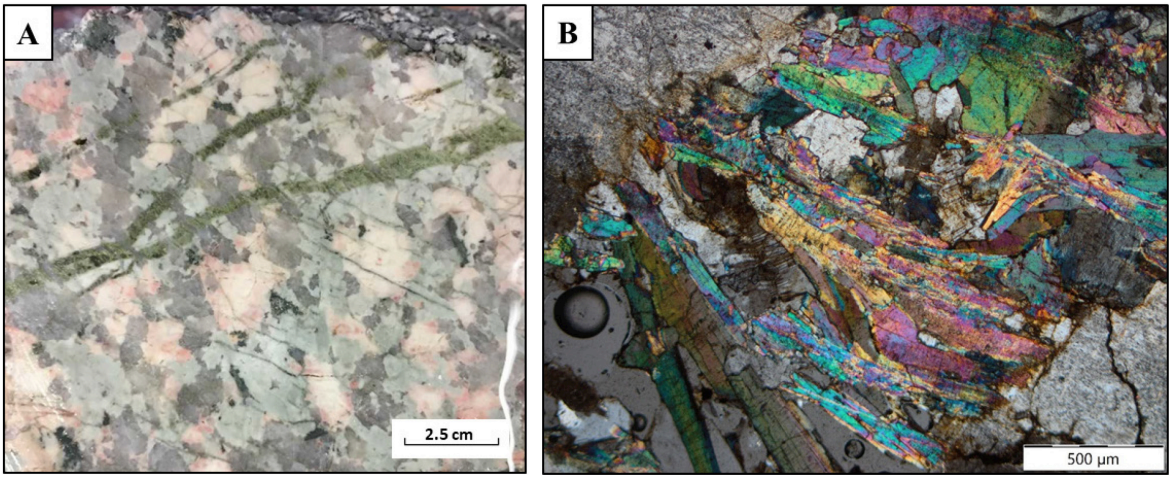

Figure 4.10: Examples of epidote veins (Stage PD-6). **(A):** Hand specimen photomicrograph of epidote veins in the Pink granite. **(B):** Cross-polarised photomicrograph of epidote vein in the Pink granite.

Quartz ± chlorite ± phengite ± carbonate veins (Stage PD-7A)

Quartz ± chlorite ± phengite ± carbonate veins are the most abundant vein type at Prince Darwin. Stage PD-7A occurs in all geological units in the study area and are texturally and mineralogically diverse. PD-7A veins typically have a boudin-neck fibrous texture (Fig. 4.11A and B), although massive texture (Fig. 4.11C) has been observed in CVC dacite but are generally less common. Boudin-neck fibrous quartz veins have characteristically bladed quartz crystals as a consequence of later vein re-opening. The remaining open space between quartz crystals infilled with later chlorite ± phengite (Stage PD-8) and carbonate (Stage PD-11B) assemblages. Median lines running through the quartz veins were observed locally (Fig. 4.11B). In the field area, open space filling minerals have been eroded away. Boudin-neck quartz veins are generally thinner in the Darwin granite. PD-7A vein in the White granite is characterised by quartz ± sericite assemblages and lack of chlorite. Stage PD-7A in the volcanic rocks are the main host of disseminated bornite – chalcopyrite. No sulfide minerals have been found in this vein type within the Darwin granite and quartz porphyry.

Massive and barren quartz veins (Stage PD-7B)

Stage PD-7B is another common quartz vein phase in volcanic rocks (Fig. 4.11E). No occurrence has yet been recognised within the Darwin granite and quartz porphyry. Vein width varies from 1 to 15 cm. Some quartz veins are sheared or foliated, implying deformation after their formation. Variation in grain size of quartz crystals can be observed within individual quartz veins. In places, quartz recrystallisation results in irregular distribution of fine-grained aggregates in the vein. PD-8B is generally barren of sulfide.

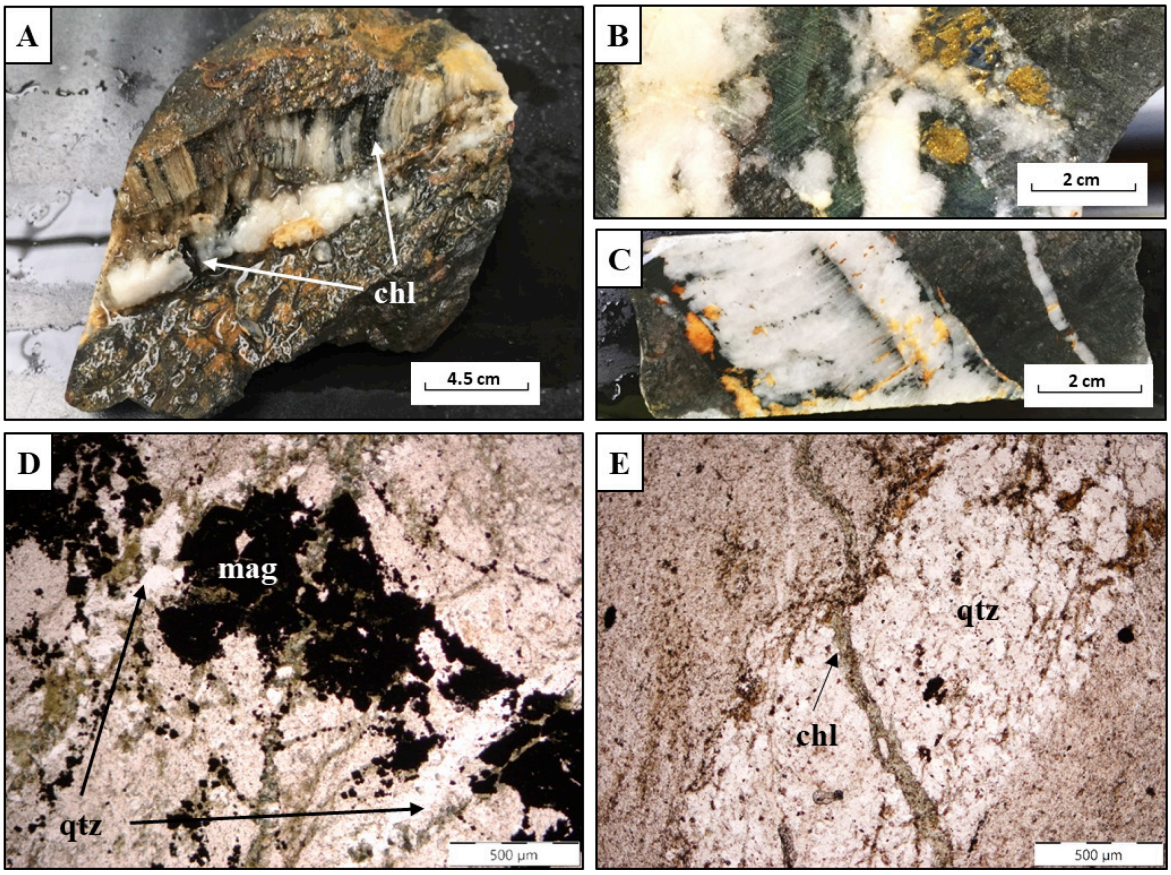

Figure 4.11: Examples of different types of quartz veins (Stage PD-7A and PD-7B) at Prince Darwin. **(A):** Hand specimen photograph of boudin-neck quartz – chlorite vein in dacite. **(B):** Drill core photograph of mineralised massive quartz – chlorite vein (Stage PD-7A) in dacite**. (C):** Drill core interval of a thick boudin-neck fibrous quartz – chlorite ± phengite vein (Stage PD-7A), with a median line running through the vein. **(D):** Plane-polarised photomicrograph of dacite that has been crosscut by an early-stage magnetite vein (Stage PD-1A), followed by quartz – chlorite veins (Stage PD-8A) and chlorite veins (Stage PD-8). **(E):** Plane-polarised photomicrograph of a barren quartz vein crosscut by chlorite ± phengite vein (Stage PD-8) crosscut by a chlorite veinlet. Abbreviations: chl = chlorite, mag = magnetite, qtz = quartz.

Chlorite – magnetite ± tourmaline alteration (Stage PD-8)

Stage PD-8 consists of widespread, weak to intense selective replacement and breccia infill cement. Chlorite – magnetite selectively replaced ferromagnesian minerals, primarily biotite and plagioclase phenocrysts in the Pink granite (Fig. 4.12A) and the

volcanic rocks (Fig. 4.14B). Lenticular chlorite clots have been observed in places (Fig. 4.12B). Stage PD-8 also occurs as cement within the CVC rocks (Fig. 4.12D). Fine-grained magnetite and tourmaline are commonly present within the chlorite cement. Weak chlorite alteration imparts a dusting texture in plagioclase within the groundmass of the volcanic rocks.

Chlorite ± phengite veins (Stage PD-8A)

Vein PD-8A is restricted in the Pink granite and the CVC but absent in the White granite and quartz porphyry. Vein PD-8A occurs as straight-walled and continuous veins (Fig. 4.12E). PD-8A veins are locally stockwork to sheeted in the Pink granite. In the CVC rocks, chlorite veinlets are more common. Chlorite veins in the volcanic rocks are relatively thinner, locally stockwork textured, continuous to discontinuous and straight-walled to branching. Chlorite veins appear to have crosscut early-formed magnetite (Stage PD-1A; Fig. 4.12F), tourmaline (Stage PD-2A) and quartz veins (Stage PD-7A and 5B; Fig. 4.14E).

Pervasive chlorite ± phengite ± pyrite ± magnetite replacement (Stage PD-8B)

This stage is texturally similar to Stage PD-M2 but is dominated by chlorite and its occurrence is typically restricted within the volcanic rocks outboard of the Darwin intrusions, generally within 200 m from their contacts. Pervasive, intense to moderate chlorite ± sericite ± pyrite ± magnetite alteration results in conspicuous massive dark green patches within silicified and K-feldspar-altered dacitic rocks (Fig. 4.12). Pyrite are finely disseminated to absent in this alteration. There are no clear crosscutting relationships with any other alteration stage. The occurrence of pyrite has resulted in their classification as part of syn-mineralisation alteration.

Plagioclase ± quartz veins (Stage PD-9)

Plagioclase ± quartz veins are relatively rare but are locally concentrated. Plagioclase veins have only been observed within the dacite (Fig. 4.13A and C) and White granite (Fig. 4.13B). They are commonly discontinuous and branching, and can be sheeted in dacite. In the Pink granite, PD-1D veins occur as striaght-walled veins with coarser plagioclse crystals than those in the CVC (Fig. 4.13B). Pyrite may be present but are mostly rare to absent. Stage PD-9 has crosscut phengite – chlorite alteration (Stage PD-8; Fig. 4.13C).

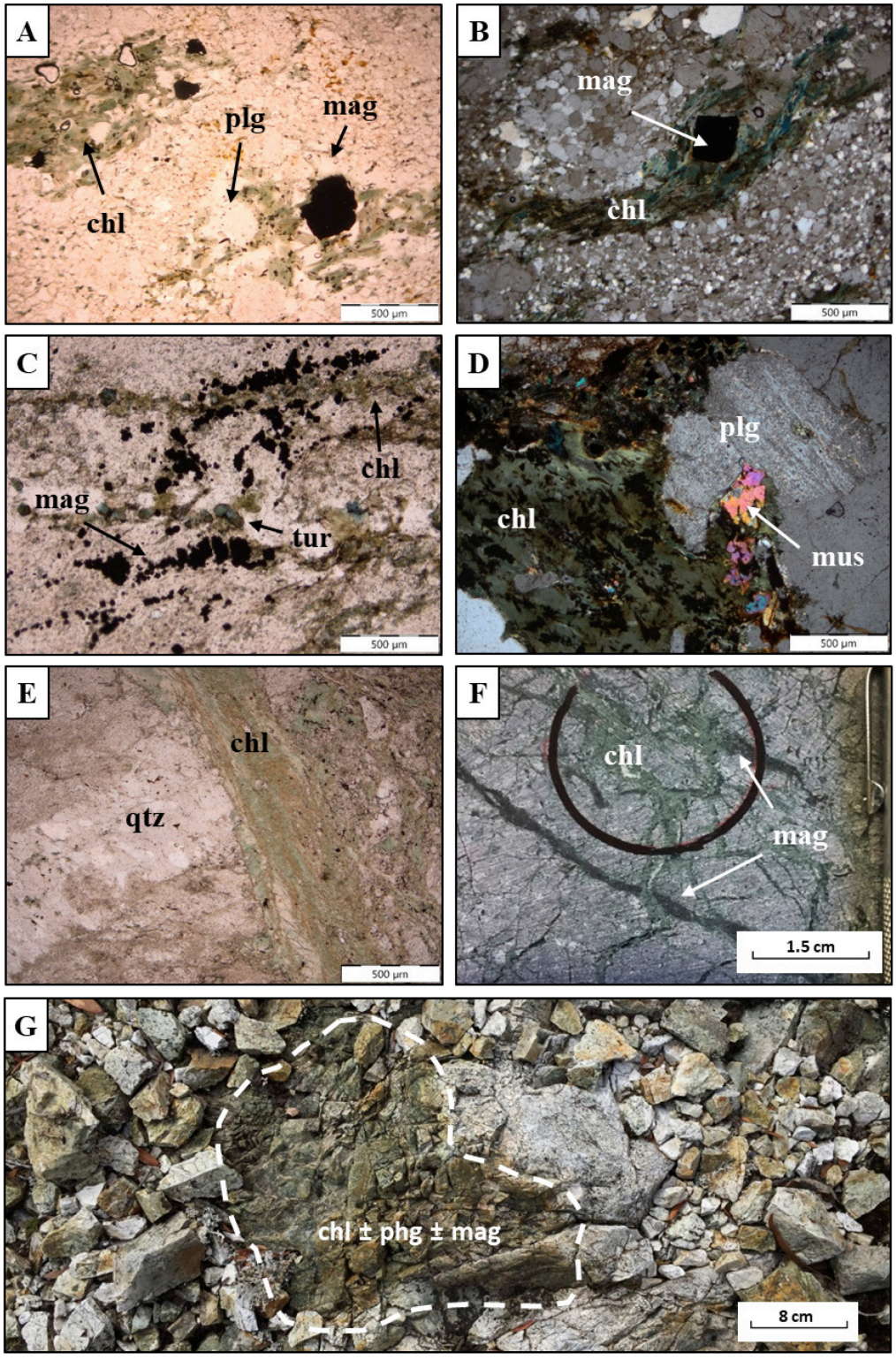

Figure 4.12: Examples of chlorite – magnetite ± tourmaline alteration (Stage PD-8), chlorite ± phengite veins (Stage PD-8A) and pervasive chlorite ± phengite ± pyrite ± magnetite replacement (Stage PD-8B). **(A):** Plane-polarised photomicrograph illustrating partial chlorite – magnetite replacement after feldspar phenocrysts in dacite. **(B):** Cross-polarised photomicrograph showing sigmoidal chlorite – magnetite clot in dacite. **(C):** Cross-polarised photomicrograph illustrating the chlorite – magnetite alteration after the primary biotite in the Pink granite**. (D)** Plane-polarised photomicrograph of chlorite – magnetite ± tourmaline-cemented dacite. **(E):** Plane-polarised photomicrograph of straight-walled chlorite vein that crosscut early barren quartz vein (stage PD-7B). **(F):** Hand specimen photo of magnetite vein (stage PD-1A) crosscut by chlorite stockwork (Stage PD-8A) in rhyolite. **(G)**: Field photo of pervasive chlorite ± phengite ± pyrite ± magnetite replacement (Stage PD-8B) in intensely silicified CVC surface outcrop. Abbreviations: chl = chlorite, mag = magnetite, mus = muscovite, phg = phengite, plg = plagioclase, qtz = quartz, tur = tourmaline.

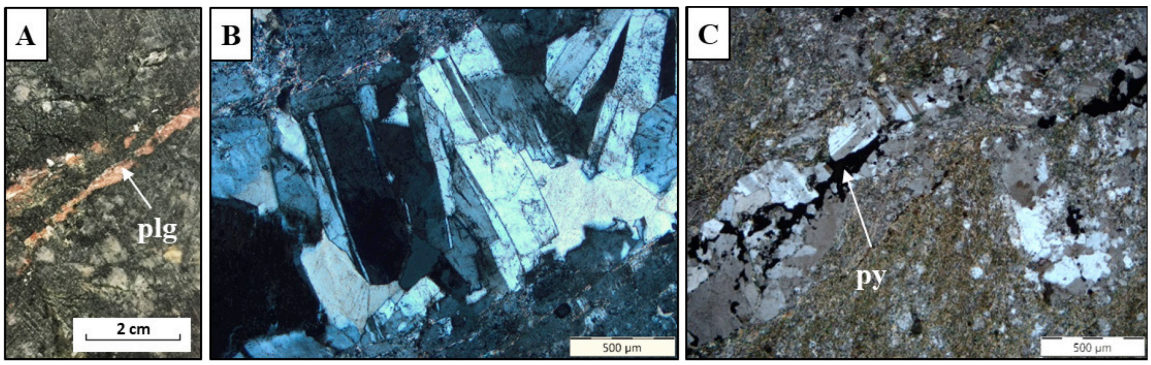

Figure 4.13: Example of plagioclase ± quartz veins (Stage PD-9). **(A):** Interval of albite – chlorite-altered (Stage PD-M1) dacite crosscut by plagioclase veins. **(B):** Cross-polarised photomicrograph of plagioclase vein in the White granite. **(C):** Cross-polarised photomicrograph of phengite – chlorite-altered dacite crosscut by a pyrite-bearing plagioclase vein. Abbreviation: plg = plagioclase, py = pyrite.

Biotite ± chlorite ± phengite alteration (Stage PD-10)

Stage PD-10 is composed biotite ± chlorite ± phengite and is restricted to the volcanic rocks. It may occur as selective alteration of feldspar phenocrysts (Fig. 4.14A), pervasive alteration in groundmass or fracture-controlled alteration (Fig. 4.14B). In places, biotite veins show sigmoidal texture, which is suggestive of tectonic disturbance. Biotite within the veins has been invariably altered to chlorite. Biotite in this vein phase consistently has a brownish appearance at microscopic scale and is distinctly different from the biotite associated with Stage PD-4. PD-10 veins have crosscut barren quartz veins (stage PD-7B) and pervasive phengite ± chlorite alteration (Stage PD-5; Fig. 4.14B).

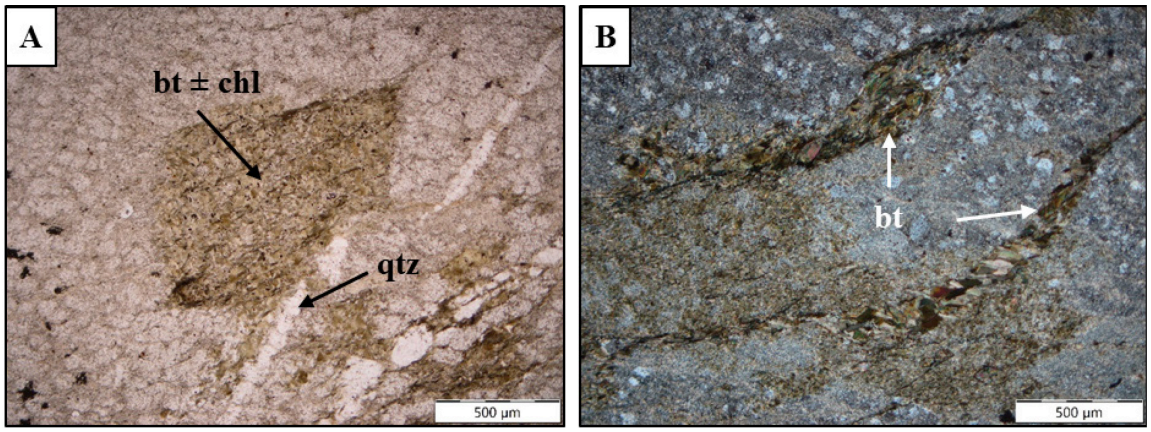

Figure 4.14: Examples of biotite ± chlorite ± phengite alteration (Stage PD-10). **(A):** Plane-polarised photomicrograph of biotite – chlorite-altered feldspar phenocryst in dacite. **(B):** Cross-polarised photomicrograph of biotite – phengite replacement along the fracture and within the groundmass.

Phlogopite – biotite – muscovite ± pyrite ± chlorite alteration (Stage PD-11)

A narrow zone (10 m) of moderate to intense, pervasive phlogopite – biotite – muscovite alteration has been observed in the dacite. The intense alteration has resulted in

conspicuous dark green domains (Fig. 4.15). Chaotic to rotated, subrounded to angular magnetite, apatite and quartz fragments are abundant and are cemented with phlogopite – biotite – muscovite (Fig. 4.15A). Quartz fragments are commonly more amorphous than the magnetite clasts. Breccias of boudin-neck quartz veins (Stage PD-7A) are also observed. In places, magnetite fragments have elongated shapes and show clast alignments (Fig. 4.15B). Some magnetite fragments are rimmed by pyrite ± chalcopyrite assemblages. Pyrite are commonly absent in the magnetite and quartz fragments, but are more often finely disseminated throughout the micaceous cement. Biotite and phlogopite in the cements have been variably chloritised.

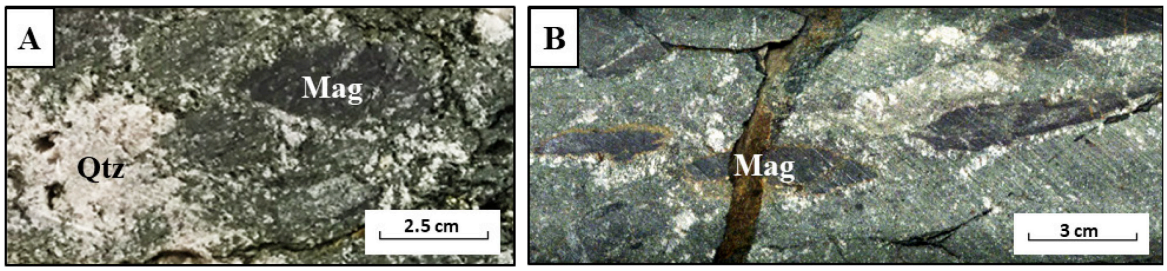

Figure 4.15: Examples of phlogopite – biotite–muscovite ± pyrite ± chlorite alteration (Stage PD-11). **(A):** Core interval of biotite – phlogopite-cemented quartz and magnetite breccias. **(B):** Interval of elongated magnetite breccia cemented in biotite – phlogopite. Magnetite breccias show weak alignment. Abbreviations: qtz = quartz, mag = magnetite.

Carbonate-cemented breccia (Stage PD-12A)

Carbonate-cemented breccia pipes are restricted to the magnetite – apatite replacement zone between the rhyolite and dacite (Stage PD-3; Fig. 4.16A). Presence of brecciated magnetite – pyrite ± chalcopyrite clasts implies that this stage is late- to post-mineralisation. Chaotic to rotated clast arrangement suggests that the carbonate pipes are related to hydrothermal, rather than tectonic events. Where crosscutting relationships have been observed, the carbonate pipes are truncated by later-stage carbonate ± chlorite ± phengite veins (Stage PD-12B; Fig. 4.16B).

Carbonate ± chlorite ± phengite veins (Stage PD-12B)

No carbonate veins have been recognised within the Darwin granite. Occurrence of carbonates have only been observed in the CVC rocks in drill core. Carbonate veins have crosscut all mineralised alteration and vein stages. This crosscutting relationship and absence of associated sulfide minerals suggest that they post-date mineralisation (Fig. 4.16B and 4.16C).

Different types of carbonate veins have been recognised using hyperspectral data, varying from Ca-rich (calcite), Mg-rich (dolomite) to Fe-rich (ankerite and siderite) in composition. The carbonate assemblages at Prince Darwin are typically zoned, with Mg-rich towards the Darwin granite and more Fe-rich with increasing distance from the intrusive centre. The alteration zonation extends laterally and grades outwards from an inner calcite-dominated, to dolomite-dominated to ankerite-dominated subzones.

Vein width is varied, ranging from 1 mm to 25 mm wide. Presence of wispy shapes are indicative of deformation after their formation. Calcite and dolomite veins are creamy white to pale yellow. Occasional feldspar and quartz crystals and sericite aggregates are present within the veins.

Some quartz veins and carbonate veins show open-space filling texture, evident by zoned monomineralic band striking perpendicular to the strike of quartz veins, which results in ladder-like texture to some PD-7A veins (Fig. 4.16D) and crustiform texture in carbonate veins (Fig. 4.16E). This suggests there were re-opening events of quartz veins (Stage PD-7A and PD-7B).

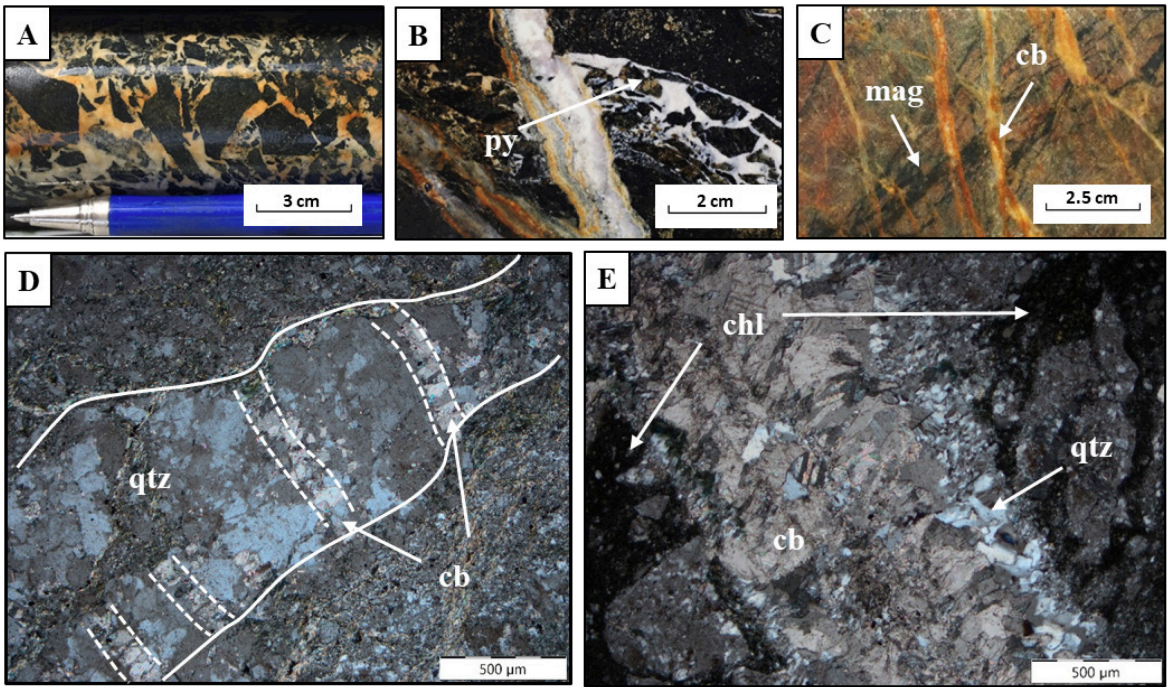

Figure 4.16: Example of late-stage carbonate-cemented breccia (Stage PD-12A) and carbonate ± chlorite ± phengite veins (stage PD-12B). **(A):** Interval of carbonate-cemented magnetite-altered breccias (Stage PD-1). **(B):** Drill core photograph showing the carbonate-cemented pyritic magnetite-altered clasts crosscut by a later carbonate vein (Stage PD-11B). **(C):** Interval of albite – K-feldspar-altered dacite crosscut by early magnetite vein (Stage PD-1A) and late stage carbonate vein (Stage PD-12B). **(D):** Cross-polarised photomicrograph of carbonate-infilled ladder-like quartz vein (Stage PD-8A). **(E):** Cross-polarised photomicrograph of carbonate vein with quartz – plagioclase envelope. Abbreviations: cb = carbonate, chl = chlorite, mag = magnetite, plg = plagioclase, py = pyrite, qtz = quartz.

Selective chlorite – carbonate ± phengite ± magnetite ± biotite alteration (PD-13)

Stage PD-13 is exclusive to the quartz porphyry and the lower part of feldspar-phyric dacites where they have been intruded by the quartz porphyry. Absence of this alteration stage within other parts of the CVC and the Darwin granite indicates that this stage post-dates the emplacement of the quartz porphyry. Selective replacement of feldspar phenocrysts by chlorite – carbonate ± phengite assemblages result in dark speckles in the rock (Fig. 4.18). At microscopic scale, the cores of feldspar phenocrysts are altered to carbonate; whereas, the rims are replaced by chlorite ± magnetite ± phengite (Fig. 4.17B and 4.17C). Remnants of the precursor mineral biotite are present in places.

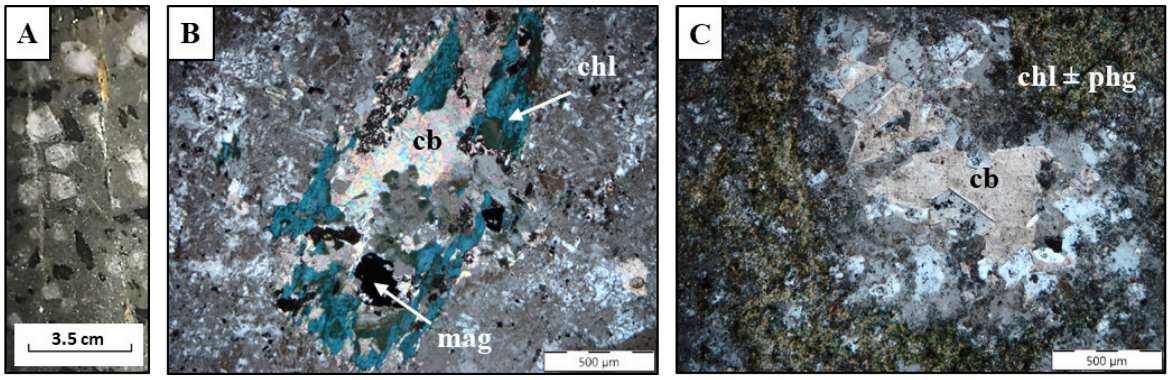

Figure 4.17: Examples of selective chlorite – carbonate ± magnetite ± biotite ± sericite alteration (Stage PD-13). **(A):** Drill core photograph of quartz porphyry. The dark speckles are attributed to the intense, selective chlorite – carbonate alteration of feldspar phenocrysts. **(B):** Cross-polarised photomicrograph of feldspar phenocryst that has been completely altered by carbonate in the core and chlorite on the rim in the quartz porphyry. **(C):** Cross-polarised photomicrograph of a chlorite – phengite – carbonate-altered plagioclase phenocryst in dacite. Carbonate selectively replaced the plagioclase in the core, with fine-grained aggregate of chlorite – phengite ± biotite rim. Abbreviations: cb = carbonate, chl = chlorite, mag = magnetite, phg = phengite.

4.5 Discussion

Ten hydrothermal alteration assemblages and twelve vein types were documented from drill core and field mapping (Table 4.1). Multiple intrusions have resulted in complex and overlapping alteration zones extending into the surrounding volcanic rocks. Hydrothermal alteration within Prince Darwin includes pervasive K-feldspar and selective sericite and chlorite alteration, with minor magnetite, tourmaline, allanite and biotite. These alteration assemblages are representative of early potassic, propylitic and late phyllic alteration that are characteristic hydrothermal alteration styles in porphyry-related magmatic-hydrothermal systems (Sillitoe, 2010). A simplified cross section was constructed to illustrate spatial distribution of the main hydrothermal alteration assemblages at Prince Darwin (Fig. 4.18).

Table 4.1: Schematic table summarising the alteration and mineralisation paragenesis at Prince Darwin. Alteration events are listed in chronological order from left to right.

	Early-stage alteration		**Main-stage alteration and vein (associated with intrusions)**										**Late-stage alteration and vein**		
	Albite alteration (PD-M1)	Phengite alteration (PD-M2)	K-feldspar – magnetite – tourmaline – hematite alteration (PD-1, 1A, 1B, 2A, 2B)	Magnetite – apatite replacement (PD-3)	Allanite – biotite alteration (PD-4)	Phengite alteration (PD-5)	Epidote veins (PD-6)	Quartz ± chlorite ± phengite veins (PD-7A)	Massive, barren quartz veins (PD-7B)	Chlorite – magnetite alteration (PD-8, 8A and 8B)	Plagioclase veins (PD-9)	Biotite alteration (PD-10)	Phlogopite – biotite – muscovite alteration (PD-11)	Carbonate veins (PD-12A, 12B)	Selective chlorite – carbonate alteration (PD-13)
Albite															
Chlorite															
Phengite															
Phengitic illite															
K-feldspar															
Magnetite															
Tourmaline															
Hematite															
Quartz															
Apatite															
Allanite															
Biotite															
Fluorapatite															
Monazite															
Muscovite															
Epidote															
Plagioclase															
Phlogopite															
Carbonate															
Pyrite															
Chalcopyrite															
Bornite															

Strong **Moderate** **Weak**

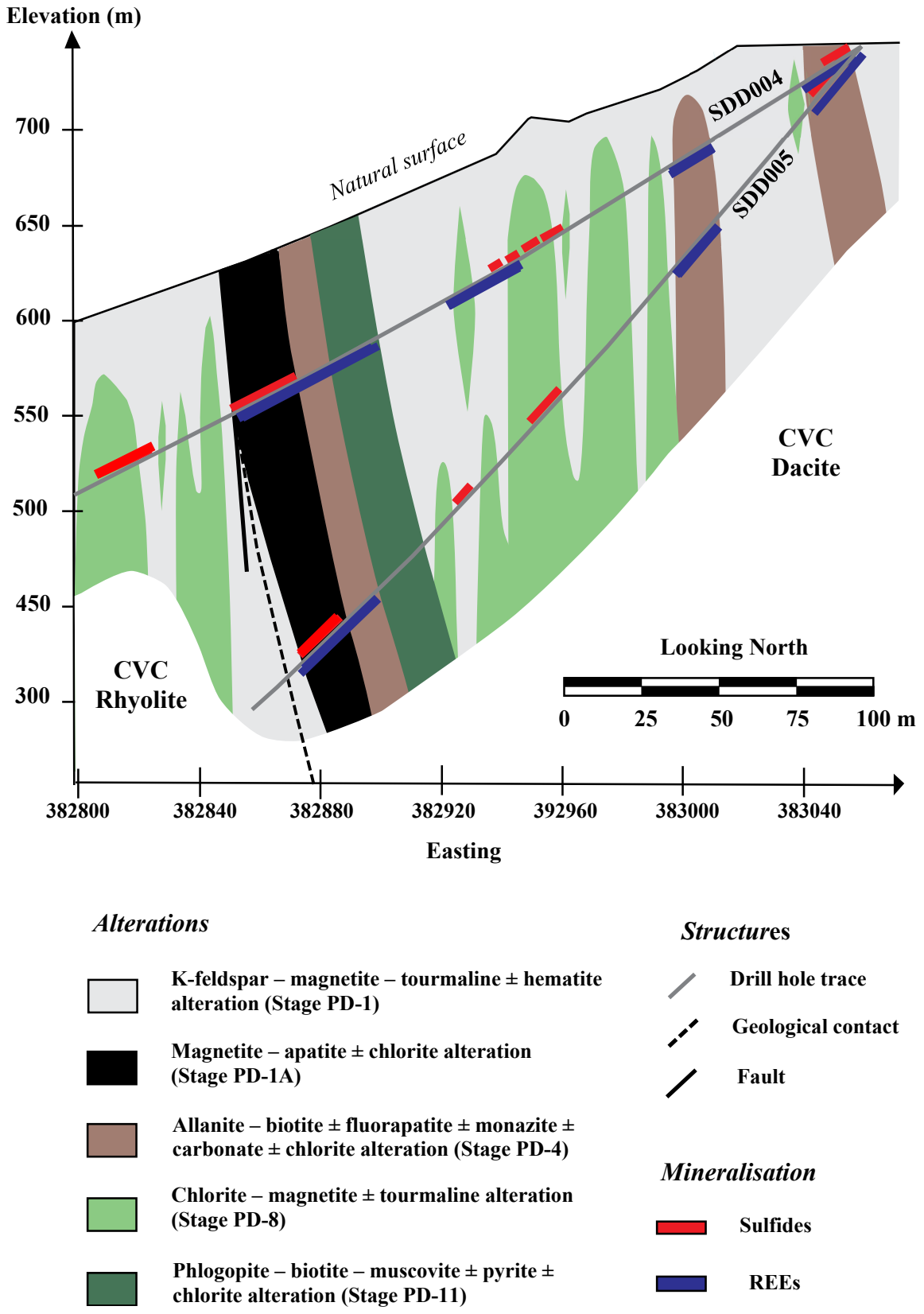

Figure 4.18: Cross section of drill holes SDD004 and SDD005, with distribution of the key alteration stages, sulfide and REE mineralisation, and geology. The alteration stages, except for the phlogopite – biotite stage, were overprinted by phengite-related alteration. Alteration and mineralisation at the Prince Darwin prospect appear to be pipe-like in shape. Occurrence of REE deposits is restricted in the CVC dacite. Cross section location is shown in Fig. 3.1.

Magnetite – apatite (Stage PD-2), allanite – biotite (Stage PD-4) and phlogopite – biotite (Stage PD-11) alteration domains can be traced across drill holes and are typically fault-controlled. The prevalent occurrence of Fe-oxide alteration across Prince Darwin is suggestive of an oxidised nature for the hydrothermal fluids. Hydrothermal tourmaline breccias observed across the Darwin Plateau are also common in some porphyry copper deposits (e.g., Rio Blanco, Chile: Frikken, 2003; Copper Creek, U.S.: Eichenlaub, 2007). Widespread occurrence of tourmaline veins and breccias also suggests the presence of boron-rich hydrothermal fluids. Such occurrence is generally attributed to magmatic-hydrothermal events related to magma emplacement (Demirel et al., 2009).

Similar granite-related hydrothermal alteration styles have also been described for the Elliott Bay granite to the south of Macquarie Harbour (Large et al., 1987) and the Murchison granite in the northern MRV (Eastoe et al., 1987; Abbott, 1992). Prince Darwin also shows some similarities, in terms of hydrothermal alteration and copper – iron mineralisation styles, with several nearby Cu-Au prospects within the MRV, such as Jukes Proprietary prospect (Jones, 1993), Garfield prospect (Duncan, 1996) and South Darwin – Mt. Darwin prospects (Wyman, 2001). Despite these similarities, Prince Darwin differs significantly from other MRV-hosted prospects due to the occurrence of REE-rich minerals and IOCG-like magnetite – apatite alteration assemblages (Williams et al., 2015). Magnetite – apatite alteration assemblages have been documented at two localities in western Tasmania: Prince Lyell (Raymond, 1996) and Savage River Fe mine (Bottrill, 2001). This suggests that Prince Darwin, Prince Lyell and Savage River may represent a similar style of mineralisation that differs from other MRV-hosted deposits.

4.6 Summary

Hydrothermal alteration at Prince Darwin is complicated, with multiple overprinting stages forming due to emplacement of several discrete intrusions. Prince Darwin shows some similarities with other MRV-hosted prospects in terms of hydrothermal alteration styles and copper – iron mineralisation. However, the occurrence of REE mineralisation suggests that Prince Darwin may be representative of a different type of ore system.

Chapter 5

Igneous Geochemistry

5.1 Introduction

This chapter presents the results of whole rock geochemical analyses of intrusive and volcanic rocks from the Prince Darwin prospect, for purposes of petrographic classification and comparison with pre-existing data from igneous rocks in the Darwin granite and CVC. The data are also used to assess the nature and the degree of alteration associated with the host rocks.

5.2 Previous studies

A large number of geochemical studies on the volcanic rocks of the Mount Read Volcanic belt (MRV) has been carried out over the past 40 years (e.g., White, 1975; Solomon, 1980; Crawford, 1987; Corbett & Solomon, 1989; Doyle, 1990; Crawford et al., 1992; Jones, 1993; Gadaloff, 1996; Wyman, 1996; 2001). The MRV comprises an extensive range of igneous rocks, ranging from basalt to rhyolite. Crawford et al. (1992) developed a geochemical discrimination scheme for classification of MRV suites to study the magmatic affinities using immobile elements. Whole-rock geochemical studies on the Darwin granite are limited (e.g., White, 1975; Crawford et al., 1992; Jones. 1993; Gadaloff, 1996; Wyman, 1996). The Darwin granite has been suggested to be co-magmatic with CVC by Solomon (1980). Jones (1993) also proposed that the CVC and Darwin granite were sourced from the same parental magma, whereas Wyman (2001) suggested that Darwin granite was not co-magmatic with the CVC but was instead sourced from a magma which is compositionally similar to the Murchison granite.

5.3 Methods

A total of 18 volcanic and intrusive rocks from the Prince Darwin prospect were selected for whole rock geochemical analysis in this study. Rocks at the Prince Darwin prospect have been subjected to varying degrees of alteration due to regional metamorphism

and hydrothermal events (Chapter 4). All rocks show at least a weak degree of alteration. Least-altered samples are the primary target for petrogenetic studies whereas moderately altered samples are targeted for comparative purposes. Samples from both surface outcrops and drill cores were selected for a good spatial coverage across the field area. Out of 18 samples, 9 samples (3 Pink granite, 2 White granite and 4 volcanic rocks within the CVC) are surface samples from the field area, with the remaining 9 samples (2 quartz porphyry and 7 volcanic rocks) collected from drill core. The samples were analysed at Bureau Veritas Analytical Labs, Canada for their major and trace element compositions. Analyses of CVC samples from north and south of the Henty Fault, which here represent 'least altered' samples of the CVC (Crawford et al., 1992), are included in this study for comparative purpose.

5.4 Results

5.4.1 Effects of hydrothermal alteration

Least-altered and unweathered samples were targeted in the sampling program for geochemical analysis in this study; however, all selected samples have been subjected to at least a weak to moderate degree of hydrothermal alteration and regional metamorphism. Assessment on the effects of hydrothermal alteration on whole-rock geochemistry was done using a series of bivariate element diagrams.

Loss on ignition (LOI) has been widely used as a proxy for the degree of hydrothermal alteration on rocks (e.g., Lechler and Desilets, 1987). High LOI content within host rocks is typically indicative of high degrees of alteration. Whole-rock geochemical data in this study and from previous studies across Jukes-Darwin area (White, 1975; Doyle, 1990; Jones, 1993; Wyman, 2001) are plotted in an alteration box plot diagram (Fig. 5.1A). Volcanic and intrusive rocks are plotted on total alkali-silica (TAS) diagrams separately for lithotype classification. Symbol sizes of data points of these diagrams are scaled to their corresponding LOI contents (Fig. 5.1B and C).

No analyses from this study plot within the least-altered box of the AI versus CCPI diagram, with the exception of two samples from the Pink granite (Fig. 5.1). The majority of the volcanic rocks and intrusions from the Jukes-Darwin area deviate towards sericite alteration, with minor deviations towards the chlorite – pyrite alteration field. Pink granite analyses deviate towards the K-feldspar alteration corner, whereas the White granite forms

a broad trend towards albite alteration. The 'least altered' samples from the CVC typically plot within the least-altered box (Fig. 5.1A).

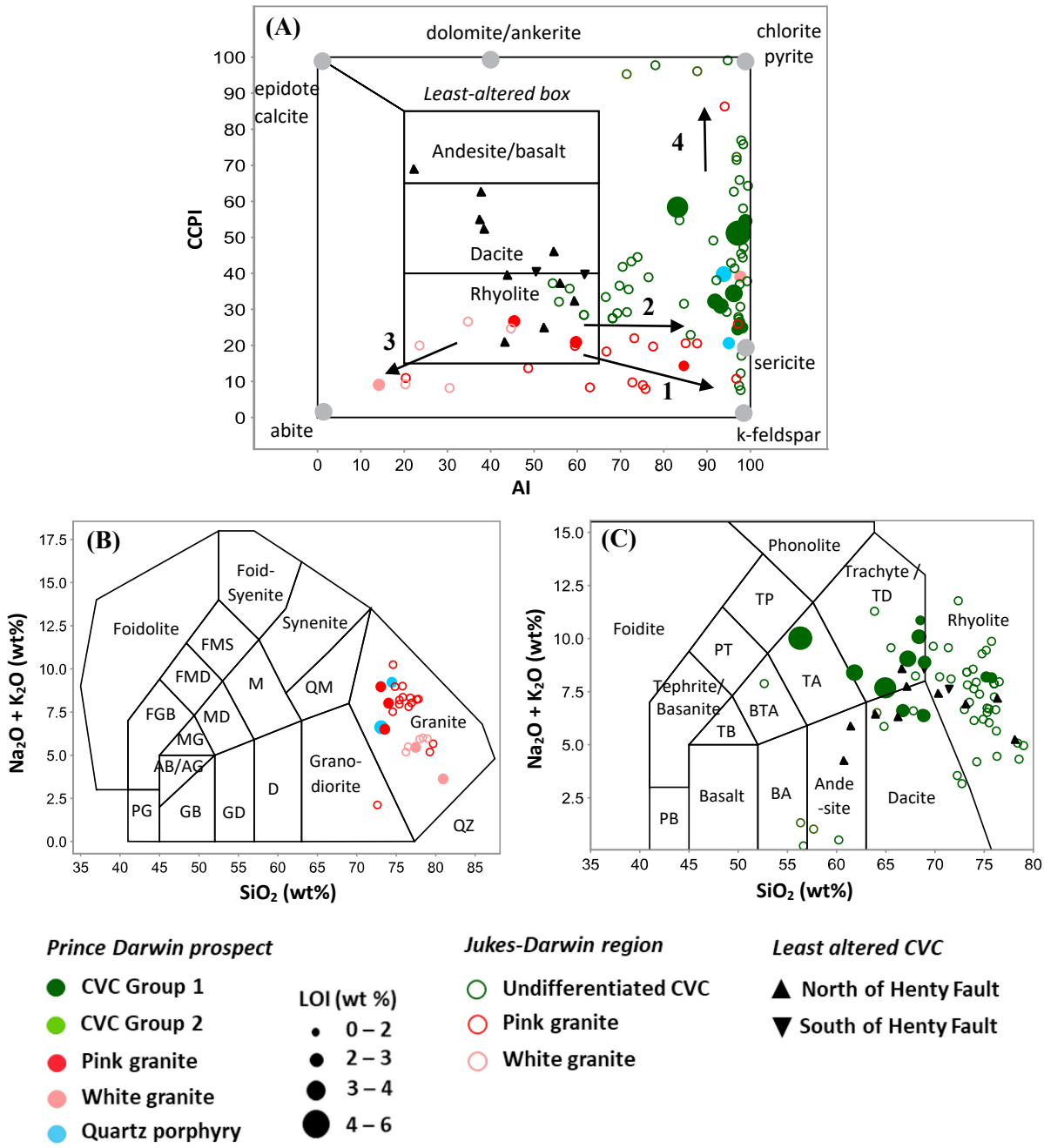

Figure 5.1: Assessment of the hydrothermal alteration effects on the geochemistry of the volcanic and intrusive rocks from the Prince Darwin prospect. **(A):** Alteration box plot (cf. Large et al., 2001). All samples, except two samples of Pink granite, plot outside the least-altered box. Arrows indicate K-feldspar (1), sericite (2), albite (3) and chlorite – pyrite (4) alteration trends. **(B):** TAS plutonic classification diagram (cf. Middlemost, 1994). All intrusions plot within the granite field, though the White granite has been described as granodiorite by petrographic inspection. **(C):** TAS volcanic classification diagram (cf. Le Maitre, 1989). Volcanic samples show a considerable scatter throughout the trachytic and rhyodacitic fields. Data from Crawford et al. (1992), Jones (1993) and Wyman (2001). Abbreviations: AB = alkalic basalt, AI = alteration index, AG =Alkalic Gabbro, CCPI = chlorite-carbonate-pyrite index, BA = basaltic andesite, BTA= basaltic trachyandesite, D = diorite, FGB = foid=-gabbro, FMD = foid-monzodiorite, FMS = Foid-monzosyenite, GB = gabbro, GD = gabbroic diorite, M = monzonite, MD = monzodiorite, MG = Monzogabbro, PB = picrobasalt, PG = perdotgabbro, PT = phonotephrite, TA = trachyandesite, TB = trachybasalt, TD = trachydacite, TP = Tephriphonolite, QM =quartz monzonite, QZ = quartzolite.

On the TAS diagram, intrusive samples invariably plot within granite field (Fig. 5.1B). This result is not consistent with the lithotype interpretations made in Chapter 3 and previous studies, as the White granite has been widely described as granodiorite. Volcanic rocks analysed in this study fall within trachytic fields, whereas the samples from previous studies predominantly fall within the rhyolite – dacite compositional field (Fig. 5.1C). This suggests there is strong remobilisation of alkali elements in the samples analysed in this study.

5.4.2 Major and minor element chemistry

Petrographic descriptions of volcanic rocks have been presented in Chapter 3 and CVC rocks at Prince Darwin broadly consists of two lithofacies: dacite and rhyolite. It is noted that volcanic samples analysed in this study can be divided into two populations with distinct Ti concentrations, irrespective of LOI contents (Fig. 5.2). Group 1 is relatively less Ti-rich (< 2,000 ppm) whereas Group 2 is more Ti-rich (> 3,000 ppm). The variation in Ti concentrations may be a reflection of lithofacies in the volcanic rocks.

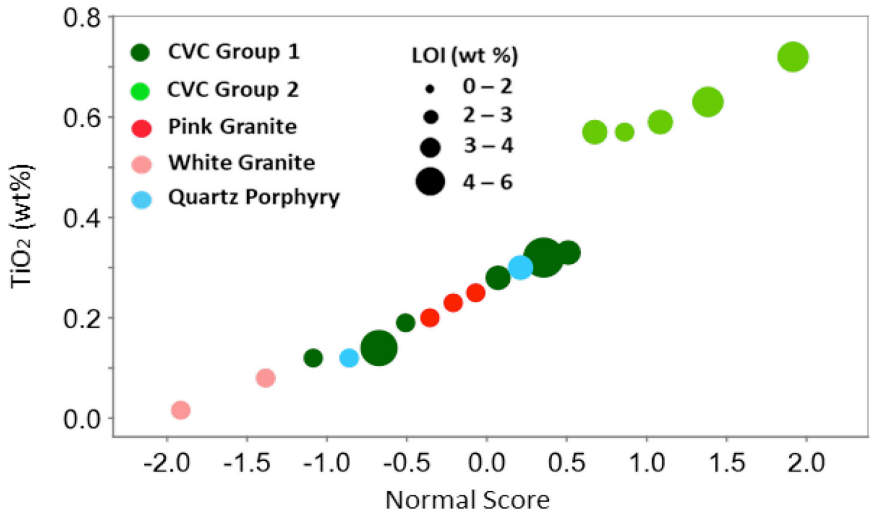

Figure 5.2: Probability diagram of Ti contents in the intrusive and volcanic rocks from the Prince Darwin prospect. There is a distinct separation between low-Ti (Group 1) and high-Ti (Group 2) CVC analyses.

The compositions of major elements from the Prince Darwin samples are plotted in Fig. 5.3. Igneous rocks from the Jukes-Darwin region are generally well-correlated; however, they do not conform to the compositional trends in alkali elements of the least altered CVC rocks (CaO, Na_2O and K_2O). Volcanic rocks and the quartz porphyry are notably depleted in CaO and Na_2O, whereas Darwin granite analyses are typically enriched in Na_2O. These relationships suggest remobilisation of these elements during hydrothermal alteration. Out of the major compositions, Al_2O_3, Fe_2O_3 and MgO exhibit well-correlated smooth trends which mimic magma fractionation trends.

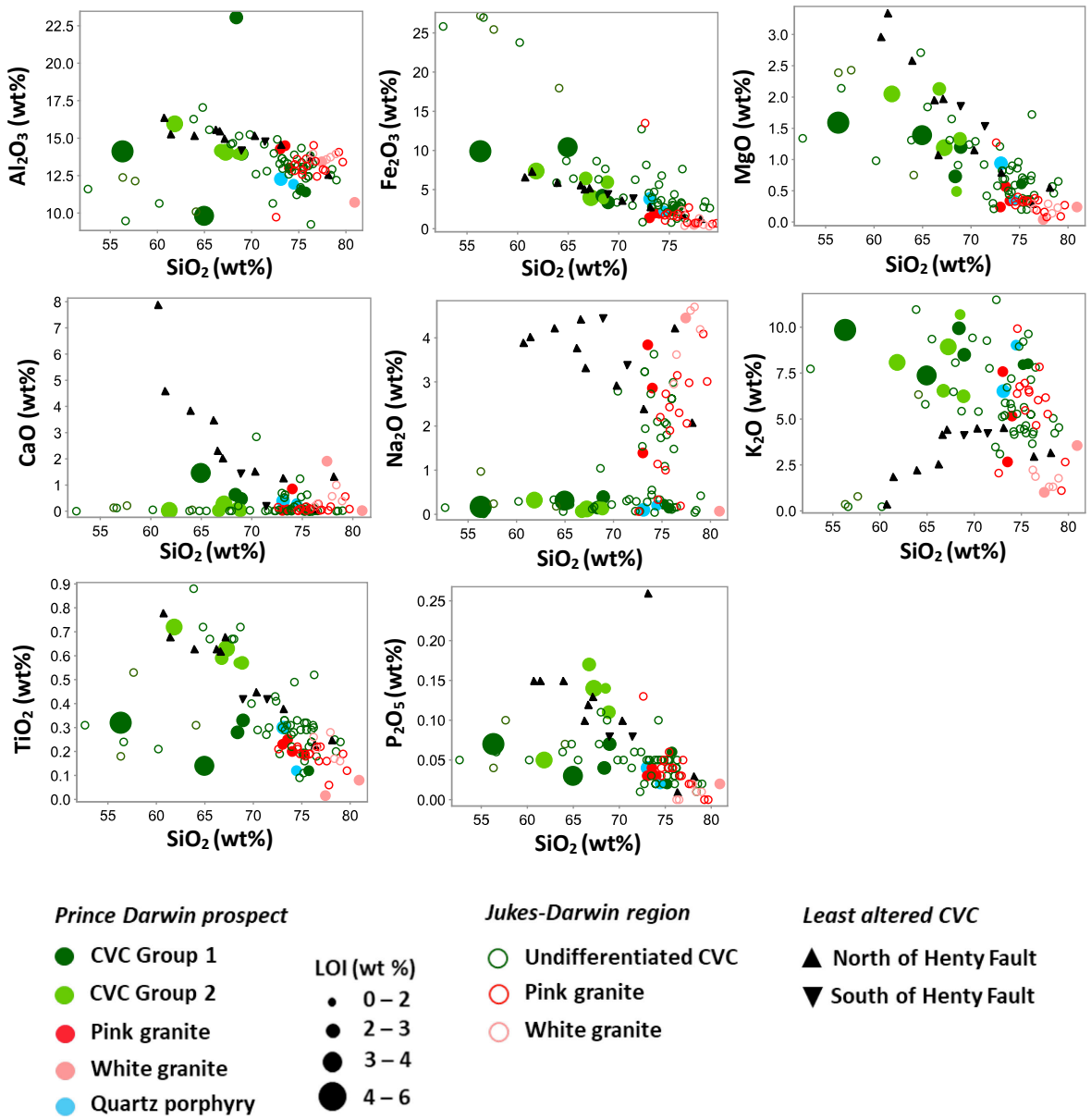

Figure 5.3: Harker diagrams for the intrusive and volcanic rocks from Prince Darwin. Data in this study are compared with samples from Jukes – Darwin prospect and representative least altered CVC. Data from Crawford et al. (1992), Jones (1993) and Wyman (2001).

The compositions of major elements from the Prince Darwin samples are plotted in Fig. 5.4. A weak negative relationship is shown between large ion lithophile (LIL) elements (e.g., Rb, Sr and Ba) and SiO_2. Similar trends are observed in high field strengths (HFS) elements (e.g., Ti, V, Zr). These elements are more relatively more enriched in Group 2 and depleted in Group 1 and intrusions. As LIL elements are more sensitive to hydrothermal processes, these LIL elements, particularly Sr, show more scatter in the plot relative to HFS elements. Overall, minor and trace elements show better correlations and broad congruent trends in the multi-element plots, compared to major element compositions, implying they are relatively less affected by the secondary processes and may be useful in geochemical lithotype classification.

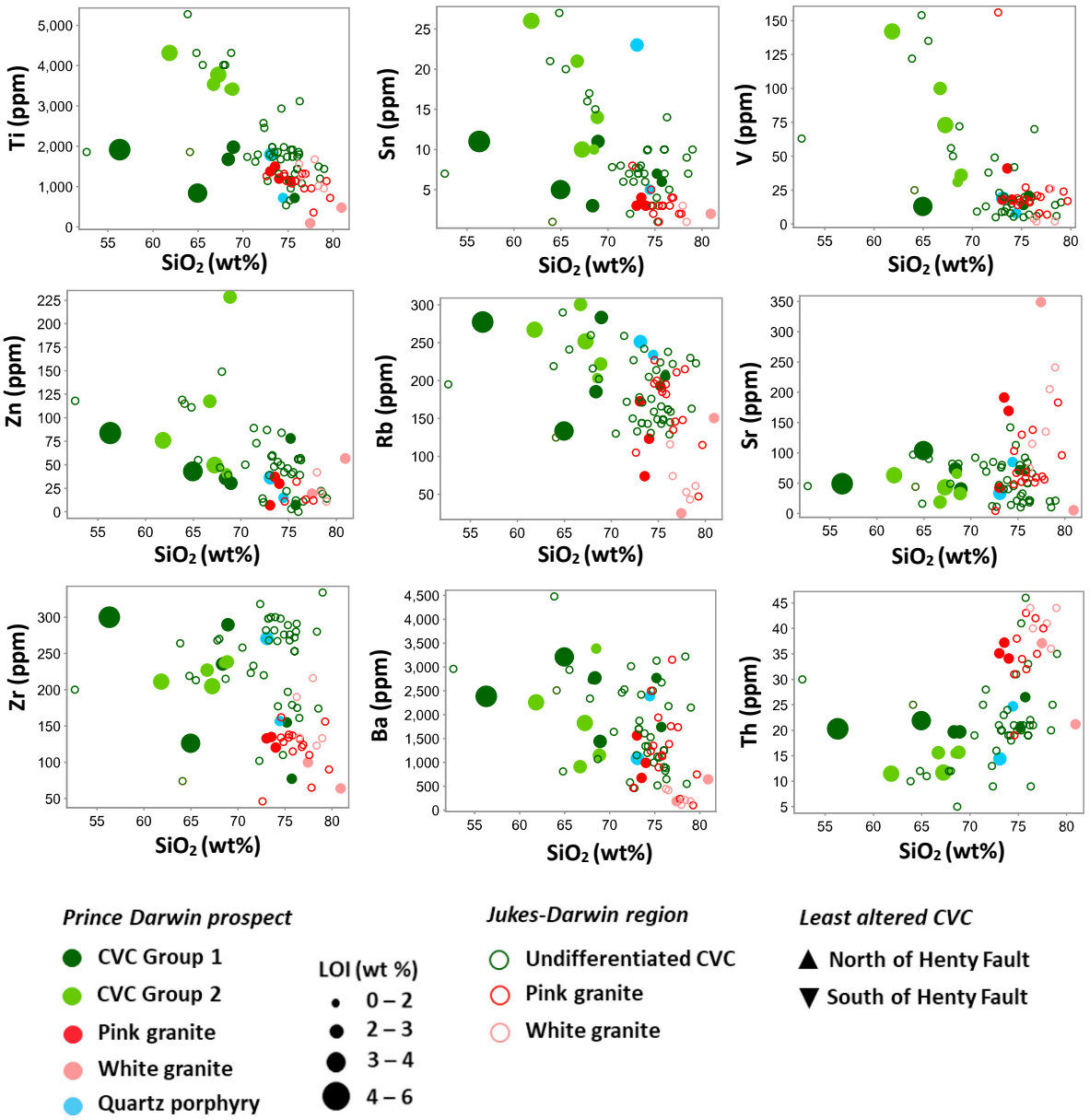

Figure 5.4: Minor and trace element bivariate diagrams for the intrusive and volcanic rocks from Prince Darwin (this study), compared with samples from Jukes – Darwin prospect and representative least altered CVC. Data from Crawford et al. (1992), Jones (1993) and Wyman (2001).

5.4.3 Assessment of element mobility

Due to the effects of intense hydrothermal alteration and weathering, classification of the lithologies, particularly for the volcanic rocks, in this study are primarily based on immobile elements (Crawford et al., 1992; Gemmell and Large, 1992). Aluminium, Ti, Zr, Nb, Y and P are the least mobile under low-grade metamorphism and hydrothermal alteration conditions and have previously been used for the geochemical classification of hydrothermally altered volcanic rocks in the MRV (Crawford et al., 1992; Stoltz, 1992;

Pascual et al., 1997; Jiang et al., 2000). However, it is important to assess the mobility of the "immobile elements" prior to their use.

Stolz (1992) summarised that elements that have not been mobilised should show coherent geochemical behaviours and well-defined trends which pass through the zero with high correlation coefficients in bivariate diagrams. Bivariate diagrams plotted against Ti are shown in Figure 5.5. Both intrusive and volcanic rocks in this study show congruent trends with the least altered CVC rocks, though some show considerable scatter (e.g., Zr, Nb). Immobile element concentrations of Group 1 analyses largely overlap with intrusions. Group 2 typically has less SiO_2, is Zr-poor, and P_2O_5-rich relative to Group 1. Group 2 is compositionally identical to the least altered CVC from the north of the Henty Fault, whereas Group 1 is compositionally similar to those from the south of the Henty Fault. Group 2 also shows weak negative relationships between Ti and Zr, and Ti and Nb (Fig. 5.5D and E), which contrasts with Group 1 and other intrusions.

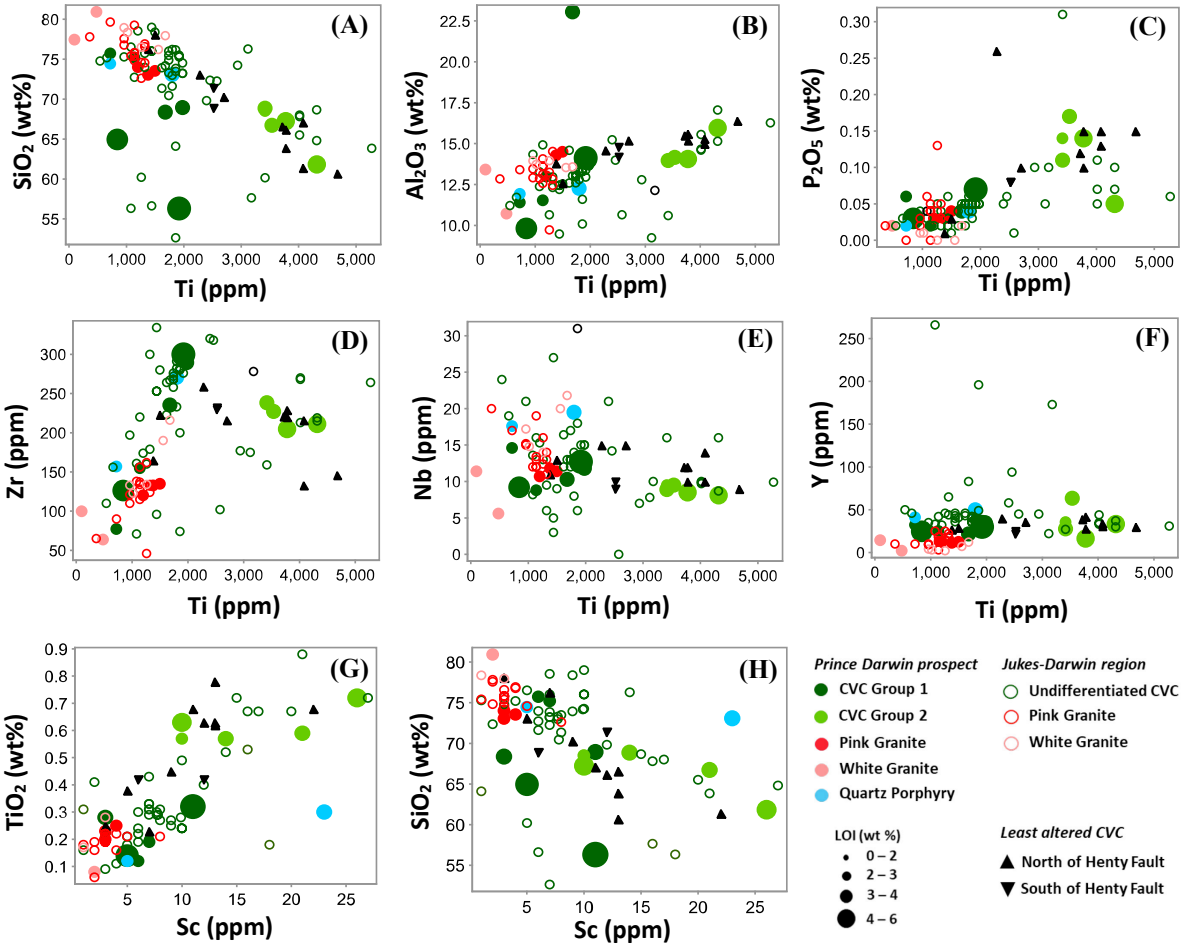

Figure 5.5: Bivariate diagrams of immobile elements from Prince Darwin. **(A) to (F):** Bivariate diagrams of SiO_2, P_2O_5, Al_2O_3, Zr, Nb and Y plotted against Ti. **(G) and (H):** Plots of SiO_2 and TiO_2 relative to Sc. Sc enrichment in Group 2 relative to other samples reflects the 'mafic' nature relative to Darwin granite and Group 1. Data from Crawford et al. (1992), Jones (1993) and Wyman (2001).

Sc is another useful immobile element under hydrothermal conditions (Halley, 2013). Sc commonly substitutes for Fe into common silicate minerals such as biotite, chlorite and amphibole. It can therefore be used as a proxy for the Fe content as it is significantly less mobile than Fe during hydrothermal alteration (Halley, 2013). In general, rhyolites contain less than 10 ppm, dacites 10 to 20 ppm, andesites 20 to 30 ppm, and basalts 30 to 50 ppm. By plotting major elements against Sc (Fig. 5.5G and H), Group 2 samples appears to be more enriched in Sc relative to Darwin granite and Group 1 samples, which is likely to reflect their relatively more 'mafic' nature compared to the intrusions and Group 1. This result is also consistent with the observation of fewer quartz phenocrysts in Group 2 samples. Notable Sc enrichment in one of the quartz porphyry samples is likely due to intense selective chlorite replacement after feldspar phenocrysts (see Chapter 3).

5.4.4 Geochemical classification

Volcanic rocks are geochemically classified on the Zr/TiO_2 – Nb/Y plot (Winchester and Floyd, 1977), as the elements used in this classification scheme are demonstrated to have limited mobilisation during hydrothermal alteration. The volcanic rocks across Jukes-Darwin prospect are geochemically dominated by rhyodacitic or dacitic compositions (Fig. 5.6A). Group 1 typically borders on the rhyolite – rhyodacite boundary, reflecting their relative felsic nature. This result is in accordance with the lithotype classifications presented in Chapter 3 and in previous studies (Jones, 1993; Wyman, 2001).

The geochemical classification scheme for granitic rocks is largely based upon major element compositions. Consequently, the classification scheme developed by Crawford et al. (1992) was used (Fig. 5.6B and C), which has been used to study the geochemical affinities of igneous suites in the MRV. The results show that both intrusions and volcanic rocks from the Jukes-Darwin area, including the least altered CVC rocks from Henty Fault, belong to suite I, with a few samples plotting outside the defined suites (Fig. 5.6B and C).

Overall, all samples show consistent REE patterns on multi-element diagrams (Fig. 5.6D and 5.6E), with the exception of the White granite samples which displays more varied REE patterns. Both intrusions and volcanic rocks at the Prince Darwin prospect are more enriched in LREEs relative to HREEs. The quartz porphyry is most enriched in REEs amongst all intrusions. HREEs are more heavily depleted in the Darwin granite relative to the quartz porphyry. Both volcanic rocks and the quartz porphyry are characterised by

negative Eu anomalies. In contrast, the Pink granite shows smooth trends with no Eu anomalies, whereas one of the analyses from the White granite shows a positive Eu anomaly.

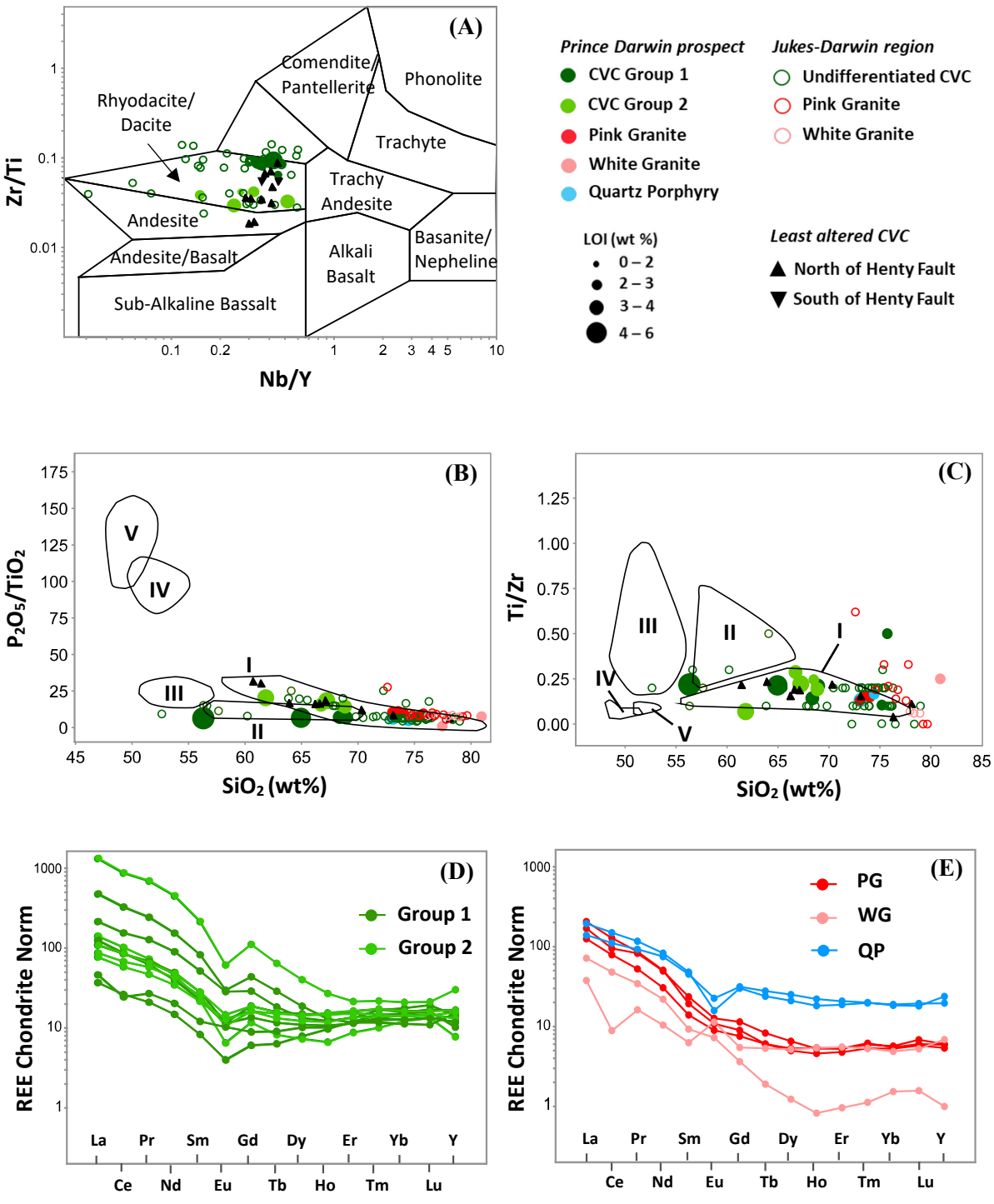

Figure 5.6: Igneous geochemistry classification diagrams and multi-element diagrams for volcanic and intrusive rocks from Prince Darwin. **(A):** Volcanic rock classification (after Winchester and Floyd, 1977). **(B):** P_2O_5/TiO_2 vs. SiO_2 (cf. Crawford et al., 1992). **(C):** Ti/Zr vs. SiO_2 (cf. Crawford et al., 1992). **(D):** Chondrite-normalised REE diagram of volcanic rocks. **(E):** Chondrite-normalised REE diagram of volcanic rocks. Normalising values from Taylor and McLennan (1985). Data from Crawfored et al. (1992), Jones (1993) and Wyman (2001). Abbreviations: PG = Pink granite, QP = Quart Porphyry, WG = White Granite.

5.5 Discussion

Hydrothermal alteration has led to issues in the geochemical classification of igneous rocks at the Prince Darwin prospect using major element compositions. Remobilisation of alkali elements due to hydrothermal alteration is evident by the incongruent compositional trends relative to the least unaltered CVC in major element bivariate diagrams (Fig. 5.3). Consequently, classification of the samples using immobile elements is particularly useful in studying the geochemical nature of the altered volcanic rocks at the Prince Darwin prospect, with the results more consistent with the lithotype interpretations presented in Chapter 3. The consistent trends towards albite and K-feldspar-dominated alteration in the Pink and White granite samples are due to their primary igneous composition, as the Pink granite is typically K-feldspar-rich whereas the White granite is plagioclase-rich.

The most popular classification schemes for granitic rocks are I- and S-type (White and Chappell, 1983), and the magnetite- and ilmenite-series classification (Ishihara, 1981). Two of these classification schemes are based upon whole-rock geochemical data, normative mineral calculations and stable isotopes. The intense hydrothermal alteration and element remobilisation, particularly for K_2O, Na_2O and CaO, prohibit the use of these classification schemes. However, field observations of widespread magnetite alteration and association with sulfide mineralisation support the hypothesis that the Darwin granite belongs to the I-type granite series (Ishihara, 1981; White and Chappell, 1983). The Darwin granite is also classified as volcanic arc-related granitoid (Fig. 5.7). This interpretation is consistent with interpretations previously made by Solomon (1980), Jones (1993) and Wyman (2001). In contrast, samples of the quartz porphyry plot within the 'within plate-granite' field, suggesting that it may be genetically different from the Darwin granite. The quartz porphyry may be an S-type or A-type granite which commonly involve significant crustal contamination.

The classification system proposed by Crawford et al. (1992) assigns both intrusive and volcanic rocks at the Prince Darwin prospect to Suite I, which has been interpreted to represent the medium to high K calc-alkaline and the least LREE-enriched suite in the MRV (Table 5.1; Crawford et al., 1992). This is consistent with observations from previous studies (Jones, 1993; Wyman, 2001), implying that the CVC of the Mount Darwin – South Darwin region forms part of Suite I. The decreasing trend of Ti/Zr with increasing SiO_2 in Figure 5.6B is attributed to the precipitation of Fe-Ti oxides, whilst Zr continues to be retained in the melt during fractionation, a common feature in calc-alkaline rocks (e.g., Jones, 1993).

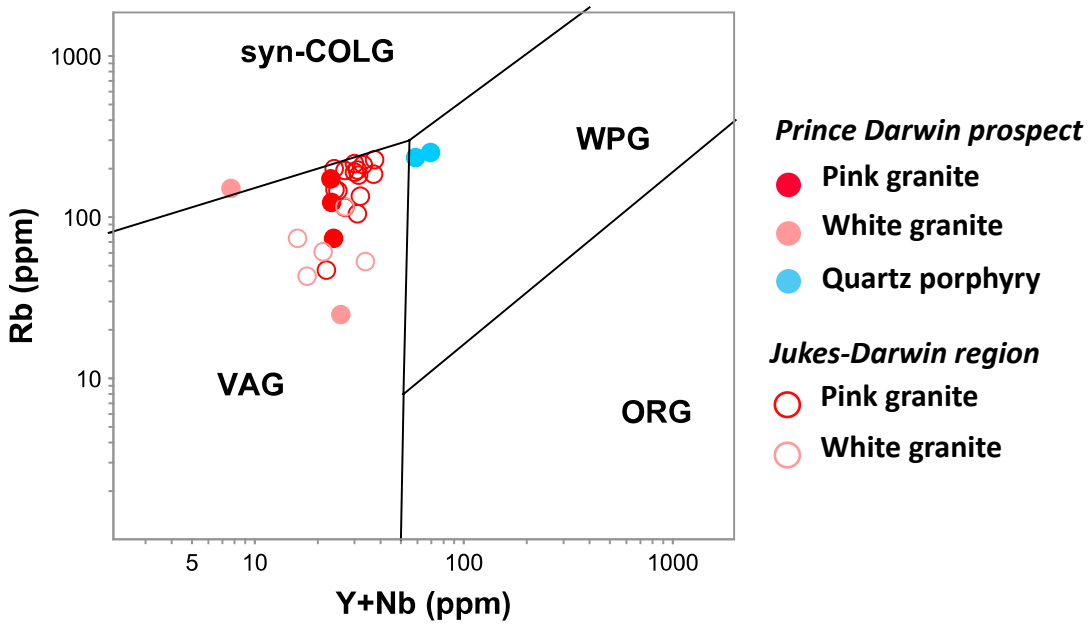

Figure 5.7: Tectonic classification of intrusive rocks at Prince Darwin (cf. Pearce et al., 1984). Abbreviations: syn-COLG = syn-collisional granites, ORG = ocean ridge granitoid, VAG = volcanic arc granitoid, WPG = within-plate granitoid. Data from Jones (1993) nad Wyman (2001).

The enrichment of LREEs relative to HREEs in both the intrusions and volcanic rocks at the Prince Darwin prospect is indicative of subduction-related magmas (Winter, 2014). By comparing the data in this study with previous work conducted on the Darwin granite and the Cambrian-aged Murchison granite (Appendix E; Crawford et al., 1992), they broadly show similar REE patterns and negative Eu anomalies (Fig. 5.8A). The negative Eu anomalies in the intrusions are most likely the consequence of feldspar removal by crystal fractionation or feldspar retention in the residual source after partial melting (Rollinson, 1993).

The White granite shows more varied compositions and REE patterns (Fig. 5.8B). The White granite is also invariably characterised by positive Eu anomalies that are not recognized in any phase in the Prince Darwin granite and Murchison granite. The positive Eu anomalies are owing to the enrichment of plagioclase relative to other igneous phases at Prince Darwin. The wide geochemical variations in the White granite may be attributed to the hydrothermal alteration or compositional heterogeneity, as it has been described as the most texturally and compositionally diverse phase at Prince Darwin (Chapter 3).

REE geochemistry, particularly the strong negative Eu anomaly and congruent REE trends, suggests that the volcanic rocks and the quartz porphyry may have had a comagmatic relationship (Fig. 5.6D and 5.6E). Absence of negative Eu anomalies in Darwin granite suggest that it is not co-magmatic with the volcanic rocks and quartz porphyry. This interpretation is consistent with previous studies by Jones (1993) and Wyman (2001).

Table 5.1: Summary of different geochemical suites in the MRV (after Crawford et al., 1992).

Suites	Geochemical characteristics	Corresponding unit in MRV
I	Medium to high K calc-alkaline, the least LREE-enriched suite in the MRV, $(La/Yb)_N$ = 5 – 12 (avg. 8.1)	Eastern sequence, Central Volcanic Complex, Tyndall Group, quartz-feldspar porphyries and granitoids andesitic lavas of the Que Hellyer footwall sequence
II	High K calc-alkaline affinities, more P_2O_5 and LREE-enriched than suite I, $(La/Yb)_N$ = 10 – 26 (avg. 16.7)	Hornblende-porphyritic andesites and dacites in the upper part of the southern Central Volcanic Complex
III	High K calc-alkaline, striking compositional range: - Low TiO_2 (0.4 – 0.5 %), low P_2O_5 (<0.1 %), $(La/Yb)_N$ = 8 – 12 with almost flat HREE patterns - Low TiO_2 (0.4 – 0.8 %), strongly to exceptionally enriched in P_2O_5 and LREEs up to 350 times chondritic La with $(La/Yb)_N$ up to 34. This group is regarded as shoshonite	Basaltic and andesitic lavas of the Que-Hellyer hanging-wall Sequence, Lynch Creek Basalts, intrusive of Howards Plain area
IV	Tholeiitic, high TiO_2 (1 – 1.6 %), depleted Nb contents (<3 ppm), only slightly enriched in LREEs, $(La/Yb)_N$ = 1.4 – 3.4.	Tholeiitic basalts of Henty Fault Wedge and Henty Dike Swarm
V	Tholeiitic, low TiO_2 (<0.7 %), strong LREE depletion, $(La/Yb)_N$ = 0.9	Miners Ridge Basalts, which have been considered as part of the pre-MRV basement

5.6 Summary

Immobile elements are particularly useful in geochemical classification in intensely altered volcanic and intrusive rocks at Prince Darwin. Both intrusive and volcanic rocks form part of Suite I, which is the least LREE-enriched suite in the MRV. The quartz porphyry may be co-genetic with volcanic rocks. Igneous rocks at Prince Darwin were formed from subduction-related magmatism but are not co-magmatic.

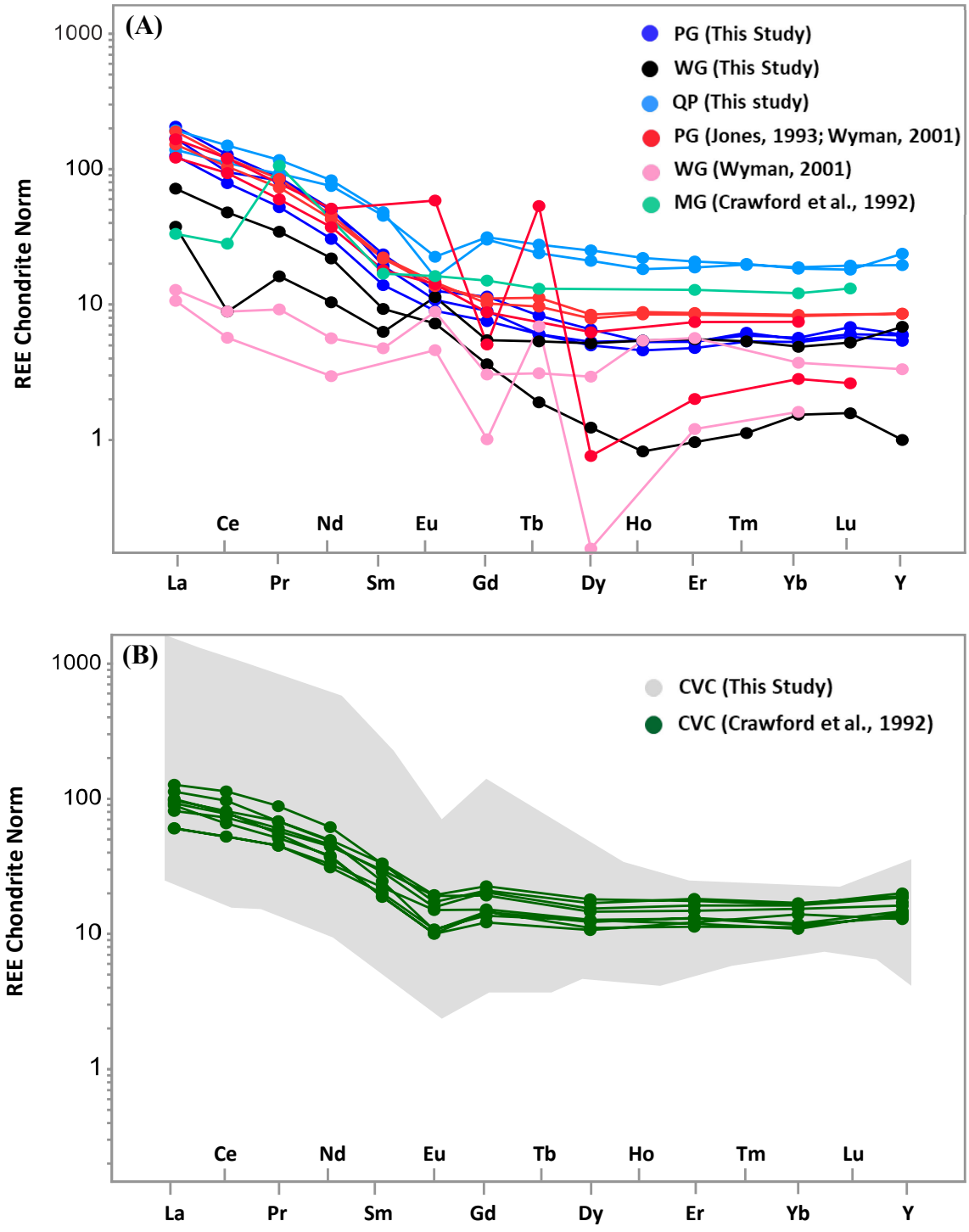

Figure 5.8: Comparison of REE patterns of intrusive rocks at the Prince Darwin prospect with previous work on the Darwin granite and Murchison granite (normalising values after Taylor and McLennan, 1985). **(A):** REE patterns of intrusions from the Prince Darwin prospect, from Mt. Darwin – South Darwin region and Murchison granite. **(B):** REE patterns of the CVC from the Prince Darwin prospect relative to least-altered CVC rocks. Data from Crawford et al. (1992), Jones 91993) and Wyman (2001). Abbreviations: CVC = Central Volcanic Complex, MG = Murchison granite, PG = Pink granite, QP = Quartz porphyry, WG = White granite.

Chapter 6

Hydrothermal Mineral Chemistry

6.1 Introduction

This chapter presents the chemistry of key hydrothermal minerals (chlorite, epidote, allanite and tourmaline) at the Prince Darwin prospect, to ascertain their usefulness as indicators for mineralisation fertility and as exploration vectoring tools towards high-grade mineralisation. Discussions on the physiochemical conditions of the melt and associated mineralising fluids, such as oxidation state, pH and water content, and constrains on the genesis of the mineralisation at the Prince Darwin prospect interpreted from the mineral chemistry are also included in this chapter.

6.2 Overview of chlorite, epidote, allanite and tourmaline chemistry

Chlorite

Chlorite is a common hydrothermal mineral in propylitic alteration domains surrounding porphyry-epithermal systems (Cooke et al., 2014). It has a general chemical formula of $(X,Y)_{4\text{-}6}(Si,Al)_4O_{10}(OH,O)_8$, where X and Y can be Li^{+1}, Fe^{2+}, Fe^{3+}, Mg^{2+}, Mn^{2+}, Al^{3+} or Ti^{4+} (Foster, 1962). Chlorite group minerals can be broadly divided into four sub-groups: clinoclore (Mg-rich), chamosite (Fe-rich), nimite (Ni-rich) and pennantite (Mn-rich; Foster, 1962). Substitutions of ions into chlorite are typically controlled by host rock chemistry, temperature, oxygen fugacity, pH and fluid chemistry (Shikazono and Kawahata, 1987; Deer et al., 2009; Beaufort et al., 2015). Recently, several studies have commented the potential of trace element contents in propylitic chlorite serving as proximity and fertility tools for porphyry-epithermal systems (e.g., Cooke et al., 2014; 2017; Wilkinson et al., 2015; 2017).

Epidote and Allanite

Epidote is another common mineral in propylitic alteration assemblages. Epidote is one of the end-members in epidote supergroup (Table 6.1). The chemical formula of epidote

is generalised to $A_2M_3[Si_2O_7]$ $[TO_4](O,F)(OH,O)$, where A = Ca, Mn^{2+}, Sr, Pb, REE, and other divalent cations, M = Al, Fe^{3+}, Mn^{3+}, V^{3+}, Cr^{3+} and other trivalent cations, including REEs (Deer et al., 1986). Epidote in hydrothermal systems is typically characterised by composition zonation owing to variable Fe^{3+} – Al^{3+} substitution as a complex function of redox, temperature, pressure, bulk rock and fluid chemistry (Arnason et al., 1993). Complex interplay of several variables in the propylitic alteration zone often results in complexities in epidote (e.g., growth zones) and hinders the systematic zonation in the alteration halo, making the application of epidote as a vectoring tool in exploration challenging (Wilkinson et al., 2015).

Table 6.1: Chemical formulas of epidote and allanite subgroups (after Franz and Liebscher, 2004; Gieré and Sorensen, 2004; Armbruster et al., 2006; Minakawa et al., 2008; Mills et al., 2009; Chukanov et al., 2012; Skoda et al., 2012; Nagashima et al., 2013; Cooke et al., 2014).

Group	Chemical formula
Epidote Group	
Epidote	$Ca_2Al2Fe^{3+}[Si_2O_7][SiO_4]O(OH)$
Epidote-(Sr)	$CaSrAl_2Fe^{3+}[Si_2O_7][SiO_4]O(OH)$
Epidote-(Pb)	$CaPbAl_2Fe^{3+}[Si_2O7][SiO4]O(OH)$
Clinozoisite	$Ca_2Al_3[Si_2O_7][SiO_4]O(OH)$
Clinozoisite-(Sr)	$CaSrAl_3[Si_2O_7][SiO_4]O(OH)$
Mukhinite	$Ca_2Al_2V^{3+}[Si_2O_7][SiO_4]O(OH)$
Piemontite	$Ca_2Al_2Mn^{3+}[Si_2O_7][SiO_4]O(OH)$
Piemontite-(Sr)	$CaSrAl_2Mn^{3+}[Si_2O_7][SiO_4]O(OH)$
Piemontite-(Pb)	$CaPbAl_2Mn^{3+}[Si_2O_7][SiO_4]O(OH)$
Manganipiemontite-(Sr)	$CaSrMn_3$+$AlMn^{3+}[Si_2O_7][SiO_4]O(OH)$
Allanite	
Allanite-(Ce), -(La), -(Y), -(Nd)	$Ca(REE)^{3+}Al2Fe^{2+}[Si_2O_7][SiO_4]O(OH)$
Vanadoallanite-(La)	$CaLa^{3+}$ $V^{3+}AlFe^{2+}[Si_2O_7][SiO_4]O(OH)$
Dissakisite-(Ce), -(La)	$Ca(REE)^{3+}Al2Mg[Si_2O_7][SiO_4]O(OH)$
Ferriallanite-(Ce), -(La)	$Ca(REE)^{3+}$ $Fe^{3+}AlFe^{2+}[Si_2O_7][SiO_4]O(OH)$
Manganiandrosite-(La), -(Ce)	$Mn^{2+}(REE)Mn^{3+}AlMn^{2+}[Si_2O_7][SiO_4]O(OH)$
Vanadoandrosite-(Ce)	$Mn^{2+}Ce^{3+}V^{3+}AlMn^{2+}[Si_2O_7][SiO_4]O(OH)$

The rare earth element (REE)-rich epidote subgroup is commonly known as allanite (Gieré & Sorensen, 2004; Table. 6.1). The general formula of allanite is $(Ca,Mn,REE,Th)_2(Fe^{2+},Fe^{3+},Ti)(Al,Fe^{3+})_2Si_3O_{12}(OH))$ (Gieré & Sorensen, 2004). Formation of allanite is related to the coupled substitution of REE^{3+} in epidote group minerals: $REE^{3+} + Fe^{2+} \rightarrow Ca^{2+} + Fe^{3+}$ (Khvostova, 1963; Ploshkl and Bogdanova, 1963). Allanite-(Ce) is the most common species in the allanite group. Deer et al. (1986) indicated

that allanite is a potential carrier of Sr^{2+}, Pb^{2+}, Th^{4+}, U^{4+}, Mn^{3+}, Mn^{2+}, Cr^{3+}, Ti^{4+}, Zr^{4+} and Ba^{2+} (Gieré & Sorensen, 2004). Presence of allanite has been reported in various hydrothermal deposits and geological settings, with common occurrences in skarn environments (e.g., Exley, 1980; Chen and Zhou, 2014; Uher et al., 2015; Fu et al. 2007). Th and U contents in allanite are particularly useful for geochronological purposes (Morrison, 2004; Cox et al., 2012; Smye et al., 2014). The U contents in allanite are also useful to study the oxygen fugacity of ore-forming fluids, with high U concentrations indicative of high fo_2 (Pal et al., 2011).

Tourmaline

Tourmaline is a complex borosilicate mineral with more than 25 end-member compositions due to its complicated crystal structure and arrangement (Hawthorne and Henry, 1999; Henry et al., 2011; Hawthorn and Dirlam, 2011). The chemical formula of the tourmaline group can be generalised to: $XY_3Z_6(T_6O_{18})(BO_3)_3V_3W$, where X = Na^+, K^+, Ca^{2+} and vacant, Y = Li^+, Mg^{2+}, Mg^{2+}, Mn^{2+}, Fe^{2+}, Fe^{3+}, Al^{3+} and Cr^{3+}; Z = Mg^{2+}, Al^{3+}, Fe^{3+}, and Cr^{3+}; T = Al^{3+}, and B^{3+}, Si^{4+}; B = B^{3+}; V = OH^- and O^{2-}; and W = OH^-, F^-, and O^{2-} (Henry et al., 2011). In broad terms, tourmaline group minerals can be divided into three sub-groups: schrol (Fe-rich), dravite (Mg-rich) and elbaite (Li-rich), and the occurrences of these sub-types vary with hydrothermal systems (Table 6.2; see reviews by Slack, 1996; Henry et al., 2011; Slack and Trumbull, 2011; Bosi, 2018).

Table 6.2: Varieties of tourmaline groups in different hydrothermal environments (from Plimer and Lees, 1988; Slack et al., 1993, 2011; Slack 1996; Williamson et al., 2000; Jiang et al., 2008).

Hydrothermal ore deposit style	Common tourmaline end-member	Reference
Submarine massive sulfide deposits	Dravite-schorl series	Plimer and Lees, 1988; Slack et al., 1993
- *Adjacent to the submarine veins*	Fe-rich dravite or schorl	
Reduced granite-related Sn-W deposits	Schorl group	Williamson et al., 2000; Jiang et al., 2008
Porphyry Cu-Mo-Au deposits and IOCG	Schorl-dravite	Slack, 1996

Due to its chemically and physically refractory properties, many studies have successfully demonstrated the roles of tourmaline in constraining the genesis of magmatic-hydrothermal ore deposits, petrogenetic indicators in fingerprinting environments and vectoring potential in mineral exploration (e.g., Slack et al., 1993; Henry and Guidotti, 1985; Jiang et al., 1995; 2004; Yavuz et al., 1999; Williamson et al., 2000; Garda et al., 2003; Marschall et al., 2008; Galbraith et al., 2009; Tornes et al., 2012). The complex interplay of chemical parameters (e.g., pH, redox, temperature, fluid flux, wall rock interaction) account

for more varied tourmaline compositions in hydrothermal environments compared to those in igneous and metamorphic terranes (Table 6.2; Henry and Guidotti, 1985; Slack, 1996; Slack and Thumbull, 2011; Mark et al., 2013).

6.3 Previous studies

Extensive studies have demonstrated the applications of hydrothermal mineral chemistry as fertility and vectoring tools in porphyry ore systems to optimise the ability for explorationists to locate high-grade ore deposits during early the early stages of exploration (Wilkinson et al., 2015, 2017; Cooke et al., 2014; Galbraith et al., 2009; Chang et al., 2011; Marks et al., 2013; Piziak et al., 2015). However, studies focussed on mineral chemistry across the southern Mount Read Volcanics are limited. Wyman (2001) conducted microprobe analyses on chlorite, apatite and sericite in Jukes-Darwin area. He noted that the Fe contents in chlorite increase towards the mineralised zone. Similar zonation was observed around the Murchison granite as the function of outward increase in fO_2 and decline in temperature (Poyla et al., 1986).

6.4 Sampling and analytical methods

Hydrothermal minerals analysed in this study include chlorite, epidote, allanite and tourmaline. There is a variety in the mode of occurrence for these minerals, including as disseminations, veins, pervasive replacement and matrix in-fill in hydrothermal breccias. Chlorite, epidote and tourmaline were easily identified from hand specimens due to their diagnostic colours and properties. Later validation of the presence of chlorite, epidote and tourmaline was achieved by short wave infra-red (SWIR) analysis using a TerraSpec instrument. Identification of allanite from hand specimens proved more difficult. In-situ analyses were conducted on potential allanite-bearing samples with portable X-ray fluorescence (pXRF) to determine the presence of allanite. Samples with selected minerals were then made into 1-inch diameter laser ablation mounts. A total of 24 laser ablation mounts were analysed in this study, including six chlorite, two epidote, nine allanite and seven tourmaline-bearing samples.

Reflected light microscopic studies were performed on the laser mounts, followed by scanning electron microscopy (SEM) analysis to test for the presence of targeted hydrothermal minerals prior to laser ablation inductively-coupled plasma mass spectrometry

(LA-ICP-MS) analysis, that was subsequently used to determine trace and major element concentrations in these minerals. The quantitative multi-element analyses were performed by ablating spots 30 μm in size, with a laser repetition rate of 5 Hz on a ASI Resolution S155 SE laser system housed at the CODES Analytical Laboratory, University of Tasmania. The laser beam fluence was set to 3.41 J/cm^2.

Isotopes analysed by ICP-MS for chlorite, epidote and allanite included ^{7}Li, ^{11}B, ^{23}Na, ^{24}Mg, ^{27}Al, ^{29}Si, ^{39}K, ^{43}Ca, ^{47}Ti, ^{49}Ti, ^{51}V, ^{53}Cr, ^{55}Mn, ^{57}Fe, ^{59}Co, ^{60}Ni, ^{65}Cu, ^{66}Zn, ^{75}As, ^{88}Sr, ^{89}Y, ^{90}Zr, ^{107}Ag, ^{109}Ag, ^{118}Sn, ^{121}Sb, ^{137}Ba, ^{139}La, ^{140}Ce, ^{153}Eu, ^{157}Gd, ^{172}Yb, ^{175}Lu, ^{178}Hf, ^{181}Ta, ^{197}Au, ^{205}Tl, ^{208}Pb, ^{209}Bi, ^{232}Th, and ^{238}U. For tourmaline, ^{9}Be, ^{31}P, ^{71}Ga, ^{85}Rb, ^{93}Nb, ^{111}Cd, ^{133}Cs, ^{141}Pr, ^{146}Nd, ^{147}Sm, ^{159}Tb, ^{163}Dy, ^{165}Ho, ^{166}Er, ^{169}Tm, and ^{182}W were also included. Data with poor-quality due to ablation across grain boundaries or inclusions were discarded during post-analysis processing using in-house proprietary data regression software.

6.5 Results

6.5.1 Chlorite

Chlorite samples analysed in this study can be divided into four groups based on the alteration styles: (1) chlorite veinlets in volcanic rocks; (2) quartz – chlorite – phengite ± pyrite ± bornite ± chalcopyrite assemblage; (3) magnetite – chlorite – altered breccia; and (4) chlorite vein in the Pink granite (Table 6.3). The first three chlorite groups are hosted within volcanic rocks of the CVC.

Table 6.3: List of chlorite samples analysed, with descriptions on the modes of occurrences.

Sample	Occurrence	Group
001 - 77.9	Chlorite veinlets in quartz – phyric rhyolite	Chl 1
002 - 103.3	Quartz – chlorite – phengite vein in K-feldspar - chlorite - altered rhyolite	Chl 2
004 - 92.1	Quartz - chlorite - sericite vein in intensely phengite-altered dacite	Chl 2
005 - 185.7	Chlorite - quartz veins in K-feldspar - chlorite -altered dacite	Chl 2
005 -387.7	Magnetite – chlorite - altered breccias in K-feldspar - altered rhyolite	Chl 3
MD069	Chlorite vein in the Pink granite	Chl 4

Two chlorite populations can be defined based on Fe-Mg compositions (Fig. 6.1): (1) Fe-rich (>230,000 ppm) in volcanic-hosted chlorites; and (2) relatively Fe-poor (<23,000 Fe) and Al-rich (>110,000 ppm) in the Pink granite. The chlorites from volcanic rocks show

negative correlation between Fe and Mg contents, which is typical for main-series chlorites, whilst those in the Pink granite show a weak positive correlation (Fig. 6.1). In the volcanic rocks, the chlorite Fe contents vary with different modes of occurrence. Chl 1 has the highest Fe content, followed by those in Chl 3 and Chl 4. The highest Mg content is reported in sample 005-185.7m from Chl 2. Occasional K-Ba-rich and Ti-Nb-rich inclusions are present. Analyses with significant inclusions were discarded during data processing. However, the presence of these minor inclusions typically has a negligible effect on the overall chlorite chemistry.

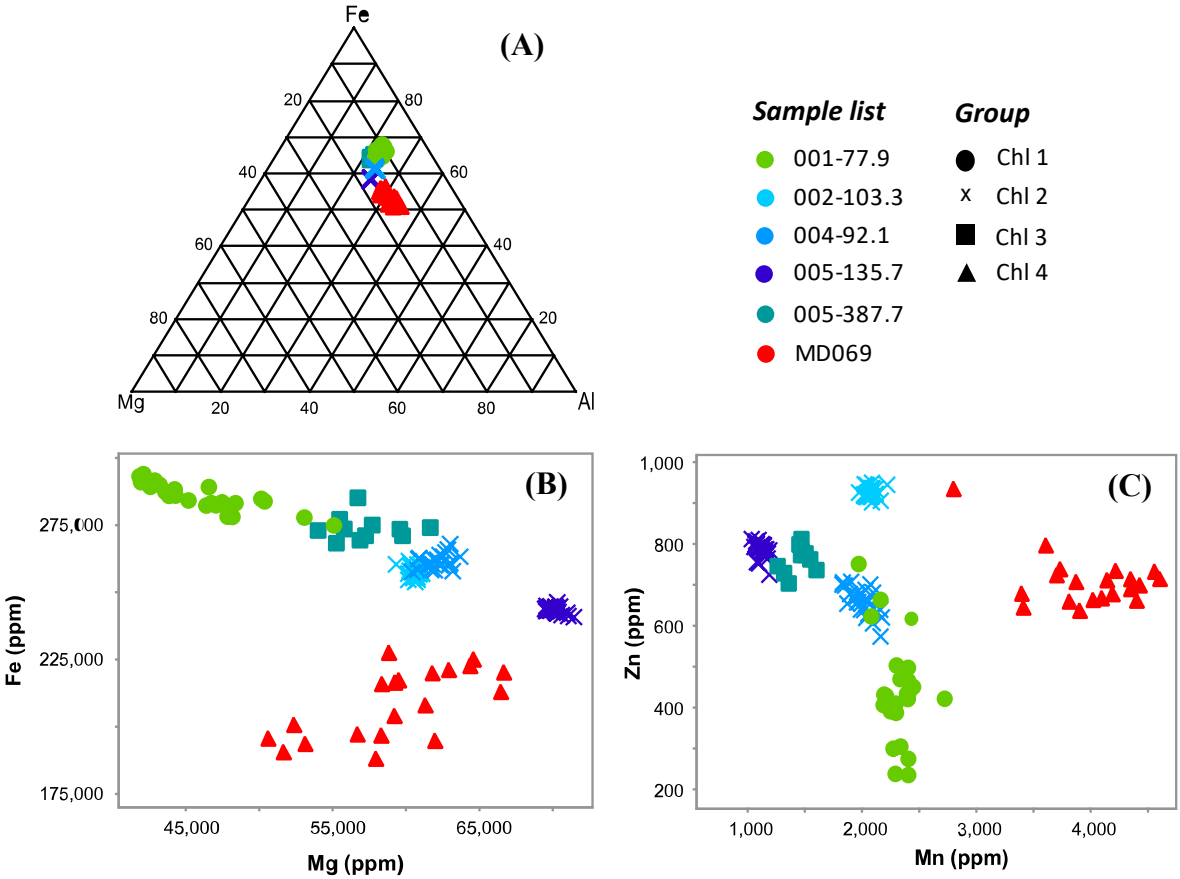

Figure 6.1: Major and minor element chemistry of chlorites from the Prince Darwin prospect. **(A):** Fe-Mg-Al ternary diagram of chlorite compositions. Pink granite-hosted chlorites (Chl 4) are more Al-rich compared to other chlorite analyses from this study. **(B):** Plot of Fe-Mg compositions in chlorite. Two distinct populations are clearly defined based on Fe contents within chlorite. **(C):** Plot of Mn-Zn compositions in chlorite Volcanic-hosted chlorites (Chl 1, 2 and 3) are comparatively Fe-rich and Mn-poor compared to Pink granite-hosted chlorites (Chl 4).

Mn, Zn, Ti, V and Ni (in decreasing order of abundance) are the most common trace elements found in chlorite, after the major elements. As, Ba, Cu, La, Li, Sn, Sr, Ti, Zr, U and Th were detected in more than three quarters of the analyses. Volcanic rock-hosted chlorites (Chl 1, 2 and 3) are generally Mn and REE-poor (Fig. 6.2). REE concentrations were typically below detection limit in all volcanic rock-hosted chlorites but were detectable in Pink granite chlorite analyses (Chl 4). The lowest Co (< 3 ppm) and Zn contents (200 – 700

ppm) are reported in Chl 1. Chl 3 are typically high in Ti, Zr and Sn and depleted in V (<22 ppm). Chl 4 is depleted in Ti and enriched in Li, Cr, Mn, Co, Cu, Sr, Ba, Pb, U, Th and REEs relative to analyses from volcanic samples.

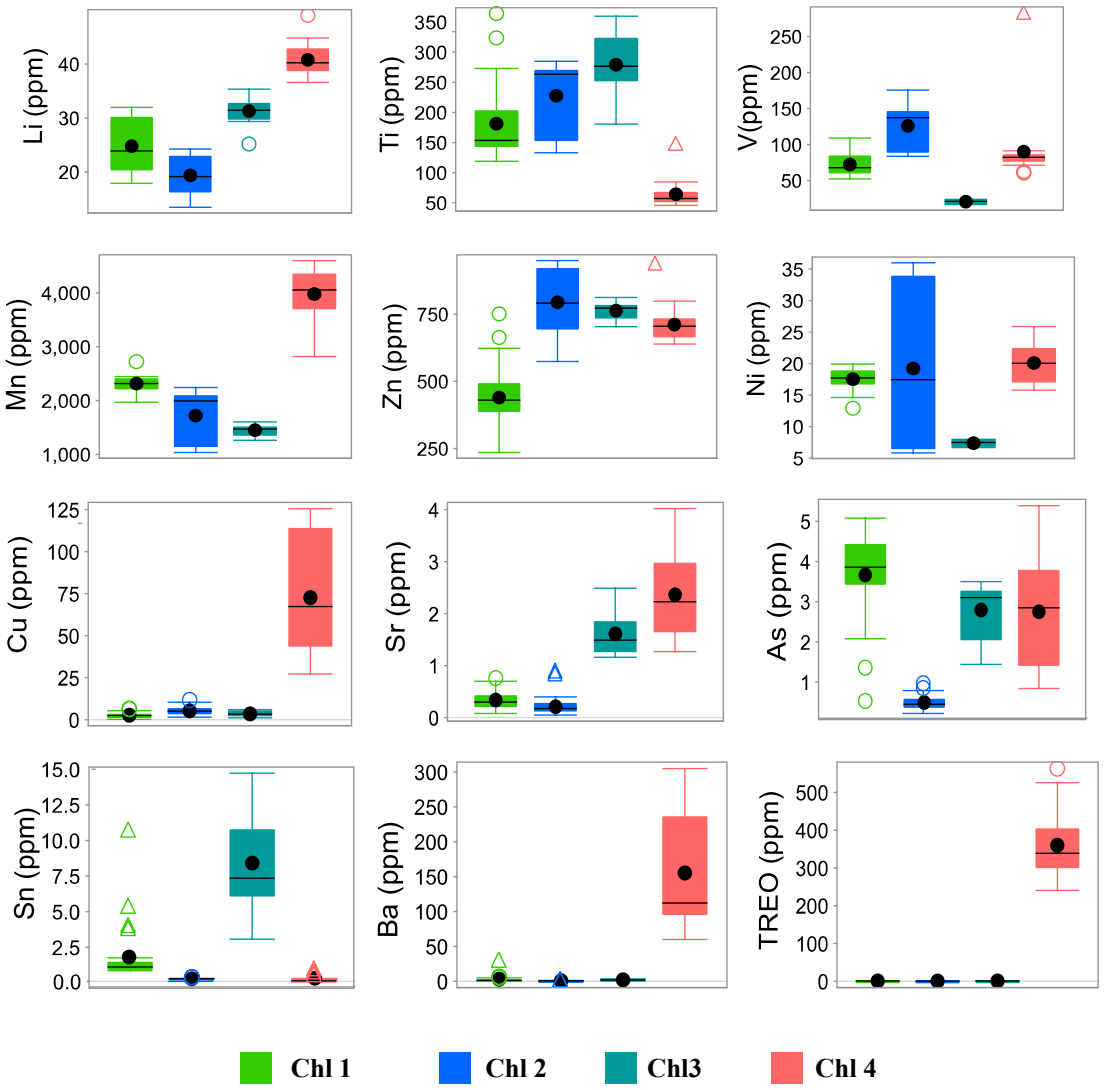

Figure 6.2: Tukey Box Plots of trace element compositions in chlorite groups defined in Table 6.3. Chl 4 analyses are notably enriched in rare earth elements compared to other chlorite groups.

6.5.2 Epidote-group minerals

Both allanite and epidote occur within hydrothermal veins in the Prince Darwin prospect. Allanite-bearing veins are confined to the dacitic volcanic rocks, whereas epidote-bearing veins are restricted to the Pink granite. Allanite invariably occurs with biotite, along with minor magnetite. LA-ICP-MS analysis has revealed the presence of K-Ba, Na-K, and Ce-La-rich inclusions in epidote. These inclusion-rich analyses were typically excluded from the final results due to their effects on the overall epidote or allanite chemistry.

Major element compositions of epidote correspond to epidote and allanite solid solutions. ICP-MS analyses show a clear systematic negative Ca-Fe and positive Al-Fe relationship in both minerals (Fig. 6.3). Allanite is typically more Fe-rich, Ca- and Al-poor compared to epidote. Ca contents in epidote (median 160,000 ppm) are twice as much as in allanite (median 88,000 ppm).

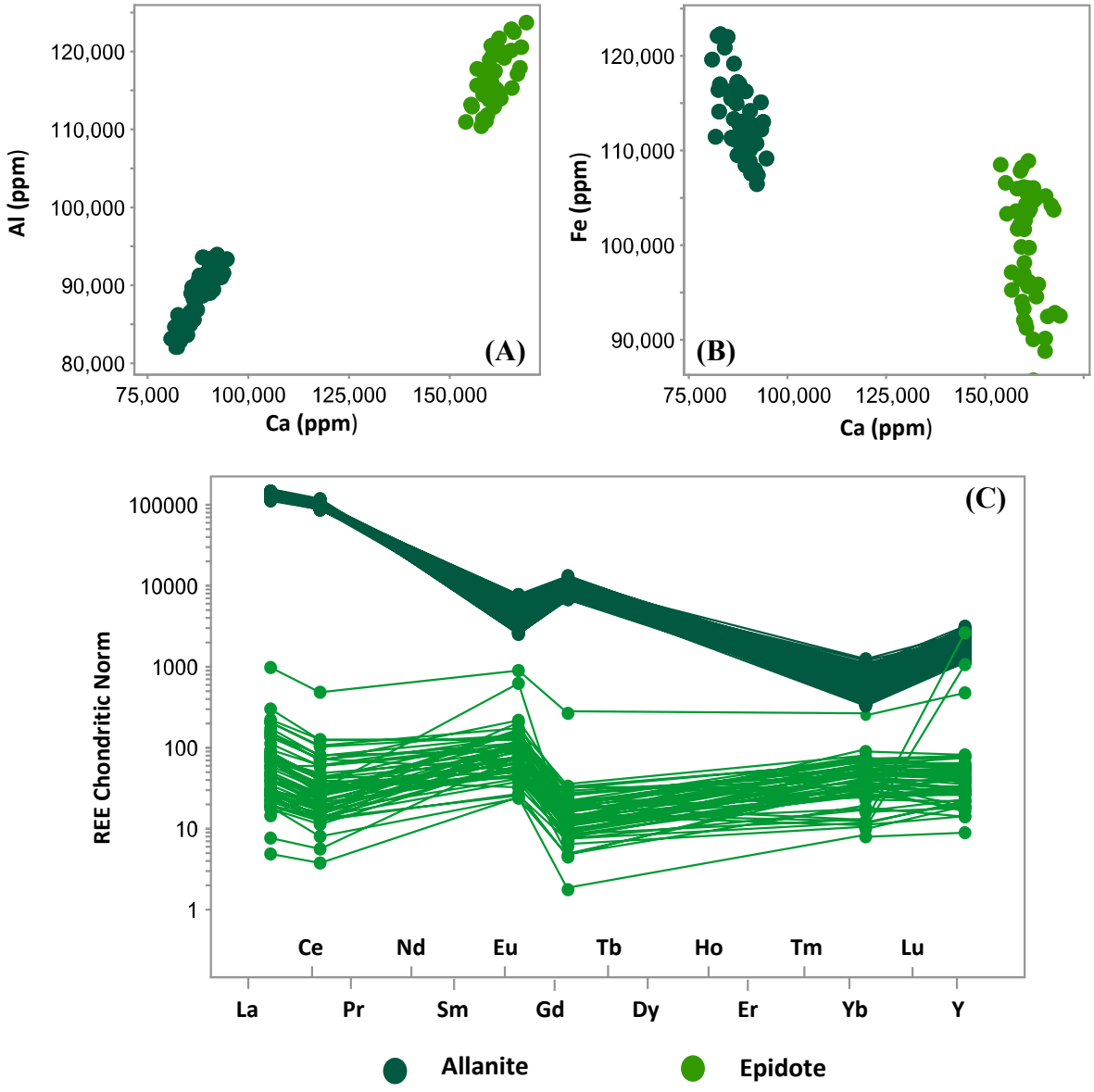

Figure 6.3: Bivariate plots of major element compositions of allanite (n = 172) and epidote (n = 53). **(A):** Ca vs. Al; and **(B):** Ca-Fe. Allanite is notably Al-poor, Ca-poor and Fe-rich relative to epidote. **(C)**: Normalised chondritic REE patterns of allanite and epidote. Normalising values after Taylor and McLennan (1985).

Rare earth elements are notably high in allanite and are typically present in concentrations between 10 to 100,000 ppm. Allanite is more enriched in LREEs relative to HREEs (Fig. 6.3C). REEs occur as trace element in epidote, with concentrations between 300 ppb to 460 ppm. It is also noted that allanite and epidote show different REE patterns, particularly the notable variation in Eu anomalies. Epidote from Prince Darwin shows

positive Eu anomalies, whereas allanite shows a negative anomaly (Fig. 6.3C). In addition to REEs, Mn and Sr the most abundant trace elements detected in both epidote and allanite (Fig. 6.4). Mn and Sr are generally lower in concentrations in allanite compared to epidote. Other trace elements detected in epidote and allanite, in decreasing order, include Ti, V, Th, Pb, U, As, Sb, Sn, Zn and Cu. In general, all allanite samples show a similar or narrow range in trace element concentrations, except for 004-29.4, which is particularly enriched in Ti, V, Cr and Cu. Ce in allanite correlates positively with Co, and negatively with Sn, Ce and U (Fig. 6.5A to D). Lanthanum broadly shows similar relationships with these elements, though the trends are relatively weak compared to Ce, except for Zn which shows weak negative correlation. A positive relationship between As and Sb is observed in epidote, but not in allanite (Fig. 6.5E). Allanite is notably depleted in Sb (<1 ppm) but enriched in As (median 90.8 ppm) relative to epidote (median 4.7 ppm).

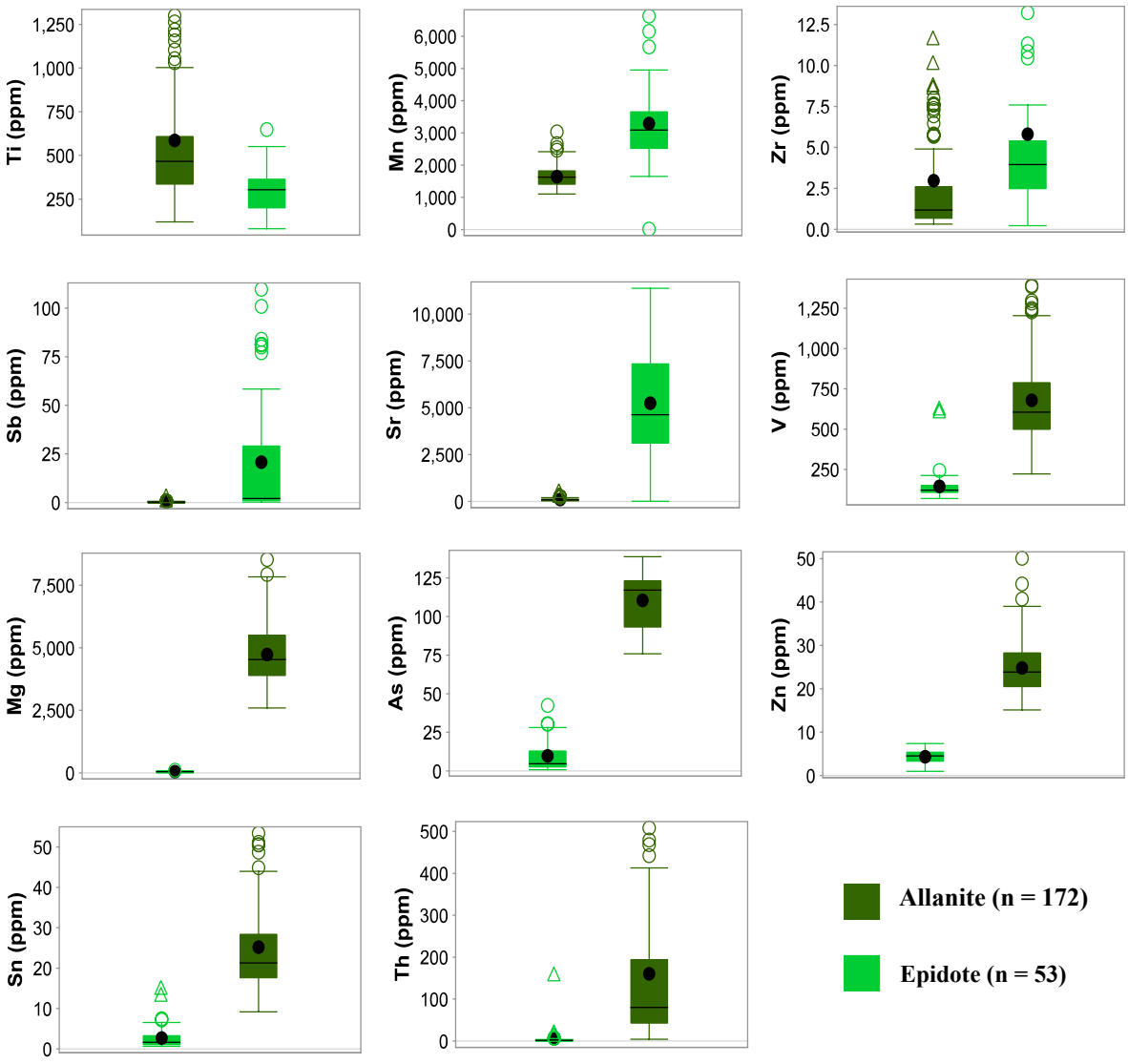

Figure 6.4: Tukey Box Plots of trace element compositions of allanite and epidote. The top two rows show the elements that are typically more enriched in allanite relative to epidote.

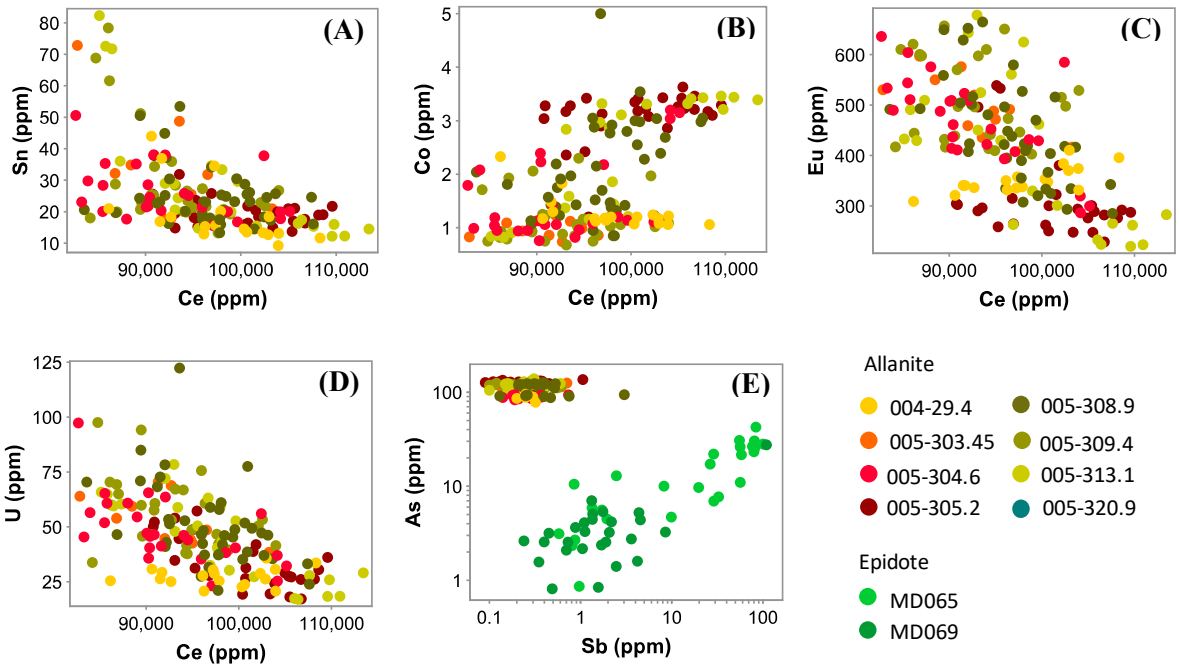

Figure 6.5: Minor and trace element compositions in allanite and epidote. **(A) to (D):** Bivariate plots of trace elements relative to Ce in allanite. **(E):** Comparative plot of Sb and As in allanite and epidote.

6.5.3 Tourmaline

Tourmalines analysed in this study can be grouped into three sub-types in terms of the mode of occurrence: (1) tourmaline-cemented breccias; (2) tourmaline vein in the White granite; and (3) tourmaline veins in volcanic rocks (Table 6.4).

Table 6.4: Tourmaline samples analysed in this study, including modes of occurrence.

Sample	Occurrence	Group
MD002	Tourmaline-cemented breccia in silicified aureole	Tur 1
MD007	Tourmaline cement / vein in brecciated White granite	Tur 2
MD018	Clast-bearing tourmaline vein in K-feldspar – magnetite – altered dacite	Tur 3
MD028	Tourmaline vein in K-feldspar – chlorite – altered rhyolite	Tur 3
SDD001-215.2m	Tourmaline cement / vein in K-feldspar-altered dacite	Tur 3
SDD004-207.9m	Tourmaline vein with bleached selvage in dacite	Tur 3
SDD005-53m	Tourmaline ± pyrite vein in albite ± chlorite- altered dacite	Tur 3

Major element compositions in tourmaline reflect the Fe – Al-Li – Mg solid solution series. Ternary Fe – Al-Li – Mg composition is plotted to reveal the compositional end-members of tourmaline at the Prince Darwin prospect and the result shows that the tourmalines are Fe-rich and Al-Li-rich, with the compositions intermediate between dravite and schorl (Fig. 6.6). Major element compositions of Tur 1 and 3 largely overlap in Fe, Al and Ca concentrations, except for Mg which is relatively depleted in Tur 1. Both Tur 1 and

3 form positive trends in Fe-Al and Fe-Mg diagrams (Fig. 6.6C and D). Tur 2, which is hosted in the White granite, is compositionally distinct from volcanic-hosted tourmalines (Tur 1 and 3) with elevated Ca and, Mg (Fig. 6.6).

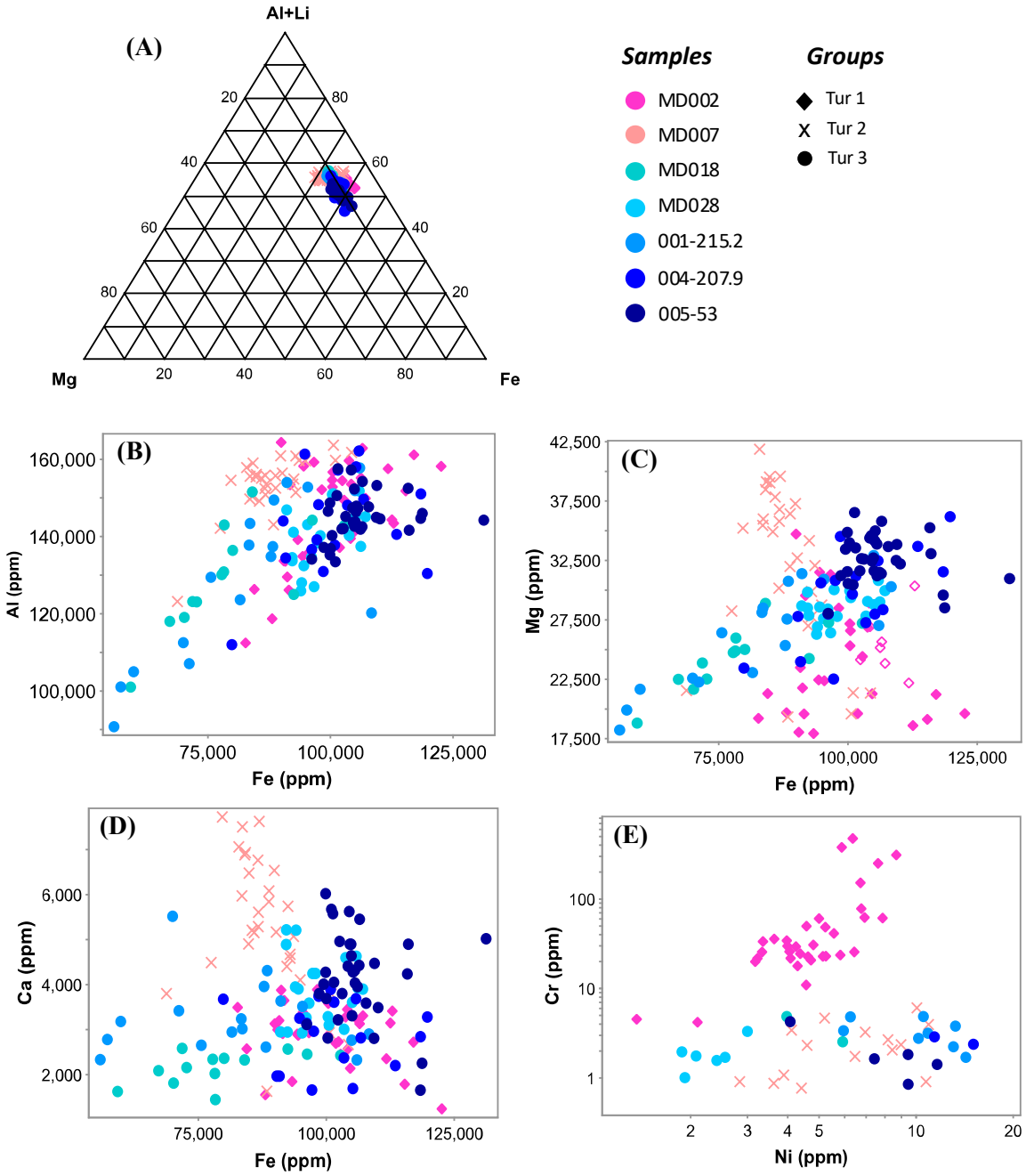

Figure 6.6: Major and minor element compositions of tourmaline from the Prince Darwin prospect. **(A):** Al+Li – Mg – Fe ternary diagram; **(B)** Al vs. Fe. **(B):** Al vs. Fe. **(C):** Mg vs. Fe. **(D):** Ca vs. Fe. **(E):** Cr vs. Ni.

Ti, P, Sn, Mn and Cu are the most common elements occurring (in decreasing order of abundance) after the major elements in tourmaline (Fig. 6.6). There is no large variation in trace element composition in tourmaline. Cr content in Tur 1 is notably higher compared to other groups, with variation up to two orders of magnitude (Fig. 6.6E). Tur 2 appears to contain a small amount of LREEs, which are typically present at concentrations between 2 ppm and 25 ppm, whereas REE concentrations are mostly below detection limit in volcanic-

Table 6.5: Trace element variations of different tourmaline subtypes at Prince Darwin. Abbreviation: BLD = Below detection limit.

Element (ppm)	Group 1	Group 2	Group 3
P	BDL–28.1	BLD–68.2	BLD–511
K	242–914	172–2,523	242–19,572
Ti	1,199–3,628	1,060–2,479	455–3,950
Cr	4.20–476	BLD–6.07	BLD–4.87
Mn	94.5–219	119–442	68.1–1,400
Sr	55.5–150	69.5–139	72.0–337
Cu	BDL–4.82	BLD–4.29	BLD–513
Sn	50.6–1,624	11.9–216	544–1,469
Zr	0.34–13.9	0.15–2.10	1.02–39.2

hosted tourmalines. P was detected in two dacite-hosted tourmaline samples (004-207.9 and 005-53) from Tur 3, with a median concentration of 300 ppm. The rhyolite-hosted tourmaline vein sample (MD028) is generally more enriched in Ti, Sr, Zr and Mo relative to the other tourmaline samples (Appendix F).

6.6 Discussion

Chlorite

The compositional differences in chlorite reflect the different modes of occurrences. Chlorites at Prince Darwin are predominantly Fe-rich, with an exception of the Pink granite-hosted chlorite (Chl 4). The Al-, Li-, Si- and Na-enrichments in Chl 4 are likely to reflect protolith chemistry of the Pink granite. The comparatively high REE contents in Chl 4 relative to other groups are probably attributed to the leaching of granite by hydrothermal fluid flux.

Mg-rich chlorite is favourably formed under oxidised and lower pH conditions, whereas relatively reduced and higher pH conditions are more favourable for the formation of Fe-rich chlorite (Inoue, 2010). Fe/(Fe+Mg) in chlorite provides an alternative approach to compare the fO_2 conditions of the fluids in chlorite-bearing rocks. The higher the values, the more reduced the conditions of formation. This suggests that chlorite veins of Chl 2 and 4 were formed under relatively oxidised and acidic condition relative to those from Chl 1 and 2 (Table. 6.6).

Table 6.6: Fe/(Fe-Mg) ratios for investigated chlorite samples. Abbreviations

Sample	Occurrences	Fe/(Fe+Mg)	Group
001-77.9	Chlorite veinlets in quartz – phyric rhyolite	0.86	Chl 1
004-92.1	Quartz – chlorite – phengite vein in K-feldspar - chlorite - altered rhyolite	0.81	Chl 2
002-103.3	Quartz - chlorite - sericite vein in intensely phengite-altered dacite	0.81	Chl 2
005-185.7	Chlorite - quartz veins in K-feldspar - chlorite -altered dacite	0.78	Chl 2
005-387.7	Magnetite – chlorite - altered breccias in K-feldspar - altered rhyolite	0.83	Chl 3
MD069	Chlorite vein in the Pink granite	0.78	Chl 4

Formation of veins are commonly the results of open space precipitation from hydrothermal fluids. The compositions of the precipitated minerals are therefore strongly controlled by the fluid chemistry, pH, temperature, oxygen fugacity, and to lesser extent, the fluid-wallrock interaction. Vein minerals are commonly depleted in fluid immobile elements (e.g., Ti, Nb, Sc, Ga, V, Co, Ni and Cr) and enriched in fluid mobile elements (e.g., Th, Pb and Sr; Wang et al., 2018), which is consistent with chlorite data from the Pink granite (enrichment in Ti, Nb, V and Cr, depletion in Th, Pb and Sr). However, depletion-enrichment patterns of these elements are not observed in Chl 1 and 2, possibly due to the remobilisation or sequestration of these elements during fluid migrations or later alteration events.

Previous studies have demonstrated that titanium in chlorite can be a potential exploration vectoring tool, with Ti enrichment in chlorite proximal to the porphyry centre (e.g., Batu Hijau, Indonesia: Wilkinson et al., 2015; El Teniente, Chile: Wilkinson et al., 2017; Yangdong, China: Xiao et al., 2017). Wilkinson et al. (2015) proposed that the Ti substitution into chlorite in Batu Hijau is thermally controlled. However, this variation trend is not observed at Prince Darwin prospect. This suggests that temperature may not be the major control in Ti substitution into chlorite at Prince Darwin. Protolith chemistry is most likely the principal factor in controlling the substitution of Ti in chlorite (Fig. 6.7), with Ti enrichment in intermediate protoliths (dacite) relative to the felsic protoliths (rhyolite and Pink granite). Other factors such as the redox condition and the pH of the fluids may also influence the incorporation of Ti into chlorite. However, evaluation of their roles will be hard due to complex interplay between these two parameters in propylitic zone. Similar variation trends were observed in Niujian Ag-Au-Pb-Zn deposit in China (Wang et al., 2018). The strong protolith control on the chlorite chemistry suggests that an assessment on chlorite utilities as an orebody vectoring tool needs to be done in the same lithotype.

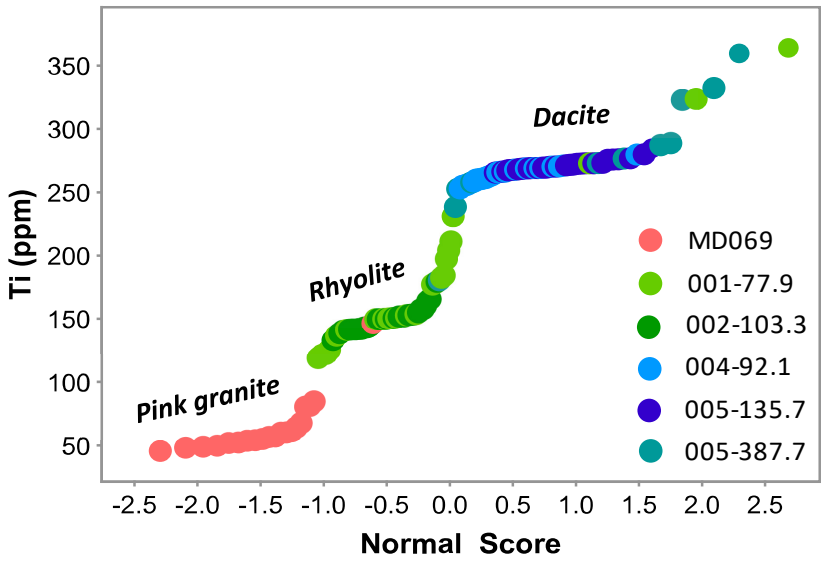

Figure 6.7: Titanium concentration in chlorite from different lithotypes at Prince Darwin. The concentration typically increases with decreasing SiO_2 content within the host rocks.

Epidote and allanite

Overall, allanite is comparatively depleted in Al, Si and Ca and enriched in Mg, Fe, Th and REEs relative to epidote. The depletion and enrichment of these major elements and REEs are related to the coupled substitution of $Ca^{2+} + (Al, Fe)^{3+} \leftrightharpoons REE^{3+} + Fe^{2+}$ (Franz and Liebscher, 2004; Gieré and Sorensen, 2004; Armbruster et al., 2006), though the relative proportion of Fe^{3+} and Fe^{2+} is unknown. The substitution can also involve $Ca^{2+} + Si^{4+} \leftrightharpoons REE^{3+} + Al^{3+}$ and $3\ Ca^{2+} \leftrightharpoons 2\ REE^{3+}$ without the involvement of Fe (Burt, 1989; Sokolova et al., 1991; Peterson and MacFarlane, 1993; Mitchell, 1996; Campbell et al., 1997; Holtstam et al., 2003; Gieré and Sorensen, 2004). HREEs, relative to LREEs, are more preferentially incorporated into epidote crystal lattice.

Allanite at the Prince Darwin prospect is typically enriched in LREE relative to HREE and is predominantly allanite-(Ce), with narrow range of compositional variation. Allanite in the study area is also characterised by low Mn. The Mn-poor character contrasts with the Mn-rich allanite from Japanese Granitoids in continental margins and intracontinental settings (e.g., Peterson and MacFarlane, 1993; Broska et al., 2000; Smith et al., 2002; Oberli et al., 2004; Hoshino et al., 2006). The presence of Mn-poor allanite implies that the Darwin granite belongs to the magnetite series (Ishihara, 1981; Takagi, 2004; Hoshino et al, 2006; Ishihara et al., 2011), supporting the interpretation of the geochemical classification of the Darwin granite (Chapter 5). The magnetite series character suggests that the hydrothermal or mineralising fluids are derived from an oxidised magma source and are responsible for the widespread magnetite alteration in the prospect.

Previous studies have proposed that an appreciable amount of REEs can be mobilised by hydrothermal processes (Alderton et al., 1980; Gieré, 1986, 1990; Costantopouios, 1988; Mean, 1990; Wood, 1990; Haas et al., 1995; Lewis et al., 1998). The ligands involved in carrying REEs still remain controversial. Occurrences of allanite at Prince Darwin are generally associated with biotite, fluorapatite, carbonate, monazite, magnetite, quartz, and, but less commonly, thorium oxide, as revealed by SEM and petrological studies. The mineral occurrences are largely consistent with those documented in Olympic Dam in Australia (Alderton et al., 1980; Costantopouios, 1988), Bagjata Uranium Mine in India (Pal et al., 2011) and Stupné in Slovakia (Uher et al., 2015). Similar mechanisms may account for the REE mineralisation. The mineralogy also suggests that REE mineralisation is potentially associated with K-, Fe-, F-, P- and Ca-rich fluids.

Arsenic, Sb and Th show remarkable variation in concentrations in allanite and epidote, with variations up to two orders of magnitude. The relative Th and As enrichment in allanite implies preferential substitution of these elements. Several authors have proposed a mechanism for Th substitution into allanite, using the following equations (Gromet and Silver, 1983; Gieré et al., 1999; Wood and Ricketts, 2000):

(1) $$Th^{4+} + Fe^{2+} \leftrightharpoons REE^{3+} + Fe^{3+}$$

(2) $$Th^{4+} + Fe^{2+} \leftrightharpoons REE^{3+} + Al^{3+}$$

(3) $$Th^{4+} + Ca^{2+} \leftrightharpoons 2\ REE^{3+}$$

(4) $$Th^{4+} + 2\ Fe^{2+} \leftrightharpoons Ca^{2+} + 2\ Fe^{3+}$$

The mechanism of Th incorporation into allanite at Prince Darwin requires more work, as equations (1) to (3) were proposed for an Mg-free system (Gieré et al., 1999), which is unlikely to be the case at Prince Darwin given the prevalence of chlorite alteration across the region. There is no significant variation in U concentrations between epidote and allanite. This suggests that U is equally incorporated into both phases. The higher Th contents relative to U suggests that Th is more preferentially partitioned into allanite relative to U. Positive correlation between As and Sb in epidote implies that they were incorporated into epidote crystal structure together. In contrast, there is no relationship between As and Sb substitution in allanite. This indicates that the substitution of As is independent of Sb, and As incorporation into allanite is more favoured.

The varied multielement trends between allanite and epidote suggest that they were formed from different sources (Fig 6.8). Epidote shows some similar REE characters with White granite (Figure 6.8A). The REE patterns of allanite, however do not conform with the

trends of Darwin granite. but is more comparable with the volcanic rocks and quartz porphyry which have been interpreted to have had co-magmatic relationship in Chapter 5. This suggests that quartz porphyry may be the potential source of REEs responsible to the REE-rich mineralisation at Prince Darwin.

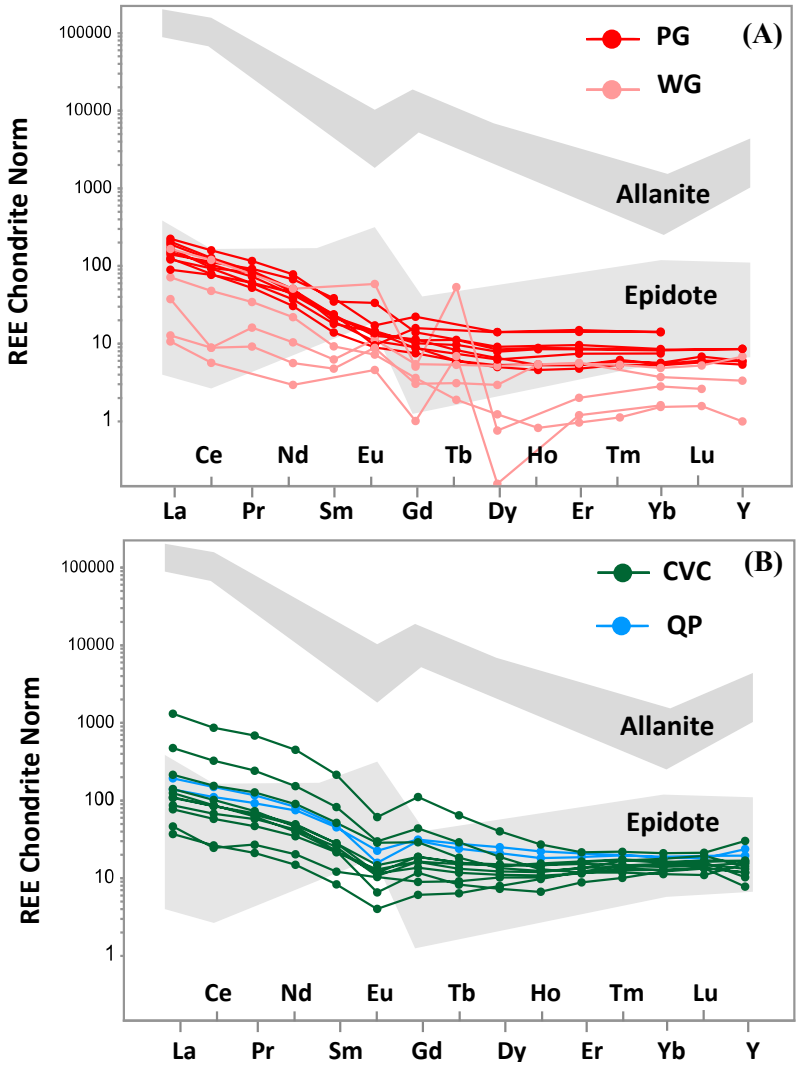

Figure 6.8: REE patterns of allanite and epidote relative to the volcanic and intrusive rocks at Prince Darwin. **(A):** Pink (PG) and White granite (WG). **(B):** Volcanic rocks (CVC) and quartz porphyry (QP). Compositional field of allanite and epidote are coloured and labelled in the plots. Allanite is more enriched in LREEs relative to HREEs, whereas LREEs and HREEs show similar concentrations in epidote. Normalising values after Taylor and McLennan (1985).

Europium anomalism in epidote group minerals can be an indicator of redox conditions (Wilkinson et al., 2015). Eu^{3+} typically behaves similar to other REE^{3+} cations in oxidised fluids. Epidote from Prince Darwin shows positive Eu anomalies, whereas allanite shows a negative anomaly (Fig. 6.8). The positive Eu anomalies in epidote indicate the oxidising nature of fluids responsible for epidote formation. As previously discussed, allanite at Prince Darwin formed from oxidised fluids, given by the Mn-poor character. The negative Eu anomaly is likely due to one or both of the following reasons: (1) Eu, together with other

HREEs, was attained in the fluids while LREEs were incorporated into allanite, monazite and apatite; and (2) selective removal of Eu during later alteration (e.g., Alderton et al., 1980).

Tourmaline

Overall, tourmalines from Prince Darwin are primarily schorlitic to dravitic in composition, though there are some compositional variations. Previous studies have established that the major element compositions of tourmalines formed in hydrothermal environments may broadly correspond to the chemistry of the host rocks (London and Manning, 1995; Slack and Trumbull, 2011; Albert et al., 2018).

Tourmaline in hydrothermal breccia cement (Tur 1) shows considerable variation in chemical composition, particularly for Mg. This variation may imply multiple episodes of fluid associated with the two-stage emplacement of the Darwin granite. Consequently, there may be a progressive change in fluid chemistry (from Mg-rich to Mg-poor) that is responsible for the element variability seen in Tur 1. Similar Fe and Ca compositions, and partial overlap in Mg composition between Tur 1 and 3 suggest that they may initially share similar hydrothermal origin, which is most likely sourced from the Pink granite. The Mg depletion in Tur 1 is probably due to several reasons: (1) White granite-derived hydrothermal fluids which came in later were Mg-poor. This may be supported by the lack of Mg-bearing phases in the White granite; (2) Mg has been sequestered by Tur 2 (and potentially Tur 3), evident by Mg-enrichment in those sub-types. In addition, both Tur 1 and 2 show negative correlations in Fe-Mg diagrams (Fig. 6.6C) and the trends of these two groups may represent a continuum in terms of fluid evolution; and (3) Mg was preferentially taken up by biotite – allanite and chlorite alteration in the CVC and Pink granite. The interpretation of a multi-stage evolution in hydrothermal fluids also seems to be true for Tur 3. Field observations of widespread occurrences of tourmaline veins in the Darwin granite and CVC and cross-cutting relationships with magnetite veins (Chapter 4) suggest a dynamic system with a minimum of two generations of tourmaline crystallisation.

In terms of trace elements, there is no distinct variation between the tourmaline sub-groups, except for high Cr in Tur 1. Chronium is unlikely to have been transported by fluids as it is a transition metal and fluid immobile element (Humphris and Thompson, 1978). The high Cr in Tur 1 is therefore likely to reflect the strong control of protolith chemistry on the tourmaline composition. However, the lithotype could not be positively identified as the host rocks were all intensely silicified.

All tourmaline groups at Prince Darwin show positive Eu anomalies (Fig. 6.9). White granite-hosted tourmalines (Tur 2) are more enriched in LREEs relative to HREEs, whereas the volcanic-hosted tourmalines are more depleted in LREEs. This suggests that the White Granite may be the potential fluid source account for formation of Tur 2. The enrichment in LREEs relative to HREEs in tourmaline contrasts with REE trends in all intrusive and volcanic rocks identified in the study area. The depletion in LREE relative to HREE in volcanic-hosted tourmalines (Tur 3) may be account for the removal of LREE during biotite – allanite formation.

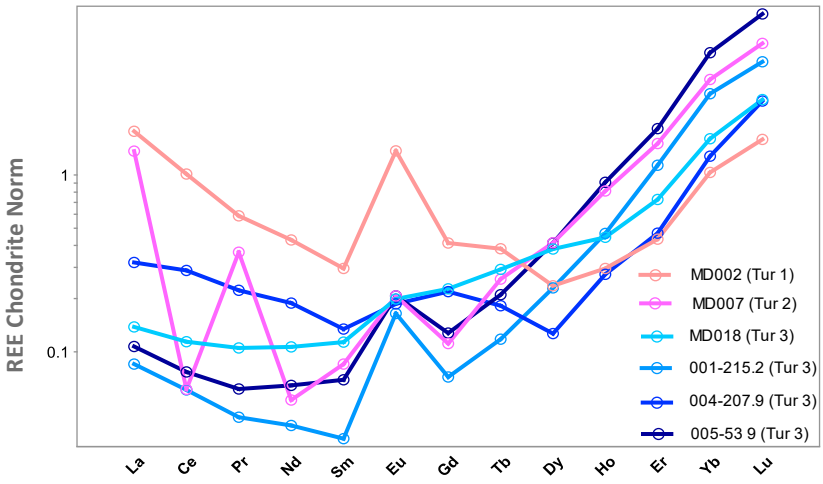

Figure 6.9: Multi-element diagram for tourmaline sub-groups at Prince Darwin. Median values of the REE contents for different tourmaline groups are illustrated. Normalising values from Taylor and McLennan (1985).

In terms of vectoring, few trace elements in Tur 3 (volcanic-hosted) show good spatial variation. For example, distal tourmalines appear to be enriched in Zn, Zr, Hf, W, Pb, Th, U and depleted in Na, Mn, Ni, Ga, Sn, Yb, Lu and Ta, even over such a short distance (Fig. 6.10). Given that the ore grades gradually increase with depth as reported by Corona Minerals (2011), CVC-hosted tourmalines may be potential in vectoring towards higher-grade mineralisation. Nevertheless, there is a lack of confidence in assessing the potential of tourmaline trace elements in this study. More samples are required to assess the potential of tourmalines as proximitor with higher confidence.

6.7 Summary

Mineral chemistry of key hydrothermal alteration minerals at the Prince Darwin prospect reveal that multiple episodes of hydrothermal fluid flow were associated with the two-stage emplacement of the Darwin granite. Minerals from different alteration stages have distinct geochemical compositions, which provides insights into the potential chemistry of the associated hydrothermal fluids. The Mn-poor character of allanite and positive Eu

anomalies in epidote and tourmaline suggest an oxidised nature of the hydrothermal fluids affecting the Prince Darwin.

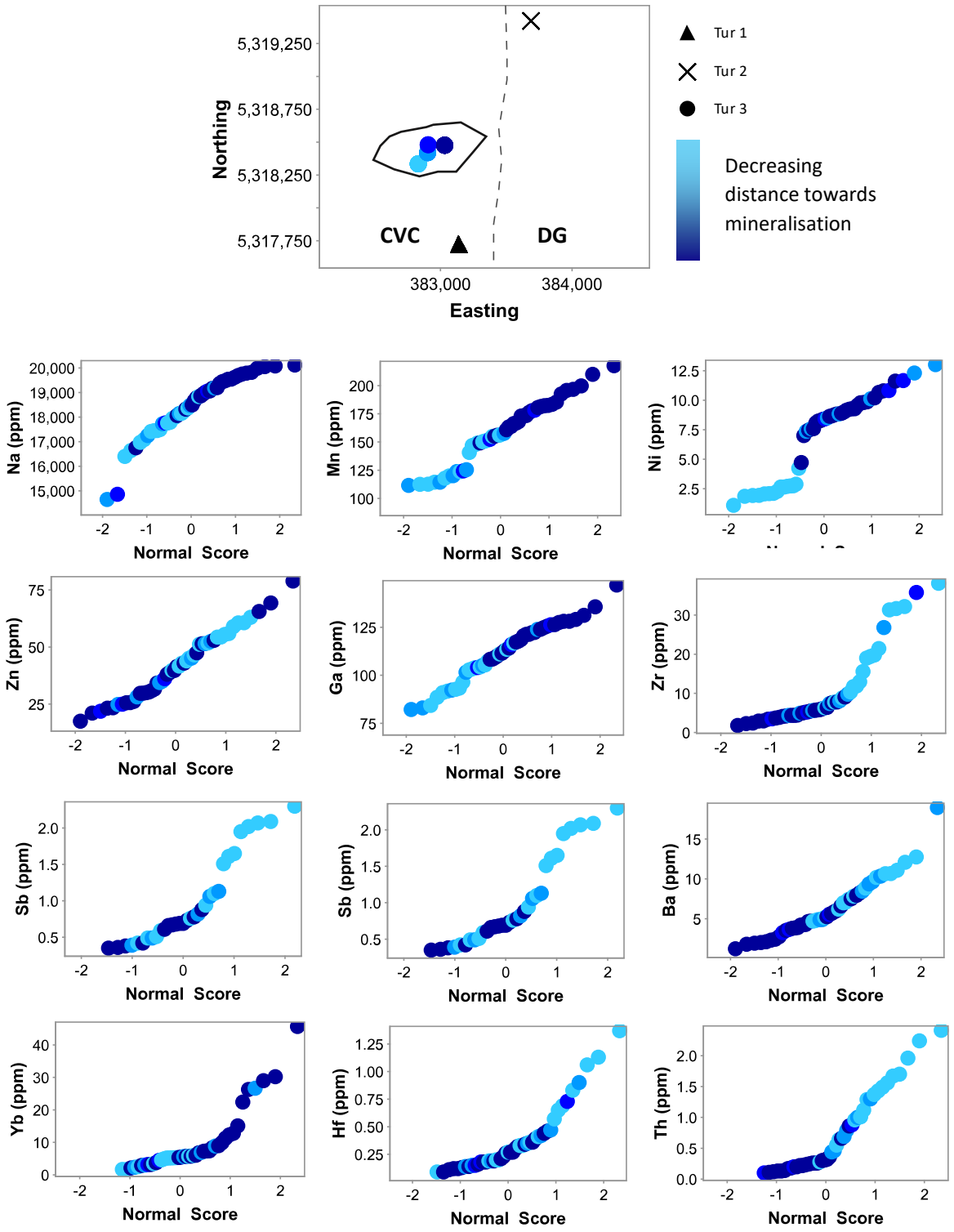

Figure 6.10: Variation of trace elements in tourmalines at Prince Darwin. Areas with known occurrences of mineralisation are outlined for reference. The dashed-line represents the contact between the Central Volcanic Complex (CVC) and Darwin granite (DG). Symbol colours are equivalenet to the distance from the Darwin granite. The darker the symbol, the further it is from mineralisation. The attribute map shows the locations of investigated tourmaline samples, followed by twelve probability plots of trace elements in volcanic-hosted tourmalines. Tur 1 and 2 are excluded from the probability plots to avoid protolith controls on the assessment. Zn, Zr, Hf, W, Pb, Th and U are generally more enriched in distal tourmalines, whereas enrichment of Na, Mn, Ni, Ga, Sn, Yb, Lu and Ta occura within tourmalines proximal to the Darwin granite.

Chapter 7

Sulfur Isotopes

7.1 Introduction

This chapter presents the sulfur isotopic compositions of pyrite from the Prince Darwin prospect to determine the potential sources of ore-forming fluids and constrain the physicochemical environment of mineralisation. Data from this study were plotted in Leapfrog 3D in order to visualise and interpret any sulfur isotopic zonation.

7.2 Sampling and analytical methods

Twelve pyrite samples were submitted for sulfur isotopic analysis. All pyrite samples were from volcanic rocks, as no pyrite was observed in any of the intrusive phases. Eleven of the pyrite samples were collected from drill holes and one from surface. The intense weathering of outcrops precluded an effective pyrite surface sampling campaign. The analysed samples were constrained to pyrite-bearing rocks associated with magnetite – apatite – tourmaline alteration and quartz – chlorite – phengite veins. In some samples, chalcopyrite preferentially replaced pyrite along fractures, resulting in possible contamination in the analysis. Samples where this was observed have been noted in the results. Careful selection and sampling of coarse-grained pyrite allowed preparation of 1–5 mg of pyrite powders by hand drilling using a *Dremel Multipro 225 T2 Flex-shaft drill*. Visible impurities were discarded if present. The powders were submitted to the CSL, University of Tasmania and were analysed by conventional methods using the techniques of Robinson and Kusakabe (1975). Isotopic measurements were performed on a *VG Sira Series II mass spectrometer*, with an estimated analytical uncertainty of ±0.2‰.

7.3 Overview of sulfur isotopes

Systematic studies of sulfur isotopes have been crucial to understanding the evolutionary processes of magmatic-hydrothermal systems and ore genesis. A number of

studies have been carried out in many porphyry-epithermal systems from around the world (e.g., Müller et al., 2002; Field et al., 2005; Cooke et al., 2011; Mao et al., 2011; Alizadeh Sevari and Hezarkhan, 2014; Jo and Shin, 2015). More recently, systematic sulfur isotopic zonation around mineralised centres have been observed in several porphyry-epithermal deposits (e.g., Mt Polley, Columbia: Deyell, 2005; Cadia, Australia: Wilson et al., 2007; Didipio, Philippines: Wolfe and Cooke, 2011; Golpu, Papua New Guinea: Rinne et al., 2018; Wainaulo, Fiji: Orovan et al., 2018), implying that sulfur isotopes have potential use in vectoring in mineral exploration.

Seal (2006) summarised the range of sulfur isotopic values in different natural sulfur reservoirs (Fig. 7.1). Isotopic variations in hydrothermal ore deposits depends upon the physicochemical conditions of the magmatic-hydrothermal systems (e.g., redox, pH, and temperature), the nature of the progenitor intrusion, and mixing with external water (Ohmoto, 1986; Rollinson, 1993; Seal, 2006). For example, sulfur isotopes in Cu-Au-Mo porphyry systems, which are commonly associated with I-type (oxidised) granitoids, are generally more varied due to the presence of both oxidised (SO_2) and reduced (H_2O) sulfur components in sub-equal proportion, as opposed to the H_2S-dominated Sn-W porphyry systems associated with S-type reduced granitoids (Burnham and Ohmoto, 1980; Seal, 2006). Probable processes on controlling the sulfur isotopic values in hydrothermal deposits are reviewed in details by Ohmoto (1986), Rollinson (1993), Seal et al. (2000), Field et al. (2005), Rye (2005), Seal (2006) and Shanks (2013).

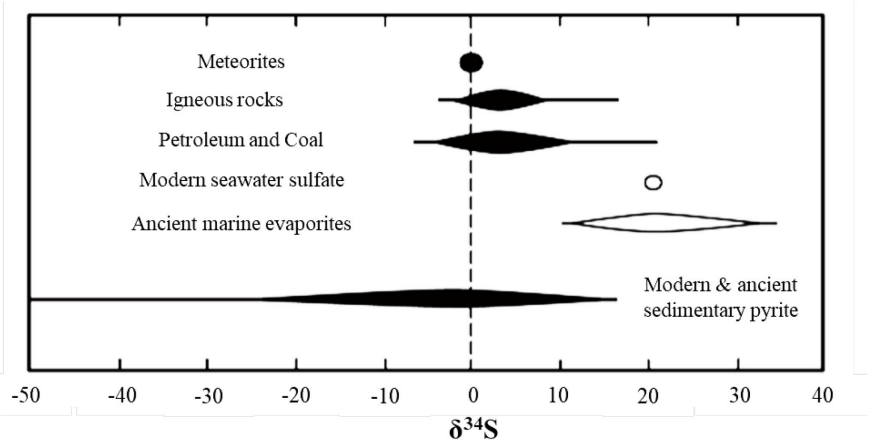

Figure. 7.1: Range of $\delta^{34}S$ values of different geologic reservoirs (Seal, 2006).

7.4 Previous work in the district

Sulfur isotopic studies of hydrothermal minerals have been previously carried out for several deposits and prospects associated with the Darwin granite (e.g., Solomon et al., 1988;

Green et al., 1981; Poyle et al., 1986; Eastoe et al., 1987; Jones, 1993; Gadaloff, 1996; Wyman, 2001). The study by Eastoe et al. (1987) summarised pyrite $\delta^{34}S$ values from the Mt. Darwin region, which range from +7 to +16.5‰ (Table 7.1). A general trend of increasing $\delta^{34}S$ values with increasing distance from the Darwin granite was interpreted by Jones (1993), although Wyman (2001) refuted this zonation pattern.

Table 7.3: Summary of $\delta^{34}S$ values obtained across Jukes–Darwin district.

Reference	Region	Mineral	$\delta^{34}S$ value (‰)
Solomon et al., 1986	Findons	Pyrite	+13.6–17.5
	Prince Darwin and area	Pyrite	+8.6–16.3
	(South-southwest of Prince Darwin)	Pyrite	+12.4, +13.5
	(Near Prince Darwin Audit)	Pyrite	+12.6
	Darwin granite and contact area	Pyrite	+9.3–13.5
	Near Mount Darwin	Pyrite	+11
Doyle, 1990	Central Complex Rhyolites	Pyrite	+11.0–11.7
	Central Complex Rhyolites	Chalcopyrite	+10.8
Jones, 1993	Darwin granite	Pyrite vein	+9, +14.5
	Darwin granite	Barite	+29.0
	East Darwin	Diss. Pyrite	+13.4, +14.3
Wyman, 2001	Mt. Darwin	Pyrite	+8.0 –17.0
	Darwin granite (whole rock)		+12.7
	Prince Darwin prospect		
	Population 1	Pyrite	+7.1–9.3
	Population 2	Pyrite	+10.3–17.0
	Jukes Prospect		
	Adits	Pyrite	+10.5–13.5
	Altered feldspar-phyric dacite	Pyrite	+10.8–15.7
	Altered quartz-phyric dykes	Pyrite	+11.3–19.0

Jones (1993) interpreted that the progressively heavier $\delta^{34}S$ values away from the Darwin granite is due to the increasing input of reduced Cambrian seawater sulfate ($\delta^{34}S$ ~30‰; Claypool et al., 1980) compared with magmatic sulfur in the hydrothermal fluids. The lower $\delta^{34}S$ values in the vicinity to the Darwin granite represent the maximum proportion of magmatic to seawater sulfur in the fluids. Similar $\delta^{34}S$ values have been obtained from sulfides from many of the VHMS deposits in the Mount Read Volcanics (+8 to +15‰; Solomon et al., 1988).

7.5 Results

Twelve pyrite samples from the Prince Darwin prospect have been analysed in this study and the results are listed in Table 7.2. There is a broad range in isotopic values from +8.6 to +15.8‰. A significant variation in $\delta^{34}S$ values is observed with respect to different alteration and vein stages. Heavier $\delta^{34}S$ values (>+13‰) are associated with pyrite from late-stage quartz – chlorite – phengite veins; whereas, sulfur isotopic values ranging from +10–13‰ are associated with pyrite from early-stage magnetite – apatite – tourmaline alteration. In broad terms, the $\delta^{34}S$ values increase from early-stage alteration to late-stage alteration. The lowest $\delta^{34}S$ value (+8.6‰) reported in this study is from carbonate vein-hosted pyrite.

Table 7.4: List of sulfur isotopic data from Prince Darwin pyrite.

Sample	Easting (m)	Northing (m)	RL (m)	Occurrence	$\delta^{34}S$ (‰)
MD062	383239	5318508	739	Pyrite in chlorite – muscovite schist	+13.5
SDD001-80.9	382861	531850	509	Pyrite ± chalcopyrite clot in magnetite ± chlorite-altered volcanics	+10.5
SDD001-199.8	382898	5318429	427	Pyrite veins in magnetite-cemented volcanic breccia	+14.0
SDD001-215	382902	5318419	417	Pyrite in magnetite cement	+12.2
SDD001-320	382930	5318344	349	Pyrite in magnetite vein	+10.8
SDD002-25.8	382849	5318328	620	Pyrite in magnetite cement	+10.3
SDD004-83.2	382996	5318475	681	Pyrite in magnetite replacement band at dacite-rhyolite contact	+9.7
SDD004-195.5	382915	5318479	604	Pyrite veins in K-feldspar – chlorite-altered dacite	+14.4
SDD005-41.9	383037	5318475	703	Pyrite vein in magnetite-altered dacite	+13.9
SDD005-185.7	382969	5318479	576	Pyrite – chlorite vein	+15.8
SDD005-320.9	383900	5318487	460	Pyrite in carbonate vein hosted in biotite – allanite-altered volcanic rock	+8.6
SDD005-356.3	382880	5318488	431	Pyrite in magnetite replacement band at dacite-rhyolite contact	+ 10.7

7.5 Discussion

The $\delta^{34}S_{pyrite}$ values in the Prince Darwin prospect extend well above the typical range of porphyry Cu deposits ($\delta^{34}S_{sulfide}$: -3 to +1‰; Seal, 2006). The heavy sulfur isotopic

composition (>+8.6‰) precludes the dominance of a magmatic source and suggests alternative sulfur sources were in involved during the evolution of the system.

$\delta^{34}S$ values from various types of ore deposits hosted in MRV (e.g., VHMS, epithermal and porphyry) are summarised in Fig 7.2. Solomon et al. (1988) noted that there is an increase in $\delta^{34}S$ values within the Darwin granite and volcanic rocks: +9.3–13.5‰ in the Darwin granite, +7.1–16.3‰ in the CVC near its contact (+7 to 9‰ within metres of the contact) and +11–15.8‰ in the contiguous CVC rocks. Similar zonation in $\delta^{34}S$ has also been observed around the Murchison granite (Polya et al., 1986). In general, the $\delta^{34}S_{pyrite}$ values obtained in this study (+8.6–15.8‰) are within the range of values from previous studies across the Jukes-Darwin area (+7 to +17‰) and similar to many other Cambrian hydrothermal deposits hosted in the MRV, suggesting they share a similar origin of sulfur. The high $\delta^{34}S_{pyrite}$ values in the Prince Darwin prospect, including other prospects hosted within the MRV, are most likely due to the involvement of reduced Cambrian seawater.

A simple zonation pattern can be discerned from the cross section in this study, with higher $\delta^{34}S$ values in the middle of the cross section and lower $\delta^{34}S$ values on the periphery (Fig. 7.3). The lighter isotopic values (+9.0–14.0‰) occur within the early K-feldspar – magnetite – tourmaline alteration zone; whereas, the heavier isotopic values (>+14.0‰) occur in the later chlorite alteration domain. The lowest $\delta^{34}S$ value (+8.6‰) in the Prince Darwin prospect is derived from carbonate vein-hosted pyrite. Crosscutting relationships show that the carbonate veins post-date the K-feldspar – magnetite – tourmaline and chlorite alteration (see Chapter 4). It is possible that further sulfur isotopic analyses of carbonate vein-hosted pyrite could delineate a separate population with a distinct isotopic range.

Figure 7.2: Summary of sulfur isotopic values from the Prince Darwin region, compiled from this study and previous studies. **(A):** Regional map showing the locations of the Prince Darwin prospect and major Cambrian hydrothermal deposits in western Tasmania (after Solomon et al., 1988). **(B):** Comparison of $\delta^{34}S_{sulfide}$ data for the Prince Darwin prospect and Cambrian hydrothermal deposits listed in Figure 2A. $\delta^{34}S_{sulfide}$ data for the Prince Darwin prospect are coloured with respect to different pyrite populations: K-feldspar – magnetite – tourmaline alteration (grey) and quartz – chlorite – phengite veins (blue). The variability in the sulfur isotopic compositions in the Prince Darwin prospect may be affected by redox. The heavier sulfur isotopic compositions in the quartz – chlorite – phengite veins is attributed to increased seawater input in the hydrothermal fluids. The green arrows show the typical range of $\delta^{34}S_{sulfide}$ values for porphyry Cu deposits (Ohmoto and Rye, 1979) and reduced Cambrian seawater (Claypool et al., 1980), while the red arrows indicate the probable source of sulfur. The Garfield prospect may be a porphyry deposit, supported by the near-zero $\delta^{34}S_{sulfide}$ values; whereas, many of the other Cambrian ore deposits in western Tasmania show isotopic signatures consistent with significant input from Cambrian seawater, with an exception of the Chester prospect. Negative $^{34}S_{sulfide}$ values in the Chester massive sulfide ores are attributed to bacteriological seawater sulfur reduction (Collins, 1981). Data from Solomon et al. (1988), Collins (1981), Walshe and Solomon (1981), Green (1983), Eastoe et al. (1987), Lees (1987), Jack (1989), Doyle (1990), Gemmell and Large (1992), Raymond (1992), Jones (1993), Gadaloff (1996), Wyman (2001), Green and Vicary (2002), Martin (2004) and this study.

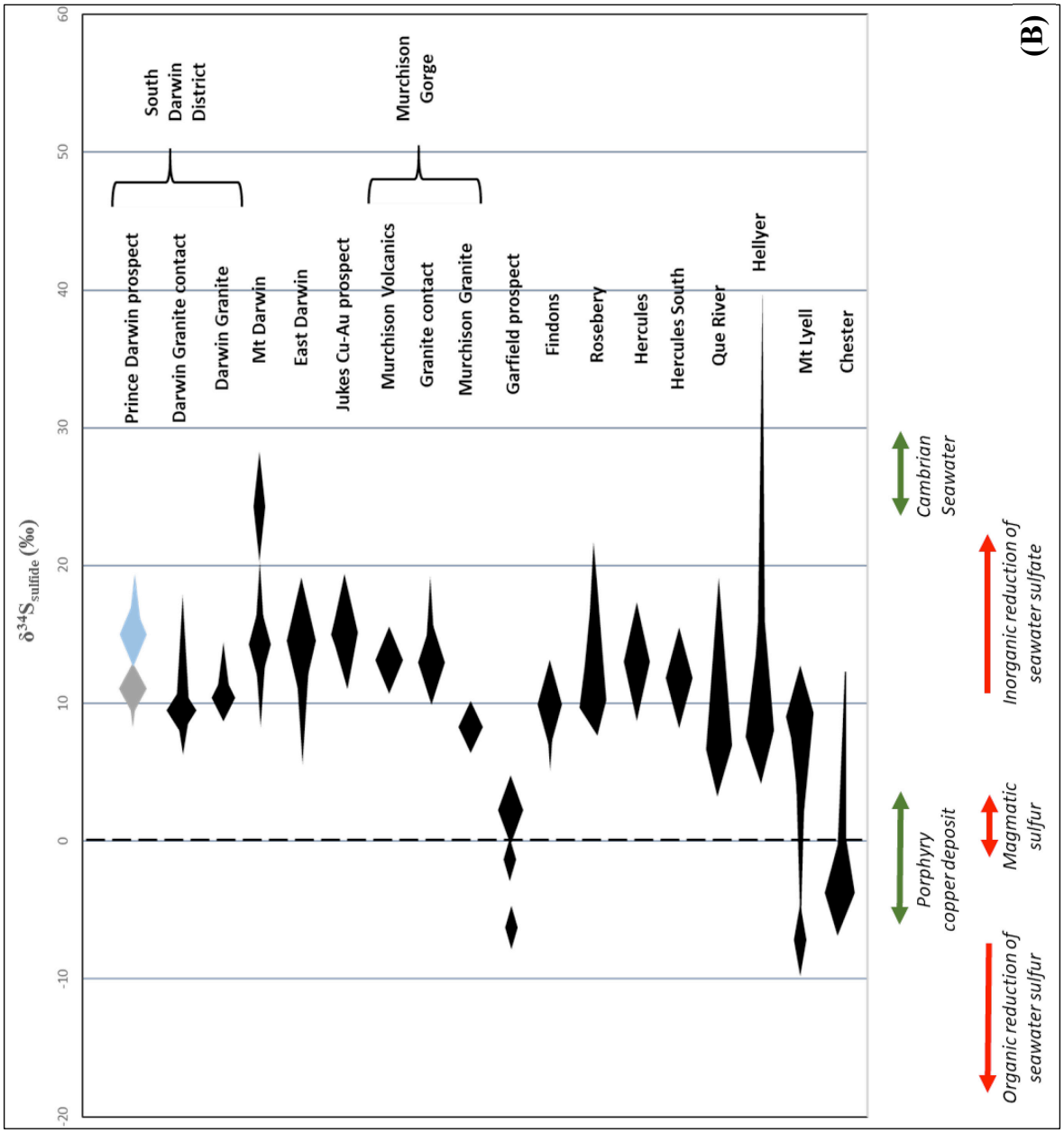
(B)
$\delta^{34}S_{sulfide}$ (‰)
60
50
40
30
20
10
0
-10
-20
South Darwin District
Murchison Gorge
Prince Darwin prospect
Darwin Granite contact
Darwin Granite
Mt Darwin
East Darwin
Jukes Cu-Au prospect
Murchison Volcanics
Granite contact
Murchison Granite
Garfield prospect
Findons
Rosebery
Hercules
Hercules South
Que River
Hellyer
Mt Lyell
Chester
Cambrian Seawater
Inorganic reduction of seawater sulfate
Porphyry copper deposit
Magmatic sulfur
Organic reduction of seawater sulfur

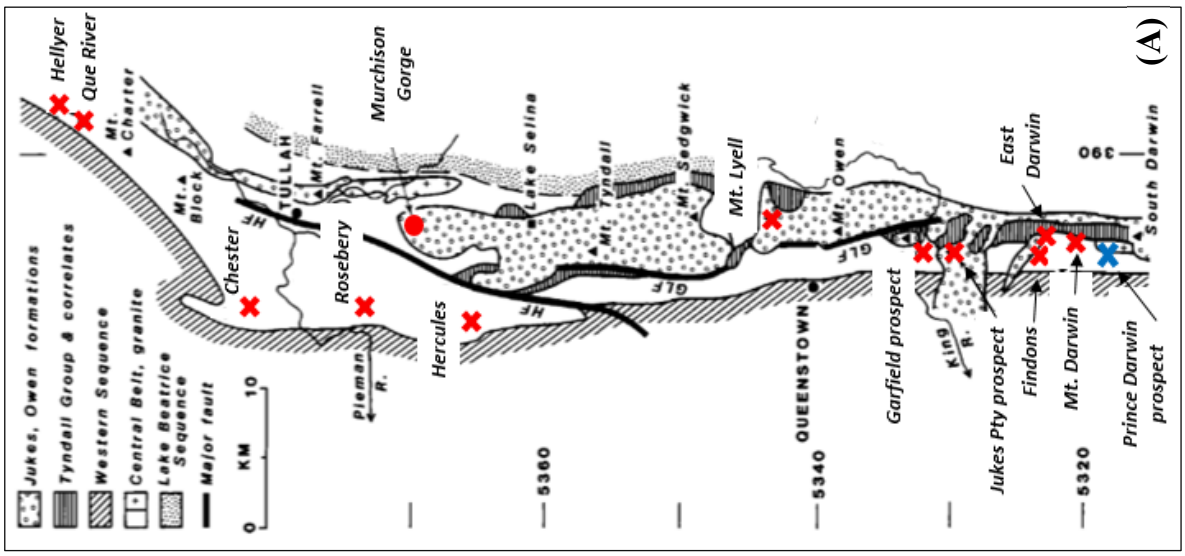
(A)
Jukes, Owen formations
Tyndall Group & correlates
Western Sequence
Central Belt, granite
Lake Beatrice Sequence
Major fault
0 KM 10
Hellyer
Que River
Mt. Charter
Mt.A Block
TULLAH
Mt. Farrell
Murchison Gorge
Lake Selina
Mt. Tyndall
Mt. Sedgwick
Mt. Lyell
Mt. Owen
Chester
Rosebery
Hercules
Pieman R.
HF
GLF
QUEENSTOWN
5360
5340
5320
Garfield prospect
King R.
Jukes Pty prospect
Findons
Mt. Darwin
Prince Darwin prospect
East Darwin
South Darwin

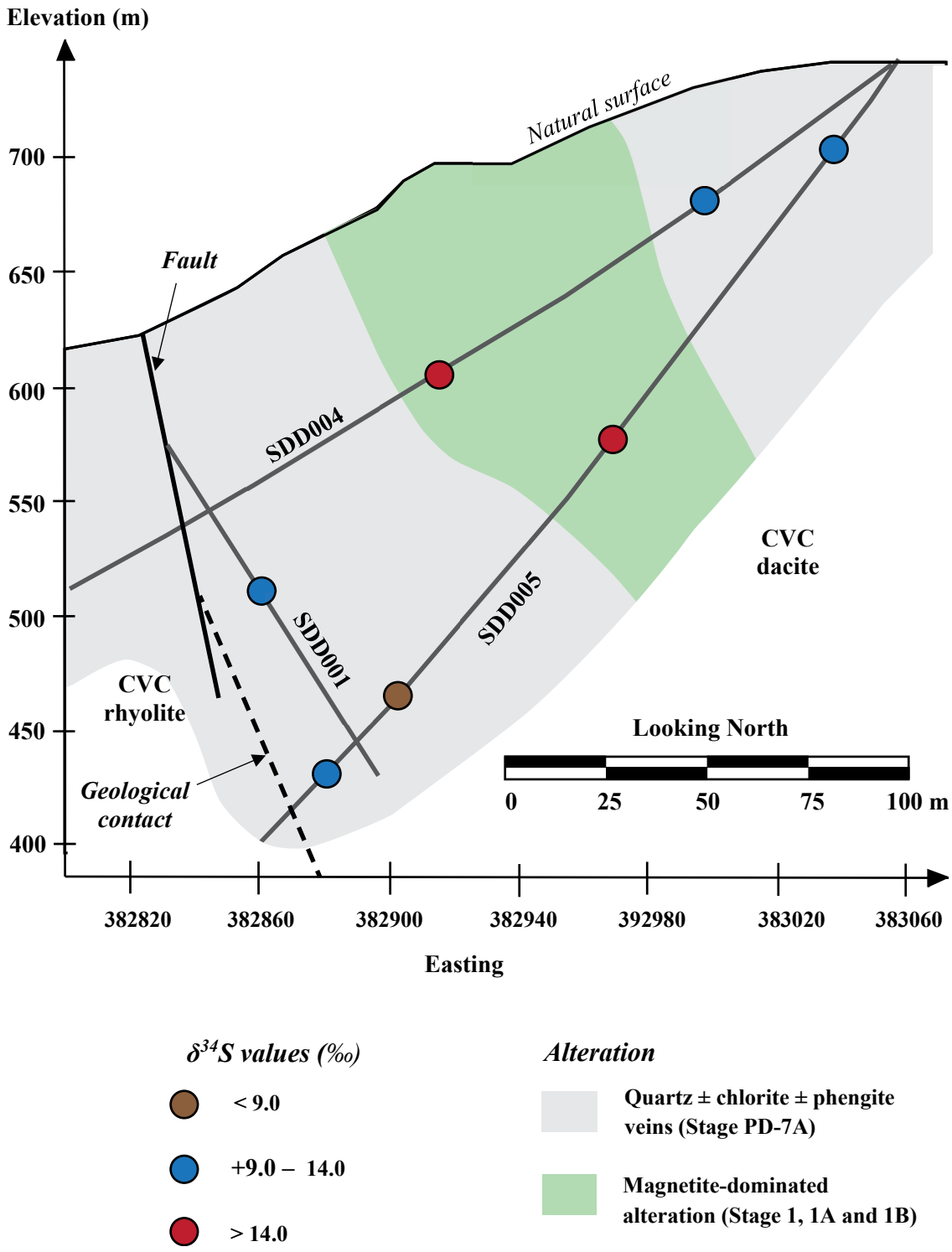

Figure 7.3: Distribution of $\delta^{34}S$ values in the CVC rocks at the Prince Darwin prospect. In broad terms, $\delta^{34}S$ values in magnetite-altered domains are generally lower than those in chlorite-altered domains (see Chapter 3).

In general, $\delta^{34}S_{sulfide}$ values under oxidising conditions (SO_4-dominated) are expected to span a broad range of near-zero values and progressively become more negative with time during its cooling history. In contrast, a narrow range of positive $\delta^{34}S_{sulfide}$ compositions (Ohmoto and Rye, 1979; Rye, 1993) are expected under more reduced conditions (H_2S-dominated). The variability of $\delta^{34}S_{sulfide}$ values associated with different alteration stages

may reflect the control of redox condition on the sulfur isotopic composition. Crosscutting relationships provide strong evidence that the K-feldspar – magnetite – tourmaline alteration was overprinted by later chlorite alteration (see Chapter 4). Considering this temporal relationship, the heavier sulfur isotopic compositions in the chlorite alteration may indicate more reduced condition, or increased Cambrian seawater involvement.

7.6 Summary

The overall heavy sulfur isotopic values from the Prince Darwin prospect are consistent with the presence of Cambrian seawater in the hydrothermal fluids. The high isotopic values do not resemble what is expected for porphyry Cu deposits worldwide. The sulfur isotopic compositions may be further controlled by the relative redox conditions associated with the different alteration stages producing a sulfur fractionation zonation pattern. More samples are required to test this zonation pattern for mineral exploration purposes.

Chapter 8

Genetic Model and Conclusions

8.1 Source of rare earth elements at Prince Darwin

Most REE deposits are associated with alkaline igneous rocks, including carbonatite (e.g., Mountain Pass, U.S.A: Castor, 2008; Bayan Obo, China: Wu, 2008; Smith et al., 2015) or syenite (Lovozero, Russia; Kogarko et al., 1995; Orris and Grauch, 2002), including Olympic Dam in Australia (Schlegel et al., 2015) and Sin Quyen Mine, Vietnam (Ishihara, 2011). Several studies (Murata et al., 1957; Kosterin et al., 1961; Fleischer, 1965; Lee and Bastron, 1967) have also observed the correlation between the presence of allanite and the bulk chemical composition of REE in the host rocks. For example, Lee and Bastron (1967) noted that the degree of REE fractionation is controlled by the CaO content of granitic rocks, whilst Murata et al. (1957) and Fleischer (1965) pointed out that the REE enrichment in allanite varies with host rock. These theories were largely premised on the alkali nature of the host rocks.

Allanite at Prince Darwin has shown similar REE characters with quartz porphyry; however, the Darwin granite, quartz porphyry, and volcanic rocks in this study are typically calc-alkaline in composition and low in CaO (less than 1 wt%). There is a lack of association of alkali magmatism or REE-rich host rocks (e.g., Suite II or III in MRV; Crawford et al., 1992) in the area. In terms of the source of REEs at Prince Darwin, there remains a possibility that a parental magma of alkali nature has not yet been encountered. Previous studies at the Thomas Creek Cu ± Au prospect, which is located approximately 15 km away from Prince Darwin, show that the hydrothermal alteration in the area is characterised by a lack of quartz veins, phyllic and argillic alteration, and abundance of sodic-calcic assemblages and magnetite (Reid, 2001). These features are comparable to alkaline porphyry copper deposits (e.g., British Columbia, Canada: Lang et al., 1995; Cadia, Australia: Wilson et al., 2003, 2007). These observations support the possibility of the existence of alkali magmatism in the area.

8.2 Genetic model for the Prince Darwin prospect

Prince Darwin shows a number of similarities to granite-related magmatic-hydrothermal mineral systems. Table 8.1 compares the key features of Cu-bearing intrusion-related deposit types, including porphyry Cu deposit, skarn and IOCG, with features observed at Prince Darwin.

Hydrothermal alteration, breccia- or stockwork-hosted copper-iron mineralisation styles, and association with I-type granites at Prince Darwin are broadly analogous to many calc-alkaline porphyry Cu deposits (e.g., Batu Hijau: Garwin, 2002; Ok-Tedi and Wafi-Golpu, Papua New Guinea: Large et al, 2018; Rinne et al., 2018). The occurrence of quartz veins and chemistry of the associated intrusions precludes its classification as an alkalic porphyry (Holidays and Cooke, 2007). The massive magnetite replacement at the geological contact between the dacite and rhyolite is comparable to Fe-skarn. Allanite, as a hydrous calc-silicate, may occur as part of retrograde skarn; however, REE deposits rarely occur within base metal-rich porphyry-skarn deposit systems that commonly develop in association with voluminous calc-alkaline magmatism (Giere, 1996; Goodenough et al., 2016). Consequently, REE-rich mineralisation at Prince Darwin does not conform to the typical porphyry-skarn model.

REE-rich base metal mineralisation is rare; however, there are a few examples of significant base metal prospects or deposits which also host appreciable amounts of REEs (e.g., Olympic Dam, Australia: Schlegel et al., 2015; Ernest Henry, Australia: Williams et al., 2015; Sin Quyen Mine, Vietnam: Ishihara, 2011). Most of these provinces fall within the IOCG deposit class. Prevalent K-rich and iron oxide alteration, occurrence of magnetite – apatite alteration, structurally controlled hydrothermal alteration and mineralisation at Prince Darwin are analogous to many IOCG systems (Groves et al., 2010; Williams et al., 2015). In addition, REE-host minerals at Prince Darwin are typically associated with biotite, fluorapatite and carbonate. Similar mineralogical associations have been documented by several authors at Olympic Dam (e.g., Williams et al., 2005; Ehrig et al., 2012; and Schmandt et al., 2017). The presence of F- and P-rich fluids, as suggested by this mineralogical association, is not common in porphyry and skarn deposits (Williams et al., 2005; Sillitoe, 2010; Barton, 2013).

Table 8.1: Summary of the key features observed at Prince Darwin, compared with different types of intrusion-related Cu-rich deposit types. Data compiled from Ishihara (1981); Hitzman et al. (1992); Barton and Johnson (1996); Pollard (2000; 2006); Porter (2000, 2002); Williams (2000); Kerrich et al. (2005, 2010); Seedorff et al. (2005); Williams et al. (2005); Sinclair (2007); Groves et al., (2010, 2016); Deb and Sarkar (2017).

Key Features	Prince Darwin prospect	Porphyry Cu deposit	Cu-rich skarn	Iron – oxide copper gold (IOCG) deposit
Common commodities	Cu, Au, Fe, LREEs	Cu, Au, Mo (± Re, Sn, W, Ag, Pd, Te, Se, Bi, Zn, and Pb)	Cu, W, Sn, Mo, Cu, Fe, Zn, Pb, Ag, Au	Cu, Au (± LREEs, U, Ag, Mo, Ba, Co, Bi, F, P)
Alteration styles	K-feldspar – magnetite – tourmaline – hematite, magnetite – apatite, chlorite, phengite, allanite – biotite and carbonate	Deep sodic-calcic, proximal potassic, propylitic, phyllic, argillic, advanced argillic	Ca-rich calc-silicates (e.g., garnet, pyroxene, wollastonite, pyroxene, amphibole, epidote, scapolite). Retrograde minerals such as actinolite, biotite, muscovite, chlorite, talc and carbonate may be brought in.	Proximal potassic (k-feldspar and biotite) or hydrolytic (sericite, chlorite). Also associated with pervasive regional and local sodic (ab), and sodic-calcic (ab, amp) alteration
Mineralisation styles	Stockwork, disseminated, breccia-hosted, structurally controlled hydrothermal breccias	Stockwork, disseminated and breccia-hosted	Massive replacement, dissemination and vein-hosted	Epigenetic, structurally-controlled hydrothermal breccias, replacements and vein stockwork
Tectonic settings	post-collisional submarine volcanic setting	Subvolcanic environment within magmatic arc settings above subduction zones, where volcanism is active	Related to convergent place margins and commonly associated with porphyry Cu-Mo-Au deposits	Compressional arcs, extensional arcs, back acs, intraplate and rift settings
Igneous associations	Adjacent to the Darwin granite	Centred above porphyries	At the contact of a felsic intrusive and a reactive rock (most commonly carbonate-rich rocks or mafic igneous rocks)	Back arc or post-collisional setting, cratonic margin, intra-continental rift zone
Lithological associations	Associated with volcanic arc-related I-type series (Darwin granite) and within-plate granites (quartz porphyry). All intrusive and volcanic host rocks are calc-alkaline in composition	Exclusively I-type and magnetite-series affiliation, metaluminous and medium K calc-alkaline. May fall into the high K calc-alkaline (shoshonitc) or alkaline fields but less common.	Calc-alkaline, I-type intrusions of mafic to intermediate compositions. Reactive rocks include dolomite, limestone, calcareous shale, or basalt	I-type, high K to shoshonitic character or A-type granites with alkaline to sub-alkaline affinity
Sulfur isotope signatures	+8.6 to 15.8 per mil	0 ± 5 per mil	0 ± 5 per mil	-10 to 30 per mil, with most spreads of 5 to 20 per mil.
Examples		Batu Hijau, Indonesia (calc-alkaline; Garwin, 2002)	Cadia, Australia (Forster, 2004)	Olympic Dam, Australia (Schmandt et al., 2017)
		Wafi-Golpu, Papau New Guinea (calc-alkaline; Rinnie et al., 2018)	King Island, Australia (Kwak and Tan, 1981)	Ernest Henry, Australia (Williams et al., 2015)
		Mt Polley, Canada (alkalic-type; Pass, 2010)	Ancash, Peru (Love et al., 2004)	Candelaria, Chile (Ulrich and Clark, 1999)

This study has shown that there are multiple mineralisation phases at Prince Darwin, characterised by different sulfide minerals and alteration assemblages, including pyrite ± chalcopyrite assemblages associated with magnetite-dominated alteration, and pyrite ± bornite ± chalcopyrite hosted within quartz – chlorite – phengite veins. Copper mineralisation in IOCG deposits typically occurs within magmatic-hydrothermal breccias associated with iron oxide alteration (e.g., Oliver et al., 2008; Groves et al., 2010; Schmandt et al., 2017). However, the occurrence of quartz – chlorite – phengite vein-hosted mineralisation is more comparable with the mineralisation styles in porphyry Cu deposits.

It has been well-established that hydrothermal alteration in IOCG deposits is characterised by early sodic-calcic, potassic and hydrolytic assemblages as a consequence of intense and voluminous Na-Ca-K metasomatism (Barton, 2013). At Prince Darwin, the presence of albite, K-feldspar, chlorite and phengite suggest that this style of alteration may have occurred, although there is still some uncertainty in identifying the origin of albite alteration (i.e., metamorphic, diagenetic or hydrothermal-related). Heavy sulfur isotopic compositions at Prince Darwin are not consistent with the dominance of magmatic sulfur in fluids typical of porphyry Cu deposits (Rye, 1993). The high and wide range of sulfur isotopic values is more comparable with IOCG deposits which commonly have values between +5 – 20 ‰ due to mixing of two or more fluid sources (metamorphic, basinal, marine, evaporitic and magmatic origin) (Bastrakove et al., 2007; Benavides et al., 2007; Chen, 2011; Rieger et al., 2012; Torris et al., 2012).

The tectonic model of the MRV belt is more comparable with the tectonic setting of IOCG deposits, i.e. post-collisional or back-arc setting (e.g., Candelaria, Chile: Ryan et al., 1995; Ullrich and Clark, 1999), relative to porphyry Cu deposits (Sinclair, 2007; Sillitoe, 2010). Whole-rock geochemical data for the intrusions at Prince Darwin are also consistent with magmas associated with porphyry and IOCG deposit types. Lack of reactive host rocks (e.g., carbonate and mafic rocks) and apatite enrichment within the magnetite replacement zone are not compatible with a skarn model.

In summary, Prince Darwin shows features most in common with the IOCG deposit class. However, the IOCG model represents a broad family of mineralisation styles that lack well-defined tectonic, igneous, fluid and geochemical associations relative to better-constrained porphyry-skarn hydrothermal systems. Consequently, Prince Darwin cannot be explained by any single ore deposit model within the current framework. Instead, it may represent a hybrid porphyry-IOCG system that involved atypical hydrothermal fluid sources and magmatism.

8.3 Implications for exploration and metallogenic potential of MRV

The outcomes of this study have implications for future exploration activities across the South Darwin district, and potentially other MRV-hosted prospects and similar REE-rich base metal prospects:

- This study has revealed the potential of the MRV belt in hosting REE resources. Prince Darwin prospect is representative of a different class of ore deposit compared to other known MRV-hosted VHMS and porphyry-epithermal base metal prospects.
- REE-rich base metal prospects can be hosted within submarine volcanism. Heavy sulfur isotopic signature at Prince Darwin, consistent with other MRV-hosted prospects, suggests involvement of non-magmatic sulfur source in the mineralisation. Saline seawater may play an important role in mobilising REEs at Prince Darwin.
- CVC-hosted tourmaline shows subtle geochemical variation, even over short distance. This suggests that tourmalines may be a potential orebody vectoring tool in the district or other intrusion-related prospects in the MRV.
- Chlorite trace element chemistry at Prince Darwin is strongly protolith-controlled and this has affected its application as vectoring tool for mineralisation.
- Comparable REE patterns in volcanic rocks and quartz porphyry suggest that they may be co-magmatic. Similar REE character between allanite and quartz porphyry also suggest that quartz porphyry may be the potential source of REEs at Prince Darwin.
- Comparable ages of formation and field observations of the Pink and White granite in this and previous studies suggest that they may be co-magmatic; however, the Pink and White granite show distinct Eu anomalies, which do not support this interpretation.

8.4 Recommendations for future work

To further improve our understanding of the genesis of the Prince Darwin prospect, as well as mineralisation throughout the southern portion of the Mount Read Volcanic belt, the following work should be considered:

- The source of the REEs at Prince Darwin remains unresolved. Future studies should focus on determining the likely source of the REEs and the nature of the associated igneous suites. Some ideas for resolving this issue include:

- Dating of REE carrier minerals, including allanite, monazite, apatite and zircon is highly recommended. Comparison with the age of the known porphyries in the area will give an insight into their relative ages of formation. If REE-host minerals pre-date the Darwin granite and quartz porphyry, this may suggest that the Darwin granite and quartz porphyry are not related to REE mineralisation.
- Additional LA-ICP-MS analyses on REE-host minerals to study their REE profiles. Comparison of the REE profiles could help in constraining their genetic relationship (e.g., Krneta et al., 2017)
- Stable isotope studies, including $\delta^{18}O$ and δD analyses could be undertaken on the main-stage alteration minerals (e.g., biotite, chlorite, phengite) at Prince Darwin, to improve the constraints on the likely sources and chemistry of hydrothermal fluids involved in the ore formation and hydrothermal alteration.

- It has been well established that the mineralisation in IOCG provinces are commonly associated with crustal-scale fault network and re-activated orogenic events (e.g., Hitzman et al., 1992; Hitzman, 2000; Haynes, 2000; Pollard, 2006; Goodenough, 2017). A systematic study of district-scale structures would help in determining the structural controls on mineralisation at Prince Darwin.
- Considering the documentation of magnetite – apatite alteration at Savage River and Prince Lyell, revision of the genetic models of these two prospects is recommended as they may represent a similar hydrothermal system.

References

Abbott, P.D.B., 1992, Geology of a Barite-Galena Occurrence exposed in the Anthony Power Development Tunnel, Western Tasmania: Unpublished B.Sc.(Honours) thesis, University of Tasmania.

Adams, C.J., Black, L.P., Corbett, K.D., and Green, G.R., 1985, Reconnaissance isotopic studies bearing on the tectonothermal history of Early Palaeozoic and Late Proterozoic sequences in western Tasmania: Australian Journal of Earth Sciences, v. 32, p. 7−36

Alberta, C., Lanaa, C., Gerdesb, X., Schannora, M., Narduzzia, F., and Queirogaa, G., 2018, Archean magmatic-hydrothermal fluid evolution in the Quadrilátero Ferrífero (SE Brazil) documented by B isotopes (LA MC-ICPMS) in tourmaline: Chemical Geology, v. 481, p. 95–109.

Alderton, D.H.M., Pearces, J.A., and Potts, P. J.,1980, Rare-earth element mobility during granite alteration: evidence from southwest England: Earth and Planetary Science Letters, v. 49, p. 149–165.

Alizadeh Sevari, B., Hezarkhani, A., 2014, Hydrothermal evolution of Darreh-zar porphyry copper deposit, Iran: evidence from fluid inclusions: Arabic Journal of Geosciences, v. 8, p. 1463–1477.

Armbruster, T., Bonazzi, P., Akasaka, M., Bermanec, V., Chopin, C., Giere, R., Heuss-Assbichler, S., Liebscher, A., Menchetti, S., Pan, Y., and Pasero, M., 2006, Recommended nomenclature of epidote-group minerals: European Journal of Mineralogy, v. 18, p. 551–567.

Arnason, J.G., Bird, D.K., and Liou, J.G., 1993. Variables controlling epidote composition in hydrothermal and low-pressure regional metamorphic rocks: 25 Jahre Knappenwand - 125 years Knappenwand, Proceedings of a Symposium, p. 17–25.

Ballie, P. W. 1989, Stratigraphy, sedimentology and structural setting of the Cambrian Sticht Range Formation, western Tasmania: Tasmania Geological Survey Bulletin 65.

Barton, M.D. and Johnson, D.A., 1996, Evaporitic-source model for igneous-related Fe oxide–(REE–Cu–Au–U) mineralization: Geology, v. 24, p. 259–262.

Barton, M.D. and Johnson, D.A., 2004, Footprints of Fe-oxide(-Cu-Au) systems: SEG 2004: Predictive Mineral Discovery Under Cover. Centre for Global Metallogeny, Special Publication 33, The University of Western Australia, p. 112–116.

Bastrakov, E.N., Skirrow, R.G., and Davidson G.J., 2007, Fluid evolution and origins of iron oxide Cu-Au prospects in the Olympic Dam District, Gawler craton South Australia: Economic Geology, v. 102, p. 1415–1440.

Beaufort, D., Rigault, C., Billon, S., Billault, V., Inoue, A., Inoue, S., Patrier, P., 2015, Chlorite and chloritization processes through mixed-layer mineral series in low-temperature geological systems – a review: Clay Minerals, v. 50, p. 497–523.

Benavides, J., Kyser, TK., and Clark, A.H., 2007, The Mantoverde iron oxide-copper-gold district, III Region, Chile: The role of regionally-derived, non-magmatic fluids contributions to chalcopyrite mineralisation: Economic Geology, v. 102, p. 415–440.

Berry, R.F., 1994, Tectonics of western Tasmania: Late Precambrian–Devonian, in Cooke, D.R., and Kitto, P.A., eds., Contentious issues in Tasmania geology, Abstract: Geological Society of Australia, v. 39, p. 6–8.

Berry, R.F., and Keele, R.A., 1993a, Cambrian Structure in Western Tasmania, Structure and Mineralisation in Western Tasmania: AMIRA Project P291, p. 55–68.

Berry, R.F., and Keele, R.A., 1993b, Structure and Mineralisation of Western Tasmania: Final Summary, Structure and Mineralisation of Western Tasmania: AMIRA Project P291, p. 69–94.

Berry, R.F., and Keele, R.A., 1997, Cambrian Tectonics and Mineralisation in western Tasmania: Third International Mining Geology Conference, AUSIMM publication series 6/97, p. 13–16.

Berry, R.F., Chmielowski, R.M., Steele, D.A., and Meffre, S., 2007, Chemical U–Th–Pb monazite dating of the Cambrian Tyennan Orogeny, Tasmania: Australian Journal of Earth Sciences, v. 54, p. 757–771.

Black, L.P., Seymour, D.B., Corbett, K.D., Cox, S.E., Streit, J.E., Bottril, R.S., Calver, C.R., Everard, J.L., Green, G.R., McClenaghan, M.P., Pemberton, J., Taheri, J., and Turner, N.J., 1997, Dating Tasmania's oldest geological events: Australian Geological Survey Organisation Record 1997/15, 57 p.

Bosi, F., 2018, Tourmaline Crystal Chemistry: American Mineralogist, v. 103, p. 298–306.

Bottrill, R.S., 2001, A mineralogical field guide for a Western Tasmania minerals and museum tour: Tasmania Geological Survey Record 2001/2008, Mineral Resources Tasmania.

Burnham, C. W., and Ohmoto, H., 1980, Late stage processes of felsic magmatism. In Granitic Magmatism and Related Mineralization. In: Ishihara, S., and Takenouchi, S., eds, Granitic magmatism and related mineralisation: Mining Geology Special, v. 8, p. 1–11.

Burt, D. M., 1989, Compositional and phase relations among rare earth element minerals: Reviews in Mineralogy and Geochemistry, v. 21, p. 260 – 307.

Campbell, L., Henderson, P., Wall, F., and Nielsen, T.F.D., 1997, Rare earth chemistry of perovskite group minerals from the Gardiner Complex, East Greenland: Mineralogical Magazine, v. 61, p. 197–212.

Canil, D., Grondahl, C., Lacourse, T., and Pisiak, L.K., 2016, Trace elements in magnetite from porphyry Cu–Mo–Au deposits in British Columbia, Canada: Ore Geology Reviews, v. 72, p. 1116–1128.

Carey, S. W. and Banks, M.R., 1954, Lower Paleozoic Uncomformities in Tasmania: Papers and Proceedings of the Royal Society of Tasmania, v. 88, p. 245–269.

Castor, S.B., 2008, The Mountain Pass Rare-Earth Carbonatite and Associated Ultrapotassic Rocks, California: Canadian Mineralogist, v. 46, p. 779–806.

Cayley, R., Taylor D.H., Vandenberg, A., and Moore, D., 2002, Proterozoic – Early Palaeozoic rocks and the Tyennan Orogeny in central Victoria: The Selwyn Block and its tectonic implications: Australian Journal of Earth Sciences, v. 49, no. 2, p. 225–254.

Chen, W.T. and Zhou, M.F., 2014, Ages and compositions of primary and secondary allanite from the Lala Fe–Cu deposit, SW China: implications for multiple episodes of hydrothermal events: Contribution to Mineralogy and Petrology, v. 168, p. 1–20.

Chmielowski, R.M., 2009, The Cambrian Metamorphic History of Tasmania: Unpublished PhD thesis, University of Tasmania.

Chmielowski, R.M., and Berry, R.F., 2012, The Cambrian metamorphic history of Tasmania: The Metapelites: Australian Journal of Earth Sciences, v. 59, p. 1007–1019.

Chukanov, N.V., Varlamov, D.A., Nestola, F., Belakovskiy, D.I., Goettlicher, J., Britvin, S.N., Lanza, A., and Jancev, S., 2012, Piemontite-(Pb), CaPbAl2Mn3+[Si_2O_7][SiO_4]O(OH), a new mineral species of the epidote supergroup: Journal of Mineralogy and Geochemistry, v. 189, p. 275–286.

Claypool, G.E., Holser, W.T., Kaplan I.R., Sakai, H., and Zak, I., 1980, The age curves of sulur and oxygen isotopes in marine sulfate and their mutual interpretation: Chemical Geology, v. 28, p. 199–260.

Collins, P.L.F., 1981, Sulfur Isotope Study of the Chester Massive Pyrite Deposits, Western Tasmania: Tasmanian Mines Department Report 1981/27.

Cooke, D.R., Baker, M., Hollings, P., Sweet, G., Chang, Z., Danyushevsky, L., Gilbert, S., Zhao, T., White, N., Gemmell, J.B., & Inglis, S., 2014, New Advances in Detecting the Distal

Geochemical Footprints of Porphyry Systems - Epidote Mineral Chemistry as a Tool for Vectoring and Fertility Assessments: SEG Special Publication 18, Building Exploration Capability for the 21st Century.

Cooke, D.R., Deyell, C.L., Waters, P.J., Gonzales, R.I. and Zaw, K., 2011, Evidence for Magmatic-Hydrothermal Fluids and Ore-Forming Processes in Epithermal and Porphyry Deposits of the Baguio District, Philippines: Economic Geology, v. 106, p. 1399–1424.

Cooke, D.R., Hollings P., Wilkinson J.J., and Tosdal R.M., 2014, Geochemistry of porphyry deposits: Treatise on Geochemistry, v. 13, p. 357−381.

Corbett, K.D., 1990, Cambro-Ordovician stratigraphy, West Coast Range to Black Bluff: Tasmania – a Generalists Influence, p. 8–13.

Corbett, K.D., 1992, Stratigraphic-volcanic setting of massive sulfide deposits in the Cambrian Mount Read Volcanics, Tasmania: Economic Geology, v. 87, p. 564–586.

Corbett, K.D., 2002, Bedrock geological map of the Mt Read Volcanics belt andadjacent areas, South Darwin Peak to Hellyer: West Tasmanian Regional Minerals Program, Mineral Resources Tasmania.

Corbett, E.B., and Cuffley, B.W., 1970, Geology of the Jukes-Darwin Mining field, Southwest Tasmania: Tasmania Department of Mines Report on EL/65.

Corbett, K.D., Perberton, J., and Vicary, M.J., 1993, Geology of the Mt. Jukes – Mt. Darwin area, Map 13: Geological Survey of Tasmania.

Corbett, K.D., Quilty, P.G., and Calver, C.R., 2014, Geological Evolution of Tasmania: Geological Society of Australia Special Publication 24.

Corbett, K.D., and Solomon, M., 1989, Cambrian Mt. Read Volcanics and Associated Mineral Deposits, in Burrett, C.F. and Martin, E.L., eds., Geology and Mineral Resources of Tasmania Special 15, p. 84-153

Corona Resources, 2011, IPO NI 43-101 Technical Report on the Corona Gold Limited Base Metal and Gold Projects Located on the West Coast of Tasmania, Corona Mineral.

Costantopouios, J., 1988, Fluid inclusions and rare-earth element geochemistry of fluorite from South-Central Idaho: Economic Geology, v. 83, p. 626–636.

Cox, S.E., Farley, K.A., and Hemming, S.R., 2012, Insights into the age of the Mono Lake Excursion and magmatic crystal residence time from (U-Th)/He and ^{230}Th dating of volcanic allanite: Earth and Planetary Science Letters, v. 319–320, p. 178–184.

Crawford, A.J., 1987, Progress report on the petrology, geochemistry and tectonic implications of the Mount Read Volcanics Second Annual Report (August, 1987): Controls on gold

and silver grades in volcagenic sulphide deposits: AMIRA 84/P210, University of Tasmania, p. 79–108.

Crawford, A.J. and Berry, R.F., 1992, Tectonic implications of Late Proterozoic-Early Paleozoic igneous rock associations in western Tasmania: Tectonophysics, v. 214, p. 37–56.

Crawford, A.J., Corbett, K.D. and Everard, J.L., 1992., Geochemistry of the Cambrian volcanic-hosted massive sulfide-rich Mount Read Volcanics, Tasmania, and some tectonic implications. Economic Geology, v. 87, 597–619.

Deb, M., and Sarakr, S.C., 2017, Geodynamic Context of Metallogeny: Minerals and Alied Natural Resources and their Sustainable Development, p. 293–339.

Deer, W.A., Howie, R., and Zussman, J., 1986, Rock-forming minerals, Disilicates and ring silicates: Wiley, v. 1B.

Deer, W.A, Howie, R.A. and Zussman, J., 1992, An introduction to the rock forming minerals, 2nd eds.: Longrnan Scientific and Technical.

Deer, W. A., Howie, R. A., and Zussman, J., 2009, Layered Silicates Excluding Micas and Clay Minerals, Rock-Forming Minerals, Volume 3B: London, Geological Society, p. 314.

Demirel, S., Göncüoglu, M.C., Topuzm G., Ishik, V., 2009, Geology and chemical variations in tourmaline from the quartz-tourmaline breccias within the Kerkenez Granite-Monzonite Massif, Central Anatolian Crystalline Complex, Turkey: The Canadian Mineralogists, v. 47, p. 787–799

Deyell, C. L., 2005, Sulfur Isotope zonation at the Mt. Polley alkalic porphyry Cu-Au deposit, British Columbia, Canada, in Mao, J., and Bierlein, F.P., eds, Mineral Deposit Research: Meeting Global Challenge: 8th Biennial Society for Geology Applied to Mineral Deposits meeting, v. 1, p. 373–376.

Doyle, M.G., 1990, The Geology, Mineralisation and Alteration of the Jukes Proprietry Prospect, Western Tasmania: Unpublished Honours thesis, University of Tasmania.

Duncan, S.M., 1997, Geology, Geochemistry and Genesis of Cu-Au and Magnetite-Apatite Mineralization at the Garfield prospect, Western Tasmania: Unpublished B.Sc (Honours) thesis, University of Tasmania.

Eastoe, C.J., Solomon, M., and Walshe, J.L., 1987, District scale alteration associated with massive sulfide deposits in the Mount Read Volcanics, western Tasmania: Economic Geology, v. 82, p. 1239–1258.

Ehrig, K., McPhie, J., and Kamenetsky, V., 2012, Geology and mineralogical zonation of the Olympic Dam Iron Oxide Cu-U-Au-Ag deposit, South Australia: Society of Economic Geologists, Special Publication 16, p. 237–267.

Eichenlaub, A.B., 2007, Exploration of Genetic Links between Breccia Pipes and Porphyry Copper Deposits in a Laramide Hydrothermal System, Sombrero Butte, Pinal County, Arizona: Thesis of Master of Science, the University of Arizona.

Exley R.A., 1980, Microprobe studies of REE-rich accessory minerals: implications for Skye granite petrogenesis and REE mobility in hydrothermal systems: Earth and Planetary Science Letters, v. 48, p.97–110.

Field, C.W., Zhang, L., Dilles, J.H., Rye, R.O., and Reed, M.H., 2005, Sulfur and oxygen isotopic record in sulfate and sulfide minerals of early, deep, pre-main stage porphyry Cu-Mo and late main stage base-metal and mineral deposits, Butte district, Montana: Chemical Geology, v. 215 p. 61–93.

Fleischer, M., 1965, Some aspects of the geochemistry of yttrium and the lanthanides: Geochimica et Cosmochimica Acta, v. 29, p. 755–772.

Foster, M.D., 1962, Interpretation of the Composition and a Classification of the Chlorites: Shorter Contributions to General Geology: Geological Survey Professional Paper 414-A.

Foster, D.B.., Seccombe, P.K., Phillips, P., 2004, Controls on Skarn Mineralization and Alteration at the Cadia Deposits, New South Wales, Australia: Economic Geology, v. 99, p. 761–788.

Franz, G., and Liebscher, A., 2004, Physical and chemical properties of the epidote minerals—an introduction: Reviews in Mineralogy and Geochemistry, v. 56, p. 1–82.

Frikken, P.H., Cooke, D.R., Walshe, J.L., Archibald, D., Skarmeta, J., Serrano, L., and Vargas, R., 2005, Mineralogical and isotopic zonation in the Sur-Sur tourmaline breccia, Río Blanco-Los Bronces Cu-Mo deposit, Chile: Implications for ore genesis: Economic Geology, v. 100, p. 935–961.

Fu, Y., Sun, X., Li, D., Lin, D. and Lai, C., 2017, LA-ICP-MS U-Th-Pb Dating and Trace Element Geochemistry of Allanite: Implications on the Different Skarn Metallogenesis between the Giant Beiya Au and Machangqing Cu-Mo-(Au) Deposits in Yunnan, SW China: Minerals, v. 7, 251 p.

Gadaloff, 1996, Cambrian Copper-Gold Vein Mineralization in the East Darwin Area, Western Tasmania: Unpublished B.Sc. (Honours) thesis, University of Tasmania.

Galbraith, C.G., Clarke, D.B., Trumbull, R.B., and Wiedenbeck, M., 2009, Assessment of Tourmaline Compositions as an Indicator of Emerald Mineralization at the Tsa da Glisza Prospect, Yukon Territory, Canada: Economic Geology, v. 104, p. 71 –731.

Garda, G.M., Beljavskis, P., Juliani, C., and Silva, D., 2003, Geochemistry associated with iron formation and quartz veins of the Morro da Pedra Preta Formation, Serro do Itaberaba Group (Sao Paulo, Brazil): Anais da Academia Brasileira de Ciencias, v. 75, no. 2, p. 209–234.

Garwin, S., 2002, The geologic setting of intrusion-related hydrothermal systems near the Batu Hijau porphyry copper-gold deposit, Sumbawa, Indonesia: Economic Geology Special Publication, v. 9, p. 333–366.

Gemmell, J.B. and Large, R.R., 1992, Stringer systems and alteration zones underlying the Hellyer volcanic-hosted massive sulfide deposit, Tasmania, Australia: Economic Geology, v. 87, p. 620–649.

Gemmell, J.B., and Large, R.R., 1992, Stringer System and Alteration Zones Underlying the Hellyer and Que River Volcanic-Hosted Massive Sulfide Deposit, Tasmania, Australia: Economic Geology, v. 87, p. 620–649.

Giere, R., 1986, Zirconolite, allanite and hoegbomite in marble skaru from the Bergell contact aureole: implications for mobility of Ti, Zr and REE: Contribution to Mineralogy and Petrology, v. 93, p. 459–470.

Gieré, R., 1990, Hydrothermal mobility of Ti, Zr and REE: Examples from the Bergell and Adamello contact aureoles (Italy): Terra Nova, v. 2, p. 60–67.

Gieré, R., and Sorensen, S.S., 2004, Allanite and other REE-rich epidotegroup minerals: Reviews in Mineralogy and Geochemistry, v. 56, p. 431–493.

Gieré, R., Virgo, D., and Popp, R.K., 1999, Oxidation state of iron and incorporation of REE in igneous allanite: Journal of Conference Abstracts, v. 4, p. 721.

Gifkins, C.C., 2001. Submarine volcanism and alteration in the Cambrian, northern Central Volcanic Complex, western Tasmania: Unpublished PhD thesis, University of Tasmania, p. 239.

Gifkin, C.C., and Kimber, B., 2003, 3-D geological modelling and mineral systems in Tasmania. Explanatory notes for the map of volcanic facies associations and volcanic centres in the Mount Read Volcanics, Tasmania: Centre for Ore Deposit Research University of Tasmania.

Goodenough, K.M., Schilling, J., Jonsson, E., Kalvig, P., Charles, N., Tuduri, J., Deady, E.A., Sadeghi, M., Schiellerup, H., Müller, A., Bertrand, G., Arvanitidis, N., Eliopoulos, D.G., Shaw, R.A., Thrane, K., and Keulen, M., 2016, Europe's rare earth element resource potential: An overview of REE metallogenetic provinces and their geodynamic setting: Ore Geology Reviews, v. 72, p. 838–856.

Green, G.R., 1983, The Geological Setting and Formation of the Rosebery Volcanic-Hosted Massive Sulfide Orebody, Tasmania: Unpublished PhD thesis, University of Tasmania.

Green, G.R., Bottrill, R.S., Bacon, C.A.and Turner, N.J. ,1988, Mineral deposits and metallogenic map of Tasmania, scale 1:500000: Tasmanian Department of Mines.

Green,D., and Vicary, M., 2002, Chester Prospect: mineralogy and lithogeochemistry, Isotopic Response of Fluid Flow in Submarine Volcanic-Hosted Hydrothermal Systems, and its Implications of Prospectivity: Mount Read Volcanics Case Study: Industry-ARC SPIRT Project Final Report, Centre for Ore Deposits and Exploration Studies, University of Tasmania, p. 3.1–3.12.

Gromet, L.P., and Silver, L.T., 1983, Rare earth element distributions among minerals in a grandiorite and their petrogenetic implications: Geochimica et Cosmochimica Acta, v. 47, p. 925–939.

Groves, D.I., Bierlein, F.P., Meinert, L.D., and Hitzman, M., 2010, Iron Oxide Copper-Gold (IOCG) Deposits through Earth History: Implications for Origin, Lithospheric Setting, and Distinction from Other Epigenetic Iron Oxide Deposits: Geology, v. 105, p. 641–654.

Haas, J.R., Shock, E.L., and Sassani, D.C., 1995, Rare earth elements in hydrothermal systems: Estimates of standard partial molal thermodynamic properties of aqueous complexes or the rare earth elements at high pressures and temperatures: Geochimica et Cosmochimica Acta, v. 59, p. 4329–4350.

Halley, S.W., 2013. Spectral Mapping: Unpublished Internal Report, Corona Minerals.

Halley, S.W., and Roberts, R.H., 1997, Henty; a shallow-water gold-rich volcanogenic massive sulfide deposit in western Tasmania: Economic Geology, v. 92, p. 438–447.

Halley, S.W., Vicary, M., Corlettm S., and Wyman, W., 1996, Annual Report 1995/96, ELs 102/87, 55/89 and 12/92 Queenstown, Mt. Darwin and Queenstown South: Zeehan, Tasmania: RGC Exploration Ltd.

Hawthorne, F.C., and Dirlam, D.M., 2011, Tourmaline the Indicator Mineral: From Atomic Arrangement to Viking Navigation: Elements, v. 7, no. 5, p. 307–312.

Hawthorne, F.C. and Henry, D.J., 1999, Classification of the minerals of the tourmaline group: European Journal of Mineralogy, v. 11, p. 201–215.

Haynes, D. W., 2000, Iron oxide copper(-gold) Deposits: Their position in the ore deposit spectrum and modes of origin, in Porter, T. M., ed., Hydrothermal Iron Oxide Copper-Gold & Related Deposits, A Global Perspective, p. 71–90.

Hedenquist, J.W., Arribas, A., and Reynolds, T.J., 1998, Evolution of an Intrusion-Centered Hydrothermal System: Far Southeast-Lepanto Porphyry and Epithermal Cu-Au Deposits, Philippines: Economic Geology, v. 93, p. 373–404.

Henry, D.J., and Guidotti, C.V., 1985, Tourmaline as a petrogenetic indicator mineral: an example from the staurolite-grade metapelites of NW Maine: American Mineralogist, v. 70, pp. 1–15.

Henry, D.J., Novak, M., Hawthorne, F.C., Ertl, A., Dutrow, B.L., Uher, P., and Pezzotta, F., 2011, Nomenclature of the tourmaline-supergroup minerals: American Mineralogist, v. 96, p. 895–913.

Hills, C.L., 1914, The Jukes-Darwin mining field: Bulletin of the Geological Survey of Tasmania, v. 16.

Hitzman, M.W., 2000, Iron oxide-Cu-Au deposits: what, where, and why?, in Poryer, T.M., ed., Hydrothermal iron oxide copper-gold & related deposits: a global prospective, v. 1, p. 9–25.

Hitzman M.W., Oreskes, N., and Einaudi, M.T., 1992, Geological characteristics and tectonic setting of Proterozoic iron oxide (Cu-U-Au-REE) deposits: Precambrian Research, V. 58, p. 241–287

Holliday, J.R. and Cooke, D.R., 2007, Advances in Geological Models and Exploration Methods for Copper ± Gold Porphyry Deposits: Ore Deposits and Exploration Technology, v. 53, p. 791–809.

Holm, O.H., and Berry, R.F., 2002, Structural history of the Arthur Lineament, northwest Tasmania: an analysis of critical outcrops: Australian Journal of Earth Sciences, v. 49, p. 167–185.

Holtstam, D., Anderssonm U.B., Broman, C., and Mansfeld, J., 2014, Origin of REE mineralisation in the bastnäs-type Fe-REE-(Cu-Mo-Bi-Au) deposits, Bergslagen, Sweden: Mineralium Deposita, v. 49, p. 933–966.

Holtstam, D., Andersson, U.B., Mansfeld, J., 2003, Ferriallanite-(Ce) from the Basntnäs deposit, Västmanland, Sweden: The Canadian Mineralogist, v. 41, p. 1233–1240.

Hoshino, M., Kimata, M., Arakawa, Y., Shimizu, M., Nishida, N. and Nakai, S., 2007, Allanite-(Ce) as an indicator of the origin of granitic rocks in Japan: Importance of Sr-Nd isotopic and chemical composition: Canadian Mineral., v. 43, p. 1329–1336.

Hoshino, M., Kimata, M., Shimizu, M., Nishida, N., Fujiwara, T., 2006, Allanite-(Ce) in granitic rocks from Japan: genetic implications of patterns of REE and Mn enrichment: The Canadian Mineralogist, v. 44, p. 45–62.

Hughes, C., 2015, The South Darwin Cu-Au-Fe-REE Discovery in Mount Read Volcanics, West Coast Tasmania: Mineral Exploration in the Tasmanides, Mines and Wines 2015.

Humphris, S.E., and Thompson, G., 1978, Trace element mobility during hydrothermal alteration of oceanic basalts. Geochimica et Cosmochimica Acta, v. 42, p. 127–136.

Inoue, A., Kurokawa, K., and Hatta, T., 2010, Application of chlorite geothermometry to hydrothermal alteration in Toyoha geothermal system, Southwestern Hokkaido, Japan: Resource Geology, v. 60, p. 52–70.

Ishihara, S., 1981, The granitoid series and mineralization: Economic Geology 75th Anniversary Volume, p. 458–484.

Ishihara, S., Hirano, H., Hoshino, M., Can, P.N., Dung, P.T., and Tran, T-A., 2011, Mineralogical and chemical characteristics of the allanite-rich copper and iron ores from the Sin Quyen mine, northern Vietnam: Bulletin of the Geological Survey of Japan, v. 62, p. 197–209.

Jack, D.J., 1989, Hellyer Host Rock Alteration: Unpublished Honours thesis, University of Tasmania.

Jiang, S.Y., 2000. Controls on the mobility of high field strength elements (HFSE), U, and Th in an ancient submarine hydrothermal system of the Proterozoic Sullivan Pb-Zn-Ag deposit, British Columbia, Canada: Geochemical Journal, v. 34, p. 341–348.

Jiang, S.Y., Palmer, M.R., Li, Y.H., and Xue, C. J.,1995, Chemical compositions of tourmaline in the Yindongzi-Tongmugou Pb-Zn deposits, Qinling, China: implications for hydrothermal ore-forming processes: Mineralium Deposita, v. 30, p. 225–234.

Jiang, S.Y., Yu, J.M., and Lu, J.J., 2004, Trace and rare-earth element geochemistry in tourmaline and cassiterite from the Yunlong tin deposit, Yunnan, China: implication for migmatitic-hydrothermal fluid evolution and ore genesis: Chemical Geology, v. 209, p. 193–213.

Jo, J., and Shin, D., 2015, Sulfur Isotope Variations of Metallic Ore Deposits in the Gyeongsang Basin, South Korea: Resource Geology, v. 65, p. 296–310.

Jones, W.T., 1993, The Geology, geochemistry and structure of the Mt. Darwin – South Darwin Peak area, western Tasmania: Unpublished B.Sc (Honours) thesis, University of Tasmania.

Jones, A.T. 1999, Volcanology and geochemistry of the Cambrian Mount Read Volcanics in the Basin Lake area, western Tasmania: Research Master thesis, University of Tasmania.

Jonsson, E., Högdahl, K., Sahlström, F., Nysten, P., and Sadeghi, M., 2014, The Paleoproterozoic skarn-hosted REE mineralisations of bastnas-type: overview and mineralogical-geological character: European Rare Earth Resources 2014, p. 383–389.

Kerrich, R., Goldfarb, R.J., and Richards, J.P., 2005, Metallogenic provinces in an evolving dynamic framework: Economic Geology 100th Anniversary Volume, p. 1097–1136.

Kerrich, R., Goldfarb, R.J., Groves, D.I., and Garwin, S., 2000, The geodynamics of world-class gold deposits: Characteristics, space-time distribution, and origins: Reviews in Economic Geology, v. 13, p. 501–552.

Khvostova, V.A., 1963, On the isomorphism of epidote and orthite: Doklady Academy of Sciences.

Kogarko, L.N., Kononova, V.A., Orlova, M.P., and Woolley, A.R., 1995, Alkaline Rocks and Carbonatites of the World, Part Two: Former USSR. Chapman & Hall, London, 226 p.

Kosterin, A.V., Kizyura, V.E., and Zuev, V.N., 1961, Ratios of rare earth elements in allanites from some igneous rocks of northern Kirgiziya: Geochemistry, v. 5, p. 481–484.

Krneta, S., Ciobanu, C.L., Cook, N.J., Ehrig, K., and Kontonikas-Charos, A., 2017, Rare Earth Element Behaviour in Apatite from the Olympic Dam Cu–U–Au–Ag Deposit, South Australia: Minerals, v. 7, 135 p.

Kwak, T. A. P., and Tan, T.H., 1981, The geochemistry of zoning in skarn minerals at the King Island (Dolphin) Mine: Economic Geology, v.76, p. 468–497.

Lang, J.R., Stanley, C.R., and Thompson, J.F.H., 1995, Porphyry copper-gold deposits related to alkalic igneous rocks in the Triassic-jurassic arc terranes of British Columbia: Porphyry Copper Deposits of the American Cordillera: Arizona Geological Society Digest 20, p. 219–236.

Large, R.R., Doyle, M., Raymond, O., Cooke, D., Jones, A., and Heasman, L., 1996, Evaluation of the role of Cambrian granites in the genesis of world class VHMS deposits in Tasmania: Ore Geology Reviews, v. 10, p. 215–230.

Large, R.R., Gemmell, J.B., Paulick, H., and Huston, D.L., 2001, The alteration box plot: A simple approach to understanding the relationship between alteration mineralogy and

lithogeochemistry associated with volcanic-hosted massive sulfide deposits: Economic Geology, v. 96, p. 957–971.

Large, R.R., McPhie, J., Gemmell, J.B., Herrmenn, W., and Davidson, G.J., 2001, The spectrum of ore deposit types, volcanic environments, alteration halos, and related exploration vectors in submarine volcanic successions: some examples from Australia: Economic Geology, v. 96, p. 913–938.

Large, S.J.E., Von Quadt, A., Wotzlaw, J.F., Guillong, M., and Heinrich, C.A., 2018, Magma Evolution Leading to Porphyry Au-Cu Mineralization at the Ok Tedi Deposit, Papua New Guinea: Trace Element Geochemistry and High-Precision Geochronology of Igneous Zircon: Economic Geology, v. 113, p. 39–61.

Le Maitre, R.W., 1989, A classification of igneous rocks and glossary of terms: recommendations of the International Union of Geological Sciences Subcommission on the Systematics of Igneous Rocks: Blackwell Scientific Publications, Oxford, United Kingdom, 253 p.

Leanman, D.E., and Richardson, R.G., 1989. The granites of west and North-west Tasmania, a geophysical interpretation: Bulletin Geological Survey of Tasmania, v. 66, 146 p.

Lee, D.E., and Bastron, H., 1967, Fractionation of rare-earth elements in allanite and monazite as related to geology of the Mt. Wheeler mine area, Nevada: Geochimica et Cosmochimica Acta, v. 31, p. 339–356.

Lees, T.C., 1987, The Geology and Mineralisation of the Rosebery-Hercules Area, Tasmania: Unpublished MSc thesis, University of Tasmania.

Lewis, A.J., Komninou, A., Yardley, B.W.D., and Palmer, M.R., 1998, Rare earth element speciation in geothermal fluids from Yellowstone National Park, Wyoming, USA: Geochimica et Cosmochimica Acta, v. 62, p. 657–663.

London, D., and Manning, D.A.C., 1995, Chemical variation and significance of tourmaline from southwest England: Economic Geology, v. 90, p. 495–519.

Love, D.A., Clark, A.H., Keith G.J., 2003, The Lithologic, Stratigraphic, and Structural Setting of the Giant Antamina Copper-Zinc Skarn Deposit, Ancash, Peru: Economic Geology, v. 99, p. 887–916.

Mao, J., Zhang, J., Pirajno, F., Ishiyama, D., Su, H., and Guo, C., 2011, Porphyry Cu-Au-Mo-epithermal Ag-Pb-Zn-distal hydrothermal Au deposits in the Dexing area, Jiangxi province, East China – A linked ore system: Ore Geology Reviews, v. 43, no. 1, p. 203–216.

Marks, M.A.W., Marschall, H.R., Schühle, P., Guth, A., Wenzel, T., Jacob, D.E., Barth, M., and Markl, G., 2013, Trace element systematics of tourmaline in pegmatitic and hydrothermal systems from the Variscan Schwarzwald (Germany): The importance of major element composition, sector zoning, and fluid or melt composition: Chemical Geology, v. 344, p. 73–90.

Martin, N.K., 2004, Genesis of the Rosebery massive sulfide deposit, western Tasmania, Australia: Unpublished Honours thesis, University of Tasmania.

McNeil, A.W., and Corbett, K.D., 1992, Geology and mineralisation of the Mt. Murchison area: Mount Read Volcanics Project Geological Report 2, Department of Mines Tasmania.

McPhie, J., and Allen, R.L., 1992, Facies architecture of mineralized submarine volcanic sequences: Cambrian Mount Read Volcanics, western Tasmania: Economic Geology, v. 87, p. 587−596.

McPhie, J., and Allen, R.L., 2003, Submarine, silicic, syneruptive pyroclastic units in the Mt. Read Volcanics, western Tasmania – influence of vent setting and proximity on lithofacies characteristics: AGU Geophysical Monograph, v. 140, p. 245–258.

Mean, J.K., 1990, Negative Ce anomalies in Archean amphibolites and Laramide granitoids, southwestern Montana, U. S. A.: Chemical Geology, v. 81, p. 191–207.

Meffre, S., Berry, R.F., and Hall, M., 2008, Cambrian metamorphic complexes in Tasmania: Tectonic implications: Australian Journal of Earth Sciences, v. 47, no. 6, p. 971–985.

Meinert, L.D., 1992. Skarns and Skarn deposits: Geoscience Canada, v. 19, no. 4, p. 145–162.

Middlemost, E.A.K., 1994, Naming Materials in the Magma/Igneous Rock System: Earth-Science Reviews, v. 37, p. 215–224.

Mills, S.J., Hatert, F., Nickel, E.H., and Ferraris, G., 2009, The standardisation of mineral group hierarchies: Application to recent nomenclature proposals: European Journal of Mineralogy, v. 21, p. 1073–1080.

Minakawa, T., Fukishima, H., Nishio-Hamane, D., and Hiroyuki, M., 2008, Epidote-(Sr), $CaSrAl^{2}Fe^{3+}(Si_2O_7)(SiO_4)(OH)$, a new mineral from the Ananai mine, Kochi Prefecture, Japan: Journal of Mineralogical and Petrological Sciences, v. 103, p. 400–406

Mitchell, R.H., 1996, Perovskite: A revised classification scheme for an important rare earth element host in alkaline rocks, in Jones A.P, Williams, C.T., and Wall, F., eds., Rare Earth Minerals: Chemistry, Origin and Ore Deposits: Mineralogical Society Series, Chapman & Hall, London, p. 41–76.

Morrison, J., 2004, Stable and radiogenic isotope systematics in epidote group minerals: Reviews in Mineralogy and Geochemistry, v. 56, p. 607–628.

Mortensen, J.K., Gemmell, J.B., McNeill, A.W., and Friedman, M., 2015, High-Precision U-Pb Zircons Chronostratigraphy of the Mount Read Volcanic Belt in Western Tasmania, Australia: Implications for VHMS Deposit Formation: Economic Geology, v. 100, p. 445–468.

Müller, D., Kaminski, K., Uhligm S., Graupner, T., Herzig, P., and Hunt, S., 2002, The transition from porphyry- to epithermal-style gold mineralization at Ladolam, Lihir Island, Papua New Guines: a reconnaissance study: Mineralium Deposita, v. 37, p. 61–74.

Munara, K.J., Rose, H.J., JR., Carron, M.K., and Glass, J.J., 1957, Systematic variation of rare earth elements in cerium-earth minerals: Geochimica et Cosmochimica Acta, v. 11, p. 141–161.

Murphy, F.C., Denwer, K., Keele, R.A., Stapleton, P., Seymour, D.B., and Green, G.R., 2004, Tasmania mineral province: geoscientific database, 3D geological modelling, mines and mineral prospectivity: Mineral Resources Tasmania

Nagashima, M., Nishio-Hamane, D., Tomita, N., Minakawa, T., and Inaba, S., 2013, Vanadoallanite-(La): A new epidote-supergroup mineral from Ise, Mie Prefecture, Japan: Mineralogical Magazine, v. 77, p. 2739–2752.

Oberli, F., Meier, M., Berger, A., Rosenberg, C.L., an Giere, R., 2004, U- Th-Pb and 230Th/238U disequilibrium isotope systematics: precise accessory mineral chronology and melt evolution tracing in the Alpine Bergell intrusion: Geochimica et Cosmochimica Acta, v. 68, p. 2543–2560.

Ohmoto, H., 1986, Stable isotope geochemistry of ore deposits in Vallet J.W., Taylor H.P. JR., and O'Neil J.R., eds., Stable Isotopes in High Temperature Geological Processes: Reviews in Minealogy, v. 16, p. 491–559.

Ohmoto, H., and Rye, R.O., 1979, Isotopes of sulfur and carbon, in Barnes, H.L., 2nd eds., Geochemistry of hydrothermal ore deposits, p. 509–567.

Orovan, E.A., Cooke, D.R., Harris, A.C., Ackerman, B. and Lawlis, E., 2018, Geology and Isotope Geochemistry of the Wainaulo Cu-Au Porphyry Deposit, Namosi District, Fiji: Economic Geology, v. 113, p. 133–161.

Orris, G.J., Grauch, R.I., 2002, Rare earth element mines, deposits, and occurrences: U.S. Geological Survey Open-File Rep 2002–0189.

Pal, D.C., Chaudhuri, T., McFarlane, C., Mukherjee, A., Sarangi, A.K., 2011, Mineral chemistry and in situ dating of allanite, and geochemistry of its host rocks in the Bagjata uranium

mine, Singhbhum Shear Zone, India- Implications for the chemical evolution of REE mineralization and mobilization: Economic Geology, v. 106, p. 1155–1171.

Pascual, E., Nesbitt, R. W., Toscano, M., Almodóvar, G. R. and Sáez, R., 1997, Zirconium mobility in footwall hydrothermal haloes in the Iberian Pyrite Belt: geochemical and textural evidences: SEG Neves Corvo Field Conference, Abstracts, 81 p.

Pass, H.E. 2010, Breccia-hosted chemical and mineralogical zonation patterns of the northeast zone, Mt. Polley Cu-Ag-Au alkalic porphyry deposit, British Columbia, Canada: Unpublished PhD thesis, University of Tasmania.

Pearce, J.A., Harris, N.B.W., and Tindle, A.G., 1984, Trace element discrimination diagrams for the tectonic interpretation of granitic rocks: Journal of Petrology, v. 25, p. 956–983.

Pemberton, J., and Corbett, K.D. 1992, Stratigraphic-facies associations and their relationship to mineralization in the Mount Read Volcanics: Mineral Resources Tasmania, Geological Survey Bulletin 70, p. 167−176.

Perkins, C., and Walshe, J.L., 1993, Geochronology of the Mount Read Volcanics, Tasmania, Australia: Economic Geology, v. 88, p. 1176-1197.

Peterson, R.C., and MacFarlane, D.B., 1993, The rare-earth-element chemistry of allanite from the Grenville Province: The Canadian Mineralogist, v. 31, p. 159–166.

Piziak, L.K., Canil, D., Grondahl, C., Plouffe, A., Ferbey, T., and Anderson, R.G., 2015, Magnetite as a porphyry Cu indicator mineral in till: a test using the Mount Polley porphyry Cu-Au deposit, British Columbia, in Geoscience BC Summary of Activities 2014, Geoscience BC, Report 2015-1, p. 141–150.

Plimer, I.R., and Lees, T,C, 1988, Tourmaline-rich Rocks Associated with the Submarine Hydrothermal Rosebery Zn-Pb-Cu-Ag-Au Deposit and Granites in Western Tasmania, Australia: Mineralogy and Petrology, v. 38, p. 81–103.

Ploshko, V.V., and Bogdanova, V.I., 1963, Isomorphous substitutions in minerals of the epidote group from the northern Caucasus: Geochemistry, v. 1, p. 61–71.

Pollard, P.J., 2000, Evidence of a magmatic fluid and metal source for Fe oxide Cu-Au mineralization, in Porter, T. M., ed., Hydrothermal iron oxide copper-gold and related deposits: A global perspective: Adelaide, Australian Mineral Foundation, p. 27–41.

Pollard, P.J., 2006, An intrusion-related origin for Cu-Au mineralization in iron oxide-copper-gold (IOCG) provinces: Mineral Deposita, v. 46, p. 179–187.

Porter, T.M., 2002, Hydrothermal iron oxide copper-gold and related deposits: A global perspective: Adelaide, PGC Publishing, v. 2, 367 p.

Poyla, D.A., Solomon, M. and Eastoe, C.J., 1986, The Murchison Gorge, Tasmania – a Possible Cross Section through a Cambrian Massive Sulfide System: Economic Geology, v. 81, p. 1341–1355.

Raymond, O.L., 1992, Geology and Mineralisation of the Southern Prince Lyell Deposits, Queenstown, Tasmania: Unpublished MSc. Thesis, University of Tasmania

Raymond, O.L., 1996, Pyrite composition and ore genesis in the Prince Lyell copper deposits, Mt. Lyell mineral field, western Tasmania, Australia: Ore Geology Reviews, v. 10, p. 231–250.

Reid, K.O., 1977, Jukes-Darwin area, E.L. 21/76, Annual Progress Report No. 1: The Mount Lyell Mining and Railway Company Ltd..

Reid, R 2001, Cambrian intrusion-related copper mineralisation at the Thomas Creek prospect, Southwestern Tasmania: Coursework Master thesis, University of Tasmania

Rieger, A., Marschik, and Díaz, M., 2012, The evolution of the hydrothermal IOCG system in the Mantoverde district, northern Chile: new evidence from microthermometry and stable isotope geochemistry: Mineralium Deposita, v. 47, p. 359–369.

Rinne, M., Cooke, D., Harris, A., Finn, D., Allen, C., Heizler, M., and Creaser, R, 2018, Geology and geochronology of the Golpu porphyry and Wafi epithermal deposit, Morobe Province, Papua New Guinea: Economic Geology, v. 113, p. 271–294.

Robinson, B.S., and Kusakabe, M., 1975, Quantitative preparation of sulfur dioxide, for $^{34}S/^{32}S$ analyses, from sulfides by combustion with cuprous oxide: Analytical Chemistry, v. 47, p. 1179–81.

Rollinson, H.R, 1993, Using geochemical data: evaluation, presentation, interpretation: Longman geochemistry series, Burnt Mill, Harlow, Essex, England.

Ryan, P.J., Lawrence, A.L., Jenkins, R.A., Matthews, J.P., Zamora, J.C., Marino, E., and Urqueta, I., 1995, The Candelaria copper-gold deposit, Chile: Arizona Geological Society Digest, v. 20, p. 625–645.

Rye, R.O., 1993, The evolution of magmatic fluids in the epithermal environment: the stable isotope perspective: Economic Geology, v. 88, p. 733–753.

Rye, R.O., 2005, A review of the stable-isotope geochemicatry of the sulfate minerals in selected igneous environments and related hydrothermal systems: Chemical Geology, v. 215, p. 5–36.

Schlegel, T. U. and Heinrich, C. A., 2015, Lithology and Hydrothermal Alteration Control the Distribution of Copper Grade in the Prominent Hill Iron Oxide-Copper-Gold Deposit (Gawler Craton, South Australia): Economic Geology, v. 110, p. 1953–1994

Schmandt, D.S., Cook, N.J., Ciobanu, C.L., Ehrig, K., Wade, B.P., Gilbert, S., and Kamenetsky, V.S., 2017, Rare Earth Element Fluoracarbonate Minerals from the Olympic Dam Cu-U-Au-Ag Deposit, South Australia: Minerals, v. 7, 202 p.

Seal, R.R., 2006, Sulfur isotope Geochemistry of sulfide minerals: Reviews in Mineralogy and Geochemistry, v. 61, p. 633–677.

Seal R.R., Alpers C.N., and Rye, R.O., 2000, Stable isotope systematics of sulfate minerals: Reviews in Mineralogy and Geochemistry, v. 40, p. 541–602.

Seedorff, E., Dilles, J.H., Proffett, J.M., Einaudi, M.T., Zurcher, L., Stavast, W.J.A., Johnson, D.A., and Barton, M.D., 2005, Porphyry deposits: Characteristics and origin of hypogene features: Economic Geology 100th Anniversary Volume, p. 251–298.

Selley, D.B., 1997, A re-evaluation of the structural significance of the Boat Habour Fault, northwestern Tasmania: Mineral Resources Tasmania Record 1997/09.

Selley, D.B, Green, G.R., and Calver, C.R., 2006, The geology and mineral deposits of Tasmania: a summary: Tasmania Geological Survey Bulletin 72.

Seymour, D.B., and Calver, C.R., 1995, Explanatory notes for the time-scape diagram and stratatectonic elements map of Tasmania: Tasmanian Geological Survey Record 1995/01, Mineral Resources Tasmania

Seymour, D.B., and Calver, C.R., 1998, Proterozoic rock sequences of western Tasmania: Proceedings of the 14th Australian Geological Convention (Townsville).

Seymour, D.B., Green, G.R., and Calver, C.R., 2007, The Geology and Mineral Deposits of Tasmania: a summary: Tasmania Geological Survey Bulletin 72, Mineral Resources Tasmania.

Shank, W.C.P., 2014, III, Stable isotope geochemistry of mineral deposits, Treatise on Geochemistry, 2nd eds., p. 59–85.

Shikazono, N., and Kawahata, H., 1987, Compositional Differences in Chlorite from Hydrothermally Altered Rocks and Hydrothermal Ore Deposits: Canadian Mineralogist, v. 25, p. 465–474.

Sinclair, W.D., 2007, Porphyry deposits, in Goodfellow, W.D., ed., Mineral Deposits of Canada: A Synthesis of Major Deposit-Types, District Metallogeny, the Evolution of Geological

Provinces, and Exploration Methods: Geological Association of Canada, Mineral Deposits Division, Special Publication No. 5, p. 223-243

Skoda, R., Cempírek, J., Filip, J., Novák, M., Veselovsky, F., and Ctvrtlik, R., 2012, Allanite-(Nd), $CaNdAl_2Fe^{2+}(SiO_4)(Si_2O_7)O(OH)$, a new mineral from Askagen, Sweden: American Mineralogist, v. 97, p. 983–988.

Slack, J.F., 1996, Tourmaline associations with hydrothermal ore deposits: Reviews in Mineralogy and Geochemistry, v. 3, p. 559–664.

Slack, J.F. and Trumbull, R.B., 2011, Tourmaline as a Recorder of Ore-Forming Processes: Elements, v. 7, p. 321–326.

Slack, J.F., Palmer, M.R., Stevens, B.P.J., and Barnes, R.G., 1993, Origin and significance of tourmaline-rich rocks in the Broken Hill district, Australia: Economic Geology, v. 88, no. 3, p. 505–541.

Smith, M.P., Campbell, L.S., and Kynicky, J., 2015, A review of the genesis of the world class Bayan Obo Fe–REE–Nb deposits, Inner Mongolia, China: multistage processes and outstanding questions: Ore Geology Reviews, v. 64, p. 459–476.

Smith, M.P., Henderson,P., and Jeffries, T., 2002, The formation and alteration of allanite in skarn from the Beinnan Dubhaich granite aureole, Skye: European Journal of Mineralogy, v. 14, 471–486.

Smith, M.P., Moore, K., Kavecsánszki, D., Finch, A.A., Kynicky, J. and Wall, F., 2016, From mantle to critical zone: A review of large and giant sized deposits of the rare earth elements: Geoscience Frontiers, v. 7, p. 315–334.

Smye, A.J., Roberts, N.M.W., Condon, D.J., Horstwood, M.S.A., and Parrish, R.R., 2014, Characterising the U-Th-Pb systematics of allanite by ID and LA-ICP-MS: Implications for geochronology: Geochimica et Cosmochimica Acta, v. 135, p. 1–28.

Sokolova, E.V., Nadezhina, T.N., Pautov, L.A., 1991, Crystal structure of a new natural silicate of manganese from the epidote group: Soviet Physics – Crystallography, v. 36, p. 172–174

Solomon, M., 1960. The Dundas group in Queenstown area: Papers and Proceedings of the Royal Society of Tasmania, v. 94, p. 33–49.

Solomon, M., 1981, An introduction to the geology and metallic ore deposits of Tasmania: Economic Geology, v. 76, p. 194–208.

Solomon, M., Eastoe, C.J., Walshe, J.L., and Green, C.R., 1988, Mineral deposits and sulfur isotope abundances in the Mount Read Volcanics between Que River and Mount Darwin, Tasmania: Economic Geology, v. 83, p. 1307–1328.

Solomon, M., Rafter, T.A., and Jensen, M.L., 1969, Isotope studies on the Rosebery, Mount Farrell and Mount Lyell Ores, Tasmania: Mineralium Deposita, v. 4, p. 172–199.

Stacey, A.R., and Berry, R.F., The structural history of Tasmania: a review for petroleum explorers, in Boult, P.J., Johns, D.R., and Lang, S.C., eds., Eastern Australian Basin Symposium II, Adelaide 19–22 September 2004, p. 151–162.

Stolz, J., 1992, The use and abuse of immobile element geochemistry for rock classification and identification of paleotectonic setting of ancient volcanic sequences: Unpublished CODES Master of Economic Geology, Coursework Manual 10, University of Tasmania.

Streckeisen, A.L., 1973, Plutonic rocks, classification and nomenclature recommended by the IUGS subcommission on the systematics of igneous rocks: Geotimes, v. 18, 26–30.

Streckeisen, A., 1974, Classification and nomenclature of plutonic rocks recommendations of the IUGS subcommission on the systematics of Igneous Rocks, Geologische Rundschau, v. 63, p. 773–786.

Takagi, T., 2004, Origin of magnetite- and ilmenite-series granitic rocks in the Japan arc. American Journal of Science, v. 304, 169–202.

Taylor, S.R., and McLennan, S.M., 1985, The continental crust: its composition and evolution: Blackwell Scientific Publication, Carlton, 312 p.

Tornos, F., Wiedenbeck, M., and Velasco, F., 2012, The boron isotope geochemistry of tourmaline-rich alteration in the IOCG systems of northern Chile: implications for a magmatic-hydrothermal origin: Mineralium Deposita, v. 47, p. 483–499.

Torresi, I., Xavier, R.P., Bortholoto, D.F.A., and Monteiro, L.V.S., 2012, Hydrothermal alteration, fluid inclusions and stable isotope systematics of the Alvo 118 iron oxide–copper–gold deposit, Carajás mineral province (Brazil). Implications for ore genesis: Mineralium Deposita, v. 47, p. 299–323.

Turner, N.J., Black, L.P., and Kamperman, M., 1998, Dating of Neoproterozoic and Cambrian orogenies in Tasmania: Australian Journal of Earth Sciences, v. 45, p. 789−806.

Uher, P., Ondrejka, M., Bačík, P., Broska, I., and Konečnýc, P., 2015, Britholite, monazite, REE carbonates, and calcite: Products of hydrothermal alteration of allanite and apatite in A-type granite from Stupné, Western Carpathians, Slovakia: Lithos, v. 236–237, p. 212–225.

Ullrich, T.D., and Clark, A.H., 1999, The Candelaria copper-gold deposit, región III, Chile: Paragenesis, geochronology and fluid composition, in Stanley, C.J., ed., Mineral deposits: Processes to processing: Rotterdam, Balkema, p. 201–204

Walshe, J.L., and Solomon, M., 1981, An investigation into the environment of formation of the volcanic-hosted Mt. Lyell copper deposits using geology, mineralogy, stable isotopes, and a six-component chlorite solid solution model: Economic Geology, v. 76, p. 246–284.

Wang, Z., Chen, B., Yan, X., and Li, S., 2018, Characteristics of hydrothermal chlorite from the Niujuan Ag-Au-Pb-Zn deposit in the north margin of NCC and implications for exploration tools for ore deposits: Ore Geology Reviews, v. 101, p. 398–412.

White, N.C., 1975, Cambrian volcanism and mineralisation, SW Tasmania: Unpublished PhD thesis, University of Tasmania.

White, M.J., and McPhie, J., 1996, Stratigraphy and paleovolcanology of the Cambrian Tyndall Group, Mt. Read Volcanics, western Tasmania: Australian Journal of Earth Sciences, v. 43, p. 147–159.

Williams, E., McClenaghan, M.P., Collins, P.L.F., Brown, S.G., Camacho, A., Dronseika, E.V., Higgins, N.C., Morland, R., Reid, E.J., and Seymour, D.B., 1989, Mid-Paleozoic deformation, granitoids and ore deposits, in Burrett, C.F., and Martin, E.K., ed., Geology and Mineral Resources Tasmania: Geological Society of Australia Special Publication 15.

Williams, P.J., Barton, M.D., Johnson, D.A., Fontbote, L., De Haller, A., Mark, G., and Oliver, N.H.S., 2005, Iron Oxide Copper Gold Deposits: Geology, Space-time Relationships and Possible Modes of Origin: Economic Geology 100th Anniversary Volume, p. 371–405.

Williams-Jones, A.E., Migdisov, A.A., and Samson, I.M., 2012, Hydrothermal mobilisation of the rare earth elements – a Tale of "Ceria" and "Yttria": Elements, v. 8, p. 355–360.

Williamson, B.J., Spratt, J., Adams, J.T., Tindle, A.G., and Stanley, C.J., 2000, Geochemical Constraints from Zoned Hydrothermal Tourmalines on Fluid Evolution and Sn Mineralization: an Example from Fault Breccias at Roche, SW England: Journal of Petrology, v. 41, p. 1439–1453.

Wilson, A.J., Cooke, D.R., and Harper, B.L., 2003, The Ridgeway gold-copper deposit: A high-grade alkalic porphyry deposit in the Lachlan fold belt, New South Wales, Australia: Economic Geology, vol. 98, p. 1637–1666.

Wilson, A.J., Cooke, D.R., Harper, B.J., and Deyell, C.L., 2007, Sulfur isotopic zonation in the Cadia district, southeastern Australia—Exploration significance and implications for the

genesis of alkalic porphyry gold-copper deposits: Mineralium Deposita, v. 42, p. 465–487.

Wolfe, R.C., and Cooke, D.R., 2011, Geology of the Didipio region and genesis of the Dinkidi alkalic porphyry Cu-Au deposit and related pegmatites, northern Luzon, Philippines: Economic Geology, v. 106, p. 1279–1315.

Wood, S.A., 1990, The aqueous geochemistry of the rare-earth elements and yttrium: 2. Theoretical predictions of speciation in hydrothermal solutions to 350°C at saturation water vapour pressure: Chemical Geology, v. 88, p. 99–125.

Wood, S.A., and Ricketts, A., 2000, Allanite-(Ce) from the Eocene Casto Granite, Idaho: Response to Hydrothermal Alteration: The Canadian Mineralogist, v. 38, p. 81-100.

Wu. C., 2008, Bayan Obo Controversy: Carbonatites versus Iron Oxide-Cu-Au-(REE-U): Resource Geology, v. 58, p. 348–354.

Wyman, W., 2001, Cambrian Granite-related Hydrothermal Alteration and Cu-Au Mineralisation in the Southern Mt. Red Volcanics, Western Tasmania. Australia: Unpublished PhD thesis, University of Tasmania.

Xiao, B., Chen, H., Wang, Y. Han, J., Xu, C., and Yang, J., 2017, Chlorite and epidote chemistry of the Yandong Cu deposit, NW China: Metallogenic and exploration implications for Paleozoic porphyry Cu systems in the Eastern Tianshan: Ore Geology Reviews, v. 100, p. 168–182.

Yavuz, F., Iskenderoglu, A., and Jiang, S.Y., 1999, Tourmaline compositions from the Salikvan porphyry Cu-Mo deposit and vicinity, northeastern Turkey: The Canadian Mineralogist, v. 37, p. 1007–1023.

Yavuz, F., Jiang, S.Y., Karakaya, N., Karakaya, M.C., and Yavuz, R., 2011, Trace-element, rare-earth element and boron isotopic compositions of tourmaline from a vein-type Pb-Zn-Cu +/- U deposit, NE Turkey: International Geology Review, v. 53, p. 1–24.

Appendix A

Literature Review

on

Granites and Porphyry Ore Deposits in Convergent Arc Settings

Xin Ni Seow

May 2018

UNIVERSITY OF TASMANIA

Honours Degree, University of Tasmania

Table of Contents

Chapter 1: Introduction

Porphyry ore deposits have been important targets for modern mineral exploration as they are the world's largest reserves of high tonnage Cu-Mo-Au, along with substantial Ag, Pd, Te, Bi, Re, Zn, Ag and Pb credits (Sillitoe, 2010). Many of the porphyry ore deposits around the world show intimate relationship with multiphase intermediate to felsic magmatism above subduction zones (i.e. Batu Hijau, Indonesia: Garwin, 2002; Ok Tedi and Wafi-Golpu, Papua New Guinea: Large et al., 2018; Rinne et al., 2018). This relationship poses questions around the source of metals from arc-related magmas that are the source of porphyry deposits, and how they are transported. Igneous petrologists are primarily interested in the petrogenesis of the evolved magmas, whereas economic geologists seek the source of potential valuable metals.

Granite petrogenesis has been widely debated over several decades (e.g., Barbarin, 1990; Brown and Campbell, 1992; Brown, 1994; Chappell and White, 2001). Granites commonly have a complex origin, being the end product of geological processes involving contributions from both mantle and crustal material (Barbarin, 1990). Partial melting, fractionation, assimilation, magma mixing and crustal contamination as the magma ascends to the site of emplacement play important roles in enriching crustal melts to varying degrees (Petford et al., 2000). It is widely accepted that granite is the end-product of these differentiation processes. However, due to the diversity of sources, geochemical enrichment processes and tectonic settings involved in granite genesis, the formation of specific granitic suites must be considered on a case-by-case basis.

Economic geologists are broadly in agreement that porphyry mineralisation is triggered by magma enrichment processes involving soluble metals, brines and hydrous fluids in the deep crust, saturation of magmas with sulfide-bearing fluids, efficient metal transfer into magmatic-hydrothermal fluids exsolved from the crystallising magma source, fluid-wallrock interaction and localised precipitation of ore minerals in the crust (Cooke and Gemmell, 1996; Sillitoe, 2010; Halley et al., 2015). However, current models do not fully address the factors for the broad variation of metal contents in porphyry systems, from Cu-rich, Cu-Au, to Mo-rich, while Sn-W-F-APGE deposits may be present if the system is associated with reduced granite.

This review intends to merge different geological perspectives on the genesis of granite, which is a common igneous rock in convergent arcs, and its association with porphyry deposits from geochemical and petrological aspects. Hydrothermal processes involved in

mineralisation and alteration in the porphyry environment will also be examined, closing with a discussion on the exploration models that are widely applied in the search for magmatic hydrothermal systems.

Chapter 2: Intrusive Rocks in Convergent Arc Settings

Convergent arc can involve multi-source and multi-stage magmatism (Winter, 2001). The complexities in sources contributing to arc magmas result in a broad array of arc magma composition (Murphy, 2006). General petrogenetic models of convergent arcs will be reviewed in this section, with an emphasis on the processes involved in arc magmatism, formation of granitic rocks and development of porphyry ore systems in arc settings.

2.1 Convergent Arc

Island arc (ocean-ocean convergence), continental arc (ocean-continent convergence) and continental collision (continent-continent convergence) are three end-members of convergent arcs (Murphy, 2006). Magmatism in island arcs is less complicated than in continental arcs as the effects of crustal contamination are limited. The crust is generally thinner and has stronger petrological affinities with more primitive melts (Stern, 2001). Potential sources for arc magmas include the subducting oceanic slab, subducted seafloor sediment, metasomatized asthenospheric mantle wedge above the slab and upper lithospheric plates (see Appendix 1; Richards, 2011).

Subduction of oceanic crust along the mantle wedge results in the influx of fluids released from dehydration reactions in the hydrous slab into the fore-arc mantle wedge (Tatsumi and Eggins, 1995). This instigates the partial melting of the metasomatized mantle wedge, producing mafic melts with higher oxidation states, volatiles, and concentrations of incompatible elements (Ishizuka et al., 2010). Enrichment of these oxidizing components in the melt is critical to the metallogenesis of porphyry deposits. The melts only erupt onto the surface where crust is thin, for example in young island arcs. In most cases, the primitive magmas tend to pond at the base of the arc crust and form high alumina basalts. Partial melting of the overlying arc crust occurs, resulting from the upward heat transfer from underplating magmas. Fractional crystallization, assimilation and magma mixing may all take place when the melts ascend to the surface, subsequently producing more evolved and silicic magmas (see Appendix 2; Richards, 2011).

More mafic and thinner crusts in island arcs limit the interaction of the primitive mantle-derived magmas with the arc crusts en route to the surface consequently. The resulting magmas are less differentiated, contaminated, and are dominated by lavas with basaltic to

andesitic compositions (Stern, 2010). Felsic plutons may occur if there is extreme magma differentiation from the mafic melts (e.g., Kermadec Island Arc, New Zealand: Haase et al., 2004). In continental arcs, the presence of thick continental crust acts as an effective density trap for magma stagnation, leading to remelting of crusts and commonly other magma enrichment processes such as crustal contamination, assimilation, magma mixing, fractional crystallization, influx of terrestrial-derived sediments and participation of the sub-continental lithospheric and accretionary prism (Brown and Rushmer, 2006). Interplay of these processes is reflected by the broad spectrum of igneous rock associations in continental arcs, with a predominance of felsic to intermediate magma compositions (Winter, 2001). Despite the broad array of rock associations, the resulting arc magmas are typically characterized by calc-alkaline compositions and high volatile contents, attributed to metasomatism in the mantle wedge by hydrous subducting slabs (Stern, 2001).

Subduction reversals, arc collision and rifting events may follow the detachment of a subducting slab when it becomes too buoyant to be further subducted into the mantle (Tulloch and Kimbrough, 2003). The tectonic regime switches from compressional or transpressional to an extensional setting. Post-subduction magmatism is primarily derived from partial melting of the subduction-modified upper lithospheric plate during post-subduction asthenospheric upwelling (Richards, 2011). Small volumes of calc-alkaline to weakly alkaline magmas are generated, and the magmas may contribute to the formation of alkalic porphyry systems (e.g., Cadia, Australia; Wilson, 2003).

2.2 Granite genesis

Granite is the most abundant igneous rock in the upper continental crust and is generally considered to be the end-product of fractionation of mantle-derived magmas. Granite batholiths often span a large range of sizes (10^{-5} to 10^{6} m; Brown, 1994). In addition to the range of sources, origins and enrichment processes, the origins of granitic intrusions still remain a subject of controversy (Petford et al., 2000). Many petrologists agree that both mantle and crust contribute to the formation of granites (e.g., Brown, 1994; Kemp et al, 2007; Wilkinson, 2013) though some suggests that granites are derived exclusively from crustal material (Tischendorf and Palchen, 1985) or the mantle (Lameyre et al., 1976). The relative contribution between mantle and crust to granite genesis is still an evolving issue in igneous petrology.

Brown (1994) stated that generation, segregation, ascent and emplacement of silicic melts are the four principal processes responsible for granite emplacement. Melt generation occurs as the result of partial melting of underplated mafic magmas (Petford et al., 2000). Viscosity

and density of melt accounts for the small-scale migration of melt from the molten zone (Brown, 1994). Ascent of the magma depends on the rheological contrast between granitic melt and surrounding rocks (Petford et al., 2000). Mechanisms of segregation, ascent and emplacement remain controversial, but many studies have demonstrated the role of deformation associated with these processes (e.g., Clemens and Mawer, 1992; Paterson and Vernon, 1995; Rosenberg, 2004; Weinberg et al., 2009). These processes are fundamental to understanding how the mantle-derived melts interact with crustal components and evolve into granitic magmas.

Early studies into the geochemistry and isotopic composition of granites have put forward several hypothesis for their formation. Bowen (1928) postulated that magma differentiation from a mafic magma to granite is a single process. This theory was revised through later experiments on fractional crystallization by Allègre and Minster (1978), partial melting (Pitcher, 1997), assimilation combined with fractional crystallization (DePaolo, 1981) and magma mixing (Langmuir, 1989), implying that granite formation involves several processes. Fractionation and magma mixing are popular models put forward to account for the compositional variation of granites (Chappell et al., 2000). Peritectic assemblages of entrainment, where the chemistry of granite is controlled by the chemistry of the peritectic minerals that can be derived from the magmatic source or wallrocks during magma mixing and assimilation, has also been postulated to explain the compositional variation of natural granites (Clemens and Stevens, 2012).

More recently, partial melting of various types of protolith, mostly under fluid-absent condition involving dehydration melting of hydrous minerals during subduction has been recognized as the principal mechanism for generating granites in convergent arcs (Clemens et al., 2016). However, the significance of other petrogenetic processes are still debated. Experiments by Gao et al. (2016) demonstrated that the roles of fractional crystallization and open-system processes (wallrock assimilation and mixing of mantle-derived melt with felsic melts) may not be as significant as previously thought. Fractional crystallisation and restite fractionation are important in governing the composition of granites (Dahlquist et al., 2007; Chappell et al., 2000).

2.3 Porphyry genesis

Porphyry is a textural term given to igneous rocks consisting of large crystals (phenocrysts) embedded within fine-grained groundmass or matrix. The conspicuous difference in grain size implies that porphyritic rocks have undergone two distinctly different stages of cooling (Winter, 2001). The first stage occurs when ascending magmas are trapped due to neutral

buoyancy and thermal insulation is efficient (Winter, 2001). The slow cooling rate allows the formation of phenocryst. This is followed by a second cooling event at or near to the surface (faster cooling rate) where the fine-grained ground mass is more rapidly crystallized. The texture of the matrix, ranging from hyaline (glassy), aphanitic to phaneritic, depends on the cooling rate. Phenocrysts phases in porphyries vary with the temperature, timing of emplacement or eruption, magma composition and abundance of fluids in the magma. The sequence of crystallization in a magma chamber was determined by Bowen (1992; Appendix 3). Addition or loss of water content, the relative rate between cooling and chemical reaction as the magma evolves, and replenishment of the magma by new material may interrupt Bowen's reaction series (Winter, 2001).

The base metal mineralisation that evolves from magmatic-hydrothermal systems with ore-forming fluids exsolved from a crystallizing porphyry stock is termed 'porphyry deposits' (Cooke et al., 2005). This type of system is characterized by the presence of large volumes of hydrothermally altered host rocks surrounding one or several porphyrytic stocks (Sillitoe, 1972, 2010; Pirajino, 1992). Annen et al. (2006) suggested that porphyry intrusions are sourced from crustal magma chambers at 4 – 10 km depth. Magma chambers associated with porphyry systems can typically remain active for millions of years (Sillitoe, 2010). This suggests that there may be continuous introduction of new material into the magma source over time. Multiple discrete intrusions and associated dike swarms can be emplaced upwards from the magma chambers to mid to upper crustal depths (4-10 km; Cooke et al., 2014). Emplacement of the melts is driven by geological structures, rate of melt extraction, buoyancy of magma in relative to the surrounding crust and ascending tendency of magma (Hutton, 1988). The melts evolve and subsequently crystallize to form intermediate to felsic plutons after emplacement and cause volatile saturation, providing an ideal scenario for porphyry ore formation (Annen et al., 2006).

Chapter 3: Granite-related ore deposits

Granite-related ore deposits host a diversity of metals with different mineralisation styles, including Sn, W, U, Fe, Cu, Au, Mo, Pb, Zn, Ag, Nb, Ta, Be, Li, Y, Zr and other metals (Sial et al., 2001). The systematic relationship between metallogenic potential of granite-related ore deposits and the geochemistry of granite, tectonic setting, composition of magma source, degree of partial melting and fractionation processes has been widely addressed by numerous studies (Candela, 1997; Monecke et al., 2002; Blevin, 2004; Cerny et al., 2005; Sial et al., 2001; Kirwin, 2012). This chapter aims to review the geochemistry of granites

and some granite classification schemes, with a focus on the alphabetic nomenclature model, as well as address the relationship between compositional variation in granite and the diverse range of related ore deposits.

3.1 Geology and geochemistry of granite

Granite can occur in all types of convergent arc environment. Streckeisen (1979) applied the term "granite" to a broad array of felsic plutonic rocks such as granodiorite, monzogranite, syenite, and tonalities, incorporated with the felsic modal content classification by IUGS. Granite spans a broad geochemical spectrum due to the complexity of tectonic settings, pressure, temperature, composition of magma source, degree of partial melting and differentiation processes from which it can form. Despite the broad variation in geochemistry, granite is typically characterized by a mineral assemblage of coarse-grained quartz, K-feldspar and plagioclase, with occasional muscovite, biotite, hornblende and pyroxene (Winter, 2001). Accessory minerals commonly include zircon, apatite, magnetite, tourmaline, monazite, allanite, titanite, pyrite and fluorite.

Unlike sedimentary and metamorphic rocks, the establishment of a granite classification index is problematic due to the wide variety of generative processes and source rock compositions potentially involved. Different types of classification schemes have been proposed to distinguish various types of granite depending on the criteria used (see review by Barbarin, 1990). Despite the constraining factors in each classification scheme, they provide important information for igneous petrologists when describing granites. S-I-A-M classification based on the protoliths of granite and the alumina saturation index (ASI) model based on Al_2O_3 contents (Fig. 1) proposed by Chappell and White (1974) are the most widely used classification schemes and will be discussed in details in the next section.

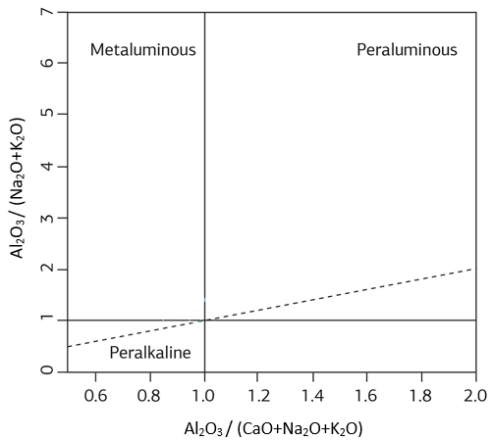

Figure 1: the alumina saturation index (ASI) developed by Chappell and White (1974) to discriminate granite based on Al2O3 contents. Granites span a broad range in ASI, from metaluminous to peralkaline. The degree of saturation varies with Al-bearing minerals (e.g., cordierite, mica, garnet and andalusite) and associated petrogenesis. Peraluminous granites are formed by melting of sedimentary components, though this is not

always the case (Frost et al., 2001; Nandedkar et al., 2014). Metaluminous granites are derived by melting of meta-igneous protoliths whereas peralkaline granites are mantle plume- or rift-related.

3.1.1 Granite sub-type classification (S-I-A-M-type)

S-I-A-M classification was first proposed by Chappell and White (1974), due to discovery of two distinctive types of granites that cannot be correlated with one another by geochemical processes, and that appeared to have been derived from isotopically and chemically different source rocks (Chappell and White, 1992). One is a more primitive, K-poor suite – termed 'I-type', derived by partial melting of igneous protoliths. I-type granites are the most common granitic suite (Wyborn, 2002). Subdivision of this group into Sr-undepleted and Y-depleted is believed to be controlled by pressure and temperature of the source regions (Patino et al., 1995). I-type granites range from metaluminous to weakly peraluminous, depending upon the source of the melt (Chappell et al., 2012). Another granite sub-type is more chemically evolved and K-rich – termed 'S-type', derived by partial melting of crustal rocks that have previously been through the erosional-sedimentary cycle (Chappell and White, 1974). S-type granites are relatively reduced and always peraluminous due to depletion in Na and Ca (Chappell et al., 2012).

A geochemically more primitive (higher mantle affinities) and K-deficient 'M-type' sub-group was later added by White (1979). Whether I-types are fractionation products of M-type is still under debate. Granitic suites formed in anorogenic settings have been termed 'A-type' by Loiselle and Wones (1979), though Whalen et al. (1987) suggested that A-type granites are not only confined in anorogenic environments. A-type granite has been interpreted to have been derived from partial melting of F- and/or Cl-rich residue in the lower crust (Bonin, 1990). Most of the A-type granites are peralkaline in composition, though metaluminous and peraluminous A-type suites can also be present (e.g., Panxi, China; Shellnutt and Zhou, 2007).

Mixing of remelted crustal material and derivation from pristine source end-members may result in transitional characteristics between each sub-type. In addition, geochemical signatures in granites can reflect their tectonic settings. Maniar and Piccoli (1989) suggested that integration of trace elements with the alphabetical nomenclature of Chappell and White (1974) is a more powerful tool in discriminating formation environment. Pithcer (1983a, 1983b, 1993), Barbarin (1990) and Winter (2001) have summarized the relationship between the geochemistry of granites and tectonic settings (Appendix 4). M-type granite is common in island arc settings, where interaction with arc crust is less likely to occur, though hybridization may still be involved to some degree, but the documentation of this interaction

is difficult as the arc crust also has a high mantle affinity (Creaser et al., 1991). Geochemical processes in continental arc settings are typically more complicated due to the participation of fertile crust and sediments. I-type granites (predominantly tonalities and granodiorites) and M-I transitional compositions are typical of continental arcs, where granites are derived by partial melting of underplated material and meta-igneous rocks, followed by fractionation and differentiation during emplacement. A mixture of numerous source components in the generative magmas can result in S-type or hybrid type granites. M-types and S-types can be emplaced during post-subduction extension where there is provision of conduits (Winter, 2001). Tectonic settings suitable for A-type granite emplacement is still the focus of ongoing debate. Eby (1992) suggested that there are two A-type geochemical groups that originate from very different sources and tectonic settings, with the first group (A_1) representing sources akin to oceanic island basalt in intraplate settings, and the second group (A_2) representing magmas derived from continent-continent collision and island-arc magmatism.

3.2 Mineralisation associated with granites

Granites are able to concentrate significant amounts of base and precious metals to economic concentrations during partial melting, ascent, emplacement and fractional crystallisation (Cerny et al., 2005). Garnett and Bassett (2005) further proposed that weathering processes may trigger in situ enrichment and formation of placer deposits of heavy minerals from altered granites. The role of granites as the metal and heat source contributing to economic mineralisation still remains controversial, as they vary in composition markedly with different styles of mineralisation.

A broad spectrum of mineralisation styles occurs around granite intrusions, including Sn-W greisen (Cornubian granite batholith, England; Atkinson and Baker, 1986), pegmatite-hosted Ta-Nb-Li-Be-REE (Yichun, China; Yin et al., 1995), intrusion-related porphyry-epithermal Cu-Mo-Au systems (Batu Hijau; Garwin, 2002), skarn (King Island, Australia; Kwak and Tan, 1981), polymetallic sulfide lodes (Cornubian Batholith, England; Simons et al., 2017), Kiruna-type iron oxide-copper-gold deposits (IOCG) (Carajás district, Brazil; Dardenne et al., 1988), polymetallic sulfide vein deposits (Yangzi River, China; Pan and Dong, 1999), intrusion-related gold deposit (IRGD) (Tintana Gold Province, Canada; Marsh et al., 2003) and uranium deposits (Mary Kathleen, Australia; Oliver et al, 1999). These mineralisation styles are typically not genetically related, with contrasting fluid composition, alteration and paragenesis, though they are all considered as part of the broad family of granite-related ore deposits (Pollard, 2006).

Geochemical characteristics of granite such as oxidation state, composition, temperature, degree of fractional crystallization and compositional evolution have been assessed by many researchers in order to study the metallogenesis of granite-related magmatic-hydrothermal

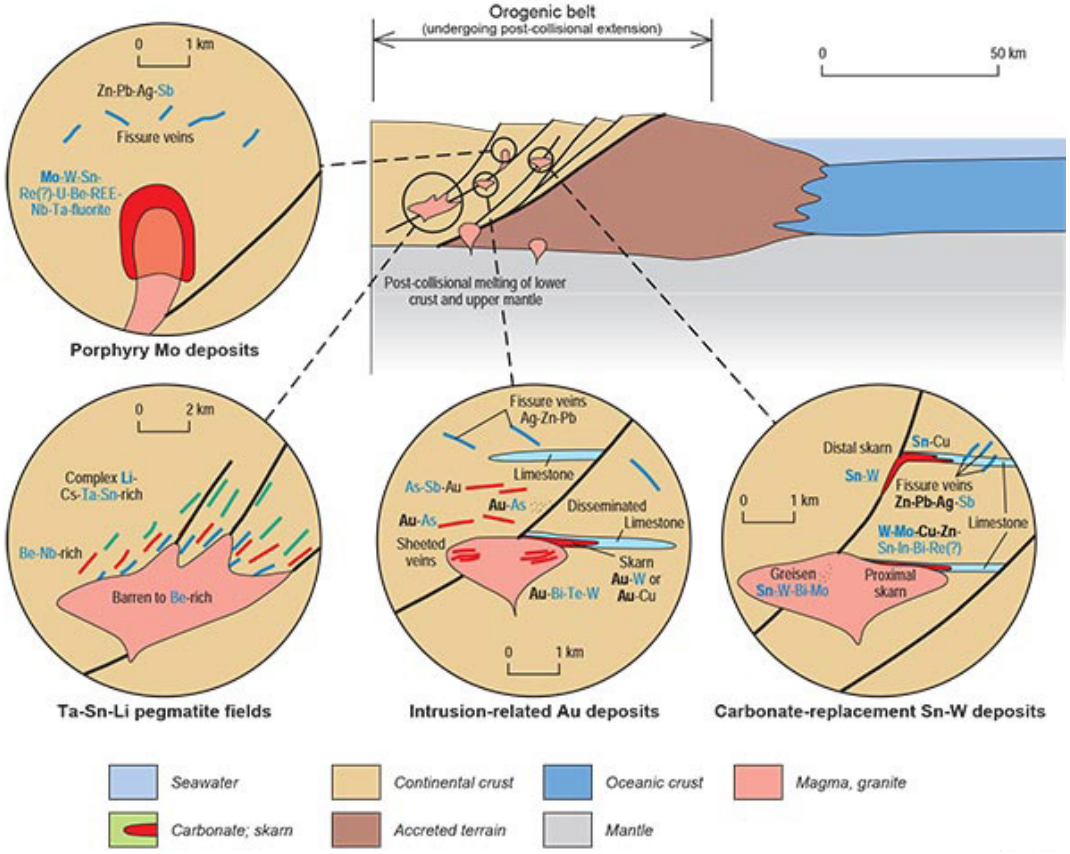

Figure 2: Illustration of the different granite-related deposit systems and the likely distribution of critical commodities associated with different types of granites within continental arc setting (Geoscience Australia, 2013). The critical commodities are indicated in blue text, major products in black. The metallogenic tenor of the mineral systems are controlled by the degrees of fractionation and oxidation states of associated granites. Progression from Cu-Au, through W to Mo mineralisation is a function of higher degrees of fractionation and oxidation within associated I-type suites (Blevin and Chappell, 1995).

mineralisation (e.g., Candela, 1992; Blevin et al., 1996; Chen et al., 1998; Wyborn, 2002; Blevin, 2004). Porphyry Cu-Mo-Au deposits are widely recognised to be associated with high-K magnetite-series I-type granites in continental arcs, though some porphyry Cu-Au systems are associated with reduced magmas (e.g., Shotgun, Alaska: Rombach, 2000). Porphyry Cu-Au deposits are more common in island arcs (e.g., Grasberg, Indonesia: Mathur et al., 2000), whereas porphyry Cu-Mo deposits are common in continental arcs (e.g., El Teniente, Chile: Cannell et al, 2005). Endako-type (subduction-related) porphyry Mo deposits are related to relatively reduced porphyritic stocks (e,g., Henderson, China: Chen et al., 2013), but may also be associated with highly oxidized intrusions (e.g., Shapinggou, China: Zhang et al., 2013). The latter is known as a Climax-type (rift-related) Mo deposit (Sinclair, 2007). The majority of Sn, W and F mineralisation is associated with both reduced

I- and, more commonly S-type granites that have undergone extended fractionation (Blevin and Chappell, 1995). IOCG deposits are genetically associated with A- to I-type, high-K and oxidized magmatism depending on the tectonic settings (Pollard, 2006). Cooling of strongly compositionally evolved peralkaline S-types granites may form result in REE-enriched pegmatite (or greisen) orebodies (Cerny et al., 2005). Intrusion-related gold deposits (IRGD) have been interpreted as being spatially associated with reduced granite at deeper crustal levels (Hart, 2005). Magnetite and sulfide skarn deposits form if there is carbonate host rock (Meinert, 1992).

3.3 Hydrothermal alteration zones around granites

Hydrothermal alteration associated with granites varies with the composition of the granite involved. The main types of hydrothermal alteration associated with aluminosilicate rocks have been outlined by Meyer and Hemley (1967). They include sodic-calcic, potassic, propylitic, sericitic, intermediate argillic and advanced argillic alteration. This classification can be also used in granite-related ore deposits (Fig. 3). Many of the arc-related granite ore deposit systems, including porphyry-epithermal deposit, skarn, IOCG, polymetallic vein system and IRGD share similar alteration styles, as the magmatic-hydrothermal processes are mostly consistent.

Absence or presence and the intensity of particular hydrothermal alteration sub-types are controlled by the composition of the granite and the chemistry of the magmatic-hydrothermal fluids associated with the granite. For example, IOCG provinces are characterized by a lack of sericitic and argillic alteration (fluids are more CO_2-rich), but are typified by common sodic (-calcic) alteration, which contrasts to porphyry-epithermal Cu-Au deposits. However, both are associated with potassic altered and oxidized intrusions (Barton and Johnson, 1996).

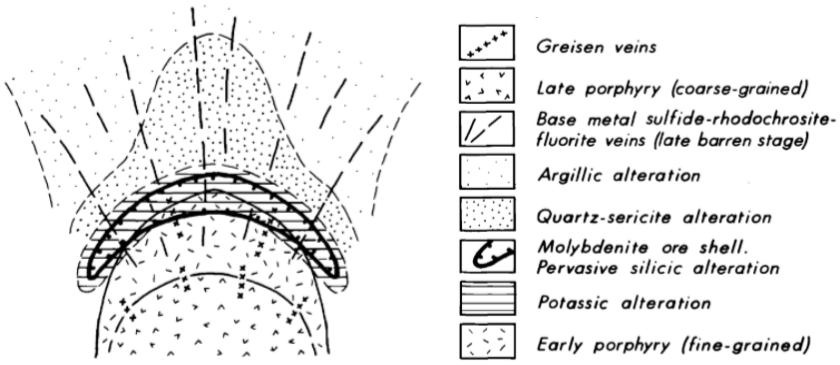

Figure 3: Generalised cross section showing the hydrothermal alteration patterns associated with S-type-granite-related molybdenite ore system (Not to scale) (Mutschler and Wright, 1981). The alteration zonation illustrated in this diagram is similar to that in a porphyry ore system (see section 4.3). It is typically zoned and characterized by the sequence of greisen – potassic – quartz-sericite – argillic alteration as one progresses away

from the porphyry centre. Greisen and fluorite vein sets occur throughout the whole system and they generally coincide with the preferential site of base metal mineralization.

Greisen alteration exclusively occurs with Sn-W-Be-Mo deposits associated with reduced S-type granites (Robb, 2004). Greisen usually forms adjacent to quartz-cassiterite-wolframite veins in the cupola of granites (Robb, 2004). It is formed by conversion of feldspar to quartz-muscovite assemblages by the interaction of wallrocks with acidic fluorine-rich fluids, accompanied with progressive F- and/or B-metasomatism (Pirajno, 2008). F- and B-rich minerals (e.g., fluorite, topaz and tourmaline) are typically present. The presence of these minerals, coarse-grained muscovite and lack of pyrite differentiates greisen from phyllic and sericite-dominated alteration assemblages (Ridley 2013). Tourmalinization may occur if intense boron metasomatism occurs in Sn-W greisens but rarely develops in IRGD (Pirajno, 2008). Albitization usually precedes greisenization in fluorine-rich peralkaline granites and results in feldspar and biotite destruction to yield Be-Nb-Ta-Zr-rich apogranite (Borodin and Pavlenko, 1974). Quartz-flooding in greisens suggest the occurrence of silicification during and after greisenization as the result of local leaching of Si within the country rocks or Si^{4+} metasomatism in the solution introduced to the system (Robb, 2005). This alteration may occur in high-sulfidation epithermal environment. Skarn deposits can be spatially and genetically related to greisen-hosted Sn-W-Mo-Be-Li-F mineralisation when carbonate wall rocks around granites are be subjected to fluorite-greisenization (e.g., Iron Mountain, Mexico: Jahns, 1944).

Chapter 4: Porphyry deposits

Porphyry Cu-Au-Mo ore deposits are one of the main targets for exploration of base metal mineralisation. The ore deposit model for porphyry systems, from both empirical and genetic aspects, are now fairly well-understood (see reviews by Seedorff et al., 2005; Cooke et al, 2005; Sinclair, 2007; Sillitoe, 2010). Systematic studies of the characteristics of porphyry systems, and innovative exploration models can facilitate and optimize discoveries of hidden porphyry deposits. This section will focus on the characteristics of porphyry ore deposits, processes of metal precipitation and hydrothermal alteration, and spatial relationship with other magmatic-hydrothermal ore systems, followed by a brief discussion on how these characteristics can be employed in exploration.

4.1 Geology and geochemistry of ore forming porphyries

Porphyry-related magmatic systems are typically restricted to the subvolcanic environment within magmatic arc settings above subduction zones (Cooke and Gemmell, 1996). Porphyry systems tend to occur as clusters aligned in a linear belt subparallel to magmatic arcs (Sillitoe,

2010). Multiphase magmatism, cyclic injection of oxidized, sulfur- and metal-enriched magmas and episodic pulses of magmatic-hydrothermal fluids in the arc environment are the main triggers for porphyry ore formation (Hendequist and Lowenstern, 1994; Halter et al., 2005). Cyclic volatile accumulation and fluid influx lead to multiple crack-seal events on fractures over time and eventually produce vein stockworks that characterize porphyry systems (Cooke et al., 2005). Polyphase magmatic activity can account for the formation of giant porphyry systems with elevated metal grades, leading to overprinting of hydrothermal alteration zones and cross-cutting relationship of veins associated with hydraulic fracturing (Seedorff et al., 2005, 2008).

Many studies have agreed that porphyry systems are structurally controlled, localizing magmatic source and ore fluids from depth to shallow crustal levels, where ores are subsequently deposited (Masterman et al., 2005; Sillitoe, 2010). The role of intersecting fault zones in localizing porphyry mineralisation has also been emphasised (Hill et al., 2002). The significance of regional structures in the localisation of deposits is yet to be resolved as there is lack of evidence that regional faults localize mineralisation in many porphyry systems (Sillitoe and Perelló, 2005).

Porphyry systems can be subdivided into alkali and calc-alkalic categories based on their geochemical affinities with intrusive rocks. Calc-alkalic porphyry systems are commonly associated subduction-related intermediate porphyritic stocks, spanning quartz monzonite to granodiorite compositions in continental arcs and quartz diorite-granodiorite compositions in island arc environments (Sinclair, 2007). Island arc porphyry systems generally have lower Mo/Cu and higher Au/Cu ratios than cordilleran types. More fractionated calc-alkalic intrusions are associated with Cu-Mo mineralization, whereas less fractionated intrusions are related to Cu-Au mineralisation (Holliday and Cooke, 2007). Alkali porphyry systems are less common. They are confined to back-arc rift settings following the cessation of subduction, and are associated with multiple “pencil”-shaped alkaline intrusions of A-type chemistry (Pirajino, 1992). Au-mineralisation generally has greater affinity with alkaline magmas, due to post-subduction magmatism and remelting of Au-rich residue in subduction modified lithosphere (Richards, 2003, 2009, 2011). The majority of the porphyry deposits associated with alkaline intrusions are smaller than calc-akaline types (Sillitoe, 2002). Both types of porphyry systems share similar geological characteristics, except for the composition of associated hydrothermal fluids and the complexity in hydrothermal alteration (Lang et al., 1995).

4.1.1 Chemistry of ore-forming hydrothermal fluids

Chemistry of hydrothermal fluids in both calc-alkalic and alkalic porphyry systems have been widely inferred from fluid inclusion, isotopic and experimental evidence in many studies (e.g., Ulrich et al., 1999; Hedenquist and Lowenstern, 1994; Bodnar, 1995; Cooke et al., 2007). The bulk of the metal budget for porphyry systems is primarily controlled by the geochemistry of the incoming fluids, which in turn are likely to control the ore-forming processes and metal precipitation (Heinrich, 1990). Many porphyry systems share similar genetic types of fluid inclusions that reflect the P-T evolution of metal-bearing magmatic fluids. The characteristics and genetic implications of each inclusion type have been summarized in numerous studies (e.g., Rusk et al., 2004; Kouzmanov and Pokrovski, 2012; Bodnar et al., 2014).

Hydrothermal fluids in alkalic porphyry systems are oxidized and relatively more enriched in CO_2, whereas hydrothermal fluids in calc-alkalic systems are S-enriched, with similar temperature and salinity in both types. In general, porphyry mineralisation is principally derived from volatile- and metal-enriched (up to 1,000's of ppm of base metals) single-phase fluids of moderately salinity (10 – 20 wt % NaCl eq.) exsolved from crystallizing porphyritic stocks (Heinrich, 2005). Mineralisation at shallow depth is introduced by a two-phase fluid, which is dominated by low-density vapour with a small fraction of hypersaline fluid (Fournier, 1999). Such assemblages are formed by exsolution from silicate melts (Shinohara, 1994) or phase separation of single-phase fluid during decompression (Bodnar, 1995). Bodnar et al. (2014) summarise the characteristics of fluid inclusions found in different types of porphyry systems. Fluid inclusions in all types of porphyry deposits have a broad range in salinity (0 to 60 wt % eq.), reflecting a combined effect of fluid-phase immiscibility, varying salinity in the primary magmatic fluids and dilution by later incursion of low-salinity meteoric fluids during cooling.

Common components of hydrothermal fluids in porphyry systems are sulfate or sulfide (CO_2 in alkali systems), alkali chlorite salts and metalloid-bearing hydroxide species. Elements selectively fractionate and partition into vapour or hypersaline liquid during phase separation. Vapour phases may contain significant amounts of Cu, Au, Ag, As, Sb, Te and B, whereas Fe, Zn, Pb, Mn and Mo preferentially partition into hypersaline liquids (Heinrich, 2005). Cu, Fe, Zn, Pb, Mn and Ag preferentially exist in chloride complexes, with some rare cases in which these base metals may form sulfate and sulfide complexes in S-concentrated brine and liquids. Au and Pt can be associated with both sulfide and chlorite complexes depending upon pH, temperature and relative abundances of Cl and S (Kouzmanov and Pokrovski,

2012). Mo and W are dominated by oxyhydroxide anions and ion pairs with Na and K (Ulrich and Mavrogenes, 2008). Metal abundances in ore-forming fluids are controlled by several parameters such as geochemistry of magma source, relative solubility of metals, temperature, abundance of complexing ligands (Cl, S) and fluid acidity (see reviews by Kouzmanov and Pokrovski, 2012; Bodnar et al., 2014). Amongst the metals in porphyry systems, Cu concentration shows the largest variation in in all types of fluid inclusions. This reflects the combined effects of silicate-melt fluid partitioning, chemistry of magmas, fluid unmixing, metal precipitation and post-entrapment modifications (Kouzmanov and Pokrovski, 2012). Attainment of Mo concentrations up to 2,000 ppm in hypersaline fluid inclusions implies Mo pre-enrichment by fluid unmixing prior to the Mo precipitation (Klemm et al., 2008).

4.2 Mineralisation associated with ore-forming porphyry intrusions

Porphyry ore minerals are deposited in veins and associated hydrothermal breccias, as well as occurring as disseminated grains. Ore minerals can be hosted within a variety of volcanic, carbonate, sedimentary and metamorphic rocks (Titley, 1993). Aqueous magmatic fluids involved in porphyry deposition and alteration may migrate outward to adjacent non-carbonate and carbonate wall rocks from the porphyry intrusions where there is provision of fluid access (e.g., structural, lithological, hydrothermal-induced permeability), allowing the formation of other magmatic-hydrothermal related mineralisation types (Fig. 4).

Many previous studies have proposed that the oxidized nature of arc magmas is due to the transfer of oxidizing components such as H_2O, CO_2, ferric iron, sulfate and possibly chloride, LILE and HFSE into mantle from subducting slabs (Alt et al., 1993; Mungall, 2002; Kessell et al., 2005). The oxidizing components act as a transport medium for metals into volatiles at a later stage. The abundance of residual sulfides within the mantle source critically controls the concentrations of the siderophile and chalcophile elements in the melt, which in turn, controls the metallogenic tenor of a porphyry system (Richard, 2011). For example, only a small amount of highly siderophile elements (e.g., Au and PGE) will be retained within the source of typical arc magmas with high O_2 and S_2 fugacity, whilst the resulting arc magmas are relatively undepleted in moderately chalcophile elements such as Cu ± Mo (Richard, 2011). Such magmas are attributed to the potential formation of porphyry Cu ± Mo deposits upon their emplacement (John et al., 2010). Au-rich porphyry deposits are associated with post-subduction remelting of residual sulfides, whereas porphyry Mo (Farmer and DePaolo, 1984) and Sn-W deposits (Wyborn, 2002) are associated with relatively reduced granites predominantly derived from melting of continental crust, though

Mo pre-enrichment derived from mantle lithosphere has also been suggested (Pettke et al., 2010; Appendix 5). Mixing of mafic derivatives with felsic and intermediate magmas prior to the mineralisation may also provide additional metals, sulfides and other volatiles to the system (e.g., Northparkers, Australia: Lickfold et al., 2007).

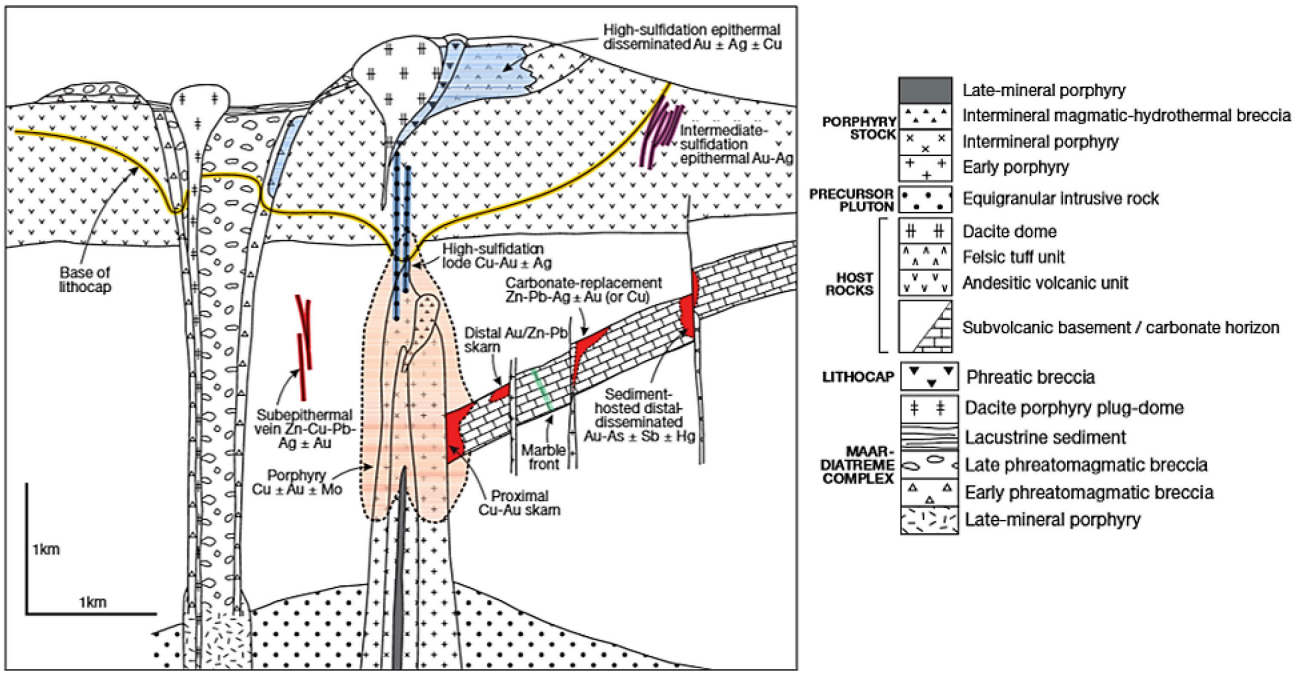

Figure 4: Anatomy of porphyry ore system showing the spatial relationship with multiphase porphyry stocks, intermediate host rocks and associated economic magmatic-hydrothermal ore deposits: peripheral proximal and distal skarn deposit, carbonate replacement, sediment-hosted deposits, polymetallic veins in non-carbonate units, shallow-level high- and intermediate-sulfidation epithermal deposits (Sillitoe, 2010).

In the early evolution of a porphyry system, saline fluids exsolved from crystallizing porphyry intrusions initiate the precipitation of Cu-Fe-Au-bearing mineral assemblages within and around the early porphyry intrusions, assisted by fluid-wall rock interaction during cooling (Ulrich et al., 1999; Rusk et al., 2008). Fracturing in and around the intrusion leads to upward decompression, rapidly decreasing the solubility of metal-carrying vapour phases, resulting in the Cu-Fe precipitation together with Au in shallowly emplaced porphyry deposits (Sillitoe, 2000; Williams-Jones et al., 2002). Oxidation, acid leaching, metal remobilization and reconcentration of hypogene mineralisation can subsequently form a near surface supergene enrichment blanket which contributes significantly to the overall metal budget of porphyry Cu systems due to increased grades (Titley and Marozas, 1995). In porphyry Mo deposits, the Mo/Cu ratio in the residual parental melt progressively increases as crystallization proceeds, resulting in separate molybdenite precipitation from the bulk Cu-Au porphyry deposit (Candela and Holland, 1986).

Zn, Pb, Ag and Mn enrichment has been widely observed in hypersaline fluid inclusions in quartz veinlets during potassic alteration, but these metals remain as chloride complexes in solution as their partitioning into sulfides precipitated in Cu ore bodies are not favoured (Bodnar 1995). Geochemical halos of these metals distal from the centre of porphyry-related mineralisation implies that their precipitation may be triggered by progressive cooling of hypersaline fluids in contact with incoming external waters and wall rocks (Henley and Hunt, 1992). The highest Zn, Pb and Ag concentrations are confined to the skarn environment, where metal precipitation is induced by fluid neutralization by carbonate host rocks (Sillitoe, 2010).

A systematic spatial and temporal relationship between porphyry ore systems and high, intermediate and low-sulfidation epithermal deposits has been established by many previous studies (e.g., Sillitoe, 2000; 2010; Williams-Jones and Heinrich, 2005; Richards, 2009; Chang et al., 2011). Condensation of voluminous sulphur-rich volatiles exsolved from the magmatic source into groundwater generates extremely acidic fluids that account for the development of advanced argillic alteration and Cu-Au mineralisation. In the lithocap environment, this is caused by intense boiling along upflow zones or fluid mixing with groundwater (Sillitoe, 1999). Outward flow of the strongly acidic hydrothermal fluids may bypass adjoining less-altered rocks and allow for the occurrence of low- and intermediate-sulfidation mineralisation (Sillitoe and Hedenquist, 2003). Most calc-alkalic porphyries are characterised by downward transition from high-sulfidation epithermal mineralisation to porphyry-style mineralisation at depth (Sillitoe, 2000). In contrast, alkaline porphyry systems transit to low- rather than high-sulfidation epithermal mineralisation due to the presence of CO_2-rich aqueous fluid that greatly increases the acid-buffering capacities of alkaline rocks and restricts acidification (Sillitoe, 2002)

4.3 Hydrothermal alteration zones associated with porphyry deposits

Hydrothermal alteration zones vary as a consequence of the outflow of magmatic-hydrothermal fluids, heating of meteoric-connate fluids within the country rocks during intrusive activity, and chemical reactions with wall rocks during subsequent cooling of fluids as they flow away from the porphyry centre (Cooke et al., 2014a). Calc-alkalic and alkalic porphyry systems have different hydrothermal alteration zonation patterns. Hydrothermal alteration zones in calc- alkalic porphyry system include sodic-calcic, potassic, phyllic, argillic and propylitic alteration (Lowell and Guilbert, 1970; Sillitoe, 2010; Fig. 5), whereas alteration zones in alkalic porphyry system generally have narrower footprint and greater complexity, from calcic, calc-potassic, calc-sodic, propylitic, to less well developed phyllic

and advanced argillic alteration (Lang et al., 1995; Holliday and Cooke, 2007; Fig. 6). The latter is also characterised by the lack of quartz veins, abundance of carbonate, anhydrite assemblages and magnetite as a consequence of enrichment of CO_2 and low sulphur concentration in the system (Cooke et al., 2007; Fig. 6).

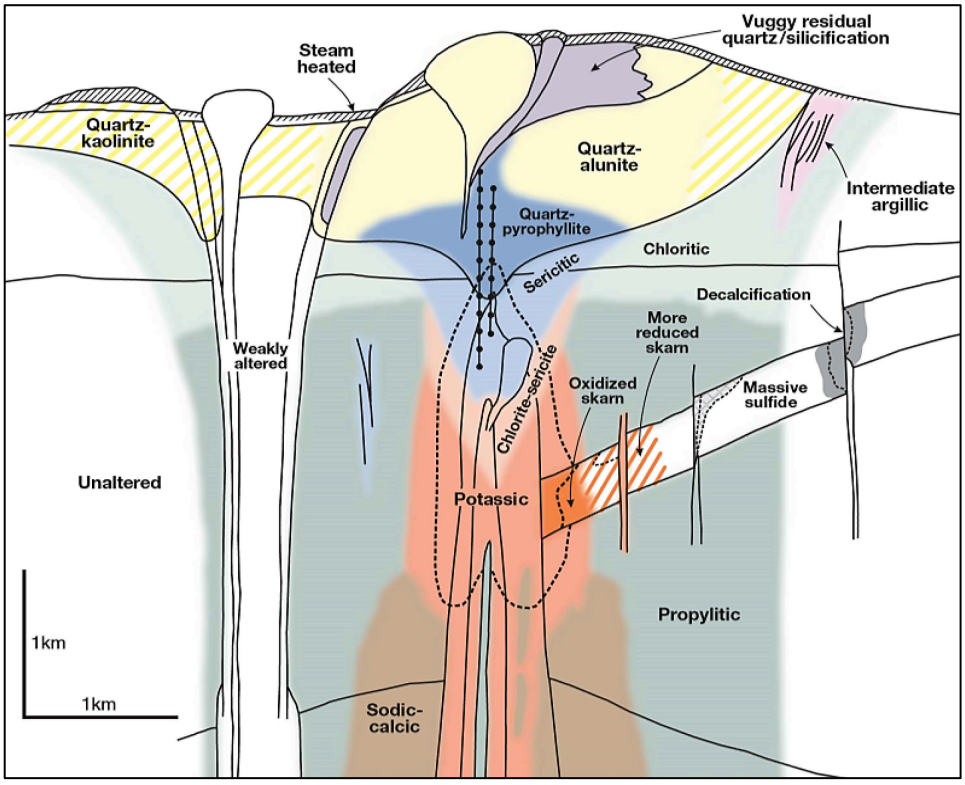

Figure 5: Cross section of alteration-mineralized zoning pattern associated with porphyry deposits (Sillitoe, 2010). The alteration-mineralization zoning pattern is commonly far more complex, particularly where there is multiphase intrusions accompanied with intense structural deformation. Sericitic alteration preferentially develops in porphyry Cu-Mo deposits, whereas chlorite-sericite alteration tends to be more abundant in the porphyry Cu-Au deposits.

Sodic-calcic alteration may characterise the centre of porphyry stocks (e.g., Koloula, British Columbia: Arancibia and Clark, 1996). However, it is generally poorly preserved at depth. This central zone is magnetite-bearing, but typically poor in sulfides and other metals (Sillitoe, 2010). Potassic alteration develops in and around the apex of the intrusive complex under relatively high temperature (> 350 °C) and near neutral pH conditions in the early evolution of a porphyry system, characterized by the presence of secondary K-silicate minerals, with biotite predominant in mafic intrusions and K-feldspar in felsic intrusions (Sillitoe, 2010). The potassic core commonly hosts high grade mineralisation associated with abundant quartz ± magnetite ± orthoclase. Intensity of alteration decreases in late-mineral intrusions and are commonly overprinted by later propylitic and phyllic assemblages (Sillitoe, 2010). The potassic zone grades upward into chlorite-sericite-pyrite and sericite-dominated phyllic alteration zones that develops under slightly lower temperature (<350 °C) and acidic conditions (4.5 - 7), typified by alteration of mafic minerals to chlorite, feldspar

to white mica and illite, and magnetite to hematite, with widespread disseminated pyrite (Sillitoe, 2010). Local weathering of pyrite in this zone is responsible to the generation of acidic fluids which account for the argillic alteration.

The phyllic-argillic alteration zone transition is characterized by the presence of clay minerals. Intermediate argillic alteration is characterized by quartz-kaolinite-illite dominated assemblages, whereas advanced argillic alteration is characterized by alunite-pyrophyllite-dickite-kaolinite-pyrite ± enargite ± covellite (Cooke et al., 2014). These mineral assemblages often overprint earlier formed potassic and chlorite-sericite alteration zones. Argillic alteration is characteristic of the lithocap environment and the progressive transition from the porphyry to epithermal environment at shallow depth (Sillitoe, 2010). The transition from the phyllic and argillic alteration zones into the chlorite zone implies the neutralization of acidic hydrothermal fluids.

Propylitic alteration typically forms outboard of the potassic core of the porphyry system. This transition implies cooling and increased wall rock interaction and wall rock buffering of hydrothermal fluids (Sillitoe, 2010). It comprises three sub-types, zoned outward from the potassic zone: an inner high-temperature actinolite sub-zone, a moderate-temperature epidote sub-zone and an outer low-temperature chlorite sub-zone. Propylitic alteration surrounding alkalis porphyries are typically reddened due to the greater abundance of hematite (Fig. 6b).

Hydrothermal fluids responsible for high-temperature potassic and phyllic alteration are dominated by the magmatic component; non-magmatic fluids are dominant in deep sodic-calcic and propylitic alteration. Intermediate argillic alteration is dominated by meteoric fluids, whereas advanced argillic alteration is dominated by condensation of magmatic vapour into meteoric water (Seedorff et al., 2015).

Magmatic-hydrothermal systems generally become progressively younger upward, with subsequent overprinting of deeper alteration by shallower alteration zones (commonly phyllic and argillic alteration) due to telescoping of ore systems. The vertical distribution of mineralisation and degree of overprinting depends upon the degree of telescoping. Lithocaps and the potassic-altered core may be separated less than 1 km with the intervening gap occupied by chlorite-sericite dominated alteration (Sillitoe, 2000), whereas the roots of argillic alteration may impinge greater than 1 km downward onto the potassic zone in highly telescoped porphyry systems (e.g., Escondida, Chile: Padilla-Garza et al., 2004).

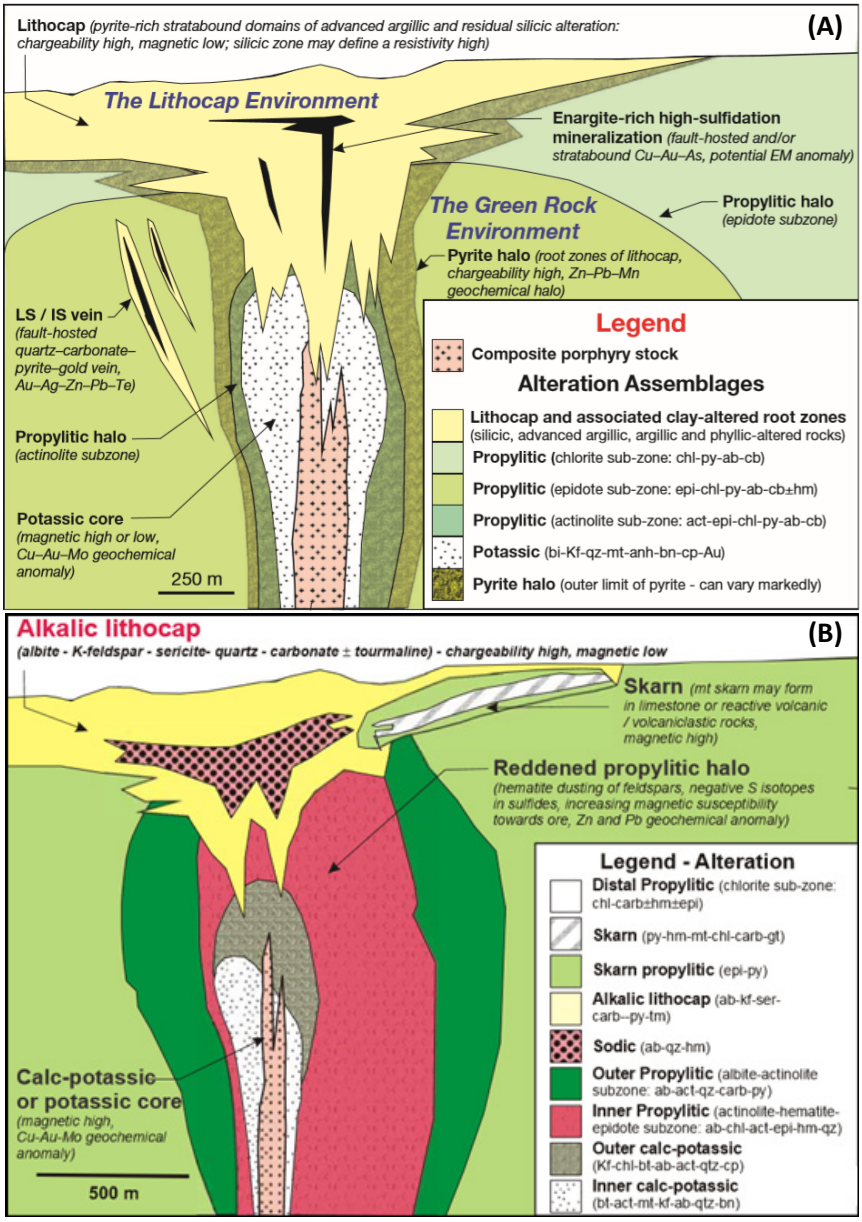

Figure 6: Comparative illustration of hydrothermal alteration zonation in calc-alkalic and alkalic sub-type porphyry. **(A):** Hydrothermal alteration zonation in calc-alkalic porphyry system (Cooke et al., 2004). Mineralization occurs within the potassic-altered core and adjacent altered wall rocks. Three propylitic alteration sub-zones occur around the porphyry centre, grading outward from actinolite sub-zone, through epidote sub-zone, to chlorite sub-zone. In this example, the porphyry system is overprinted by a lithocap (argillic alteration assemblages). This doesn't occur in every porphyry system as it is contingent on the degree of telescoping of the system (i.e. rates of uplift and erosion at the time of mineralization) over time. (B) Hydrothermal alteration zonation in alkalic porphyry system (Wilson, 2003; Cooke et al., 2007). The core of the alkalic sub-type is characterized by calcium-rich alteration minerals (e.g., calcite, epidote, actinolite, garnet). The propylitic sub-zone is typically reddened due the presence of hematite-dusted K-feldspar. The lithocap in alkalic types comprises less acidic alteration mineral assemblages such as albite, K-feldspar and sericite.

4.4 Exploration models

Understanding of the overall characteristics of porphyry ore systems significantly assists with the targeting of potentially economic ore deposits. Integration of field geology, drilling, geochemical analysis and geophysical surveys are routinely applied to optimize the likely

locations of economic deposits, especially in alkalic porphyry systems where hydrothermal alteration zones and deposit sizes are much smaller than in calc-alkalic types.

As porphyry ore systems are genetically related to geodynamic processes in subduction zones or orogenic belts, these tectonic settings are the focus of exploration studies. Hydrothermal alteration footprints have been widely used as vectoring tools and fertility indicators in targeting ore deposits (e.g., Tanaka et al., 2010; Chang et al., 2011; Cooke et al., 2014a; Halley et al., 2015). The chemical changes in wall rocks and alteration minerals may also serve as vectoring tools towards concealed porphyry orebodies (Cooke et al., 2014a, 2014b; Wilkinson et al., 2015; Yousefi, 2017). Studies of sulfur isotope compositions in sulfide minerals in Didipio (Wolfe, 2001), Mt Polley (Deyell, 2005) and Cadia (Wilson et al., 2007) have shown systematic zonation in sulfur isotopes around the mineralized centre, implying that they are a potential indicator of proximity to the mineralized core. Reconnaissance stream sediment and soil geochemistry have also been proven to be potential tools in detecting buried ore deposits (Plouffe et al., 2016).

Porphyry ore deposits may develop as clusters, resulting in overlapping of outer propylitic alteration zones (e.g., Namosi district, Fiji: Orovan et al., 2018). In addition, large alteration footprints up to 10 km may be produced by lateral outflow of hydrothermal fluids and extensive circulation of external water within the rock mass (Dilles et al., 2000). These processes often hinder effectiveness in exploration over large areas, or can serve to highlight prospective areas within districts. Remote sensing and geophysical techniques have therefore become valuable tools in regional scale exploration. Magnetic surveys are particularly useful in identifying structural patterns, magnetite in the potassic-altered core, magnetite-destructive phyllic alteration zones and magnetite replacement in the skarn environment (e.g., Marsden, Australia: Holliday et al., 2006). Induced Polarization (IP) is particularly suited to delineate the extent of pyrite-bearing phyllic alteration and radiometric survey for detecting near-surface potassic alteration zones and porphyry intrusions. Spectral analytical techniques have also been employed by some researchers to characterize the spatial variation in spectral signatures of hydrous alteration minerals associated with porphyry ore deposits (i.e. Change et al., 2011; Zadeh, 2014; Halley et al., 2015; Neal et al., 2018). Drilling still plays a significant role in gathering geological and geochemical information under cover. Core interpretation by experienced geologists is essential, and further drilling is often expected to gather more information.

It has been commonplace in the mining industry to integrate an extensive range of exploratory data to build up multi-dimensional datasets using a variety of mining software

packages such as GOCAD, GSI3D and Petrel, among others. Application of mineral prospectivity mapping has also been widely recognized to be useful in preliminary exploration stages by integrating multi-attribute geological database to localize potential zones and delimit drilling sites (Abedi and Norouzi, 2016). In this regard, the computational ability in handling big datasets is main challenge that needs to be addressed. Both knowledge-driven and data-driven approaches need continuing refinement to fill the gap between geological modelling and field-based exploration.

Chapter 5: Conclusion

Intrusion-related mineral systems constitute a wide range of base metal ore deposit classes, varying with tectonic setting, composition of the host rocks and chemistry of magmatic-hydrothermal fluids and associated intrusions. Our current understanding of these mineral systems allows explorationists to employ various geochemical and geophysical techniques with the combination of both genetic and empirical models. Nevertheless, several questions still remain unresolved: how important is an intrusion in terms of supplying metals to formation of ore deposits? How significant are mafic magmas in the development of intrusion-related deposits? What are the mechanisms of ore precipitation? As extreme temperature gradients, which are unlikely to occur in many cases, are required to generate economic ore grade (Cooke et al., 2015), is fluid cooling a feasible mechanism in forming giant porphyry ore deposits? Given that the fluids responsible for deep-seated sodic-calcic alteration is dominated by non-magmatic brine (Sillitoe, 2010), how does it reach the core at depth? It may require more sophisticated laboratory equipment in order to conduct more precise fluid inclusion studies, trace element analysis, isotopic dating and tracing, as well as more-detailed documentation of geologic conditions of intrusion-related ore deposits worldwide, to answer these questions.

References

Abedi, M., Norouzi, G.H., 2016, A general framework of TOPSIS method for integration of airborne geophysics, satellite imagery, geochemical and geological data: International Journal Applied Earth Observation Geoinformation, v. 46, p. 31–44.

Allègre, C.J. and Minster, J.F, 1978, Quantitative models of trace element behavior in magmatic processes, Earth and Planetary Science Letters, v. 38, p. 1–25.

Alt, J. C., Shanks, W. C. and Jackson, M. C., 1993, Cycling of sulfur in subduction zones: The geochemistry of sulfur in the Mariana Island Arc and back-arc trough, Earth Planetary Science Letters, v. 119, p. 477–494.

Annen, C., Blundy, J.D., and Sparks, R.S.J., 2006, The genesis of intermediate and silicic magmas in deep crustal hot zones: Journal of Petrology, v. 47, p. 505–539.

Arancibia, O.N. and Clark, A.H., 1996, Early magnetite-amphibole-plagioclase alteration-mineralization in the Island Copper porphyry copper-goldmolybdenum deposit, British Columbia: Economic Geology, v. 91, p. 402–438.

Atkinson, D. and Baker, D.J., 1986, Geology of the MacTung tungsten skarn deposit, in Abbott, J.G. and Turner, R.J.W., eds Mineral Deposits of the Northern Canadian Cordillera, Yukon–North Eastern British Columbia: Geological Survey of Canada Open File 2169, 279 p.

Barbarin, B., 1990, Granitoids: Main petrogenetic classification in relation to origin and tectonic setting: Geological Journal, v. 25, p. 227–238.

Barton, M.D. and Johnson, D.A., 1996, Evaporitic-source model for igneous-related Fe oxide–(REE–Cu–Au–U) mineralization: Geology, v. 24, p. 259–262.

Berger, B.R., Ayuso, R.A., Wynn, J.C. and Seal, R.R., 2008, Preliminary Model of Porphyry Copper Deposits: USGS Open-File Report.

Blevin, P.L. and Chappell, B.W., 1995, Chemistry, origin and evolution of mineralized granites in the Lachlan fold belt, Australia; the metallogeny of I- and S-type granites: Economic Geology, v. 90, p. 1604–1619.

Blevin, P.L., Chappell, B.W. and Allen, C.M., 1996, Intrusive merallogenic provinces in eastern Australia based on granite source and composition: Transactions of the Royal Society of Edinburgh: Earth Sciences, v. 87, p. 281–290.

Blevin, P.L., 2004, Redox and Compositional Parameters for Interpreting the Granitoid Metallogeny of Eastern Australia: Implications for Gold-rich Ore Systems: Resource Geology, v. 54, p. 241–252.

Bodnar, R.J., 1995, Fluid inclusion evidence for a magmatic source for metals in porphyry copper deposits'. In: Thompson, J.F.H., ed., Magmas, Fluids and Ore Deposits: Mineralogical Association of Canada, v. 23, p. 139–152

Bodnar R.J., Lecumberri-Sanchez P., Moncada D. and Steele-MacInnis M., 2014, Fluid Inclusions in Hydrothermal Ore Deposits, in Holland H.D. and Turekian K.K., ed., Treatise on Geochemistry, Second Edition, v. 13, p. 119–142. Oxford: Elsevier.

Bonin, B., 1990, From orogenic to anorogenic settings: Evolution of granitoid suites after a major orogenesis: Geological Journal, v. 25, p. 261–270.

Borodin, L.S. and Pavlenko, A.S., 1974, The role of metasomatic processes in the formation of alkaline rocks, in The Alkaline Rocks, Sørensen, H., ed., p. 515–534. New York: Wiley.

Bowen, N.L., 1928, The evolution of the igneous rocks. Princeton.

Bowen, N.L., 1992, The Reaction Principle in Petrogenesis: The Journal of Geology, v. 30, p. 177–198.

Brown, M, and Chappell, B.W., 1992, The second Hutton Symposium on the Origin of Granites and Related rocks. Royal Society of Edinburgh, U.K.

Brown, M, 1994, The generation, segregation, ascent and emplacement of magma: the migmatite-to-crustally-derived granite connection in thickened orogens: Earths Science Reviews, v. 36, p. 83–130.

Brown, M. and Rushmer, T., 2006, Evolution and differentiation of the continental crust. Cambridge, UK: Cambridge University Press.

Candela, P.A., and Holland, H.D., 1986, A mass transfer model for copper and molybdenum in magmatic hydrotheral systems: The origin of porphyry-type ore deposits: Economic Geology, v. 81, p. 1−19.

Candela, P.A., 1997, A review of shallow, ore-related granites: Textures, volatiles and ore metals: Journal of Petrology: v. 38, p. 1619–1633.

Cannell, J., Cooke, D.R., Walshe, J.L., Stein, H., 2005. Geology, mineralization, alteration, and structural evolution of the El Teniente porphyry Cu–Mo deposit: Economic Geology, v. 100, p. 979–1003.

Cerny, P., Blevin. P.L, Cuney, M. and London, D., 2005, Granite-related ore deposits: Economic Geology 100th Anniversary Volume, p. 337–370.

Chang, Z., Cooke, D., Roach, M., Deyell, C., Gemmell, J., Cuison, A., Hedenquist, J., White, N., Garcia Jr., J, and McKnight, S., 2011, Exploration tools for linked porphyry and epithermal deposits: Example from the mankayan intrusion-centered Cu-Au district, Luzon, Philippines: Economic Geology, v. 106, p. 1365–1398.

Chappell, B.W. and White, A.J.R., 1974, Two contrasting granite types: Pacific Geology, v. 8, p. 173–174.

Chappell. B.W., White, A.J., Williams, I.S., Wyborn, D. and Wyborn, L.A.I., 2000, Lachlan Fold Belt granites revisited: high- and low-temperature granites and their implications: Australian Journal of Earth Sciences, v. 47, p. 123–138.

Chappell, B.W. and White, A.J.R., 2001, Two contrasting granite types: 25 years later: Australian Journal of Earth Science, v. 48, p. 489–499.

Chappell, B.W., Bryant, C.J. and Wyborn, D., 2012, Peraluminous I-type granites: Lithos, v. 153, p. 142–153.

Chappell, B.W. and White A.J.R., 1992, I- and S-type granites in the Lachlan Fold Belt, Transactions of the Royal Society of Edingburgh: Earth Sciences, v. 83, p. 1–26.

Chen, Y., Guo, G., and Li, X., 1998, Metallogenic geodynamic background of Mesozoic gold deposits in granite-greenstone terrains of North China Craton, Science in China Series D: Earth Sciences, v. 41, p. 113–120.

Chen, W., Xu, Z.W., Lu, X.C., Yang, X.N., Li, H.C., Qu, W.J., Chen, J.Q., Wang, H. and Wang, S.H., 2013, Petrogenesis of the Bao'anzhai granite and associated Mo mineralization, western Dabie orogen, east-central China: constraints from zircon U–Pb and molybdenite Re–Os dating, whole-rock geochemistry, and Sr–Nd–Pb–Hf isotopes: International Geology Review, v. 55, p. 1220–1238.

Clemens, J. D & Mawer, C. K., 1992, Granitic magma transport by fracture propagation: Tectonophysics, v. 204, p. 339–360.

Clemens, J.D. and Stevens, G., 2012, What controls chemical variation in granitic magmas?: Lithos, v. 134-135, p. 317–329.

Clemens, J.D., Buick, I.S. & Stevens, G. 2016. Fluids, melting, granulites and granites: a commentary: Precambrian Research, v. 278, p. 400–404.

Cooke, D. and Gemmell, B., 1996, Porphyry Deposits: Ore Deposit Studies and Exploration Models, p. 1–86. CODES, University of Tasmania.

Cooke, D. R., Hollings, P., Wilkinson, J. J. and Tosdal, R. M. 2014a, Geochemistry of Porphyry Deposits, in Turekian, H. D., Holland, K. K., ed., Treatise on Geochemistry, p. 357–381.

Cooke, D.R., Baker, M., Hollings, P., Sweet, G., Chang, Z., Danyushevsky, L., Gilbert, S., Zhou, T., White, N. C., Gemmell, J.B., and Inglis, S., 2014b, New Advances in Detecting the Distal Geochemical Footprints of Porphyry Systems – Epidote Mineral Chemistry as a Tool for Vectoring and Fertility Assessments: Society of Economic Geologists Inc. Special Publication, v. 18, p. 127–152.

Cooke D. R., A. J. Wilson, M. J. House, R. C. Wolfe, J. L. Walshe, V. Lickfold, and A. J. Crawford, 2007, Alkalic porphyry Au-Cu and associated mineral deposits of the Ordovician to Early Silurian Macquarie Arc, NSW: Australian Journal of Earth Sciences, v. 54, p. 445–463

Cooke, D.R., Hollings, P. and Walshe, J.L., 2005, Giant porphyry deposits: Characteristics, distribution, and tectonic controls: Economic Geology, v. 100, p. 801−818.

Creaser, R.A., Price, R.C. and Wormald, R.J., 1991, A-type granites revisited: Assessment of a residual-source model, Geology, v. 19, p. 163–166.

Dahlquist, J.A., Galindo, C., Pankhurst, R.J., Rapela, C.W., Alasino, P.H., Saavedra, J. and Fanning, C.M., 2007, Magmatic evolution of the Peñón Rosado granite: petrogenesis of garnet-bearing granitoids, Lithos, v. 95, p. 177–207.

Dardenne, M.A., Ferreira Filho, C.F. and Meirelles, M.R., 1988, The role of shoshonitic and calc-alkaline suites in the tectonic evolution of the Carajás district, Brazil: Journal of South American Earth Sciences, v. 1, p. 363–372.

DePaolom D.J., 1981, Trace element and isotopic effects of combined wallrock assimilation and fractional crystallization: Earth and Planetary Science Letters, v. 53, p. 189–202.

Deyell, C. L., 2005, Sulfur Isotope zonation at the Mt Polley alkalic porphyry Cu-Au deposit, British Columbia, Canada, in Mao, J., and Bierlein, F. P., eds, Mineral Deposit Research: Meeting Global Challenge: 8th Biennial Society for Geology Applied to Mineral Deposits meeting, v. 1, p. 373–376.

Didier, J. and Lameyre, 1969, Les granites du Massif Central Français: étude comparée des leucogranites et granodiorites': Contributions to Mineralogy and Petrology, p. 219–238.

Dilles, J.H., Einaudi, M.T., Proffett, J., and Barton, M.D., 2000, Overview of the Yerington porphyry copper district: Magmatic to non-magmatic sources of hydrothermal fluids: Their flow paths and alteration effects on rocks and Cu-Mo-Fe-Au ores: Society of Economic Geologists Guidebook Series, v. 32, p.55–66.

Eby, G.N., 1992, Chemical subdivision of the S-type granitoids: Petrogenetic and tectonic implications: Geology, v. 20, p. 641–644.

Farmer, G. L. and DePaolo, D. J., 1984, Origin of Mesozoic and Tertiary granite in the western United States and implications for pre-Mesozoic crustal structure: 2. Nd and Sr isotopic studies of unmineralized and Cu-mineralized and Mo-mineralized granite in the Precambrian craton: Journal of Geophysical Research, v. 89, p. 141–160.

Fournier, R.O., 1999, Hydrothermal processes related to movement of fluid from plastic into brittle rock in the magmatic-epithermal environment: Economic Geology, v. 94, p. 1193−1211.

Garnett, R.H., & Bassett, N.C., 2005, Placer deposits: Economic Geology 100th Anniversary Volume, p. 813–843.

Gao, P., Zhengm Y and Zhao Z., 2016, Experimental melts from crustal rocks: A lithochemical constraint on granite petrogenesis: Lithos, v. 266-267, p. 133–157.

Garwin, S., 2002, The geologic setting of intrusion-related hydrothermal systems near the Batu Hijau porphyry copper-gold deposit, Sumbawa, Indonesia: Economic Geology Special Publication, v. 9, p. 333–366.

Haase, K.M., Lima, S., Krumm, S. and Garbe-Schönbergb, D., 2014, The magmatic evolution of young island arc crust observed in gabbroic to tonalitic xenoliths from Raoul Island, Kermadec Island Arc: Lithos, v. 210–211, p. 199–208.

Halley, S., Dilles, J.H., Tosdal R.M., 2015, Footprints: hydrothermal alteration and geochemical dispersion around porphyry copper deposits, Society Economic Geology Newsletter, v. 100, p. 12–17.

Halter, W.E., Heinrich, C.A., and Pettke, T., 2005, Magma evolution and the formation of porphyry Cu-Au ore fluids: Evidence from silicate and sulphide melt inclusions: Mineralium Deposita, v. 39, p. 845−863.

Hart, C. J. R., 2005, Classifying, distinguishing and exploring for intrusion-related gold systems: The Gangue, v. 87, p. 1–9.

Hattori, K., and Keith, J.D., 2001, Contribution of mafic melt to porphyry copper mineralization: evidence from Mount Pinatubo, Philippines, and Bingham Canyon, Utah, USA: Mineralium Deposita, v. 36, p. 799–806.

Hedenquist, J.W. and Lowenstern, J.B., 1994, Review article: The role of magmas in the formation of hydrothermal ore deposits: Nature, v. 370, p. 519–527.

Heinrich, C.A., 2005, The physical and chemical evolution of low-salinity magmatic fluids at the porphyry to epithermal transition: A thermodynamic study: Mineralium Deposita, v. 39, p. 864−889.

Henley, J.J., and Hunt, J.P., 1992, Hydrothermal ore-forming processes in the light of studies in rock-buffered systems: II. Some general geologic applications: Economic Geology, vol. 87, p. 23−43.

Hill, K.C., Kendrick, R.D., Crowhurst, P.V., and Gow, P.A., 2002, Copper gold mineralisation in New Guinea: Tectonics, lineaments, thermochronology and structure: Australian Journal of Earth Sciences, v. 49, p. 737 − 752.

Holliday, J. R., MacCorquodale, F., Korsch, R. J., and Jones, L. E. A., 2006, Marsden Cu-Au porphyry deposit, NSW: discovery, geology and exploration using seismic reflection: Geological Society of Australia Abstracts, v. 82.

Holliday, J.R. and Cooke, D.R. (2007) Advances in Geological Models and Exploration Methods for Copper ± Gold Porphyry Deposits: Ore Deposits and Exploration Technology, v. 53, p. 791–809.

Hutton, D.H.W., 1988, Granite emplacement mechanisms and tectonic controls: inferences from deformation studies: The Origin of Granites, v. 79, p. 245–255.

Ishizuka, O., Tani, K., Reagan, M.K., Kanayama, K., Umino, S., Harigane, Y., Sakamoto, I., Miyajima, Y., Yuasa, M., Dunkley, D.J., 2011, The timescales of subduction initiation and subsequent evolution of an oceanic island arc: Earth Planetary Science Letter, v. 306, p. 229–240.

Jahns, R. H., 1944, Beryllium and tungsten deposits of the Iron Mountain district, Sierra and Socorro Counties, New Mexico: U.S. Geological Survey Bulletin 945-C, p. 45–79.

John, D.A., Ayuso, R.A., Barton, M.D., Blakely, R.J., Bodnar, R.J., Dilles, J.H., Gray, Floyd, Graybeal, F.T., Mars, J.C., McPhee, D.K., Seal, R.R., Taylor, R.D., and Vikre, P.G., 2010, Porphyry copper deposit model, chap. B of Mineral deposit models for resource assessment: U.S. Geological Survey Scientific Investigations Report 2010–5070–B.

Kessell, R., Schmidt, M. W., Ulmer, P. & Pettke, T., 2005, Trace element signature of subduction-zone fluids, melts and supercritical liquids at 120–180 km depth: Nature, v. 437, p. 724–727.

Kemp, A.I.S., Hawkesworth, C.J., Foster, G.L., Paterson, B.A., Woodhead, J.D., Hergt, J.M., Gray, C.M. and Whitehousr, M.J., 2007, Magmatic and crustal differentiation history of granitic rocks from Hf-O isotopes in zircon: Science, v. 315, p. 980–983.

Kirwin, D., 2012, Granite-related Ore deposits: Economic Geology, v. 107, p. 383–384.

Klemm, L.M., Pettke, T., and Heinrich, C.A., 2008, Fluid and source magma evolution of the Questa porphyry Mo deposit, New Mexico, USA: Mineralium Deposita, v. 43, p. 533–552.

Ulrich, T., and Mavrogenes, J., 2008, An experimental study of the solubility of molybdenum in H2O and KCl-H2O solutions from 500°C to 800°C, and 150 to 300 MPa: Geochimica et Cosmochimica Acta, v. 72, p. 2316−2330.

Kouzmanov, K. & Pokrovski, G.S. 2012, Hydrothermal Controls on Metal Distribution in Porphyry Cu (-Mo-Au) Systems: Special Publication of the Society of Economic Geologists, v. 16, p. 573–618.

Kwak, T.A.P. and Tan, T.H., 1981, The geochemistry of zoning in skarn minerals at the King Island (Dolphin Mine): Economic Geology, v. 76, p. 468–497.

Lameyre, J., Marot, J., Zimine, S., Cantagrel, J. M., Dosso, L. and Vidal P. 1976. Chronological evolution of the Kerguelen Islands syenite-granite ring complex: Nature, London, v. 263, p. 306–307

Lang, J.R., Stanley, C.R., and Thompson, J.F.H., 1995, Porphyry copper-gold deposits related to alkalic igneous rocks in the Triassic-Jurassic arc terranes of British Columbia: Arizona Geological Society Digest, v. 20, p. 219−236.

Large, S.J.E., Von Quadt, A., Wotzlaw, J.F., Guillong, M. and Heinrich, C.A., 2018, Magma Evolution Leading to Porphyry Au-Cu Mineralization at the Ok Tedi Deposit, Papua New Guinea: Trace Element Geochemistry and High-Precision Geochronology of Igneous Zircon: Economic Geology, v. 113, p. 39–61.

Lickfold, V., Cooke, D. R., Crawford, A. J. and Fanning, C., 2007, Shoshonitic magmatism and the formation of the Northparkes porphyry Cu-Au deposits, New South Wales: Australian Journal of Earth Sciences, v. 54, p. 417–444.

Loiselle, M.C. and Wones, D.R., 1979, Characteristics and origin of anorogenic granites: Geological Society of America Abstract Programs, v. 11, 468 p.

Lowell, J.D., and Guilbert, J.M., 1970, Lateral and vertical alteration-mineralization zoning in porphyry ore deposits: Economic Geology, v. 65, p. 373−408.

Maniar, P.D. and Piccoli, P.M., 1989, Tectonic Discrimination of Granitoids: Geological Society of America Bulletin, v. 101, 635–643.

Marsh, E.E., Goldfarb, R.J., Hart, C.J.R. and Craig, A., 2003, Geology and geochemistry of the Clear Creek intrusion-related gold occurrences, Tintana Gold Province, Yukon, Canada: Canadian Journal of Earth Sciences, v. 40, p. 681–699.

Masterman, G.J., Cooke, D.R., Berry, R.F., Walshe, J.L., Lee, A.W., and Clark, A.H., 2005, Fluid chemistry, structural setting, and emplacement history of the Rosario Cu-Mo porphyry and Cu-Ag-Au epithermal veins, Collahuasi district, northern Chile: Economic Geology, v. 100, p. 835−862.

Mathur, R., Ruiz, J., Titley, S., Gibbins, S., Margotomo, W., 2000. Different crustal sources for Au-rich and Au-poor ores of the Grasberg Cu–Au porphyry deposit: Earth Planetary Science Letters, v. 183, p. 7–14.

Meinert, L.D., 1992, Skarns and skarn deposits: Geoscience Canada, v. 14, p. 145–162.

Meyer, C. and Hemley, J.J., 1967, Wall rock alteration, In: Geochemistry of Hydrothermal Ore deposits, Barnes, H.L., ed., New York: Holt, Reinehart and Winston, p. 166–235.

Monecke, T., Kempe, U., Monecke, J., Sala, M. and Wolf, D., 2002, Tetrad effect in rare earth element distribution patterns: a method of quantification with application to rock and mineral samples from granite-related rare metal deposits: Geochemica et Cosmochimica Acta, v. 66, p. 1185–1196.

Mungall, J. E., 2002, Roasting the mantle: Slab melting and the genesis of major Au and Au-rich Cu deposits. Geology, v. 30, 915–918.

Murphy, J.B., 2006, Igneous Rock Associations 7. Arc Magmatism I: Relationship between Subduction and Magma Genesis: Geoscience Canada, v. 33, p. 145–167.

Mutschler, F.E., Wright, E.G., Ludington, S. and Abbott, J.T., 1981, Granite molybdenite systems, Economic Geology, v., 76, p. 874–897.

Neal, L.C., Wilkinson J.J., Mason, P.J. and Chang, Z., 2018, Spectral characteristics of propylitic alteration minerals as a vectoring tool for porphyry copper deposits: Journal of Geochemical Exploration, v. 184, p. 179–198.

Oliver, N.H.S., Pearson, P.J., Holcombe, R.J. and Ord, A., 1999, Mary Kathleen metamorphic–hydrothermal uranium – rare-earth element deposit: ore genesis and numerical model of coupled deformation and fluid flow: Australian Journal of Earth Sciences banner, v. 46, p. 467–484.

Orovan, E.A., Cooke, D.R., Harris, A.C., Ackerman, B. and Lawlis, E., 2018, Geology and Isotope Geochemistry of the Wainaulo Cu-Au Porphyry Deposit, Namosi District, Fiji: Economic Geology, v. 113, p. 133–161.

Padilla-Garza, R.A., Titley, S.R., and Eastoe, C.J., 2004, Hypogene evolution of the Escondida porphyry copper deposit, Chile: Society of Economic Geologists Special Publication, v. 11, p. 141−165.

Pan, Y. and Dong, P., 1999, The Lower Changjiang (Yangzi/Yangtze River) metallogenic belt, east central China: Intrusion- and wallrock-hosted Cu-Fe-Au-Mo-Zn-Pb-Ag deposits: Ore Geology Reviews, v. 15, p. 177–242.

Paterson, S.R., and Vernon, R.H., 1995, Bursting the bubble of ballooning plutons: A return to nested diapirs emplaced by multiple processes: Geological Society of America Bulletin, v. 107, p. 1356–1380.

Patino Douce, A.E., and Beard, J.S., 1995, Dehydration-melting of biotite gneiss and quartz amphibolite from 3 to 15 kbar: Journal of Petrology, v. 36, p. 707–738.

Petford, N., Cruden, A.R., McCaffrey, K.J.W. and Vigneresse, J.L., 2000, Granite magma formation, transport and emplacement in the Earth's crust: Nature, v. 408, p. 669–673.

Pettke, T., Oberli, F. & Heinrich C. A., 2010, The magma and metal source of giant porphyry-type ore deposits, based on lead isotope microanalysis of individual fluid inclusions: Earth Planetary Science Letters, v. 296, p. 267–277.

Pirajino, F., 1992, Porphyry systems and skarns, Hydrothermal Mineral Deposits. Springer, Berlin, Heidelberg

Pirajno, F 2008, Hydrothermal Processes. [electronic resource], New York: Springer Oct. 2008.

Pitcher, W. S., 1983a,. Granite: typology, geological environment and melting relationships, in Atherton, M. P., & Gribble, C. D., eds., Migmatites, Melting and Metamorphism. Nantwich: Shiva Publications, p. 277–287.

Pitcher, W.S., 1983b, Granite type and tectonic environment, in Hsü, ed., Mountain Building Processes: Academic Press. London.

Pitcher, W.S., 1993, The Nature and Origin of Granite. Blackie, London

Pitcher W. S., 1997, The nature and origin of granite. Chapman & Hall, London.

Plouffe, A., Ferbey, T., Hashimi, S. and Ward, B.C., 2016, Till geochemistry and mineralogy: vectoring towards Cu porphyry deposits in British Columbia, Canada, Geochemistry: Exploration, Environment, Analysis, v. 16, p. 213 – 232.

Pollard, P.J., 2006, An intrusion-related origin for Cu-Au mineralization in iron oxide-copper-gold (IOCG) provinces: Mineral Deposita, v. 46, p. 179–187.

Richards, J.P., 2003, Tectono-magmatic precursors for porphyry Cu-(Mo-Au) deposit formation: Economic Geology, v. 98, p. 1515–1533.

Richards, J.P. 2009, Postsubduction porphyry Cu-Au and epithermal Au deposits: Products of remelting of subduction-modified lithosphere: Geology, v. 37, p. 247–250.

Richards, J.P., 2011, Magmatic to hydrothermal metal fluxes in convergent and collided margins: Ore Geology Reviews, v. 40, p. 1–26.

Ridley, J., 2013, Ore deposit geology. Cambridge Cambridge University Press.

Rinne, M, Cooke, D, Harris, A, Finn, D, Allen, C, Heizler, M, and Creaser, R., 2018, Geology and geochronology of the Golpu porphyry and Wafi epithermal deposit, Morobe Province, Papua New Guinea: Economic Geology, v. 113, p. 271–294

Robb, L 2004, Introduction to Ore-Forming Processes. [electronic resource], Wiley-Blackwell [Imprint] June 2004 Hoboken: John Wiley & Sons, Incorporated.

Rombach, C.S., 2000, Genesis and mineralization of the Shotgun Deposit, southwestern Alaska. In: Tucker, T.L., and Smith, M.T., eds., The Tintina gold belt: Concepts,exploration,and discoveries: Vancouver, British Columbia and Yukon Chamber of Mines Special Volume 2, p. 181–196.

Rosenberg, C.L., 2004, Shear zones and magma ascent: A model based on a review of the Tertiary magmatism in the Alps, Tectonics, v. 23, 3002 p.

Rusk, B.G., Reed, M.H., Dilles, J.H., Klemm, L.M., and Heinrich, C.A., 2004, Compositions of magmatic hydrothermal fluids determined by LA-ICP-MS of fluid inclusions from the porphyry copper-molybdenum deposit at Butte, MT: Chemical Geology, v. 210, p. 173–199.

Rusk, B.G., Reed, M.H., and Dilles, J.H., 2008a, Fluid inclusion evidence for magmatic-hydrothermal fluid evolution in the porphyry copper-molybdenum deposit at Butte, Montana: Economic Geology, v. 103, p. 307 − 334.

Seedorff, E., Dilles, J.H., Proffett, J.M., Einaudi, M.T., Zurcher, L., Stavast, W.J.A., Johnson, D.A., and Barton, M.D., 2005, Porphyry deposits: Characteristics and origin of hypogene features: Economic Geology 100th Anniversary Volume, p. 251–298

Seedorff, E., Barton, M.D., Stavast, W.J.A., and Maher, D.J., 2008, Root zones of porphyry systems: Extending the porphyry model to depth: Economic Geology, v. 103, p. 939−956.

Shellnutt, J.G. and Zhou, M., 2007, Permian, peralkaline, peraluminous and metaluminous A-type granites in the Panxi district, SW China: Their relationship to the Emeishan mantle plume: Chemical Geology, v. 243, p. 286–316.

Shinohara, H., 1994, Exsolution of immiscible vapor and liquid phases from a crystallizing silicate melt: Implications for chlorine and metal transport: Geochimica et Cosmochimica Acta, v. 58, p. 5215−5221.

Sial, A.N., Bettercourt, J.S., De Compos, C.R. and Ferreira, V.Z., 2001, Granite-related Ore deposits, Geological Society, London, Special Publications, v. 350, p. 1–5.

Sillitoe , R. H. , 2000 , Styles of high-sulphidation gold, silver and copper mineralisation in porphyry and epithermal environments: The AusIMM Proceedings , v. 305, pp. 19–34.

Sillitoe, R.H., 2000, Gold-rich porphyry deposits: Descriptive and genetic models and their role in exploration and discovery: Reviews in Economic Geology, v. 13, p. 315–345.

Sillitoe, R.H., 2002, Some metallogenic features of gold and copper deposits related to alkaline rocks and consequences for exploration: Mineralium Deposita, v. 37, p. 4–13.

Sillitoe, R.H., and Hedenquist, J.W., 2003, Linkages between volcanotectonic settings, ore-fluid compositions, and epithermal precious metal deposits: Society of Economic Geologists Special Publication 10, p. 315−343.

Sillitoe, R.H., and Perelló, J., 2005, Andean copper province: Tectonomagmatic settings, deposit types, metallogeny, exploration, and discovery: Economic Geology 100th Anniversary Volume, p. 845−890.

Sillitoe, R. H. 2010, Porphyry Copper Systems: Economic Geology, v. 105, p. 3–41.

Sinclair, W.D., 2007, Porphyry deposits, In: Goodfellow W.D., ed., Mineral Deposits of Canada: A Synhesis of Major Deposit-Types, District Metallogeny, the Evolution of Geological Provinces, and Exploration Methods: Geological Association of Canada, Mineral Deposits Division, Special Publication No. 5, p. 223–243.

Stern, R.J., 2001, Subduction zones, Review of Geophysics, v. 40, no. 4.

Stern, R.J., 2010, The anatomy and ontogeny of modern intra-oceanic arc systems, in Kusky, T. M., Zhai, M.-G. & Xiao, W., eds The Evolving Continents: Understanding Processes of Continental Growth. Geological Society, London, Special Publications, v. 338, p. 7–34.

Streckeisen, A.L., 1979, Plutonic rocks, classification and nomenclature recommended by the IUGS subcommission on the systematics of igneous rocks. Geotimes, v. 18, p. 26–30

Sillitoe, R.H., 1972, A plate tectonic model for the origin of porphyry copper deposits: Economic Geology, v. 67, p. 184–197.

Tanaka, T., Imai, A., Egashira, S., Sakomoto, S., Yasunaga, K. and Maeda, K., 2010, Petrological and Geochemical Characteristics of Intruisve Rocks Related to Porphyry Copper Mineralization and the Implications for the Genesis of Deposits in the Namosi area, Viti Levu, Republic of Fiji Islands: Resource Geology, v. 60, p. 31–51.

Tatsumi, Y, & Eggins, S., 1995, Subduction zone magmatism. Cambridge, Mass., USA: Blackwell Science.

Titley, S.R., 1993, Characteristics of porphyry copper occurrence in the American Southwest', Geological Association of Canada Special Paper 40, p. 433−464.

Titley, S.R., and Marozas, D.C., 1995, Processes and products of supergene copper enrichment'. In: Pierce, F.W., and Bolm, J.G., eds., Porphyry copper deposits of the American CordilleraArizona Geological Society Digest, v. 20, p. 156–168.

Tischendorf, G. and Palchen, W. 1985. Zur klassifikation von Granitoi'den: Zeitschrift für Geologische Wissenschaften, v. 13, p. 615–627.

Tulloch, A.J., Kimbrough, D.L., 2003, 'Paired plutonic belts in convergent margins and the development of high Sr/Y magmatism: Peninsular Ranges batholith of Baja California and Median batholith of New Zealand: Special Paper, 374'. Geological Society of America, p. 1–21.

Ulrich. T., Gunther, D. and Heinrich, C.A., 1999, Gold concentrations of magmatic brines and the metal budget of porphyry copper deposits: Nature, v. 399, p. 676–679.

Vigneresse, J. L., Barbey, P. & Cuney, M., 1996, Rheological transitions during partial melting and crystallisation with application to felsic magma segregation and transfer: Journal of Petrology, v. 37, p. 1579–1600.

Weinberg, R.F., Mark, G., and Reichardt, H., 2009, Magma ponding in the Karakoram shear zone, Ladakh, NW India: Geological Society of America Bulletin, v. 121, p. 278–285.

White, A.J.R., 1979, Source of granite magmas: Geological Society of America Abstract Programs, v. 11, 539 p.

Winter, J.D., 2001, An introduction to igneous and metamorphic petrology. Upper Saddle River, NJ: Prentice Hall.

Wilson, A. J., 2003, The geology, genesis and exploration context of the Cadia gold-copper porphyry deposits, NSW, Australia: Ph.D. thesis, University of Tasmania.

Wilkinson, J.J., 2013, Triggers for the formation of porphyry ore deposits in magmatic arc: Nature Geosccience, v. 6, p. 917–925.

Wilkinson, 2015, The chlorite proximitor: A new tool for detecting porphyry ore deposits: Journal of Geochemical Exploration, v. 152, p. 10–26.

Williams-Jones, A.E., Migdisov, A.A., Archibald, S.M., and Xiao, Z.F., 2002, Vapor-transport of ore metals: Geochemical Society Special Publication 7, p. 279−305.

Wilson, A.J., Cooke, D.R., and Harper, B.L., 2003, The Ridgeway gold-copper deposit: A high-grade alkalic porphyry deposit in the Lachlan fold belt, New South Wales, Australia: Economic Geology, v. 98, p. 1637–1666.

Wilson, A. J., D. R. Cooke, B. J. Harper, and C. L. Deyell, 2007, Sulfur isotopic zonation in the Cadia district, southeastern Australia: exploration significance and implications for the genesis of alkalic porphyry gold–copper deposits: Mineralium Deposita, v. 42, p. 465–487.

Wolfe, R. C., 2001, Geology of the Didipio region and paragenesis of the Dinkidi Cu-Au porphyry deposit: Ph.D. thesis, University of Tasmania.

Wyborn, L.A.I., 2002, Granites and copper gold metallogenesis in the Australian Proterozoic Geoscience Australia Record 2001/12, p. 5–51

Yin, L., Pollard, P.J., Shouxi, H., and Taylor, R.G., 1995, Geological and geochemical characteristics of the Yichun Ta-Nb-Li deposit, Jiangxi province, south China: Economic Geology, v. 90, p. 577–585.

Yousefi, M., 2017, Recognition of an enhanced multi-element geochemical signature of porphyry copper deposits for vectoring into mineralized zones and delimiting exploration targets in Jiroft area, SE Iran: Ore Geology Reviews, v. 83, p. 200–214.

Zadeh, M.H., Tangestani, M.H., Roldan F.V., and Yutsa, I., 2014, 'Spectral characteristics of minerals in alteration zones associated with porphyry copper deposits in the middle part of Kerman copper belt, SE Iran', Ore Geology Reviews, v. 62, p. 191–198.

Zhang, H., Li, C.Y., Yang, X.Y., Sun, Y.L., Deng, J.H., Liang, H.Y., Wang, R.L., Wang, B.H., Wang, Y.X., Sun, W.D., 2013, Shapinggou: the largest Climax-type porphyry Mo deposit in China: International Geology Review, v. 56, p. 313–331.